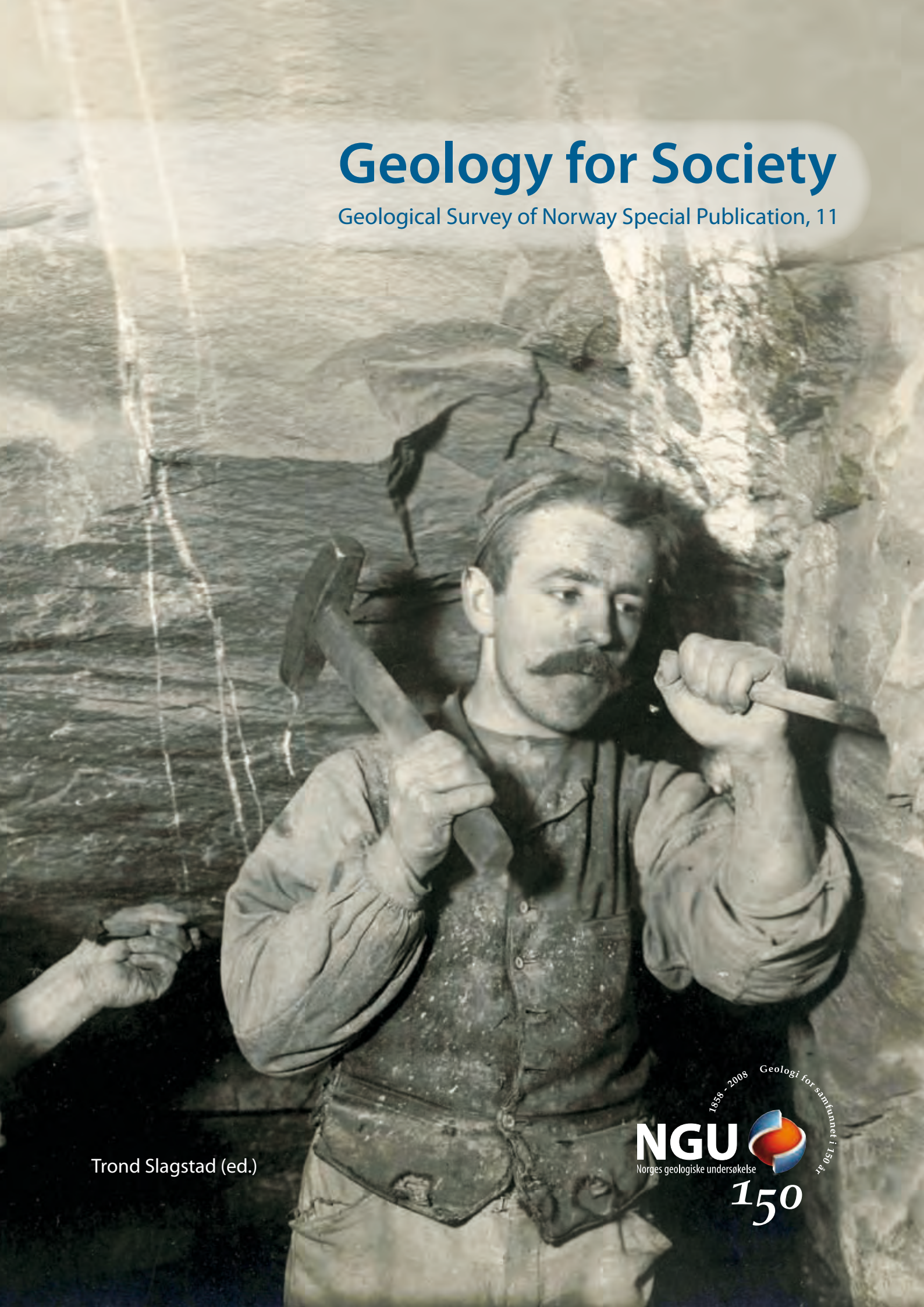


Geology for Society

Geological Survey of Norway Special Publication, 11



Trond Slagstad (ed.)

1858 - 2008 Geologi for samfunnet i 150 år
NGU
Norges geologiske undersøkelse
150



Geological Survey of Norway Special Publication, 11

The NGU Special Publication series comprises consecutively numbered volumes containing papers and proceedings from national and international symposia or meetings dealing with Norwegian and international geology, geophysics and geochemistry; excursion guides from such symposia; and in some cases papers of particular value to the international geosciences community, or collections of thematic articles. The language of the Special Publication series is English.

Editor: Trond Slagstad

©2008 Norges geologiske undersøkelse
Published by
Norges geologiske undersøkelse
(Geological Survey of Norway)
NO-7491 Norway

All Rights reserved

ISSN: 0801-5961
ISBN: 978-82-7385-130-7
Design and print: Skipnes kommunikasjon 103851/0508

Cover illustration:

Miners working 295 metres below the surface in the silver mines in Kongsberg in 1912.
Photo: Mimi Johnson.

Contents

Introduction <i>Trond Slagstad (ed.)</i>	3
National treasure of global significance. Dimension-stone deposits in larvikite, Oslo igneous province, Norway <i>Tom Heldal, Idunn Kjølle, Gurli B. Meyer and Sven Dahlgren</i>	5
Geology of the soapstone deposits of the Linnjavri area, Hamarøy, Nordland, north Norwegian Caledonides—Norway’s largest reserves of soapstone <i>Ingvar Lindahl and Lars Petter Nilsson</i>	19
Aggregates in Norway—Properties defining the quality of sand, gravel and hard rock for use as aggregate for building purposes <i>Eyolf Erichsen, Arnbild Ulvik, Knut Wolden and Peer-Richard Neeb</i>	37
From Hyllestad to Selbu: Norwegian millstone quarrying through 1300 years <i>Tor Grenne, Tom Heldal, Gurli B. Meyer and Elizabeth G. Bloxam</i>	47
Groundwater monitoring and modelling from an archaeological perspective: possibilities and challenges <i>Hans de Beer and Henning Matthiesen</i>	67
Global geochemical mapping and sediment-associated flux of major world rivers <i>Jim Bogen and Rolf Tore Ottesen</i>	83
Ground-Source Heat Pumps and Underground Thermal Energy Storage— Energy for the future <i>Kirsti Midttømme, David Banks, Randi Kalskin Ramstad, Ola M. Sæther and Helge Skarphagen</i>	93
Factors influencing shallow (< 1000 m depth) temperatures and their significance for extraction of ground-source heat <i>Trond Slagstad, Kirsti Midttømme, Randi Kalskin Ramstad and Dag Slagstad</i>	99
Sediment fluxes and sediment budget in Latnjavagge and the potential of applying unified methods for integrating investigations on sediment fluxes and budgets in cold-environment catchments <i>Achim A. Beylich</i>	111
Airborne gamma-ray spectrometer mapping for relating indoor radon activity concentrations to geological parameters in the Fen region, southeast Norway <i>Björn Henning Heincke, Mark Smethurst, Arne Bjørlykke, Sven Dahlgren, Jan Steinar Rønning and John Olav Mogaard</i>	131
Testing the performance of a recent radon-hazard evaluation in the municipality of Gran, eastern Norway <i>Mark A. Smethurst, Aud Venke Sundal, Terje Strand and Bernard Bingen</i>	145

Introduction

Geology has always had a significant impact on human society and the way it has evolved. The names of important epochs in this evolution, such as the Bronze Age, Iron Age, Oil Age—not to mention the Stone Age—reflect geology’s significance in shaping society. However, the days when one could strike it rich by drilling a well at random or accidentally stumble across a Mother Lode are all but gone, and discovering, utilising and managing geological resources and hazards today require significant knowledge about the underlying geological processes.

This volume of NGU Special Publication presents some of the ongoing research at the Geological Survey of Norway and shows how geology and geological knowledge influence many areas of society. The global demand for geological resources is on the rise, and knowing where to look for these resources is becoming increasingly more important. In addition, quantifying these resources is vital to ensure present-day as well as future supplies. As society and technology evolve (cf., the Stone Age-, Bronze Age-, Iron Age-progression) so does the demand for geological resources. A sagacious assessment of geological resources therefore requires a broad, research-based approach.

Although surprising to many, we as geologists are well aware that Earth is a dynamic, ever-changing planet. As Earth’s population grows and formerly uninhabited areas are inhabited, understanding the effects of these changes on the land on which we live becomes increasingly important. Furthermore, managing and sustaining the environment that today’s and future societies depend on require understanding of how our actions affect our surroundings both on a local and global scale. As societies have expanded and continue to expand into uncharted territories, knowing what hazards lie ahead—not to mention above and below—requires insight into geology and geological processes.

Rather than highlighting a particular topic, which is often the case with Special Publications, the purpose of this volume is to emphasise the span of what we consider to be ‘geology’ and show how these diverse topics come together under the common topic ‘Geology for Society’—the motto of the Geological Survey of Norway. Although 150 years old and counting, the arrows continue to point up and out with regard to society’s need and demand for geological knowledge.

Trond Slagstad
Editor

National treasure of global significance. Dimension-stone deposits in larvikite, Oslo igneous province, Norway

Tom Heldal¹, Idunn Kjølle², Gurli B. Meyer¹ and Sven Dahlgren³

¹*Geological Survey of Norway (NGU), 7491 Trondheim, Norway.*

²*Directorate of mining, 7491 Trondheim, Norway.*

³*Geological advisor, Buskerud, Telemark and Vestfold, Fylkeshuset, 3126 Tønsberg, Norway.*

E-mail: tom.heldal@ngu.no

Larvikite has for more than a hundred years been appreciated as one of the world's most attractive dimension stones, and at present, its production and use is more extensive than ever. The main reason for the continuous success of larvikite on the world market is the blue iridescence displayed on polished surfaces, which is caused by optical interference in microscopic lamellae within the ternary feldspars. The larvikite complex consists of different intrusions, defining several ring-shaped structures, emplaced during a period of approximately five million years. Following this pattern, several commercial subtypes of larvikite, characterised by their colour and iridescence, have been mapped. Four of these subtypes are being exploited at the present time and define the most important reserves in the short run. Some other subtypes are less attractive in the present market situation, but may provide an interesting potential for the future. However, the industrial value of the larvikite also depends on other geological features, such as various types of dykes, faults and fractures, ductile deformation zones, late-stage magmatic and hydrothermal alteration and deep weathering. When combining the distribution pattern of such features with the map of the larvikite subtypes, it is possible to delineate various types of larvikite deposit that are considered to have commercial value in the short or long term. Finally, reserve estimates for the different types have been made, showing that some of the most attractive types have rather limited known reserves if the present level of production is maintained or increased.

Introduction

The name ‘larvikite’ was first applied by Waldemar Brøgger in his descriptions of the monzonitic rocks within the southern part of the Carboniferous–Permian Oslo igneous province (Brøgger 1890, see also Dons 1978) (Figure 1). The rock name

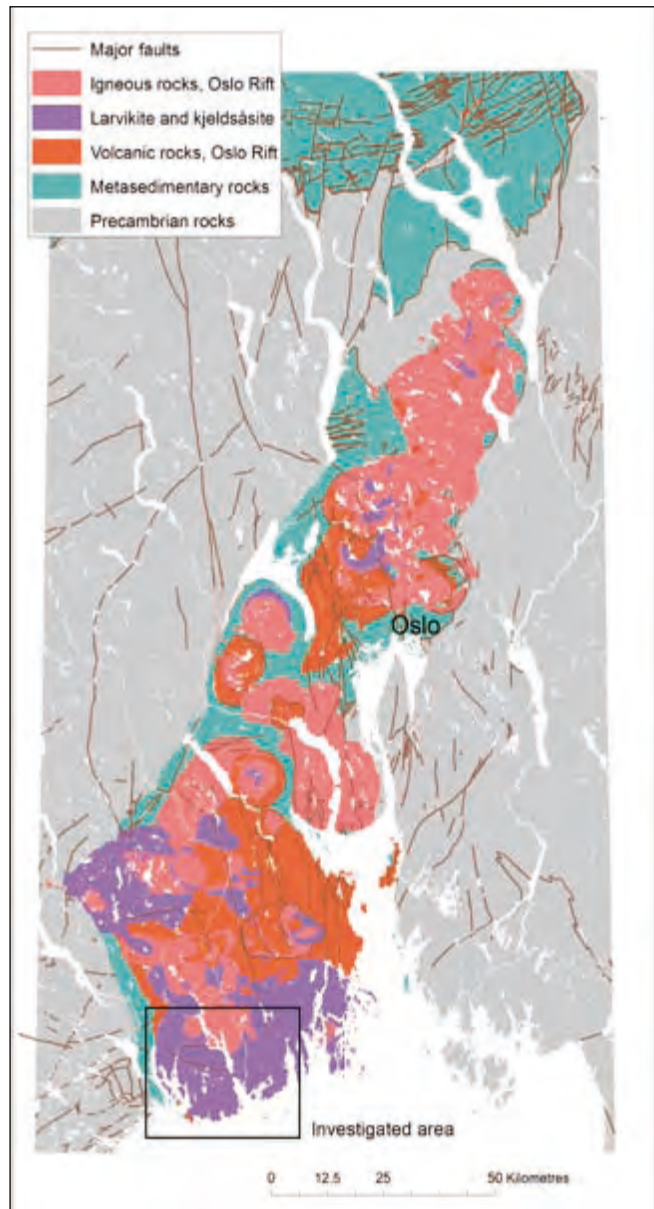


Figure 1. Overview of the Oslo Rift and distribution of larvikite and similar rocks. Modified from NGU digital maps of the Oslo region.

was later changed to ‘larvikite’ having its origin in the small coastal town of Larvik (Laurvik in Brøgger’s days), situated almost right in the centre of the main larvikite plutonic complex. The larvikites form a series of semi-circular intrusions, varying from quartz-bearing monzonite in the east (earliest phases) towards nepheline-bearing monzonite and nepheline syenite in the west (latest phases, Figure 2). From a geologist’s point of

view, the larvikites are important for understanding the tectono-magmatic processes responsible for the formation of the Oslo Rift. However, most other people see larvikite as a particularly beautiful rock. The reason for this is the abundance of ternary feldspar displaying bluish to silvery play of colours or iridescence. This aesthetic uniqueness has caused larvikite to become one of the world’s most used and appreciated dimension stones, cladding hundreds of prestigious buildings and thousands of kitchen tops world-wide, and lately also the nomination and approval of larvikite as the ‘National rock’ of Norway (Heldal 2008). Production started already in the 1880s, and at present, the export value of rough blocks of dimension stone from the Larvik region lies between a half and one billion NOK, distributed on approximately 30 individual quarries (Figures 3 and 4). Different types of larvikite have different market value, and the customers can choose between a range of types and qualities under trade names such as ‘Blue Pearl’, ‘Emerald Pearl’, ‘Royal Blue’ and ‘Marina Pearl’.

This paper presents the results of a more or less continuous, ten-year project aimed at mapping and characterising the most important larvikite deposits, in order to identify and delineate deposits that can be of industrial importance in the short and long run. Being located in an area with an increasing population, the larvikite deposits are certainly under pressure from other land-use interests, and thus the needs of documenting and securing future deposits are indeed urgent.

Geology and previous research

Larvikite and associated plutonic rocks compose a significant part of the bedrock within the Carboniferous–Permian Oslo Rift, predominantly in its southern part (Figure 1). Although dimension-stone quarrying has been carried out in many places, it is first of all in the vicinity of Larvik town that exploitation

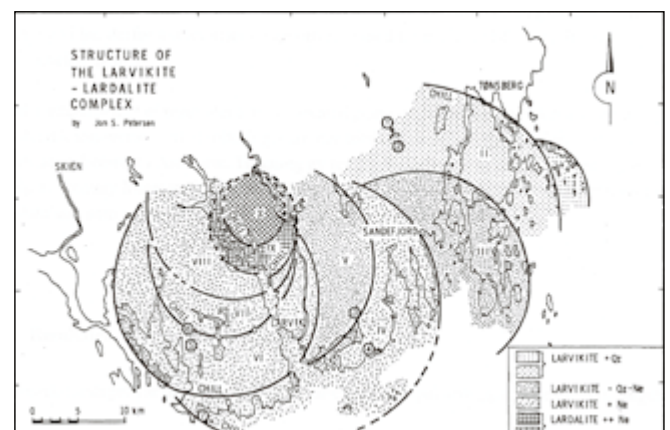


Figure 2. The larvikite ring complex as interpreted by Petersen (1978a). Map from Oftedahl and Petersen (1978).



Figure 3. Larvikite quarry at Klåstad (Emerald Pearl).



Figure 4. Stock of larvikite blocks at Tvedalen ready for shipping abroad.

has developed to a permanent and sizeable industrial activity, and which has been the target area for the present study (Figure 1).

After Brøgger's (1890) pioneering work on the igneous rocks of the Oslo Rift, little research on the larvikites, with the exception of mineralogical investigations mentioned above, was carried out until the 1970s. Petersen (1978a, b) was the first to suggest that the larvikite complex is composed of several, ring-shaped intrusions, younging from east to west. He suggested 8 such ring fragments (numbered I to VIII), based on topographic features, magnetic anomalies and field observations of some of the contact zones (chilled margins, Figure 2). Furthermore, Petersen (1978a, b) observed a systematic change in the mineralogy from quartz-bearing larvikite in the east towards nepheline-bearing larvikite to the west, approaching the lardalite and nepheline syenites in the 'centre' of the plutonic complex. This led Petersen (1978a, b) to suggest a sequential evolution from saturated to undersaturated magma fluxes. This could result from either multiple caldera collapses or a system of multiple ring intrusions from a deep-seated parental magma chamber (Neumann et al. 1977, 1988, Neumann 1978a, 1980, Petersen 1978a, b).

Neumann (1980) confirmed Petersen's model of the separate ring intrusions through geochemical analyses, and also showed geochemical evolution patterns within each ring intrusion. Neumann furthermore provided geochemical evidence that the larvikites are the plutonic equivalents to the overlying, once massive sequences of romb porphyry lava flows exposed in the surrounding areas (Neumann 1978b). Dahlgren et al. (1998) confirmed the progressive evolution of the ring intrusions through time by U–Pb dating, giving a range of ages between 297 ± 1.2 Ma (eastern larvikite) and 293.2 ± 1.3 Ma (western larvikite). Nepheline syenite, being the youngest intrusion in the sequence, was dated at 292 ± 0.8 Ma. More recently, Larsen and Olausen (2005) devised a model for the evolution of the Oslo Rift, where the larvikite/romb porphyry lavas define an intermediate step in the rift formation, i.e., in-between the

early volcanism (basalt fissure eruptions and plateau basalts) and later caldera formation.

The first record of larvikite as a source for dimension stone is a letter dated October 1811, from a certain Ohlsen to 'Headmaster Floor', where the former suggests extraction of larvikite, among other purposes, for a castle in Copenhagen (referred to in Oxaal 1916). However, nothing happened until 1884, when quarrying was initiated by Ferdinand Narvesen close to the town of Stavern, southwest of Larvik. A few years later, Theodor Kjerulf, then director of the Geological Survey of Norway (NGU), took part in the further development of the industry by recommending the deposits of dark larvikite southeast of Larvik. Oxaal (1916) did the first survey of the quarried larvikites and described the quarrying activity in the area. Reid Kvien, a geological consultant in Larvik, was the first to apply Petersen's model in his interpretation of commercial larvikite types and in compiling the first resource map for the municipality. In recent years, NGU has carried out surveys of the larvikite deposits (Heldal et al. 1999, Kjølle et al. 2003), on which this paper is based.

Larvikite is generally a coarse-grained plutonic rock consisting of tabular to prismatic crystals of ternary alkali feldspar (10–50 mm) intergrown with interstitial stubby to ragged prisms (2–5 mm) or 10–50 mm oikocrysts of augite (diopside-augite in the larvikites used for dimension stone) and/or hornblende (calcic amphiboles), interstitial grains of Fe–Ti-oxides and biotite in addition to oikocrysts or subhedral rounded grains of olivine (Fo_{25-55} in the larvikites used for dimension stone). Quartz occurs interstitially in the larvikites of the eastern part of the area while nepheline takes over for quartz in the central to northwestern part (Figure 2). Nepheline occurs both as interstitial grains and as subgrains and intergrowths in the ternary feldspars. Apatite is a minor phase forming inclusions in particular in olivine and Fe–Ti-oxides. Micro inclusions of zircon, titanite and complex Nb–Th–REE-minerals occur in all the above-mentioned mineral phases. The larvikites are generally composed of 80–95% feldspar, 1–5% Ca-rich pyroxene, 1–5% amphibole, 0–5% olivine, 1–5% Fe–Ti-oxides, ~1% apatite, 1–5% biotite, \pm 1–5% nepheline, \pm 1–5% quartz and the acces-

sory minerals zircon, baddeleyite (ZrO_2) and sphene. The bulk of the feldspar is ternary (Barth 1945), with compositions in the range $An_{4-30}Ab_{58-82}Or_{3-35}$ (Ofte Dahl 1948, Muir and Smith 1956, Smith and Muir 1958, Rosenqvist 1965, Nielsen 2007). In the larvikite types used for dimension stone, the ternary feldspar is composed of flame-like to patchy intergrowths of various phases of feldspar. Individual flames and patches range in 'bulk' composition from alkali-feldspar compositions close to sanidine, towards albite and/or anorthoclase and/or pure plagioclase compositions. Flames and patches with iridescence are composed of microscopic to submicroscopic lamellae of two phases of feldspar. A common feature of the feldspars is the occurrence of partly resorbed grains of plagioclase (oligoclase) in addition to subgrains and intergrowths with nepheline (Nielsen 2007).

The feldspars in the larvikites have bulk compositions containing significant proportions (> 5%) of Ab, Or and An. Feldspar of this composition is sometimes referred to as mesoperthite, but here we prefer the more general term ternary feldspar. As pointed out by Ribbe (1975), this composition causes instability in the crystallographic structure and leads to exsolution similar to that in alkali-feldspar. The bright optical interference colours (iridescence) seen in certain varieties of larvikite are due to optical refraction in the exsolution pattern of alternating orthoclase and anorthite (An_{15-18}) lamellae. The intensity as well as the colour of the iridescence depends on the spacing and geometry of the lamellae, and iridescence generally occurs when the thickness of lamellae is in the range 500–1000 Å (Figures 5 and 6).

Another kind of variation is in the distribution of iridescence within single feldspar crystals and three main groups can be defined: patchy (irregular patches within each crystal), homogenous (within a crystal) and zoned (see Figure 7). Partly, we can see a tendency where the younger larvikites (such as the Blue Pearl subtype) contain predominantly patchy iridescence patterns, while some of the older (such as the Emerald Pearl

subtype) more commonly have homogeneous or zoned iridescent crystals.

Quarrying larvikite — aspects of industrial quality

Larvikite is extracted in rectangular blocks aimed for export markets. To obtain the highest market value, the blocks must be large (preferably larger than 4 m³) and homogeneous. If the blocks contain flaws, veins, discolouration or other features reducing the uniformity of colour and quality, the market price for the blocks is reduced significantly, if they can be sold at all. The average block yield in the larvikite quarries is close to 10%, which means that nine out of ten cubic metres of extracted rock are not utilised as dimension stone. However, the leftover rock from dimension-stone quarrying is to an increasing extent used for other purposes. Large 'waste' blocks are shipped to the UK and other North European countries to be used for coastal protection, and some of it is crushed to rock aggregate. The rest is deposited in designated landfill areas close to the quarries.

In general, the surveys that have been carried out in the larvikite areas have focused on the main geological aspects of importance to the industrial demands, basically the fundamental success factors for the quarries.

Attractive and uniform colour is the most important issue besides the block size. In general, larvikite displaying strong blue play of colours (iridescence) is more attractive and valued than larvikite with weaker blue and/or silvery colour play (Figure 5). The variation in colour essentially follows the ring pattern identified by Petersen (1978a), i.e., related to the individual intrusive phases.

Discolouration of the larvikite is assigned to late- to post-magmatic alteration of the larvikite, varying from 'bleach-

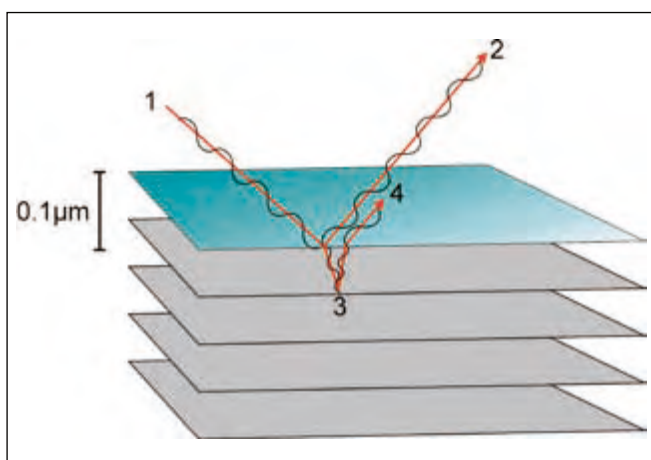


Figure 5. Principle of how iridescence forms in media, such as feldspar crystals. The reflected light beam (1–2) and the refracted beam (1–3–4) reinforce each other because their phase difference is an integral number of wavelengths. Other wavelengths present in a beam incident at this angle will interfere, resulting in the optical interference colours.

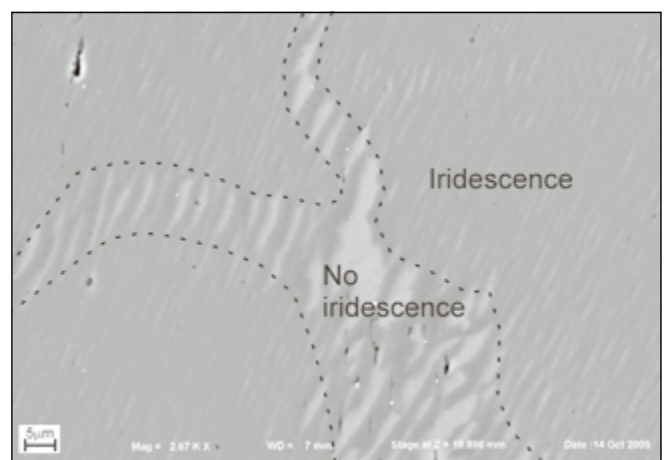


Figure 6. Scanning electron microscope photo of exsolution lamellae in larvikite. Iridescence occurs when the spacing of the lamellae is from 500 to 1000 Å (marginal parts of the photo).

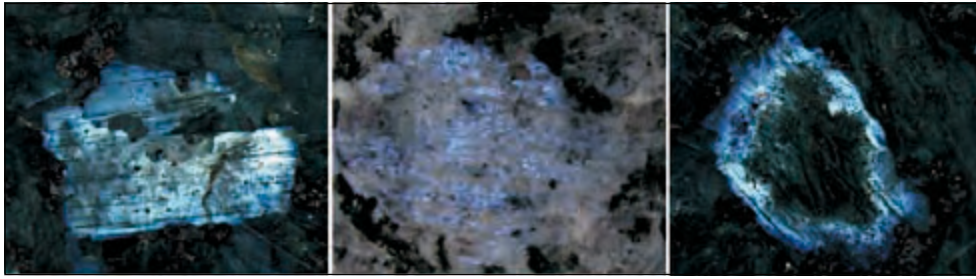


Figure 7. Types of iridescence in feldspar. Left: homogenous. Centre: patchy. Right: zoned. Each photo measures 2 cm horizontally.

ing' (sericitisation) to 'rust' (oxidation of ferrous minerals). Discolouration may be of local importance within a single quarry, or more pervasive, influencing larger bodies of larvikite. In general, all discoloured larvikite is discarded as waste rock. Similarly, dykes of basalt and romb porphyry, as well as pegmatite, make large volumes of larvikite undesirable for quarrying.

The spacing of joints and fractures determines the block size, and is thus of great importance. This feature is controlled by the physical properties of the larvikite and structures such as fault systems. In parts of the area, ductile shear zones in the larvikite similarly reduce the block potential. Moreover, modal layering and planar alignment of the feldspars ('cleavage'¹ and planes showing iridescence) are important for establishing quarrying and sawing directions of the rocks.

Methodology in the investigation of larvikite

In addressing the aspects of industrial quality as shown above, we have chosen to focus the investigations along several avenues of research. Firstly, it has been necessary to establish appropriate methods for characterising unique commercial types of larvikite in the field, without carrying out costly and time-consuming investigations such as core drilling. Polished samples of both weathered and non-weathered rocks were used as reference for evaluating the visual appearance of the iridescence colour on hand specimens (colours and intensity). The regional distribution of such types was then mapped. Secondly, the regional pattern of alteration (discolouration) was evaluated, aiming to exclude areas where such features bear a strong and penetrative impact on the quality. Thirdly, the relationship between structures (faults, fracture zones and fabric), topographic features and block-size potential was investigated. Finally, by combining these data sets, we have delineated deposits of different quality according to their market value and to their short- and long-term exploitation potential. This has, furthermore, enabled us to calculate reserves and deliver a model for management of the larvikite resources in the area.

In addition to geological mapping in the field, airborne geophysical surveys carried out in the late 1990s (Mogaard 1998, Beard 1999) proved to be of great value for the regional inter-

pretation, particularly in revealing the overall structural pattern of the larvikite complex. Digital terrain models equally proved helpful in the interpretation of fractures and joint systems.

Defining and mapping commercial larvikite types

Colour, iridescence and subtypes

For field classification of larvikite, a simple characterisation of iridescence intensity and colour (blue, light blue, silvery) proved applicable to both hand specimens and for the interpretation of commercial types of larvikite.

In addition to the iridescence, the larvikite subtypes vary in overall 'background' colour, from dark grey (almost black) to light grey, and there are also systematic variations in maximum grain size (mostly from 1 to 6 cm) and grain-size distributions. Variations may also be seen in the degree of alignment of the feldspar crystals and modal layering. Combined with the interference colours, these latter features largely define the commercial and unique subtypes of larvikite, which can be mapped in the field. Other geological aspects, such as mineral content (mode), show too small variations within the area to be of any significant help in the field survey.

In Table 1, larvikite subtypes are defined on the base of colour and texture. The most important ones are shown in Figure 8. Most of the subtypes have been given names from typical quarry areas.

Geophysical data

In addition to field surveys based on the criteria given in Table 1, airborne geophysical surveys (Mogaard 1998, Beard 1999) have proven to be of great value in the interpretation of larvikite-subtype distribution. The magnetic map (Figure 9) by far confirms the pattern of ring-shaped intrusions established by Petersen (1978a, Figure 2), although not along exactly the same lines as he proposed. In addition, the map gives us new information about faulting of the larvikites. In particular, two large faults are recognised, hereafter named the Farrisvann fault (in the east) and the Langangen fault (in the west). These two faults follow the general pattern of the Oslo Graben and the structures

¹ Cleavage is a practical term used in the stone industry describing splitting directions of rocks, generally coinciding with mineral fabric.

Table 1. Characteristics of different subtypes of larvikite.

Subtype	Iridescence intensity			Iridescence colour		Mineral orientation		Background colour			Max grain size			
	Very weak/absent	Medium	Strong	Blue	Silver/bronze + blue	Silver/bronze	Strong	Weak	Dark grey	Medium grey	Light grey	Small	Medium	Large
Kjerringvik	X	X			X		X		X		X			
Bergan		X		X			X		X			X		
Klåstad			X	X				X			X			X
Stålaker			X	X				X			X			X
Eastern Larvik		X				X		X			X			X
Larvik zone		X			X			X			X			X
Tvedal				X			X		X			X		
Bassebu-Prestskjegg		X			X		X		X		X		X	
Malerrød				X			X		X		X			X
West thin zones				X			X		X				X	
Northern zone				X			X		X				X	
North zone							X				X			X

divide the larvikite complex into three blocks, which seem to have different potential for natural stone deposits.

Although the internal structure of the larvikite complex is evident on the magnetic map, its northern borders are not clearly defined (transition to lardalite, and a circular intrusion of alkali syenite northwest of Farrisvann). However, on the thorium anomaly map (Figure 10), these two features are clearly seen, while the internal variations are more diffuse.

If we compare Petersen's (1978a) outline of the ring structures with the ones appearing on the magnetic anomaly map, there is a rough fit between the two. However, it seems that the structural complexity of the larvikite massif is higher than the simplified outline of the individual ring intrusions applied by Petersen (1978a). For example, the contact between ring IV and V in the eastern part of the area cannot be traced geochemically (Nielsen 2007). In contrast, Nielsen's geochemical profile suggests an intrusive contact slightly towards the southeast, coinciding with the anomaly pattern as seen in the easternmost part of Figure 9. To the west and northwest of Stavern, there are several thorium and magnetic anomalies that are difficult to explain from Petersen's (1978a) model, none of them actually plotting on the assumed contact of ring IV and VI. As the bedrock in the area is heavily covered by soil, it is difficult to confirm and interpret these structures in the field. However, it is likely that they represent a combination of igneous and tectonic features.

Distribution of unique larvikite types

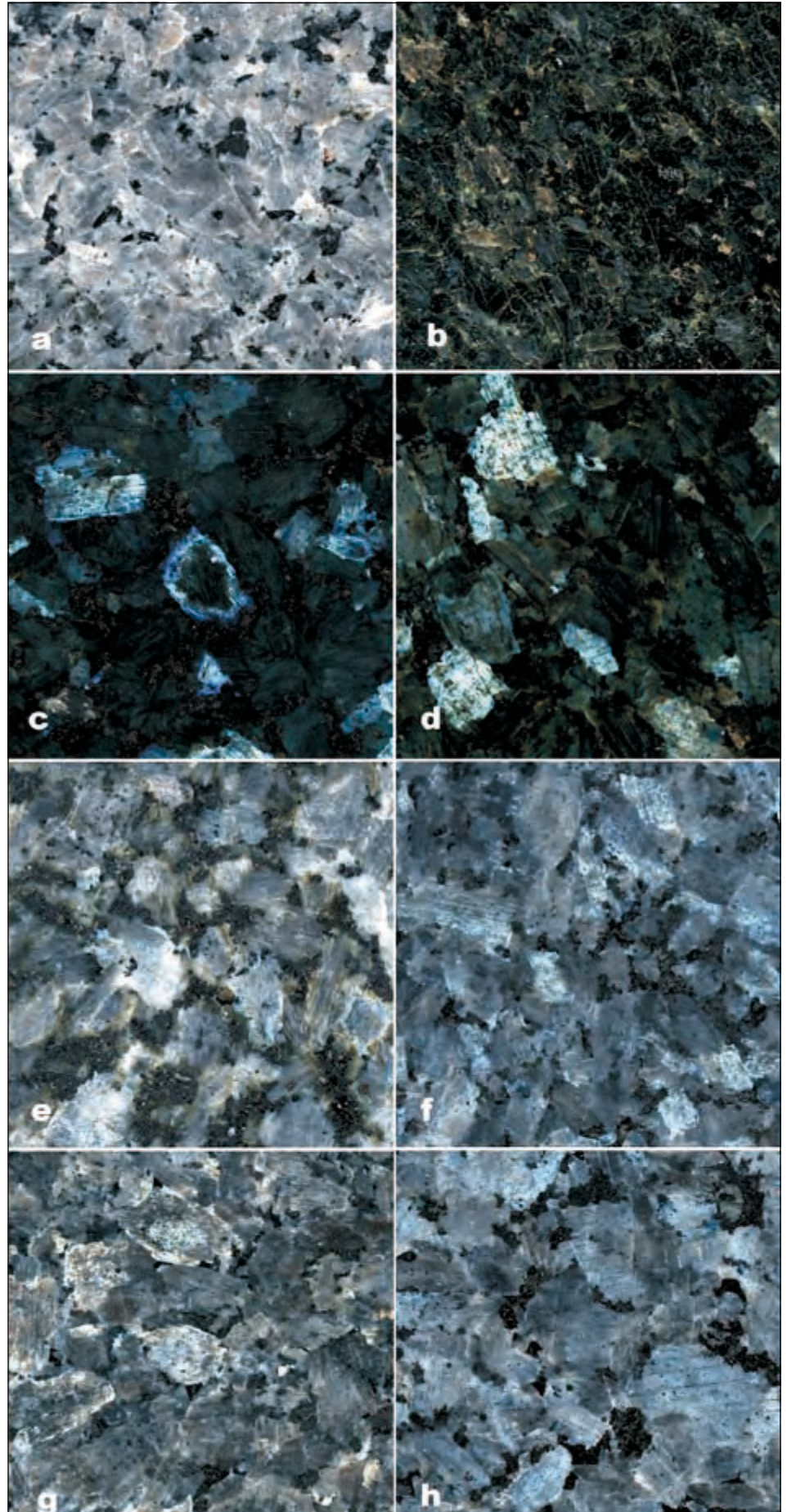
With the geophysical data in mind, mapping of larvikite subtypes was carried out. The survey confirmed that there are complex variations of larvikite, even within each subtype, particularly in the southern and eastern part of the area. Thus, the subtype map in Figure 11 (see also Table 1 and Figure 8) displays the regional variations, not taking into account the very fine-scaled differences. From east towards northwest, the subtypes can be described as follows:

The *Kjerringvik* subtype defines most of the area named ring IV by Petersen (1978a). It consists of quite homogenous, light grey larvikite with weak iridescence. In its eastern part, magmatic layering is commonly seen. There are a few abandoned quarries in this subtype, but it is considered to be of minor importance to future exploitation.

Several thin zones of dark and relatively fine-grained (most grains smaller than 1 cm) larvikite are found along the western margin of the *Kjerringvik* subtype. These are collectively named the *Bergan* subtype. Blue iridescence can be seen in the feldspars, but it is not the most distinct feature of the rock. Thus, this subtype is the only larvikite in production that predominantly is applied for non-polished workings, such as paving slabs and other outdoor uses.

The *Klåstad* subtype (also called Emerald Pearl) is one of the most attractive larvikite varieties, quarried since the 1880s. It is one of the darkest varieties of larvikite, and iridescence varies from dark blue to silver/bronze, of which the former variety is

Figure 8. Larvikite subtypes, polished slabs 7 x 7 cm. (a) Kjerringvik, (b) Bergan, (c) Klåstad strong blue (Emerald Pearl), (d) Klåstad silvery to light blue, (e) Stållaker (Marina Pearl), (f) Tvedalen (Blue Pearl), (g) Bassebu, (h) Malerød (Royal Blue).



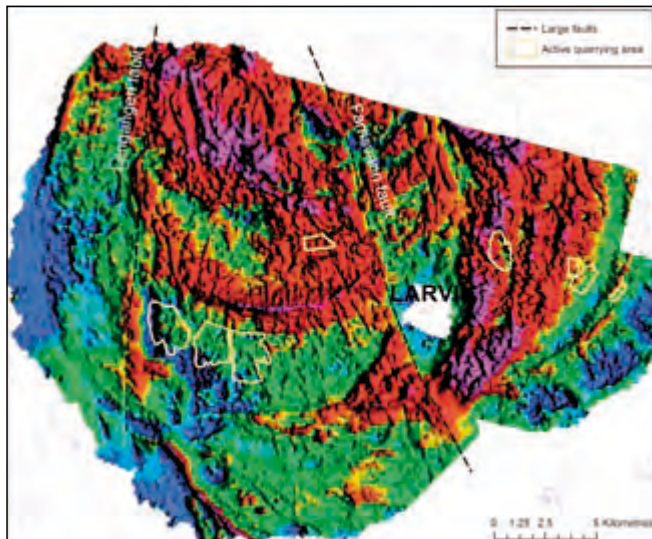


Figure 9. Magnetic anomaly map of the Larvik area, and interpretation of faults.

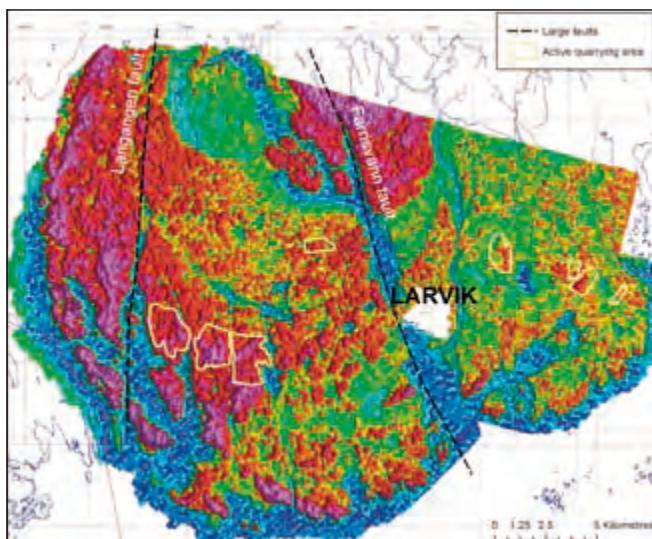


Figure 10. Thorium anomaly map of the Larvik area.

by far the most valuable. There are large, potential reserves of this subtype beneath the farmland between Larvik and Sandefjord, but so far we have little information about the quality.

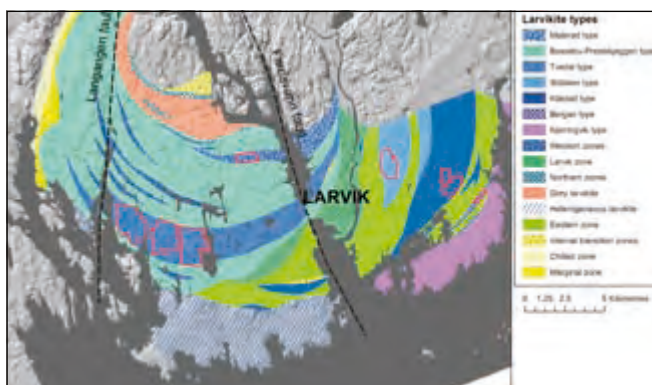


Figure 11. Distribution of unique, commercial subtypes of larvikite.

Minor occurrences, although hardly of commercial value, are found west of Larvik.

The *Stålaker* subtype is light-coloured with bluish iridescence, and has generally a higher content of mafic minerals than other light-coloured subtypes. There are a few large quarries in this subtype, marketed under the commercial name Marina Pearl. A variegated zone of non-commercial larvikite occurs in-between the former subtypes, collectively named the *Eastern Zone* on the map. A zone of *heterogenous larvikite* southwest of Larvik is also difficult to exploit on a modern industrial scale, although it was in this zone that the first quarrying was initiated in the early 1880s.

In addition to the Klåstad subtype, the light-coloured *Tvedalen* subtype (Blue Pearl), displaying strong, blue iridescence, is the best known and at present the larvikite subtype with the highest production rates. Although this subtype can be followed laterally for almost 20 km, only the present quarry areas in Tvedalen and at Auen have proven to contain homogeneous quality in sufficiently large volumes to secure long-term sustainable production. The areas just south of and north of Tvedalen are dominated by light-coloured larvikite with slightly weaker and more silvery iridescence, named the *Bassebu–Prestskjeggen* subtype, of which there might be a future potential for exploitation. Some narrow zones contain larvikite with a stronger bluish iridescence, similar to the Tvedalen type (*Western zones*).

The *Malerød* subtype (commercial name Royal Blue) was introduced commercially as late as in the 1970s, and the area has subsequently become an important production site. It is coarser grained than other light-coloured larvikite types and displays bright blue iridescence. The subtype can be followed both to the east and west of the present production area, and even east of Farrisvann. However, in the latter area, the rocks are more intensively fractured than on the western side, and thus less likely to represent an important resource.

In the far north of the area, most of the outcrops consist of grey larvikite with very weak to non-iridescent feldspar, and thus hardly of any commercial interest. A few narrow bands (*Northern zones*) of dark grey larvikite with strong, dark blue iridescence may represent an exception, but it is uncertain whether these bands are too narrow and too altered for economical production.

A marginal zone and a chilled zone occur along the eastern and northern margins of the larvikite complex, both of no commercial interest. Minor occurrences of similar chilled margins (as described by Petersen 1978a) are also found elsewhere within the complex.

Geological features and their impact on quality

Discolouration

Discolouration of larvikite due to alteration of the minerals is one of the key problems in the quality of the deposits. Not only

does discolouration influence the overall colour of the larvikite, but also, and more importantly, effaces the iridescence. The type of alteration that bears most impact on the larvikite quality is 'bleaching' of the feldspar, either locally along cracks (Figure 12) or more penetratively (Figure 13) forming aggregates of different secondary minerals (e.g., zeolites, albite, sericite, analcite, sodalite). Where the alteration is penetrative, the discolouration starts at grain boundaries and continues into the feldspar grains along the mineral cleavage (Figures 13 and 14). Blocks containing bleached larvikite are at best much lower priced than unaltered ones. Although alteration is a common phenomenon in practically all the quarries in the area, and thus contributes to the high waste ratio, it is much more severe and penetrative to the west of the Langangen fault than elsewhere. Therefore, we consider the whole area between the Langangen fjord and the western margin of the larvikite complex to be of no interest for future larvikite exploitation.

Oxidation of larvikite causes development of rusty brown discolouration along joints and fractures. It is a common phenomenon, but predominantly occurs along the major fracture zones. Since such highly fractured areas are of little interest for exploitation anyway, this type of discolouration has minor practical impact on larvikite extraction.

Joints, fractures and physical properties

In the early history of larvikite quarrying, the occurrence of parallel joints was considered useful—unless the spacing was too small—in facilitating extraction by reducing the need for drilling and blasting. In modern quarrying, however, the sizes of blocks are much larger than in the past, and most of the quarrying is aided by diamond-wire sawing. Thus, the rocks should ideally be as massive as possible. Throughout the years of production, we see clearly how the production areas have moved towards more and more massive larvikite.

The map in Figure 15 presents the regional pattern of fracturing and faulting in the area, based on a lineament analysis of the terrain features. In addition to the two large faults and related structures we see numerous smaller ones, generally having N–S to NW–SE orientation, coinciding with the general fracture pattern in the Oslo Rift. Other strong lineaments follow the planar alignment of the feldspar in the larvikite, and some of these provided the topographic features for Petersen (1978a) in his interpretation of the ring structures. Such features may indeed follow intrusive contacts (Petersen 1978a), but since they are aligned with the main plane of weakness in larvikite there might also be other explanations. Yet another set of fractures appears to be related to the igneous structure of the larvikite. Joints perpendicular to the mineral orientation may represent cooling structures and, in some cases, these are associated with fine-grained larvikite dykes. The magnetic map clearly shows the radiating nature of such structures in and around the Tvedalen area.

The major fracture systems have shaped the topography of the area; the large valleys follow the first-order structures such

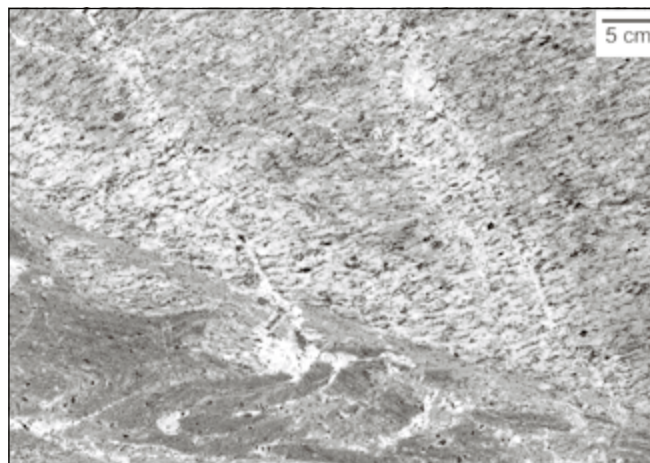


Figure 12. Shear zone along dyke in larvikite, overprinted by fracture-bound alteration (bleaching).

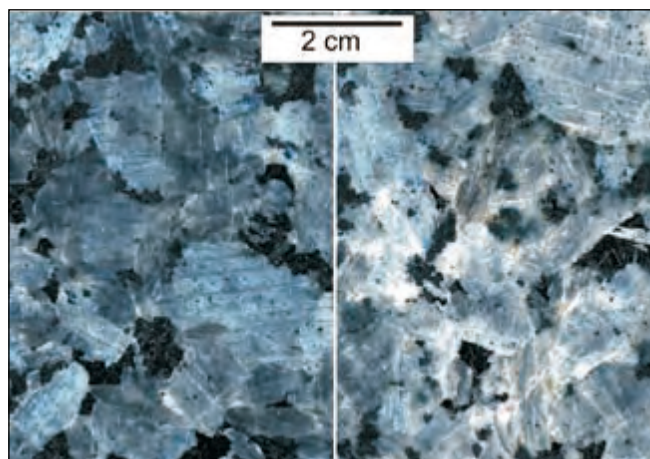


Figure 13. Bleaching of larvikite and impact on aesthetic quality. Unaltered larvikite of the Malerød subtype (left) and altered (right).

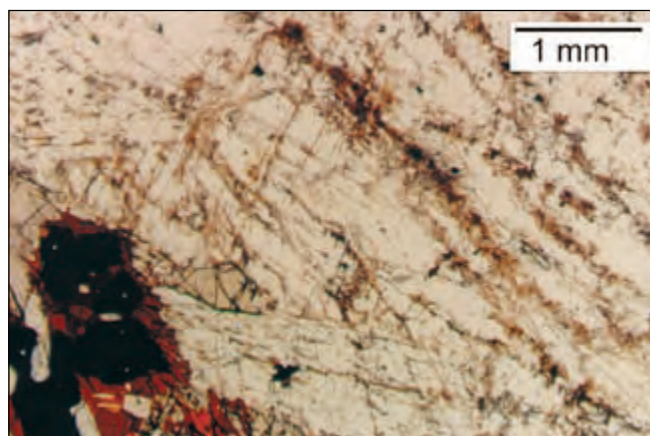


Figure 14. Alteration (brown) in thin section along cleavage planes (plane polarised light).

as the N–S to NW–SE faults and the ring structures (Figure 16). Second-order structures, such as the conjugate NE–SW-trending fractures associated with N–S-trending faults, tend to control the location of smaller valleys. On a more local scale, the pattern is even more complex; each block bordered by first-

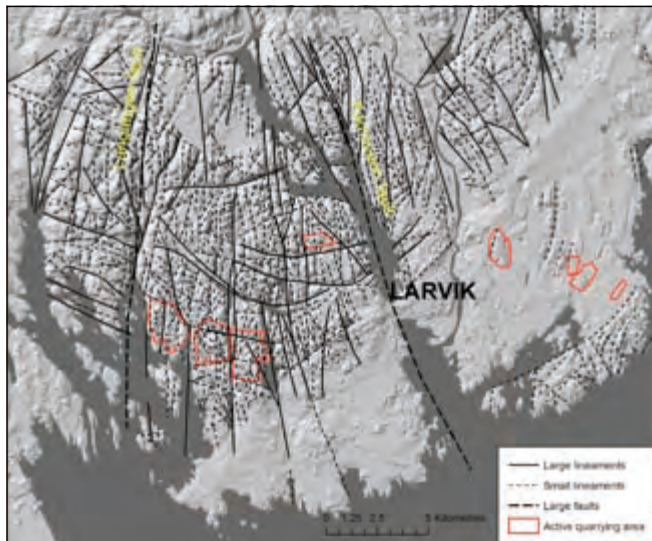


Figure 15. Lineament analysis of the larvikite area.

and/or second-order fractures may have its unique system of third- and fourth-order fractures differing from the neighbouring block. Partially, this seems to be related to a complex stress distribution in the larvikite that can vary from one hill to the next. Consequently, even within a small area, fracture and stress systems vary significantly from quarry to quarry. Not surprisingly, there is a general correlation between topography and fracturing—the topographic highs being composed of the most massive and least fractured larvikite. So, in most cases, we find the best deposits of larvikite on hills. However, even in the least fractured larvikite deposits other problems may be present, such as ‘open cleavage’, a term used by the quarrymen in Tvedalen. Open cleavage is most commonly seen on hilltops of massive, Tvedalen-type larvikite, and appears as subvertical, clay-coated fractures along the mineral orientation planes. Commonly, it only occurs in 5–15 m-wide zones below the terrain surface. The most likely interpretation of the open cleavage is that it is caused by erosional stress release. This also explains why it is mainly

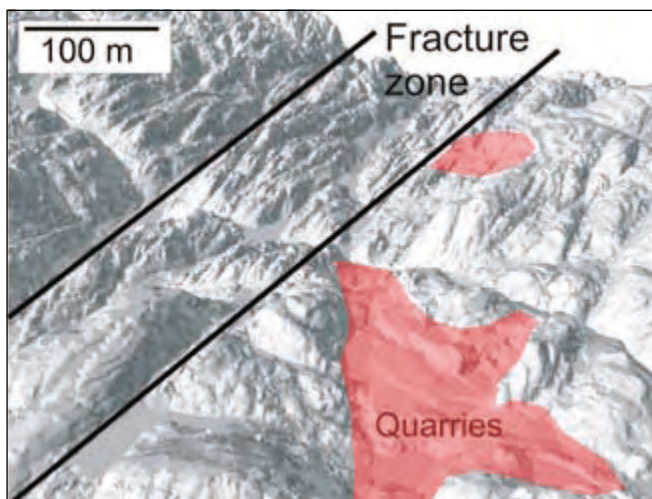


Figure 16. Digital terrain model of the topography in parts of the Tvedalen quarry area, displaying quarries located in a massive part of larvikite beside a large fracture zone.

found in the relatively massive parts of the larvikite, where the lack of abundant pre-existing fractures makes the stress release take place along other planes of weakness, i.e., mineral alignment planes.

Dykes, pegmatites and shear zones

Dykes of different composition are found in most parts of the larvikite complex and are dominantly oriented between NE–SW and NW–SE. Most common are fine-grained larvikitic dykes. The dykes are generally a minor problem in the quarrying, except from a few areas where they are particularly abundant.

Pegmatites have a more severe impact on the larvikite quality. In particular, irregular bodies of pegmatite are difficult to predict and may cause serious problems for the quarrying not only due to their presence, but also due to the commonly associated alteration and discolouration (see above). Although pegmatites are found in all of the quarry areas, they are particularly common along the margin of the complex and especially in its western part, i.e., to the west and south of Langangen. The high density of pegmatites is reflected on the thorium anomaly map since pegmatites (Ihlen et al. 2006) and nepheline syenite intrusions (Dahlgren, unpublished data) appear to be more strongly enriched in thorium than the other rocks in the larvikite massif. This area is the type locality of thorium, and the mineral thorite, and the confinement of this element/mineral to the pegmatites was established early on by Berzelius (1829) and Brøgger (1890).

Closely associated with pegmatites and nepheline syenite dykes are ductile shear zones, formed more or less contemporaneously during a late stage of the magmatic evolution (Figure 17). Locally, protomylonitic zones, several metres in thickness, are developed.

Magmatic layering and mineral orientation

Magmatic modal layering is not a common aspect of the larvikites, but is abundantly observed in some parts of the area (Figure

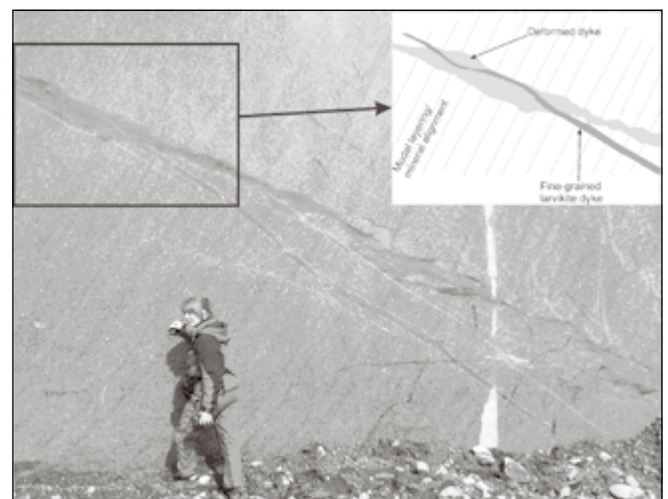


Figure 17. Larvikite dyke cutting shear zone at Malerød. Note mineral alignment and diffuse modal layering (concentration of mafic minerals) in the larvikite.

18). Since the presence of such layering by definition makes the rock inhomogenous, quarrying in such zones is generally avoided, except for the southern part of the Stålaker quarry area. The planar alignment of the feldspar is a more widespread feature of the larvikites, and of great importance in quarrying. The alignment plane represents both the primary splitting direction of the larvikite ('primary cleavage' or 'rift'²) and the plane along which the blocks should be cut in order to maximise the visible iridescence on finished slabs. Its strike follows the ring structures, and the dip varies from about 40° N to vertical. In certain areas where both modal layering and planar alignment can be seen, they are subparallel or slightly oblique to each other (Figure 19).

The importance of the planar alignment of feldspar may be illustrated with two examples. In the Klåstad area (Emerald Pearl variety), the average alignment plane dips 45° NW, but is quite diffuse with a wide scatter of orientations of the individual feldspar crystals, deviating up to 45° from the average. Thus, the blocks can be cut both vertically and horizontally without 'loosing' the iridescence completely. The possibility of varying cutting directions in such a way is favourable from the technical side of quarrying in the area.

In the Blue Pearl quarries in Tvedalen, the alignment of the feldspar is more strongly developed. Therefore, sawing cuts for slabs must be along this plane for the iridescence to be visible at all. The orientation of the plane is much steeper than at Klåstad (80–90° N). Therefore, it is more viable to follow this plane strictly in the quarrying, although the waste ratio becomes somewhat higher.

The examples above illustrate that even minor changes in the orientation and the nature of the preferred mineral orientation may have significant impact on the quarrying techniques and, thus, the economy of the quarries.



Figure 18. Modal graded layering and erosional contact in larvikite.

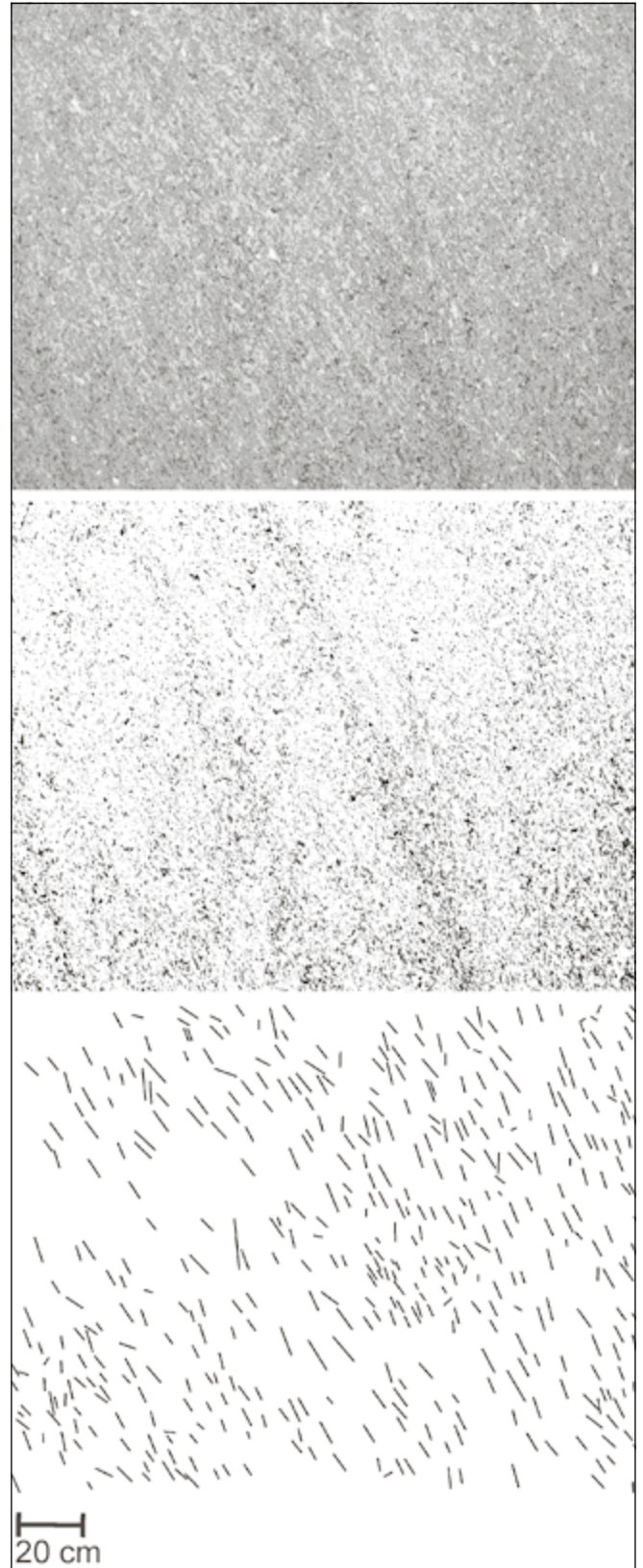


Figure 19 Mineral alignment and modal layering relations. Top: photo of quarry face at Malerød. Middle: distribution of mafic minerals in the same section, displaying diffuse, model layering. Bottom: feldspar orientation in the same section, being parallel to slightly oblique to the modal layering.

² Both terms are used by the stone industry to describe the best direction of splitting in rocks.

Synthesis: larvikite deposits in the short and long term

Towards a larvikite exploration model

The future well being of the larvikite industry depends on several factors, as illustrated in Figure 20. Most important is the international market. In particular, it is crucial to maintain a high price level to compensate for high production costs. This depends on the competition between the production companies and the aesthetic quality of the commercial blocks. The second issue relates to production techniques and strategies, efficient quarrying technology, waste handling and use (environmental aspects) and resource management (legal aspects). It is vital for the industry to continue to invest in state-of-the-art technology for improving block yield and reducing costs, and simultaneously meet more and more strict demands for environmentally friendly development.

The third issue, which is the subject of this paper, is the geological aspects—to secure that future production takes place where the geological conditions are most favourable. Based on the various features discussed above, these conditions can be summarised in an exploration model specifically applicable to the larvikite deposits (Figure 21). As shown in this figure, the first important question is the market value, in other words, whether the colour and structure of a certain subtype of larvikite meet the strict demands in the present-day market. Conversely, in cases where new commercial types are discovered, it is sometimes possible to adapt the market to the new material.

If the answer is ‘yes’ to the first question (Figure 21), there is a set of highly important geological factors that should be carefully evaluated, as described above. Clearly, the spacing and density of fractures and joints are important, as they are for all types of dimension-stone deposits. More specific to larvikite are the

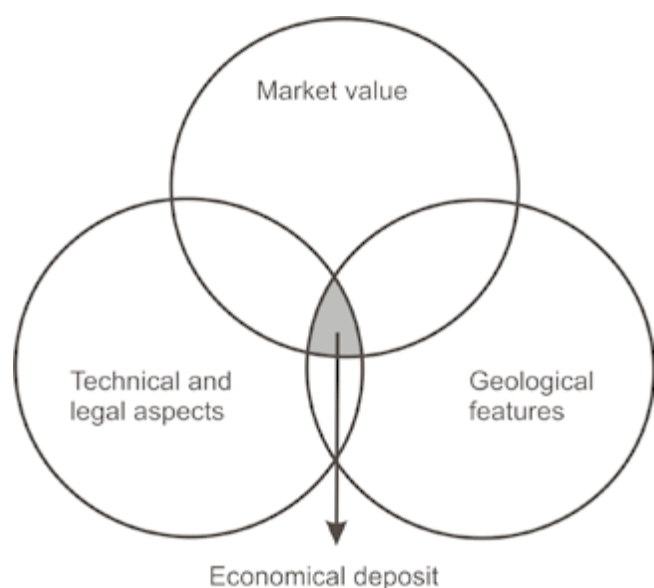


Figure 20. Aspects of economic evaluation of larvikite as dimension stone.

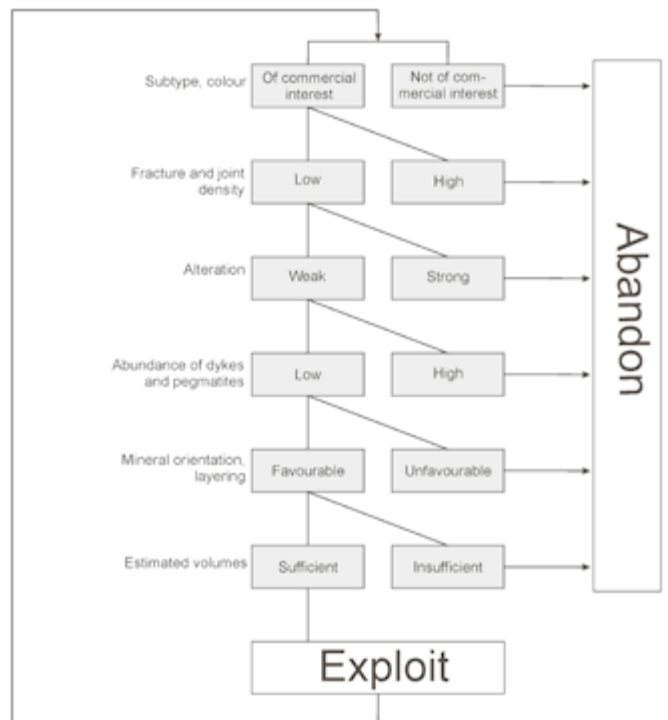


Figure 21. Exploration model for larvikite deposits.

problems of alteration/bleaching and the occurrence of dykes, pegmatites and shear zones, as well as the nature and orientation of the mineral orientation plane. If these aspects turn out in favour of production and there is sufficient volume in the deposit, quarrying may be initiated. However, it is extremely difficult to predict the exact production costs and block yield accurately. A relative change of one percent in waste ratio may mean the difference between failure and success, and in many cases it is impossible to obtain such figures without full-scale quarrying operations. Therefore, regular evaluation of the aspects mentioned above is of vital importance. If, for instance, the discolouration in some parts of a quarry is critically high, it may be necessary to abandon that part before losing too much money.

Addressing future reserves

The area around Larvik is experiencing rapid population growth and expansion of industry, tourism and infrastructure. Furthermore, since basically the whole area consists of larvikite bedrock, it is impossible to preserve all larvikite with iridescence for future exploitation without getting into conflict with other land-use interests in the region. This conflict between resources and infrastructure has caused a need for delineating the most important deposits in the area that can realistically be preserved for the future. By combining the field observations we have of larvikite types, colour, fracturing, alteration and morphology, we have delineated what we believe are the most important resources for exploitation in the future. In doing so, we have not only evaluated the larvikite types that are commercially interesting at the present time, but also included some subtypes which may represent an additional future reserve given

a positive development of the market situation for larvikite. In Figure 22, the assumed exploitable resources of larvikite are shown, characterised according to short- or long-term reserves and importance; the latter concerns a combination of subtype and commercial value (colour) balanced against the occurrence of pegmatites, alteration and other quality-reducing features. The most important category is known reserves of commercial subtypes in production within or in the vicinity of active quarry areas, whilst the least important is exploitable deposits of larvikite with weak iridescence and thus unlikely to be put into production. The map in Figure 22 forms the basis for future management of the larvikite deposits.

While looking into the crystal ball, it is also interesting to make some estimates of remaining reserves of different types of larvikite. In Figure 23, we have made estimates of known, probable and speculative reserves of different varieties³. The calculations are based on the assumption of 2.5% (pessimistic) and 5% (optimistic) average block yield and quarrying depth down to 30 m below the topographic surface. Not surprisingly, the known reserves of the Tvedalen type are the largest in volume, i.e., between 7.5 and 15 million m³. If the annual production continues as it is now (40–50,000 m³ a year), this will mean reserves for somewhere between 160 and 330 years. Similarly, the known reserves for the Klåstad type (Emerald Pearl) are between 30 and 60 years, which is not much thinking in long terms. However, there may be large potential reserves further north, beneath the farmland. Since we do not know the quality of the larvikite in most of these areas due to the soil cover, more detailed investigation of the subsurface quality should be carried out not too far into the future, and hopefully contribute to a substantial increase of known reserves.

Although such reserve estimates are uncertain, they give us an idea of the lifetime of the different deposit types, and especially where one has to put efforts to secure future extraction of unique larvikite types. Furthermore, they point at some potential new deposits that can provide an addition to the larvikite palette in some more distant future, if the market situation permits. The estimates contribute to a generally raised awareness of the importance of the larvikite resources, and last but not least, the survey underlines the responsibility for building a good management regime for a national resource of global significance.

Concluding remarks

The investigation of the dimension-stone potential of larvikite has revealed new information about important geological features controlling the commercial value of the stone and the connections between them. In particular, the role of tectono-magmatic processes in the formation of the larvikites seems to

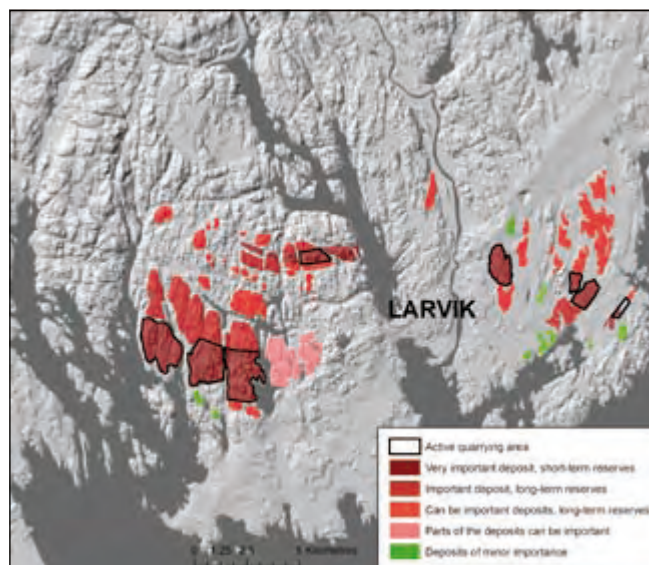


Figure 22. Distribution of larvikite deposits after their economic potential in the short and long term.

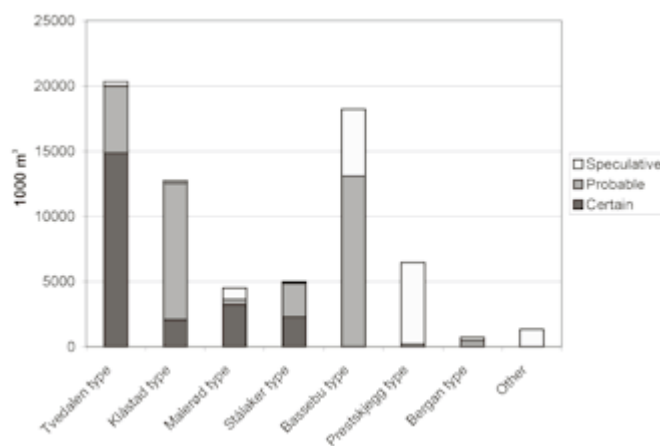


Figure 23. Reserve estimates of larvikite subtypes, in 1000 m³ (net reserves, after subtracting estimated 95% waste).

be crucial. The investigation started with obtaining an overview of the regional distribution pattern of larvikite, continued with combining these data sets with the most important structural and magmatic features that have high impact on the quality, and ended up with a distribution of deposits with potential economic importance in the short and long term. The investigation has also uncovered some new questions regarding the mechanisms behind the formation and emplacement of the larvikite complex. The contact relations between larvikite intrusions are more complex than previously assumed, and the contacts do not strictly follow the ring structures as described by Petersen (1978a). Another crucial issue is the overall structural pattern of the larvikite complex and the implications for modelling its formation. The overall relations between igneous layering, mineral orientation and syn-magmatic deformation still remain open.

³ Larvikite subtypes or deposit areas not in production are classified as probable or speculative.

Clearly, although the larvikite complex has been the subject of research for more than 100 years, many unsolved scientific problems still remain.

Acknowledgements

The present paper is the result of several projects concerning investigations of larvikite resources over the last decade. Special thanks to Håvard Gautneb, NGU, for participation in the survey of the larvikites. Many other people are thanked for contributing with their knowledge in different ways: Reid Kvien for kindly letting us borrow his collection of polished samples of larvikite, Bjørn Willemoes-Wissing for SEM work, Christian Tegner (previous colleague at NGU) for hard work in the field, and finally, the larvikite companies for their hospitality. Peter Ihlen and an anonymous reviewer are thanked for constructive comments. The work has received funding from several sources: NGU, the counties of Buskerud, Telemark and Vestfold, Larvik municipality, Statens Vegvesen and the larvikite industry.

References

- Barth, T.F.W. (1945) Studies on the Igneous Rock Complex of the Oslo Region II. Systematic petrography of the plutonic rocks. *Det Norske Videnskaps-Akademi i Oslo, Skrifter. I. Mat.-Naturv. Klasse*, **9**, 104 pp.
- Beard, L.P. (1999) Data acquisition and processing – Helicopter geophysical surveys, Larvik, 1998. *NGU Report 1999.026*, 13 pp.
- Berzelius, J. (1829) Undersökning af et nytt mineral som innehåller en förut obekant jord. *Kongliga Svenska Vetenskaps-Akademiens Handlingar*, 1829, pp. 1–30.
- Brøgger, W. (1890) Die Mineralien der Syenitpegmatitgänge der Süd-norwegischen Augit- und Nephelinsyenite. *Zeitschrift für Kristallographie und Mineralogie*, **16**, I–XVIII + 1–235 (Allgemeiner Theil), 1–663 (Spezieller Theil).
- Dahlgren, S., Corfu, F. and Heaman, L. (1998) Datering av plutoner og pegmatitter i Larvik pluton-kompleks, sydlige Oslo Graben, ved hjelp av U–Pb isotoper i zirkon og baddeleyitt. Kongsberg mineralsymposium 1998, *Norsk Bergverksmuseum Skrift*, **14**, 32–39.
- Dons, J.A. (1978) Terminology and history of investigations. In Dons, J.A. and Larsen, B.T. (eds.) *The Oslo Paleorift. A review and guide to excursions*, Geological Survey of Norway Bulletin, **45**, pp. 9–16.
- Heldal, T. (2008) Norges nye nasjonalbergart: Nasjonalhelt og verdensborger. *GEO*, **02/08**, 10–12.
- Heldal, T., Kjølle, I., Beard, L., Tegner, C. and Lynum, R. (1999) Kartlegging av larvikitt mellom Sandefjord og Porsgrunn. *NGU Report 1999.059*, 68 pp.
- Ihlen, P.M., Raaness, A., Korneliussen, A., Skår, Ø., Müller, A. and Meyer, G. (2006) Rekognoserende undersøkelser av et utvalg potensielle mineralressurser i Fritzøe Skoger. *NGU Report 2006.030*, 19 pp.
- Kjølle, I., Heldal, T. and Gautneb, H. (2003) Forekomster av larvikitt – ressurskart. *NGU Report 2003.066*, 9 pp.
- Larsen, B.T. and Olaussen, S. (2005) *The Oslo Region. A study in classical Palaeozoic geology*. Field guide to NGF's Centennial field trip, May 26–28, 2005, 88 pp.
- Mogaard, J.O. (1998) Geofysiske målinger fra helikopter ved Larvik, Vestfold, teknisk rapport. *NGU Report 1998.021*, 11 pp.
- Muir, I.D. and Smith, J.V. Jr. (1956) Crystallization of feldspars in larvikites. *Zeitschrift für Kristallographie*, **107**, 182–195.
- Neumann, E.R. (1978a) Petrogenesis of the Larvik ring-complex in the Permian Oslo Rift, Norway. In Neumann, E.R. and Ramberg, I.B. (eds.) *Petrology and Geochemistry of Continental Rifts*, D. Reidel Publ.Comp., Dordrecht, pp. 231–236.
- Neumann, E.R. (1978b) Petrology of the plutonic rocks. In Dons, J.A. and Larsen, B.T. (eds.) *The Oslo Paleorift. A review and guide to excursions*. Geological Survey of Norway Bulletin, **45**, 25–34.
- Neumann, E.R. (1980) Petrogenesis of the Oslo Region larvikites and associated rocks. *Journal of Petrology*, **21**, 499–531.
- Neumann, E.R., Brunfelt A.O. and Finstad, K.G. (1977) Rare earth elements in some igneous rocks in the Oslo rift, Norway. *Lithos*, **10**, 311–319.
- Neumann, E.R., Tilton, G.R. and Tuen, E. (1988) Sr, Nd and Pb isotope geochemistry of the Oslo rift igneous province, southeast Norway. *Geochimica et Cosmochimica Acta*, **52**, 1997–2007.
- Nielsen, A.M. (2007) *En petrologisk og geokemisk undersøgelse af ringintrusionerne IV og V i larvikitkomplekset Norge*. M.Sc. thesis. Department of Earth Sciences, University of Aarhus, Denmark, 111 pp.
- Oftedahl, C. (1948) Studies on the igneous rock complex of the Oslo Region. IX. The feldspars. *Det Norske Videnskaps-Akademi i Oslo, Skrifter. I. Mat.-Naturv. Klasse*, **3**, 71 pp.
- Oftedahl, C. and Petersen, J.S. (1978) Southern part of the Oslo Rift. In Dons, J.A. and Larsen, B.T. (eds.) *The Oslo Paleorift. A review and guide to excursions*. Geological Survey of Norway Bulletin, **45**, 163–182.
- Oxaal, J. (1916) Norsk Granitt. *Norges geologiske undersøkelse*, **76**, 220 pp.
- Petersen, J.S. (1978a) Structure of the larvikite-lardalite complex, Oslo Region, Norway, and its evolution. *Geologische Rundschau*, **67**, 330–342.
- Petersen, J.S. (1978b) Composite plutonic ring complexes: a structural characteristic and rift zone plutonism. In Neumann, E.R. and Ramberg, I.B. (eds.) *Petrology and Geochemistry of Continental Rifts*, D. Reidel Publ.Comp., Dordrecht, 217–229.
- Ribbe, P.H. (1975) Exsolution textures and interference colors in feldspars. In Ribbe, P.H. (ed.) *Feldspar Mineralogy*, *Mineralogical Society of America, short course notes*, **2**, R-73–R-96.
- Rosenqvist, I.T. (1965) Electron-microscope investigations of larvikite and tonsbergite feldspars. *Norsk geologisk tidsskrift*, **45**, 69–71.
- Smith, J.V. and Muir, I.D. (1958) The reaction sequence in larvikite feldspars. *Zeitschrift für Kristallographie*, **110**, 11–20.

Geology of the soapstone deposits of the Linnajavri area, Hamarøy, Nordland, north Norwegian Caledonides — Norway's largest reserves of soapstone

Ingvar Lindahl and Lars Petter Nilsson

*Geological Survey of Norway (NGU), 7491 Trondheim, Norway
E-mail: ingvar.lindahl@ngu.no*

The Linnajavri area, subdivided in Linnajavri northern and southern area, is located in Hamarøy municipality, Nordland county, northern Norway. During five short field seasons (1–3 weeks) from 2001 to 2006, the ultramafic bodies of the Linnajavri area have been outlined and the soapstone alteration studied in detail for evaluation of its possible potential for exploitation. The Linnajavri area is built up of Caledonian nappes thrust over Precambrian granitic basement exposed to the west of the nappe pile. Our work has focused on rocks of the Seve and Köli nappes of the Upper Allochthon. Within the Köli rocks, a number of tectonic *mélange* zones have taken up the stress built up between blocks of rock, especially in the area with ultramafic bodies, thereby preserving primary depositional structures and evidence of alteration processes in the rocks between the *mélange* zones. The ultramafic bodies, gabbros and pillow lavas are interpreted to represent ophiolite fragments. In their present setting, they are associated with conglomeratic weathering products of the ophiolites. The ultramafic rocks are dunite, peridotite and, to a subordinate degree, pyroxenite. All the ultramafic rocks are strongly serpentinised and to an extensive degree also further altered to soapstone. Listwaenite, the end product in this alteration chain, is also encountered in the Linnajavri southern area. Only one of the ultramafic bodies shows cumulate banding, probably originating from the lower, layered part of oceanic crust. Alteration of the ophiolite fragments took place at an early, probably oceanic stage, with development of serpentinite, soapstone and listwaenite. Flushing of CO₂ followed joints and brecciated zones in the ultramafic bodies. Introduction of CO₂ was focused in certain areas, most extensively in the Kleberflåget ultramafic body, producing the largest volumes of soapstone. At Kleberflåget, the CO₂ flushing continued with falling temperatures ultimately leading to breakdown of soapstone to listwaenite. The ophiolite and its alteration products were obducted and exposed for weathering processes with formation of conglomerates; e.g., serpentine conglomerates locally with soapstone pebbles, green mafic conglomerates and conglomerates with mica-schist matrix. The soapstones of the Linnajavri area represent large resources for use as dimension stone. The soapstones also represent potential resources for talc flotation. The size of the mapped reserves as well as possible additional geologically indicated resources, and the potential for exploitation over decades, implies that a thorough study of talc flotation should be undertaken.

Lindahl, I. and Nilsson, L.P. (2008) Geology of the soapstone deposits of the Linnajavri area, Hamarøy, Nordland, north Norwegian Caledonides—Norway's largest reserves of soapstone. In Slagstad, T. (ed.) *Geology for Society*, Geological Survey of Norway Special Publication, **11**, pp. 19–35.

Introduction

Our first visit to the Linnajavri¹ area (Figure 1) was a once-in-a-life-time experience for two economic geologists. During the reconnaissance trip in September 2000, very large ultramafic-hosted soapstone deposits were partly discovered for the first time, and partly rediscovered, by the authors. The trip, aimed at getting a quick overview of the soapstone potential of the area, was initiated by the authors based on the fact that there were relatively large ultramafic and mafic bodies in the area, but rather limited geological information about these bodies (Foslie 1936, 1942, Brattli and Prestvik 1985, 1987a, b). During our three-day visit to the area we discovered extensive soapstone formation both within and along the border of the Gaskavárri serpentinite ridge as well as its neighbouring body to the northwest, the Njaskasvárri 833 lens (see Figure 2). We also recognised the strong talcification of the northwest end of the Kvitfjell ultramafic lens, earlier shortly described by Foslie (1942, p. 75). On our visit to the Ridoalggičohkka ridge we discovered an overwhelmingly extensive talcification that has affected both limbs of the roughly sheet-formed 2 x 4 km ultramafic body that makes up a part of the open, shallow Ridoalggičohkka synform. The amount of soapstone we discovered, or rediscovered, during this first three-day field trip was so enormously large, at least in our eyes, and the talc content of the soapstone so high, that our findings naturally prompted us to suggest a joint collaboration project set up between landowner Statskog (State Land and Forest Managing Organization) and NGU on investigation of the soapstone deposits.

The *Linnajavri area* in this context is the area just to the north, east and southeast of lake Linnajavri and up to the Swedish border in Hamarøy municipality in Nordland county (Figure 1). Geographically, the Linnajavri area is subdivided in



Figure 1. Location map of the Linnajavri area.

the Linnajavri northern and southern area. A number of new location names are introduced in our reports, due to the scarcity of names on the 1:50,000-scale topographic map. The distance from the central part of the area to the deep-water harbour at Leirfjord is ca. 35 km, with 26 km of existing road, and 6–12 km with no road. The area is mountainous and not forested. The elevation varies between 600 and 1200 m. No signs of previous use or exploitation of the soapstone have been recognised. Parts of the deposit area may in the future be subjected to special environmental regulations.

The results from five short field seasons (1–3 weeks each) from 2001–2006 are presented here. The focus of the work in the area has mainly been to map and systematically sample the resources of soapstone and just one season for mapping the geology of the area (Lindahl and Nilsson 2001, 2002, 2005a, b, c, 2006a, b, Nilsson and Lindahl 2003a, b, Nilsson et al. 2003, Skilbrei et al. 2003, Nilsson 2004, Lindahl et al. 2005, 2006). A topographic map of the Linnajavri area in 1:5,000 scale, based on aerial photographs, has been constructed, and a geological map in ca. 1:50,000 scale is presented in Figure 2 (modified after the 1:15,000-scale map by Lindahl and Nilsson 2006b). Chain saw for sampling of the soapstone has been used extensively. The present paper is meant to give a brief overview of the soapstone deposits, their geology and mineralogy, and a contribution to the geological history of the Linnajavri area.

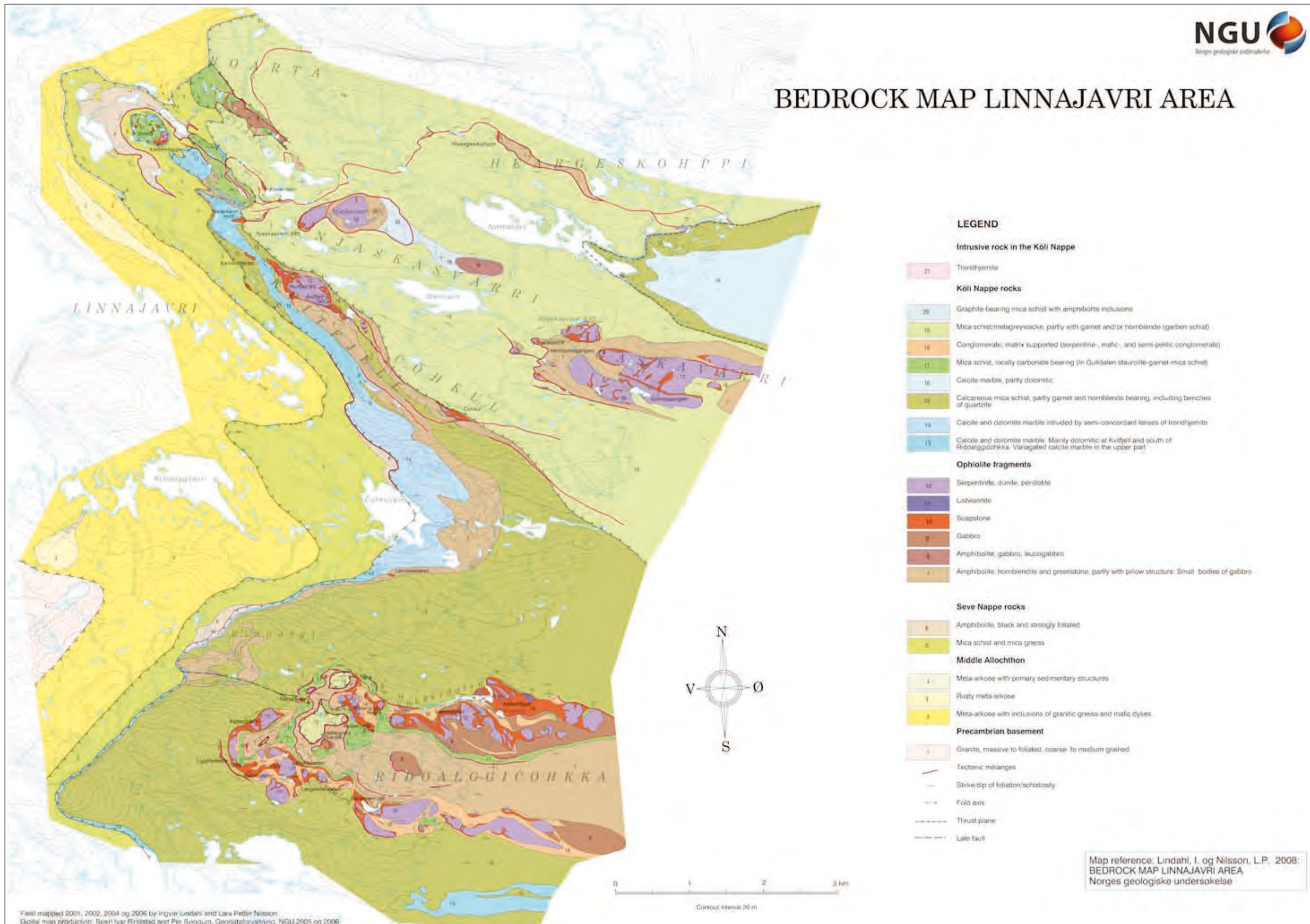
Previous work

On the Norwegian side of the border, only granite was recorded in the Linnajavri area on the maps up to 1916. Gunnar Holmsen visited the area in 1916 and was the first Norwegian geologist who registered Caledonian rocks in the area (Holmsen 1917). He also registered the ultramafic rocks at Kvitfjell and Gaskavárri in the Linnajavri northern area. However, no observations of soapstone were recorded.

NGU geologist Steinar Foslie mapped the Linnajavri area during the summer of 1929 in 1:100,000 scale (Foslie 1929, 1936, 1942). Foslie's mapping gave a relatively correct picture of the geology (lithology) of the area. He recognised the major ultramafic bodies and even described serpentinite and briefly mentioned soapstone alteration at various ultramafic bodies. Foslie did not regard the soapstone as a potential economic resource, neither for talc, nor as dimension stone. Therefore, very little information about soapstone is found in his map-sheet description. He concluded that "*No ore and mineral deposits of any importance are known within the map area*" (Foslie 1942, p. 119). However, Foslie's field diary has additional, scattered information of significant value for our investigations.

¹ Our spelling of *Linnajavri* does not follow the spelling on the latest edition of the topographic map from the Norwegian Mapping Authority (Statens Kartverk), in scale 1:50,000, where the name is spelled *Linjávri*. The spelling *Linnajavri* is, however, already introduced in NGU databases, web presentations and NGU reports. For consistency, we have, therefore, kept this spelling. All other geographical names are spelled according to the recommendations from the Norwegian Mapping Authority.

BEDROCK MAP LINNAJAVRI AREA



LEGEND

Intrusive rock in the Kõll Nappe

21 Trondhjemite

Kõll Nappe rocks

- 20 Graphite-bearing mica schist with amphibolite inclusions
- 19 Mica schist/metagreywacke, partly with garnet and/or hornblende (garnet schist)
- 18 Conglomerate, matrix supported (serpentine-, mafic-, and semi-pelitic conglomerate)
- 17 Mica schist, locally carbonate bearing (in Gulidalen staurolite-garnet-mica schist)
- 16 Calcite marble, partly dolomitic
- 15 Calcareous mica schist, partly garnet and hornblende bearing, including benches of quartzite
- 14 Calcite and dolomite marble intruded by semi-concordant lenses of trondhjemite
- 13 Calcite and dolomite marble. Mainly dolomitic at Kvittfjell and south of Ridoalggicohkka. Variegated calcite marble in the upper part

Ophiolite fragments

- 12 Serpentine, dunite, peridotite
- 11 Listwaenite
- 10 Soapstone
- 9 Gabbro
- 8 Amphibolite, gabbro, leucogabbro
- 7 Amphibolite, hornblende and greenstone, partly with pillow structure. Small bodies of gabbro

Seve Nappe rocks

- 6 Amphibolite, black and strongly foliated
- 5 Mica schist and mica gneiss

Middle Allochthon

- 4 Meta-arkose with primary sedimentary structures
- 3 Rusty meta-arkose
- 2 Meta-arkose with inclusions of granitic gneiss and mafic dykes

Precambrian basement

- 1 Granite, massive to foliated, coarse- to medium grained

- - - Tectonic mélanges
- - - Strike/dip of foliation/schistosity
- - - Fold axis
- - - Thrust plane
- - - Late fault

Map reference: Lindahl, I. og Nilsson, L.P. 2008: BEDROCK MAP LINNAJAVRI AREA Norges geologiske undersøkelse

Figure 2. Geological map of the Linnajavri area.

Modern mapping in the area with a heavy focus on tectonics and tectonostratigraphic correlation (Foslie's weakest points) was conducted by Bjørge Brattli and Tore Prestvik in the mid 1980s as part of the general upgrading before the compilation of bedrock map-sheet Sulitjelma in 1:250,000 scale (Gustavson 1996) as well as the Nordkalott-project maps (Silvennoinen et al. 1987, Krill et al. 1987). In their publication and preliminary map, Brattli and Prestvik (1987a, b) very briefly mention talc in association with the ultramafic rocks, but without considering it a possible economic resource.

On the Swedish side of the border, Fredrik Svenonius mapped the area between 1880 and 1900 on a large scale (Svenonius 1900). Already at that time, Svenonius recognised bands of ultramafic rocks, which are marked on his maps. In a mineral resource report (Svenonius 1895) he states (p. 15) that the soapstone deposits that he had just discovered on the southern side of lake Virihaure, to the south of the Linnajavri area, were associated with ultramafic rocks, had a very good quality and were plentiful at the place. The serpentinite and peridotite lenses were more densely intersected by soapstone dykes here than at any other of the numerous places where he had previously observed ultramafic rocks in Sweden.

Regional mapping on the Swedish side of the border was later undertaken by Gunnar Kautsky (1953) and Oscar Kulling (1964, 1982). Kautsky (1953) made many detailed descriptions of the rocks and was the first to describe serpentinite conglomerates in connection with the ultramafic rocks. Similar conglomerates were not described from the Norwegian side of the border until after 2000, in reports by the authors. Compilation of the geology of northern Fennoscandia was done in the Nordkalott project (Silvennoinen et al. 1987). Detailed mapping of the Vietjervaratj ultramafic body and its soapstone alteration was done by Jimmy Stigh in 1978 and 1980 (Zachrisson and Stigh 1981, Stigh 1982). The soapstone deposits at Vietjervaratj were regarded to be among the largest soapstone deposits in Sweden, and one out of only two plotted on the industrial mineral map from the Nordkalott project (Shaikh et al. 1987).

The area between Linnajavri and the Swedish border was, therefore, in geological respect not a virgin area when we started our work in 2001, but no one had paid attention to the previous work in the area concerning economic geology.

Based on the descriptions of Foslie (1942), state geologist A. O. Poulsen in his compilation of the first detailed map of industrial mineral deposits of Norway (Poulsen 1958, 1959) included two deposits of serpentinite in the Linnajavri area (Gaskavarre and Hurrejekna (note old spelling)), but none of the soapstone deposits were registered.

Geology

The rocks of the Linnajavri area are built up of Caledonian nappes thrust onto Precambrian granitic basement (Figure 2). The geology of the area is dominated by tectonic nappes and thrust sheets, separated by thrust planes of regional significance.

The Tysfjord culmination comprises Proterozoic granitic gneisses dated at 1742 ± 46 Ma (Andresen and Tull 1986, Gustavson 1996). Recent dating by Rehnström and Corfu (2004) of granite in a window in the Akkajaure Complex gives an age of 1871 ± 11 Ma. The basement also contains remnants of older, supracrustal sedimentary and volcanic rocks. The granitic basement consists of various types of granitic rock, and the Tysfjord Granite Complex is clearly indicative of multiple intrusive events (Mogaard 1992). The granites were later intruded by mafic dykes of varying density, locally associated with formation of aplitic granite. Most dykes tend to follow an approximate N–S trend with a moderate easterly dip, at least in the mountains around the upper part of Gjerdalen valley.

The basement granite due west of the Linnajavri area is massive to foliated and coarse- to medium-grained. The benching of the granite dips towards the east, parallel to the foliation of the overlying Caledonian nappes close to the contact and steeper farther (10 km) west. On the geological map (Figure 2) these rocks are shown as unit no. 1.

The lowermost Caledonian nappes in the Linnajavri area cut down into the granitic basement, with thin nappe sheets involving both basement rocks and younger sedimentary rocks. It is typically difficult to recognise the true nature and origin of these strongly sheared rocks in the field.

The major part of the nappes in the Linnajavri area are Köli rocks, with the Seve rocks wedging out towards the north in the Linnajavri northern area. The metasedimentary and metavolcanic rocks are relatively flat lying and gently folded in two open synforms with weakly dipping fold axes towards the ESE. Further, the Linnajavri area is characterised by an uncommonly dense set of tectonic *mélange* zones that are strongly altered with abundant large blocks of exotic rocks. These zones are found nearly exclusively in the Köli rocks, they are only sporadically observed in the Seve unit. In certain sub-areas, the *mélange* zones occur rather densely spaced and make up a net of zones, e.g., in the Boarta area. The tectonic *mélanges* consist of long, narrow zones of crushed and metasomatically altered rocks, and are preferably developed where bodies of serpentinite and soapstone are involved, e.g., in connection with ophiolite fragments. However, the tectonic *mélanges* also occur in the sedimentary rocks, or at the contact between sedimentary rocks (mica schist) and marble units or amphibolite units.

Ultramafic lenses constitute important parts of the rock sequences in the Caledonian mountain belt in Scandinavia, so also in the Linnajavri area. Several of these bodies, together with their associated rock suite of gabbro and greenstone, have been recognised as ophiolite complexes or more strongly dismembered and commonly spatially isolated fragments of ophiolites. In the Linnajavri area, the assembly of mafic and ultramafic bodies most probably represent dismembered ophiolite fragments, some of which are very illustrative and diagnostic for specific levels of an ophiolite pseudostratigraphy. Reviews on Caledonian ophiolites in Norway are given by Sturt et al. (1984), Sturt and Roberts (1991) and Pedersen and Furnes (1991).

The lowermost nappes — Middle Allochthon

The lowermost thrust and sheared rocks of the Caledonian nappes are in general a thicker zone than described by Foslie (1936, 1942). Most likely, this rock unit represents the Middle Allochthon of Caledonian tectonostratigraphy, as first suggested by Gee et al. (1985) and more recently by Solli and Nordgulen (2006). In the lowest part of this zone, a strongly foliated granitic gneiss dominates (i.e., strongly deformed and recrystallised Tysfjord granite) and in the upper part quartzite and meta-arkose. Some of these metasedimentary rocks are fine-grained and rusty due to thin layers of weathered biotite acting as cleavage planes. A thin layer of arkosic sedimentary rocks with preserved soft sedimentary structures is found in one of the uppermost thrust sheets towards the base of the overlying Seve Nappe. On the geological map (Figure 2), the rocks belonging to the Middle Allochthon are shown as units no. 2, 3 and 4.

Seve Nappe

The Seve Nappe in the Linnajavri area forms the lowermost part of the Upper Allochthon. On the geological map (Figure 2), two rock units are distinguished, mica gneiss/schist (no. 5) and amphibolite (no. 6).

The mica schist to mica gneiss is a monotonous greyish rock, typically with a pronounced crenulation folding and a poorly developed schistosity, locally strongly folded (Figure 3). This is in contrast to the mica schists in the Köli Nappe where the schistosity usually is well developed. In the field, the rock has a massive appearance, often forming ridges, hills and locally also steep slopes. The relief is at its most spectacular just east of lake Boartajávri where the terrain locally is very rough. The rock is coarse- to medium-grained and contains garnet (2–5 mm), on average larger than in the overlying Köli rocks, and abundant



Figure 3. Locally strongly folded mica schist to mica gneiss of the Seve Nappe. The Seve mica schist typically shows crenulation cleavage. Location: ca. 300 m north-northwest of Boartajávri.



Figure 4. Randomly oriented kyanite crystals grown upon primary layering of Seve rocks. Location: between Boartajávri and Bananvann N.

kyanite, locally up to 3 cm. Garnet and kyanite enrichments are found along the primary layering of the schist. The porphyroblasts of kyanite are randomly oriented (Figure 4). The mica schist to mica gneiss has small irregular lenses and veins of quartz. Based on the mineralogy, the metamorphism is medium grade, cf., Brattli and Prestvik (1987b, p. 68).

Three bodies of amphibolite have been mapped in the Seve Nappe, all of them in the upper part of the unit, e.g., south of Ridoalggijávri (Figure 2). The amphibolite in the Seve Nappe is dark grey to black and relatively coarse-grained. The amphibolite is strongly sheared and may represent volcanic rocks, dykes or intrusive rocks. Amphibolite interfingered in mica schist just north-northwest of lake Boartajávri may represent dykes, probably feeders to the largest body of amphibolite in the Seve unit in the Linnajavri area.

Köli Nappes

The Köli Nappes are often subdivided in a lower, middle and upper part, each with characteristic rock units. According to Brattli and Prestvik (1987b), the rocks above the garnet-mica schists (i.e., the Seve rocks) in the Linnajavri area are all metamorphosed under low-grade conditions and typical for Lower and Middle Köli lithologies. In their Table 1, Brattli and Prestvik (1987b) assign the majority of the Köli rocks in the Linnajavri area to the Middle Köli Nappes. We support their main conclusions, but we have a somewhat different division of the local nappes and their extent compared to that shown in their Figure 3 and on their preliminary 1:50,000-scale bedrock map (Brattli and Prestvik 1987a).

Our map (Figure 2) is subdivided in three local nappes. A lower nappe, here named *Ridoalggijöhkka nappe*, occurring in the Linnajavri southern area and in the western part of the northern area. Above that is a middle nappe, named *Čohkul nappe*, that makes up most of the Linnajavri northern area.

The uppermost nappe, named *Stipok nappe*, occupies a minor area in the northeast, but continues and widens significantly towards the Stipok mountain in the northeast on the Swedish side of the border.

Our local subdivision of the Kōli Nappes resembles that of (Sundblad 1986, his Figure 1). All our local nappes constitute parts of Sundblad's Stipok terrane. The ophiolite fragments are nearly exclusively found in the Kōli Nappes.

Ridoalggičohkka nappe

The base of this nappe is a unit with alternating calcite and dolomite marble (no. 13). Variegated (red and white) calcite marble is found along strike in the uppermost part of the unit. The thickness varies along strike from south of Ridoalggičohkka to Boarta, with largest thickness between Čohkuljávri and Kvitfjell, where it is mostly dolomitic (Figure 5). South of Ridoalggičohkka, the same marble unit, here developed completely as a homogenous greyish white dolomite marble, is outcropping on the Swedish side close to the national border. This carbonate comes through the carbonate mica schist in an antiform as a result of nearly horizontal and undulating fold axes in this area (Figure 2).



Figure 5. Outcropping of the thickest part of the marble unit (ca. 100 m) in the southwest slope of Kvitfjell. View towards northwest.

Trondhjemitic intrusions (unit no. 21) and small pegmatites are commonly found in connection with the marble unit. The three largest bodies occur on the northwestern part of Ridoalggičohkka, east of Kvitfjell and west of Klebervann. Around Čohkuljávri, a swarm of semi-concordant layers of trondhjemite is found within the calcite and dolomite marble unit in the open antiform that separates the Linnajavri northern and southern area (unit no. 14). The weakly dipping rocks and fold axes cause a mixed unit of semi-concordant trondhjemite sills and lenses in marble outcropping over a large area (unit no. 14 in Figure 2).

Calcareous mica schist (unit no. 15) underlies the Ridoalggičohkka ophiolite fragments, has a thickness of more than 1 km at the greatest and wedges out towards Boarta in the northwest. In the Kvitfjell area it interfingers with the ophiolite fragments. The nappe is dominated by calcareous mica schist, but also includes thin layers of quartzite, garnet-bearing, carbonate-free mica schist and smaller (a few cm to dm) and larger

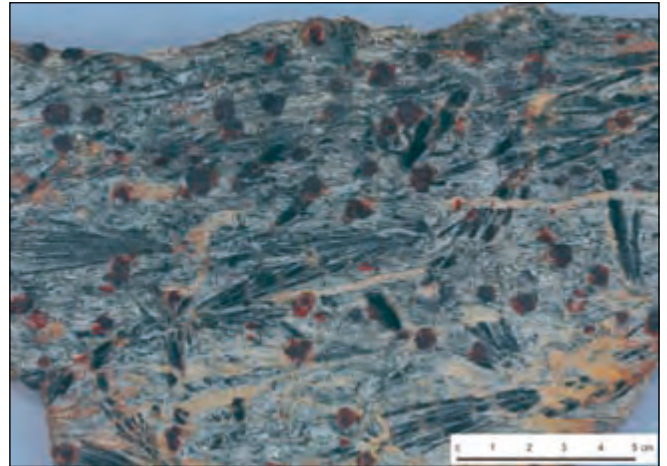


Figure 6. Polished slab of garnet-amphibole schist (garben schist) from Hurre, south of Ridoalggičohkka.

(up to 5 x 50 m) lenses of hydrothermal quartz. Strongly foliated lenses of amphibolite are found and locally thin (1 m) layers of marble occur. The metamorphic grade increases gradually southwards to garben schist south of Ridoalggičohkka, with very coarse-grained, dark green to black hornblende and reddish garnet. This rock was observed and described already by Svenonius (1896) and Foslie (1936, 1942), who both emphasised its spectacular textures and recognised it as a decorative rock. The rock has been sampled and test polished during the present work in the area (Nilsson and Lindahl 2003a) (Figure 6).

The rocks of the ophiolite fragments in the Ridoalggičohkka nappe are described below.

Čohkul nappe

The main rock type in the Čohkul nappe (unit no. 19) is garnet-mica schist to meta-psammite, representing greywacke sediments with transitions from greywacke to meta-arkose. This rock is monotonously developed over large areas. The nappe is located in the Linnajavri northern area, but with three additional small flakes, representing erosional remnants, of the nappe occurring in the western part of Ridoalggičohkka between the Klebergryta and Kleberbotn deposits (Figure 2). The rock unit lies as an open synform with the Gaskavárri ridge at the Swedish border in the central part.

The garnet in the garnet-mica schist is bright red. In a few localities, small amounts of blue kyanite has been seen. Thick (1–10 m) arkosic benches are typical for the garnet-mica schist. Typical for the unit is semi-concordant quartz lenses and near vertical N–S-trending quartz veins. Exposure of this rock unit is close to 100%. The garnet-mica schist locally contains thin, rusty layers, most likely a result of small amounts of iron sulfides. Thin layers of amphibolite occur locally within the unit.

The Čohkul nappe discordantly overlies the Ridoalggičohkka nappe and hosts the ophiolite fragments of the Klebervann–Gulldalen field, and is overlain by the Gaskavárri, Njaskavárri 985 and 833 ophiolite fragments in the core of the northern syncline (Figure 2). An extensive tectonic mélangé zone through

Heargeskohppi, hosting several small ultramafic and one large amphibolitic ophiolite fragment, has been mapped.

At all the above-mentioned locations, we find possibly inverted ophiolite sections where amphibolites are overlain by ultramafic rocks or gabbro. The observed sequence could, however, also likely be the result of stacking of individual dismembered pieces of the ophiolite during thrusting. This would not require folding with inversion involved in the process.

Underneath the ophiolite fragments, tectonic *mélanges*/ local thrust zones occur. East of the Njaskasvári 985 ultramafic body, a graphite-bearing mica schist is found. The schist is intruded by a swarm of mafic rocks, hornblendite, amphibolite and gabbroic rocks. The rock unit is strongly brecciated and represents a tectonic *mélange* beneath the ultramafite lens. The tectonics of the Guldalen field is very complex, with blocks of rock separated by tectonic *mélanges*.

Stipok nappe

Sundblad (1986) introduced the Stipok allochthon or Stipok terrane as an exotic terrane including large areas on both sides of the national border. He included all the Köli rocks in the Linnajavri area, as well as a very large part of adjoining Swedish areas extending to the south of lake Virihaure, in this terrane. In the present account, we restrict the term Stipok nappe to the tectonostratigraphically uppermost part of Sundblad's Stipok terrane, starting with his marble unit no. 3 which crops out on the Norwegian side of the border east of lake Njaskasjávri with a well-defined underlying thrust-plane. The rocks in the nappe are mostly flat lying, medium- to coarse-grained, off-white to more greyish marble. The marble is dominantly calcitic, but also with dolomitic layers (unit no. 16). The dolomite marble is mostly finer grained and white.

Underneath the marble lies a thin layer of calcareous mica schist, similar to that of the Ridoalggičohkka nappe. Based on the interpretation of Sundblad (1986), this marble and its thin,

underlying, calcareous mica schist represent a repetition of the lowermost parts of the Ridoalggičohkka nappe (Sundblad's Arajaure complex).

Tectonics

Our work has not focused on the tectonics or tectonostratigraphy of the Linnajavri area. However, the main features of thrusting, folding and faulting can relatively clearly be studied in such a well-exposed area. Structurally dominating the area are two open synclines with shallowly dipping, ESE fold axes. South of Ridoalggičohkka, the fold axes are nearly flat lying and undulating with the marble unit exposed at the surface in a valley floor (see Figure 2). The strike and dip of the sedimentary and volcanic rocks are in general less than 30° dipping easterly. Commonly, the lineation in the different rock units is better developed than the foliation. One E–W-trending fault with a few metres displacement, post-dating the tectonic *mélanges*, is mapped on the western slope of Ridoalggičohkka (Figure 2).

Thrusts

In the Linnajavri area, the Seve Nappe totally wedges out towards the northwest at Boarta in the Linnajavri northern area. In the overlying Köli Nappes, the stratigraphy of the lowermost part is repeated in the uppermost thrust sheet of the Köli Nappe succession.

The thrust planes are very commonly located in depressions in the terrain and covered by till. Discordances may be seen at several localities, but typically both lineation and foliation have the same orientation both below and above thrust planes. Outcrops of both the base and the top of the Seve Nappe can be seen. The thrust plane at the base of the Seve Nappe crops out south of Ridoalggijávri as a mylonitic zone. Here, the foliation in the Seve Nappe is clearly discordant to the underlying meta-arkoses of the Middle Allochthon. The lithologies in the lower nappe are cut by the overlying Seve Nappe (Brattli and Prestvik



Figure 7. Mylonite at the base of the Seve Nappe. Folded foliation in tectonic fragments shown in the enlarged part of the picture. Location: southwest of Čohkuljávri.



Figure 8. Elongated body of white, sheared trondhjemite (T) overlain by marble (M) at Ridoalgi, constituting the lowest unit of the Ridoalggičohkka nappe. In the background, Čohkul and Kvitfjell with the same white marble horizon. View towards north.



Figure 9. Example of pygmy folding of mylonitic trondhjemite at the base of the Ridoalggjöhokka nappe.

1987b). The border between the two nappes therefore represents a major unconformity (Figure 7). The thrust on top of the Seve rocks can be seen north of Ridoalgi on the northwestern slope of Ridoalggjöhokka. The thrust plane is located along the base of a Köli marble unit that is hosting or bordering elongated, concordant trondhjemite intrusions (Figure 8). Along the thrust, the coarse-grained trondhjemite has developed a mylonitic texture. The trondhjemite is completely ground and recrystallised and looks like an arkose, and the other rocks are mixed and phylonitic (Figure 9).

Along the thrust plane at the base of the Čohkul nappe, both discordances and rock units are being cut off. Typically, the thrust plane is covered by till or scree, but crushed and ground rocks can be seen in the southern slope of Čohkul and at Kvitfjell. The thrusting at the base of the Stipok nappe may best be seen south of the wedge east of Njaskasjávri where the foliation in the Stipok nappe is clearly discordant to that in the underlying Čohkul nappe. Further, the thrust plane of the Stipok nappe is developed as a mylonite zone where up to 3 cm, partly rotated garnet may be seen.

Tectonic mélanges

Mixed rocks of various origin has been described in a wide spectre in geology as *mélanges* (Raymond 1984a). The genesis of the rock named *mélange* is different, but mostly of tectonic origin. Raymond (1984b) has made a classification of *mélanges*. A number of tectonic *mélanges* have been described from the Appalachians as well as from the Scandinavian Caledonides.

In the well-exposed Linnajavri area, a large number of tectonic *mélange* zones can be observed. A number of these have been mapped out in different types of Köli rocks, however, preferably connected to the ophiolite fragments. The *mélange* zones have concentrated strain and thereby contributed to conserve primary structures in blocks of rock between the zones. The *mélange* zones may be characterised as both crushing zones, alteration zones and zones accommodating a large number of blocks or

fragments of rocks commonly exotic to them. We have chosen to call these zones 'mélanges' as this term denotes one of their most important, and perhaps in a more general sense, most rarely observed characteristics, namely the abundance of exotic fragments. In fact, we are not aware of similar zones reported from other parts of the Scandinavian Caledonides.

In the *mélange* zones, some rock fragments can clearly be recognised as similar to that of their immediate neighbouring rocks, e.g., the zones are crushing zones. In addition, the *mélange* zones are characterised by extensive alteration as the zones have been more permeable to volatiles than the rocks immediately surrounding them and thereby triggering mineral reactions. Especially reactions between carbonates and amphibolites have formed spectacular, coarse-grained and colourful mineral associations.

In addition to the above characteristics, the *mélange* zones host a large number of rock fragments exotic to them, foremost a large number of serpentinised rocks, or more abundantly, totally soapstone-altered ultramafic rocks. Trondhjemite bodies are also located within the zones. Most fragments or blocks of ultramafic rock are small or very small, but occasionally they may be large. The 40 x 200 m Klebervann soapstone lens is the largest individual ultramafic body associated with a *mélange* zone, and the neighbouring and equally large trondhjemite body, located just northeast of Karstdalen in the Linnajavri northern area, is the largest trondhjemite body (cf., Figure 2 and Lindahl and Nilsson 2002).

The density of the zones varies. It is at its highest in the Boarta area where they nearly make up a network. The thickness of the zones also varies a lot, from a few metres to tens of metres (Figure 10). The orientation and extent of the zones also vary a lot. They may follow the contact between different rocks or in part follow thrusts. They may also intersect rock units and thrusts. The most extensive individual *mélange* zone mapped by us has its western extremity in the Klebervann area and extends some 8–9 km to the east through Hearsgekohppi and then into Sweden (see Figure 2).



Figure 10. Tectonic *mélange* zone outcropping in Klebergryta Øvre, Ridoalggjöhokka area. View across the ca. 8 m-thick zone.

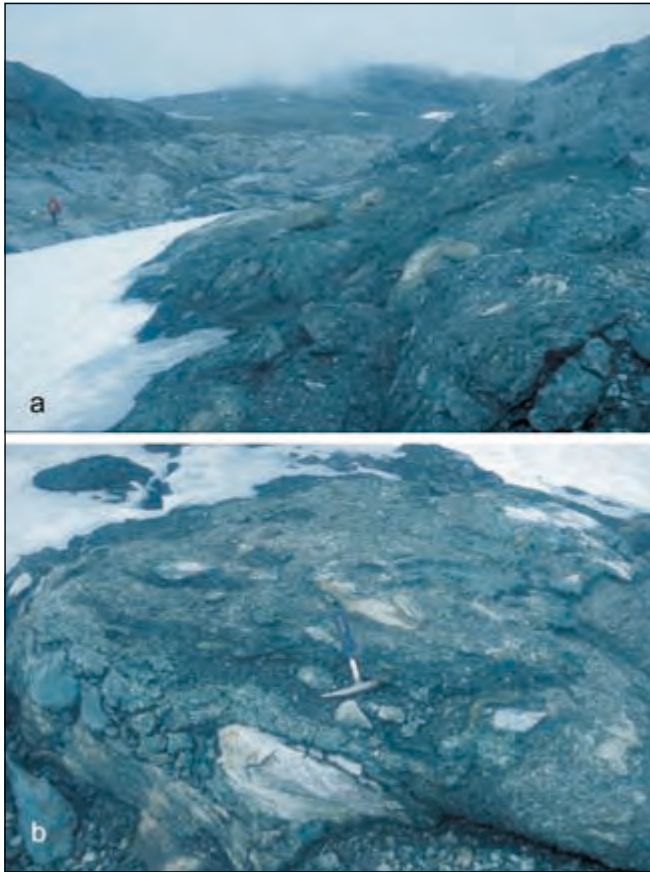


Figure 11. The mélangé zone northwest of the Klebervann deposit. (a) The ca. 15 m-thick tectonic mélangé at the base of the Klebervann deposit. View towards southeast along the zone from a location ca. 200 m northwest of the deposit. (b) Detail of the tectonic mélangé showing fragments of trondhjemite, marble, soapstone, amphibolite and mica schist in a hydrothermally altered matrix of various minerals including talc.

The deformation in the mélangé zones has mostly been plastic (Lindahl and Nilsson 2002), but some localities show a brittle deformation. The different rock fragments are both foliated and folded (Figure 11). As mentioned above, reactive solutions have percolated through the zones, especially in connection with ultramafic rocks, volcanic rocks and marbles. The result of the alteration is spectacular, coarse-crystalline, black hornblendites, intensely green serpentinite and actinolite-fels and rusty brown ferro-dolomite. The solutions have also formed unusually talc-rich soapstone bodies in gabbroic rocks in Guldalen and at Ridoalggičohkka (Klebergryta Øverste, Liggkleberen and at Grensevann). Commonly, ultramafic rocks and amphibolites are found in contact with the mélangé zones, resulting in fragments of soapstone with talc and chlorite in the matrix of the mélangé, a good lubrication for the development of the mélangé. Within the large amphibolite body making up the central part of the Ridoalggičohkka synform, a large, concordant mélangé zone is developed not far above the base of the amphibolite. Here, the mélangé zone runs parallel to the contact to the amphibolite as a 10 to 15 m-wide zone of black, strongly schistose and easily weathered chlorite schist (chlorite phyllonite) with massive amphibolite at both the hanging-wall and foot-wall sides. Other minor mélangé zones within this

amphibolite body are characterised as talc-chlorite zones.

The development of the tectonic mélangé zones seems to be more or less contemporaneous with the thrusting. The percolation of fluids, however, seems to be greater in the mélangé zones than along most of the thrusts planes.

The ophiolite fragments

Lithologies

The ophiolite fragments occur in the Kōli rocks in two different local nappes, the Ridoalggičohkka and Čohkul nappes. The most complete section is found at Ridoalggičohkka in the Linnajavri southern area and includes ultramafic rocks, pillow lava, gabbro, amphibolite and conglomeratic weathering products with well-rounded pebbles from these rocks. Well-preserved pillows are found in little deformed rock segments between mélangé zones (Figure 12). Only a single mafic dyke has so far been registered intersecting pillow lava. However, no detailed investigations looking for mafic dykes of a possible sheeted-dyke complex within the mafic rocks have been undertaken. In the Linnajavri northern area, ophiolite fragments are located both in the Ridoalggičohkka nappe and the Čohkul nappe, however, in a different lithological setting than in the southern area (see Figure 2).

The major ophiolite fragments in the Čohkul nappe in the Linnajavri northern area are more tectonically disrupted than

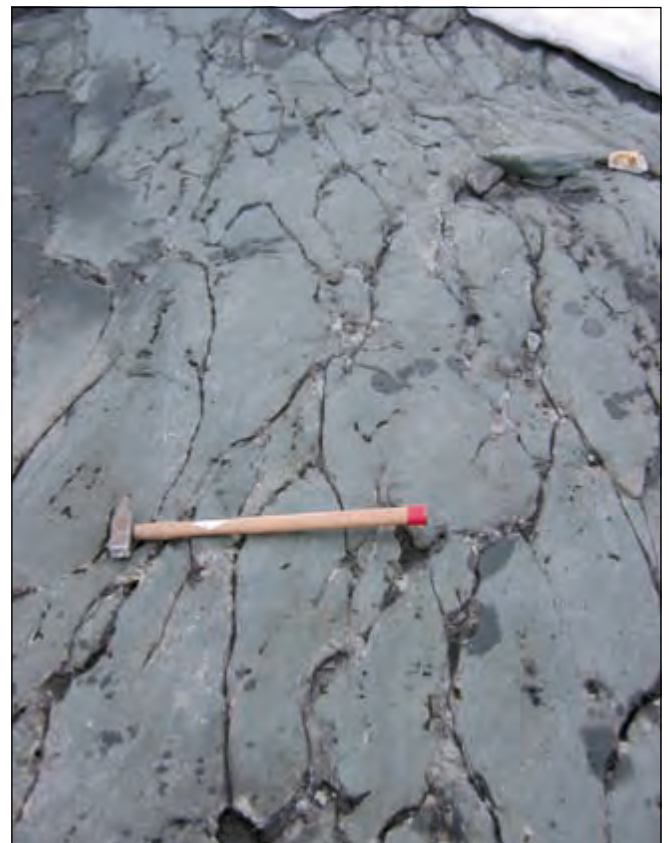


Figure 12. Weakly deformed basaltic pillow lava at Ridoalggičohkka.

Figure 13. Types of matrix-supported conglomerates at Ridoalggičohkka. The pebbles most commonly show onion-skin weathering texture. (a) Conglomerate with micaceous matrix. (b) Serpentine conglomerate with clearly developed onion-skin texture. (c) Micaceous conglomerate beds of varying facies development. (d) Conglomerate with mafic matrix and mafic and siliceous clasts.



those at Ridoalggičohkka (see Figure 2). The rock suite includes ultramafic rocks and dark, medium-grained amphibolites, the latter probably mainly with a gabbroic precursor. A body of amphibolite, gabbro and leucogabbro is located at the central portion of the Njaskavárri ridge. Ultramafic scree material and immature ultramafic breccia-conglomerate are also found as minor occurrences along the southern side of the Gaskavárri ridge. These include weakly rounded pebbles of soapstone among non-talcified boulders and gravel, one of several important key locations constraining talc formation to a pre-obduction, or at least pre-conglomerate formation stage. These tiny occurrences of ultramafic conglomerate seem to have been fixed to the ultramafic body, making this assemblage a single tectonic entity during thrusting onto its amphibolitic substrate. There is no evidence of deposition of ultramafic breccia-conglomerate onto the mafic (amphibolitic) substrate. On the contrary, the foliation in the amphibolite bends neatly around the conglomerate pockets. We do not know if and/or to what extent, these tiny conglomerate occurrences represent relics of a larger lithological unit that was excised during thrusting of the nappe pile. It should, however, be noted here that identical tiny occurrences of serpentine breccia-conglomerate are found at the same tectonostratigraphic position all the way along the southern border of the ca. 5 km-long Vietjervaratj ultramafic body, just to the east of Gaskavári (Kautsky 1953, p. 92 and map, Kulling 1972, 1982, Stigh 1982). These occurrences are 'glued' to their ultramafic substrate in a way that makes it difficult to see where the breccia-conglomerate started to develop from its pseudo-conglomerate-like base. It is definitely a matter of a transition zone.

The rocks constituting the ultramafic bodies in the Linnajavri northern and southern areas are petrographically similar, comprising dunite and peridotite, both probably basically of mantle origin, extensively serpentinised and to a large degree also talcified. Only in one ultramafic body, the Njaskavárri 985

body, a section of a well-preserved ultramafic cumulate sequence representing the lower oceanic crust in an ophiolite stratigraphy is found. This section was discovered and described for the first time by Brattli and Prestvik (1987b). The cumulate rocks of the Njaskavárri 985 body are generally less serpentinised than the rest of the ultramafic rocks in the Linnajavri area. The dunitic bodies are normally the most fine-grained and the peridotite coarser grained. The ultramafic rocks locally contain small pods of chromite, which have survived morphologically during the alteration of their host rocks to serpentine and further to soapstone. Mineralogically, however, the chromite has changed almost completely to magnetite and the pods are, therefore, now of limited or no value as depth indicators in a general ophiolite pseudostratigraphy. The gabbro bodies normally consist of medium-grained, massive metagabbro. No layered gabbros were recorded, but an example of a fresh-looking varitextured gabbro is located in the Ridoalggičohkka area, 1 km east of the national border.

The suite of rocks of the ophiolite fragments have been exposed to weathering and then become the source rock for conglomerates and grit deposits. The conglomeratic rocks (Figure 13) vary a lot in composition. At the southern side of Gaskavárri, the above-mentioned conglomeratic breccia consists of fragments and pebbles of peridotite and serpentine with barely rounded soapstone. The conglomerates at Ridoalggičohkka, on the other hand, have well-rounded pebbles, in most cases with onion-skin structure (Figures 13a, b). They vary from serpentine conglomerate, green conglomerate with large amounts of mafic material and epidote, to grey conglomerates with a micaceous matrix. The type of conglomerate varies from monomict (serpentine conglomerate) to polymict. Mostly, the conglomerates are strongly matrix supported with transitions to grit and coarse-grained sediment. The conglomerate beds vary in composition and thickness, down to half a metre (Figure 14), in an



Figure 14. Thin bed of a mafic conglomerate between two micaceous-rich beds. Location: Ridoalggjčohkka area between the 1192 and the 1248 peaks.



Figure 15. Veinlets with tourmaline, chlorite, albite and quartz with bleaching of adjacent host mica schist. Location: Klebergryta Nedre area.

alternating sequence.

Alteration of the rocks in the ophiolite fragments is extensive. In the pillow lava at Ridoalggjčohkka, sulphur- and magnesium-bearing solutions have flowed through tiny vents ('hot spots') and fissures. These solutions have caused sulphide impregnation, and in the aureole (1 m thick) around the vent, growth of flaky talc with random orientation has occurred. The sulphides are strongly weathered at the surface, and today do not make up much more than a rusty crust, where elevated values of Cu and Zn have been recorded. Along shear zones in the amphibolites within the Ridoalggjčohkka synform, magnesium has been introduced and talc growth can be seen as half centimetre unoriented flaky crystals within the more fine-grained amphibolite. Late hydrothermal activity, both in the ophiolitic rocks and the various mica schists, has bleached the rocks around veins, wherein quartz, carbonates, chlorite and tourmaline are deposited (Figure 15). Silicification along mm-thin veinlets in the conglomeratic rocks is also common, possibly a later phase than the quartz-carbonate-chlorite-tourmaline veins. This local-

ly extensive hydrothermal activity is otherwise common in the greater region, and Kautsky (1953, p. 129 and 192) reported similar development of veins from the Virihaure area and from the area east of border post 242.

Formation of soapstone

The soapstone formation in the ultramafic rocks in the Linnajavri area varies from nearly zero to extensive. The soapstones in the Linnajavri area formed where hot solutions, enriched in dissolved CO₂, penetrated the host serpentinised ultramafic rocks. Some of the ultramafic bodies are only moderately altered to soapstone whereas others are totally (e.g., Klebervann lens) or almost totally (e.g., Kleberflåget body) altered. Alteration has taken place out from cracks, joints and breccia zones in the ultramafic rocks, typically leaving a very irregular front where the pervasive alteration has ended (Figure 16). It is the reaction between serpentinite and CO₂ in hot solutions that has instantly triggered formation of talc and magnesite from the serpentinite. At the reigning high temperatures, the talc-magnesite formation seems to have happened instantaneously (at or just behind the reaction front) and been total inside the volume of serpentinite affected by the CO₂-enriched solutions. We never find soapstone with relics of serpentine (ca. 300 specimens investigated), nor

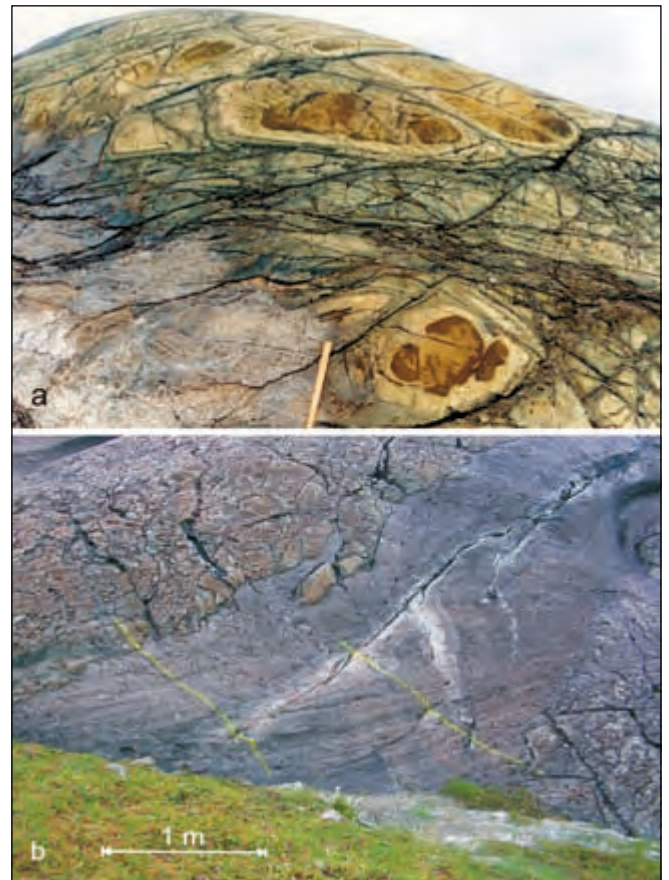


Figure 16. Soapstone alteration. (a) Alteration of dunite (dark brown weathering crust) to serpentinite (yellow to green) with a soapstone front 'moving' up from the lower left corner of the figure. Location: Klebergryta Øvre. (b) Soapstone alteration starting from a crack in serpentinite. Yellow marking prepared for slice sampling. Location: Kvitfjell NV deposit.

do we observe serpentinites with incipient talc-magnesite formation in the field. Serpentinites showing a gradual alteration to soapstone are otherwise rather abundant in many ultramafic rocks from other places within the Scandinavian Caledonides. However, we occasionally find smaller and larger xenoliths of non-talcified serpentinite within the soapstone and always with sharp borders between the two rock types.

In several places, primary magmatic textures are inherited from the dunite or peridotite. This is for example the case at the western end of the Njaskasvárri 985 body where the layered structure is visible, though faintly, in the ultramafic rocks after its alteration to soapstone. At one locality (the Kleberflåget deposit, by far the largest individual deposit in the Linnajavri area), there has been a quite massive alteration of serpentinite to soapstone. This very voluminous alteration of what was probably once part of the mantle below oceanic crust in the Iapetus Ocean, has no direct counterparts in the rest of the Scandinavian Caledonides as far as we know (see Figure 2 for dimensions of the Kleberflåget deposit). This voluminous alteration was not accompanied by visible deformation of the ultramafic body. All the structures, such as joints and fissures as well as minor textural details in the precursor serpentinite, are perfectly well preserved in the soapstone. The CO₂-enriched fluids have virtually 'flushed' through a large volume of serpentinite, probably at an early, oceanic stage, and totally changed its mineralogy. At the same time, however, the transformation process has left all the rock structures completely untouched. Elsewhere in the Scandinavian Caledonides the soapstones are typically strongly sheared.

The Kleberflåget deposit is not only by far the largest individual soapstone deposit in the Linnajavri area. At Kleberflåget, the alteration process has also taken a step further than soapstone formation. Due to excess CO₂ and falling temperature (excess in the sense that there is no more serpentinite available for soapstone formation from the local and persistently active CO₂ source), the soapstone has just started to break down to listwaenite (Figure 17 and Figure 2), a rock consisting of magnesite/dolomite and quartz. Two small areas of listwaenite have been found and mapped (Figure 2), one on each side of the Kleberflåget deposit. The formation of listwaenite is among our strongest indications/proofs that the soapstone did not form from CO₂ derived from a sedimentary source (e.g., calcite or dolomite marble, black shale) at a late, compressional stage during the Caledonian Orogeny, i.e., after such rocks had been juxtaposed or come close to the ultramafic rocks. In contrast, we believe that the CO₂ was derived from a strong and lasting mantle source at an early, probably oceanic, stage; a CO₂ source that was active even down to very low temperatures (ca. 200–300°C). This is below or near the lower stability temperature of talc in ultramafic rocks, hence the start of decomposition of talc to quartz and additional magnesite in the soapstone. The amount of listwaenite cropping out is very small compared to the volume of soapstone at Kleberflåget, i.e., we have probably just reached the critical temperature where talc started to de-



Figure 17. Border between listwaenite and soapstone (lower part of picture). The listwaenite contains ribs of quartz in a magnesite/dolomite matrix. Location: Kleberflåget deposit.

compose when the CO₂ source was turned off and the process was frozen yielding the proportions of variably altered rocks we see today. In other, more mature systems where a CO₂ source has been available at even lower temperatures, as in the Raudfjellet ophiolite fragment in Nord-Trøndelag county, central Norway (Nilsson et al. 2005), about three quarters of a 4.5 km long and up to ca. 50 m thick, sheet-formed soapstone deposit was transformed to listwaenite before the system came to rest.

The mode of formation of the Kleberflåget deposit also applies to the majority of the other soapstone deposits in the Linnajavri area, and perhaps in the whole greater region to the Sulitjelma area to the south (i.e., Sundblad's (1986) Stipok allochthon). The exception is the minor, mélange-associated, gabbro-derived soapstone occurrences.

The major parts of the ultramafic rocks are altered. Only to a limited extent are relics of the primary magmatic mineral assemblages of the ultramafic rocks found, and then typically in the cores of bodies (the Njaskasvárri 985 body makes an exception). In the centre of the Kvitfjell body, near its 914 m summit, a metaperidotite with 3–4 cm, dark, rounded spots of metamorphic olivine (forsterite) ('leopard texture'), makes up the very erosion-resistant, steep top area. This is the only case where we have encountered metamorphic olivine in the ultramafic rocks in the Linnajavri area. Most of the ultramafic rocks are serpentinites, some of them with an unusually sharp and bright green (emerald green) colour.

Hydrothermal activity has been pervasive through the whole nappe sequence of the area. Numerous small, near vertical, quartz-rich pegmatitic veins intersect the sediments, dominantly oriented N–S or parallel to the schistosity.

Mineralogy and chemistry

Soapstone is basically a talc-carbonate rock. The soapstone in the Linnajavri area is of the same type as known from other areas with abundant ultramafic rocks, basically of ophiolitic origin, in the Scandinavian Caledonides. Talc derived from alteration of

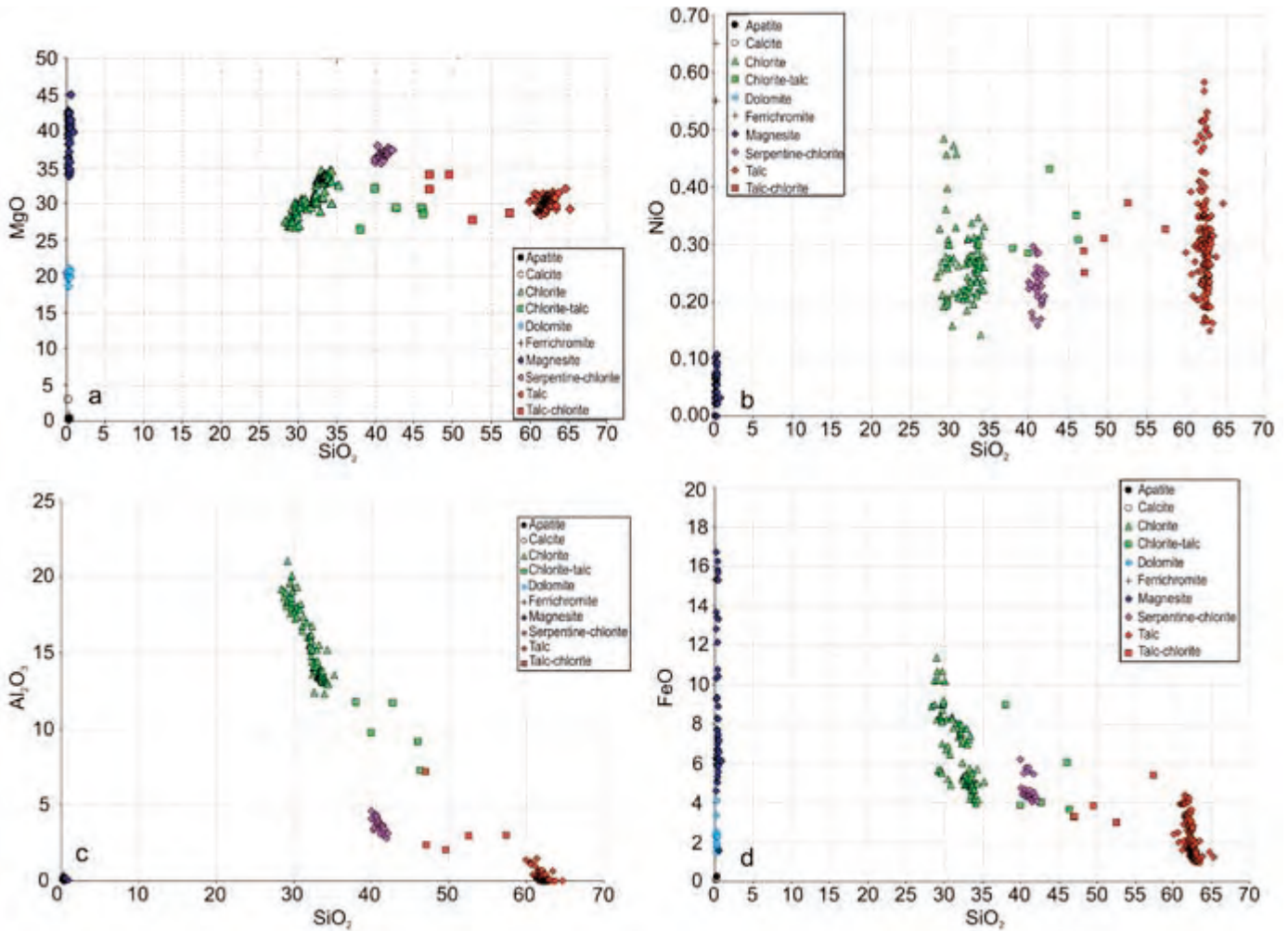


Figure 18. Scanning electron microscope (SEM) mineral analyses in various plots (a–d). Contents in weight percent. See text for discussion of results.

ultramafic rocks to a certain extent inherits both the major and trace element chemistry of the precursor ultramafic minerals (foremost olivine and serpentine).

The mineralogy of the Linnajavri soapstone is fairly simple. The number of mineral phases is strongly restricted and basically comprises talc, magnesite, chlorite and dolomite in decreasing order. Minor amounts of disseminated chromite and secondary magnetite further occur in the soapstone. Though the mineralogy is simple, the minerals’ internal proportional distribution, textural variation, grain-size distribution, intergrowths, crystal zoning and degree of recrystallisation varies. There are,

Table 1. Average values (arithmetic mean) for NiO and Cr₂O₃ in talc, chlorite, magnesite and dolomite in soapstone from the Linnajavri area. Scanning electron microscope analyses with long counting time (60 s). Analytical numbers in wt. %.

Mineral	NiO	Cr ₂ O ₃	n
talc	0.29	0.02	173
chlorite	0.25	1.27	88
magnesite	0.05	0.00	55
dolomite	0.00	0.00	13

n = number of analyses; 329 analyses in total.

for example, significant compositional differences between the soapstones of the Linnajavri northern and southern area. Further, there are differences within individual soapstone deposits within the areas. There are also significant differences at a more local scale, even down to what may be observed in thin sections from originally adjoining parts of sample slices.

The content of talc in the soapstone is about 50% on average, locally reaching as much as 70–80%. Examples of very talc-rich soapstone are found both within the ultramafic rocks and as a peculiarity where soapstone is formed directly from gabbro in association with mélangé zones, see details in Nilsson et al. (2003). The talc content is on average slightly higher in the northern area compared to the southern area. The iron content in the talc varies between 1 and 4.5 wt.% and replaces magnesium in the talc lattice (cf., Figures 18a, d). The soapstone abundantly shows a bimodal grain-size distribution with coarse and well-developed magnesite crystals set in a more fine-grained matrix of platy talc with some intergrown chlorite. The coarse-grained magnesite commonly exhibits a marked zoning with a Mg-rich core becoming gradually more Fe-rich towards the rim (Figures 18a, d). The chlorite tends to cluster in two groups: one group enriched in Si and Mg relative to the other, which in turn

is strongly enriched in Al relative to the former (Figures 18a, c). The chlorite content is otherwise significantly higher in the southern area compared to the northern area. Varying amounts of fine-grained, anhedral to subhedral dolomite occurs evenly disseminated between the silicates. Cl-apatite is recorded as an accessory mineral. In addition to the above minerals, relatively fine-grained chromite and fine-grained to very fine-grained magnetite is disseminated in the soapstone. Sulphides and other trace constituents such as sulpharsenides, arsenides and alloys, are extremely rare in the Linnajavri soapstone deposits.

The soapstone texture is mostly massive, but locally it may show a pronounced foliation or banding, schlieren structures and carbonate veining with colours varying from a soft grey tone to more greenish grey. In general, the foliation is most pronounced towards the rims of the ultramafic bodies, and close to zones of tectonic mélanges.

Where soapstone borders calcite and dolomite marble units, pale brown tremolite is locally developed close to the contact, e.g., in the Karstkleberen and Kleberveggen lenses. However, tremolite is only locally developed in the soapstones in the Linnajavri area, and not observed at all to the southeast and south of the Kvitfjell body.

A large number of bulk chemical analyses as well as mineral analyses of soapstones have been performed. In Figures 18a–d, 374 selected mineral analyses are plotted in scatter diagrams to illustrate variations in compositions.

The analyses of the trace elements Ni and Cr are summarised in Table 1. The data show that both talc and chlorite host Ni in roughly equal amounts (cf., also Figure 18b), whereas chlorite is the principal host for Cr. The carbonates, magnesite and dolomite to a very limited extent, or not at all, accommodate lattice-bound Ni and Cr.

Mineral potential for the Linnajavri area

The soapstones of the Linnajavri area may be exploited either as an ore for talc flotation or as dimension stone. Other potential mineral resources (marble, schist and gold) may be evaluated when infrastructure is established. The average content of talc in the soapstones is about 50% (Figure 19). The other minerals are carbonates (magnesite and some dolomite), chlorite and oxides, mostly magnetite. The sulphide content is very low to zero in the Linnajavri soapstones, which may be an advantage for use both as dimension stone and for talc flotation.

The soapstone reserves are calculated based on geology (geological structures and the 3D-pattern of outcrops) and detailed mapping of the size of the outcrops. For the Linnajavri northern area, the distances are surveyed using GPS, compass and laser instrument, and in the southern area from the mapping on 1:5,000-scale aerial photographs. The very good and extensive outcrops of the area, including the soapstone deposits, make it possible to carry out reliable estimates of the soapstone volumes. Close to 20 individual soapstone bodies carry in excess

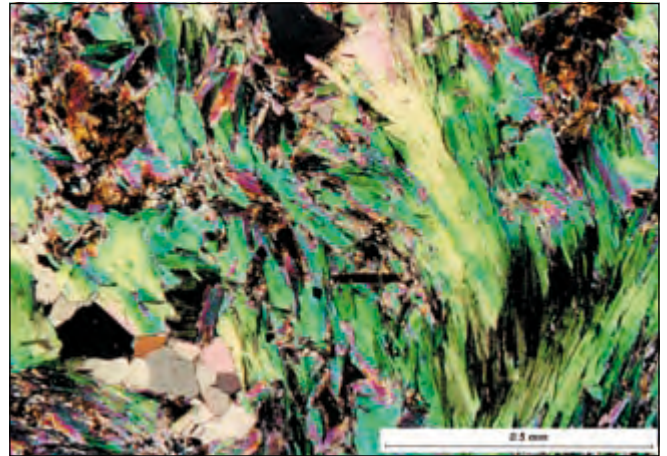


Figure 19. Thin section of talc-rich soapstone from the Linnajavri area (crossed nicols). Location: Kleberlia, Njaskasvárri 833 lens.

of 1 million tonnes each, with a total estimated reserve of some 100 million tonnes of soapstone, equivalent to some 50 million tonnes of talc. The largest single body is Kleberflåget, containing 70 million tonnes of soapstone; 50 tonnes on the Norwegian side of the border and 20 million tonnes on Swedish ground. The geological potential for possible additional soapstone resources in the Linnajavri area is estimated to be at least 2–3 times the calculated reserves. The hidden resources are basically hosted in the shallow ca. 2 x 4 km Ridoalggičohkka synform in the Linnajavri southern area. In addition, there is an unknown but relatively surface-near soapstone potential connected to the Čohkul magnetic anomaly caused by the Čohkul ultramafic body (Mogaard 1992, Skilbrei et al. 2003). This body has a thin schist cover (only about 40 m) and crops out as an 80 x 400 m soapstone deposit with large serpentinite xenoliths in the steep southern wall of the Čohkul mountain, in the Linnajavri northern area (Lindahl and Nilsson 2002).

Talc

The global market for talc as a filler mineral is relatively large at 7–8 million tonnes annually. Most of the supply comes from sedimentary deposits. However, soapstone altered from ultramafic rocks like the Linnajavri area is exploited in Finland on a large scale (Niemela 2002), where flotation of soapstone gives a talc concentrate for the paper industry. Most likely, talc from the soapstones of the Linnajavri area can also be extracted.

The very large reserves of soapstone in the Linnajavri area, sufficient for mining into the unforeseen future, justify a thorough testing of the raw material for flotation of talc. Our work on the mineralogy and mineral chemistry (Nilsson et al. 2003, Nilsson 2004) contains some of the background information needed for these tests.

Dimension stone

Scandinavia, especially Finland and Norway, is the leading region in Europe for exploitation of soapstone deposits for producing

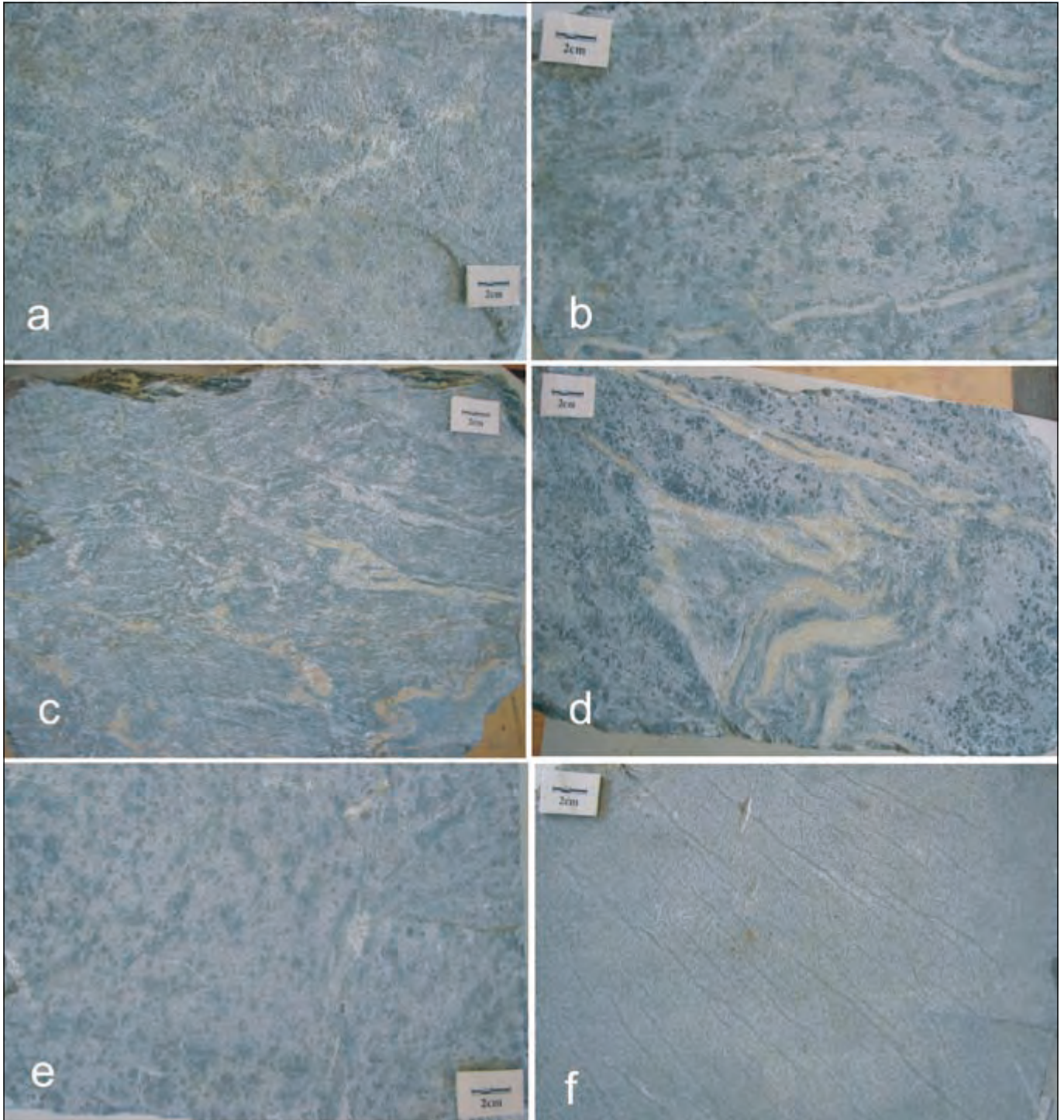


Figure 20. Selection of soapstone slabs from the Linnajavri area. See map in Figure 2 for locations. (a) Kvitfjell NV, (b) Kleberfläget, (c) Hatten, (d) Langleberdalen (e) Kleberbreen, (f) Ridoalggïohkka 1192 V.

ovens and open fire places. The market is strongly growing, both in Scandinavia and other places where winters are cold. The end product for this industry is usually made close to the quarries, and there is no international block market for soapstone. This means that exploitation of soapstone creates more local jobs than block production from other types of massive dimension stone.

The soapstones of the Linnajavri area are generally massive, only locally weakly foliated. The colour of the soapstone varies

from dark greyish to off-white. The darkest types may locally have a dull greenish tint from a certain amount of chlorite. The whitish type may be foliated and has a high content of talc, up to 70–80%, and as such has a poorer quality as dimension stone. Soapstone quarried for dimension stone normally contains minor amounts of sulphides and oxides. The sulphides may in some cases cause rusty surfaces. In the soapstones of the Linnajavri area, sulphides are absent and therefore do not have this potential problem. In Figure 20, a selection of the various

soapstone types is presented. The textures vary to a certain extent both between and within the soapstone bodies and the soapstone industry can quarry the type of stone the market wants. Because the typical soapstones from Linnajavri are massive and little sheared, the mechanical strength is probably better than for several other soapstones from the Caledonides.

The soapstone reserves in the Linnajavri area are calculated for bodies larger than 1 million tonnes. Lenses or bodies smaller than this may be exploited for soapstone quarrying for dimension stone. The very large reserves and high quality of the soapstone in the area definitely make this rock type a potential resource for the industry for a very long period of time.

Conclusions

During our work in the Linnajavri area we have documented and evaluated the economic potential of the unusually large and talc-rich soapstone deposits of the area. Geological mapping has been conducted focusing mainly on the many ophiolite fragments dispersed throughout the ca. 70 km² area (cf., Figure 2). The rather detailed geological map might also, however, be of some general interest to the study and correlation of Seve and Kõli tectonostratigraphy on a more regional scale.

The Linnajavri area is built up of granitic basement and a sequence of Caledonian nappes, the Middle Allochthon to the west and above it the Upper Allochthon with the Seve and Kõli Nappes. The Seve Nappe comprises one single nappe in the mapped area whereas the Kõli Nappes may be subdivided into three individual sub-nappes, here informally named the *Ridoalggičohkka*, *Čohkul* and *Stipok* nappes. The nappes vary considerably in thickness in the area. Both the Seve Nappe and the *Ridoalggičohkka* nappe wedge completely out in the Linnajavri northern area. Repetitions of internal Kõli Nappes also occur in the area, and we interpret the lower parts of our *Ridoalggičohkka* nappe to be repeated in the *Stipok* nappe. At three places in the core of the northern synform in the *Čohkul* nappe, we find possible inverted ophiolitic sections where amphibolites are overlain by ultramafic rocks or gabbros. In the *Ridoalggičohkka* synform in the south, we find Kõli rocks including a well-preserved assemblage of semi-continuous ophiolite fragments where ultramafic rocks are overridden by a large sheet of dominantly unspecified amphibolite, but with abundant, easily identifiable massive gabbros and basaltic pillow lavas, the opposite situation compared to the north.

The Linnajavri area is characterised by what we have chosen to call *tectonic mélange zones*. Where these are at their densest, as in the Boarta area in the northwest, they occur as a net of zones that are up to 20–30 m thick and up to several kilometres long. These zones are characterised by fragmentation and crushing of rocks as they have acted as stress releasers between large rock masses. The crushed rocks in the *mélange zones* have in turn been more permeable to fluids than the enclosing compact

rock masses and are typically strongly metasomatised. The third feature that characterises the *mélange zones* is fragments of variable size of exotic rocks, i.e., not from the immediate host rock to the zones.

The ubiquitous testimony of the soapstone alteration processes that were once at work within the ophiolitic ultramafic rocks in the Linnajavri area are impressive, and measured by volume probably unique in the Scandinavian Caledonides. The various mineralogical details concerning this alteration may be studied in great detail in the Linnajavri area due to the relatively weak deformation of the rocks between the above-described tectonic *mélange zones*. The CO₂ infiltration into dunite (Figure 16a), peridotite and serpentinite along breccia zones, joints, the *mélange zones* and a few regular, focused 'CO₂ spots' may be studied in detail. Both larger structures as well as minor textures in the ultramafic rocks are often inherited in the soapstone without any signs of accompanying deformation in the latter. The Kleberflåget deposit is the best example. After the metasomatic transformation process had ceased, fragments of the once probably large ophiolite complex were obducted and exposed to weathering. This may clearly be seen south of the Gaskavárri ridge, where slope breccia-conglomerate includes angular pebbles of intermixed, massive soapstone and serpentinite. Conglomerates are also found within the *Ridoalggičohkka* synform, where we may see various more mature conglomeratic facies developed; there are more matrix-supported conglomerates, from serpentinite conglomerates through mafic and more pelitic conglomerates and grits.

The soapstone resources in the Linnajavri area must be classified as being of *national importance for Norway and significant for Europe* both for talc flotation and as dimension stone. It is also of great importance for future mineral industry in the region and can thereby create jobs on a long-term basis. Such activity will also be important for the population pattern in the region.

Acknowledgements

Financial contributors include NGU, Statskog (landowner) and industrial partners, Nordland county council, Salten Regionråd, Hamarøy and Sørfold municipalities and the Northern Periphery Programme (NPP) of EU (PNASTINA project). Among a number of persons inside these organizations, we especially want to mention county geologist O. Torstensen and former head of development T. Langås in Hamarøy municipality for inspiring support and also their contribution to marketing the project to politicians, newspapers, local radio and TV. We also want to thank our colleagues at NGU for contributions to our work: L. Furuhaug (field work and preparing figures), T. Sørđal and A. Flaatt (Statskog) (field work), B.I. Rindstad and P. Sviggum (digital map) and B. Johansen (thin sections). The referees, B. Brattli, A. Solli, and editor T. Slagstad, are thanked for the thorough review that has substantially improved the paper.

References

- Andresen, A. and Tull, J.F. (1986) Age and tectonic setting of the Tysfjord gneiss granite, Eufjord, North Norway. *Norsk Geologisk Tidsskrift*, **66**, 69–80.
- Brattli, B. and Prestvik, T. (1985) Feltundersøkelse på kartblad Linnajavrre sommeren 1985. *NGU Map Archive 112/85.032D, Field report*, 31 pp.
- Brattli, B. and Prestvik, T. (1987a) Linnajavrre, bedrock geology map 2230 III, scale 1:50,000, preliminary edition, *Norges geologiske undersøkelse*.
- Brattli, B. and Prestvik, T. (1987b) Tysfjord granite and overlying rocks in the area of Linnajavrre, central-north Norway. *Norges geologiske undersøkelse Bulletin*, **410**, 65–72.
- Foslie, S. (1929) Feltdagbok for gradteigskartene Hellembotn og Linnajavri. Bind I og II. *NGU Map Archive*.
- Foslie, S. (1936) Linnajavrre, bedrock geology map, scale 1:100,000, *Norges geologiske undersøkelse*.
- Foslie, S. (1942) Hellembotn og Linnajavrre. Geologisk beskrivelse til kartbladene. *Norges geologiske undersøkelse*, **150**, 119 pp.
- Gee, D.G., Kumpulainen, R., Roberts, D., Stephens, M.B., Thon, A. and Zachrisson, E. (1985) Scandinavian Caledonides Tectonostratigraphic Map, scale 1:2,000,000. In Gee, D.G. and Sturt, B.A. (eds.) *The Caledonide Orogen—Scandinavia and Related Areas*, Wiley and Sons Ltd., Chichester.
- Gustavson, M. (1996) Sulitjelma, bedrock geology map, scale 1:250,000, *Norges geologiske undersøkelse*.
- Holmsen, G. (1917) Sørfolden—Riksgrensen. *Norges geologiske undersøkelse*, **79**, 46 pp.
- Kautsky, G. (1953) Der geologische Bau des Sulitelma—Salojauregebietes in den nordskandinavischen Kaledoniden. *Sveriges geologiska undersökning*, **C 528**, 232 pp.
- Krill, A.G., Kesola, R., Sjöstrand, T. and Stephens, M.B. (1987) Metamorphic, Structural and Isotopic data map of Northern Fennoscandia, scale 1:1,000,000, *Geological Surveys of Finland, Norway and Sweden*.
- Kulling, O. (1964) Översikt över Norra Norrbottensfjällens kaledonberggrund. *Sveriges geologiska undersökning*, **Ba 19**, 166 pp.
- Kulling, O. (1972) The Swedish Caledonides. In Strand, T. and Kulling, O. (eds.) *Scandinavian Caledonides*, John Wiley and Sons Ltd., pp. 149–285.
- Kulling, O. (1982) Översikt över Södra Norrbottensfjällens kaledonberggrund. *Sveriges geologiska undersökning*, **Ba 26**, 295 pp.
- Lindahl, I. and Nilsson, L.P. (2001) Kartlegging av talk/ klebersteinsforekomstene i Linnajavri-området i Hamarøy kommune, Nordland. *NGU Report 2001.112*, 91 pp.
- Lindahl, I. and Nilsson, L.P. (2002) Oppfølgende undersøkelser av talk- og klebersteinsforekomstene i området Boarta-Gaskavárri (Linnajavri Nordområde), Hamarøy kommune, Nordland. *NGU Report 2002.090*, 63 pp.
- Lindahl, I. and Nilsson, L.P. (2005a) Klebersteinsforekomstene i Linnajavri-området, Hamarøy kommune, Nordland. Statusrapport. *NGU Report 2005.034*, 57 pp.
- Lindahl, I. and Nilsson, L.P. (2005b) Prøvetakingen i Linnajavri-området feltsongen 2005: Kvitfjell NV. *NGU Notat*, 9 pp.
- Lindahl, I. and Nilsson, L.P. (2005c) Prøvetakingen i Linnajavri-området 2005: Sørområdet. *NGU Notat*, 10 pp.
- Lindahl, I. and Nilsson, L.P. (2006a) Kjemiske og mineralogiske undersøkelser av kleberstein fra forekomsten Kvitfjell NV, Linnajavri. *NGU Notat*, 38 pp.
- Lindahl, I. and Nilsson, L.P. (2006b) Geologisk oversikt over Linnajavri-området fra kartleggingen 2000–2006. *NGU Report 2006.093*, 27 pp.
- Lindahl, I., Furuhaug, L. and Nilsson, L.P. (2005) Undersøkelsene i Linnajavri-området feltsongen 2005: Guldalen. *NGU Notat*, 10 pp.
- Lindahl, I., Nilsson, L.P. and Furuhaug, L. (2006) The soapstone deposits in the Linnajavri area, Hamarøy community, Nordland county—the largest deposits in Norway—a resource of national importance. *PNASTINA project report*, 11 pp.
- Mogaard, J.O. (1992) Geofysiske målinger fra helikopter over et område i indre Tysfjord, Nordland. *NGU Report 1992.229*, 9 pp.
- Niemela, M. (ed.) (2002) Talc-magnesite deposits in Finland. In *Magnesite and Talc—Geological and Environmental Correlations. IGCP 443, Third Field Correlation*, 49 pp.
- Nilsson, L.P. (2004) Prosjekt Linnajavri talk/kleberstein. Bulkanalyser av opprednings-konsentrater samt SEM-analyser av rågods til oppredning, m.m. *NGU Notat*, 180 pp.
- Nilsson, L.P. and Lindahl, I. (2003a) Skifer i Linnajavri-området, Hamarøy og Sørfold kommuner, Nordland. *NGU Report 2003.018*, 18 pp.
- Nilsson, L.P. and Lindahl, I. (2003b) Status for Linnajavri talkprosjekt ved årsskiftet 2002–2003. *NGU Notat*, 15 pp.
- Nilsson, L.P., Lindahl, I. and Gautneb, H. (2003) Mineralkarakterisering av talk/kleberstein fra Linnajavri-området, Hamarøy kommune, Nordland. *NGU Report 2003.027*, 209 pp.
- Nilsson, L.P., Roberts, D. and Ramsay, D.M. (2005) The Raudfjellet ophiolite fragment, Central Norwegian Caledonides: principal lithological and structural features. *Norges geologiske undersøkelse Bulletin*, **445**, 99–115.
- Pedersen, R.B. and Furnes, H. (1991) Geology, magmatic affinity and geotectonic environment of some Caledonian ophiolites in Norway. *Journal of Geodynamics*, **13**, 183–203.
- Poulsen, A.O. (1958) Industrielle mineraler og bergarter, scale 1:1,000,000, *Norges geologiske undersøkelse, Bergarkivet no. K 2675*.
- Poulsen, A.O. (1959) Navneliste til kart over Industrielle mineraler og bergarter. *Norges geologiske undersøkelse, Bergarkivet*, 90 pp.
- Raymond, L.A. (ed.) (1984a) *Melanges: their nature, origin, and significance*. Geological Society of America Special Paper, **198**, 170 pp.
- Raymond, L.A. (1984b) Classification of melanges. In Raymond, L.A. (ed.) *Melanges: their nature, origin and significance*, Geological Society of America Special Paper, **198**, 7–20.
- Rehnström, E.F. and Corfu, F. (2004) Palaeoproterozoic U-Pb ages of autochthonous and allochthonous granites from the

- northern Swedish Caledonides; regional and palaeogeographic implications. *Precambrian Research*, **132**, 363–378.
- Shaikh, N.A., Tontti, M.B. and Øvereng, O. (1987) Industrial Minerals and Rocks of the Nordkalott area, scale 1:1,000,000, *Geological Surveys of Finland, Norway and Sweden*.
- Silvennoinen, A., Gustavson, M., Perttunen, V., Siedlecka, A., Sjöstrand, T., Stephens, M.B. and Zachrisson, E. (1987) Geological map of the Nordkalott area, scale 1:1,000,000, *Geological Surveys of Finland, Norway and Sweden*.
- Skilbrei, J.R., Nilsson, L.P. and Lindahl, I. (2003) Magnetisk modellberegning av talk/klebersteinforekomst ved Cohkul (Linnajavri Nord-område), Hamarøy kommune, Nordland. *NGU Report 2003.044*, 17 pp.
- Solli, A. and Nordgulen, Ø. (2006) Berggrunnskart over Norge og kaledonidene i Sverige og Finland, scale 1:2,000,000, *Norges geologiske undersøkelse*.
- Stigh, J. (1982) Talk–magnesitforekomsten i Vietjervaratj, Vestre Padjelanta, Norrbottens Kaledonidberggrund. *SGU Report 191/1982*, 19 pp.
- Sturt, B.A. and Roberts, D. (1991) Tectonostratigraphic relationships and obduction histories of Scandinavian ophiolitic terranes. In Peters, T., Nicolas, A and Coleman, R.G. (eds.) *Ophiolite Genesis and Evolution of the Oceanic Lithosphere*, Ministry of Petroleum and Minerals, Sultanate of Oman, pp. 745–769.
- Sturt, B.A., Roberts, D. and Furnes, H. (1984) A conspectus of Scandinavian Caledonian ophiolites. In Gass, I.G., Lippard, S.J. and Shelton, A.W. (eds.) *Ophiolites and Oceanic Lithosphere*, Geological Society of London Special Publication, **13**, 381–391.
- Sundblad, K. (1986) The Stipok allochthon—an exotic terrane in the northern Swedish Caledonides. *Geologiska Föreningen i Stockholm Förhandlingar*, **108**, 309–311.
- Svenonius, F. (1895) Forskningsresor i Kvikkjokks fjälltrakter åren 1892 och 1893 med särskild hänsyn till apatitforekomster. *Sveriges geologiska undersökning*, **C 146**, 36 pp.
- Svenonius, F. (1896) Några bidrag till belysning af eruptivens betydelse för fjällbildningarna. *Sveriges geologiska undersökning*, **C 164**, 31 pp.
- Svenonius, F. (1900) Öfversikt af Stora Sjöfallets och angränsande fjälltraktens geologi. 2. Berggrunden. *Geologiska Föreningen i Stockholm Förhandlingar*, **22**, 273–322.
- Zachrisson, E. and Stigh, J. (1981) Ultramafiter i fjällen. *SGU Report to NSG. BRAP 81522*, 55 pp.

Aggregates in Norway—Properties defining the quality of sand, gravel and hard rock for use as aggregate for building purposes

Eyolf Erichsen, Arnhild Ulvik, Knut Wolden and Peer-Richard Neeb

Geological Survey of Norway (NGU), 7491 Trondheim, Norway.

E-mail: eyolf.erichsen@ngu.no

Geological knowledge of aggregate deposits is fundamental in order to achieve optimum exploitation of the resources. Two site examples, Gardermoen superficial deposit and Såt hard-rock deposit, are used to demonstrate the importance of geological knowledge. Based on information from the Database for sand, gravel and hard-rock aggregates, established at the Geological Survey of Norway (NGU), general trends for the quality, as defined by several mechanical properties, are documented for different rock types. Combined with geological information, the results show that particularly the grain size of the rock has a significant influence on the product quality.

Introduction

The Norwegian production of aggregates in 2007 was 66 million tonnes, of which about 13.4 million tonnes, mostly hard-rock aggregates, were exported (Neeb 2008). The domestic consumption has remained more or less stable, while the export has increased by 95% over the last 10 years. The aggregate industry in Norway has received increased attention as an important supplier to countries in northern Europe.

Norway's geology offers a broad variation in the quality of aggregates available for use in the building and construction industry. The quality of the aggregates is determined by different mechanical and physical test methods. The term 'quality' is not precise, but depends on the use of the aggregate. In this text, the terms 'good', 'high' or 'best quality', is used for aggregate suitable for purposes where the requirements are high, for instance in wearing course for roads with high traffic density. Aggregate with poor or low quality can still be used, for instance as filling compound. The demand for high-quality aggregates is principally for use in concrete and for road purposes as pavement. Besides cement, natural sand and gravel are the principal constituents of concrete, while hard-rock aggregates and to a certain extent crushed gravel is used mainly for pavement. For instance, asphalt pavements consist of 90–95% aggregates, whereas the rest is bitumen and filler.

The mechanical and physical properties of the aggregates determine how the material can be utilised. Different mechanical and physical test methods express different properties such as resistance against impact, crushing, wearing or polishing, and

geometrical properties such as grading, shape, angularity or flakiness. The experimental mechanical test methods model the breakdown of the material, which occur in practical use. Both the mechanical and physical properties depend on geological parameters such as grain size, grain-size distribution, grain shape, texture, mineralogy and deformation (Brattli 1992, Lundqvist and Göransson 2001).

Geological knowledge

Geological knowledge of the resource is fundamental for all forms of extraction of natural raw material. The Database for sand, gravel and hard-rock aggregates at NGU gives an overview of available resources. The data are useful for both regional and local planning, but detailed geological information is only occasionally available. Two site examples will illustrate the essential need for detailed information obtained by resource mapping of the geology.

Sand and gravel—Gardermoen

One of the largest Quaternary deposits of sand and gravel in Norway, which also is a huge groundwater resource, is located near Gardermoen, north of Oslo (Figure 1).

In 1998, a new main airport for Oslo was opened at Gardermoen. The airport and its infrastructure occupy large areas of land. Consequently, available areas for industry and trade, as well as areas designated for sand and gravel exploitation, have become scarce. However, future development of this area requires access

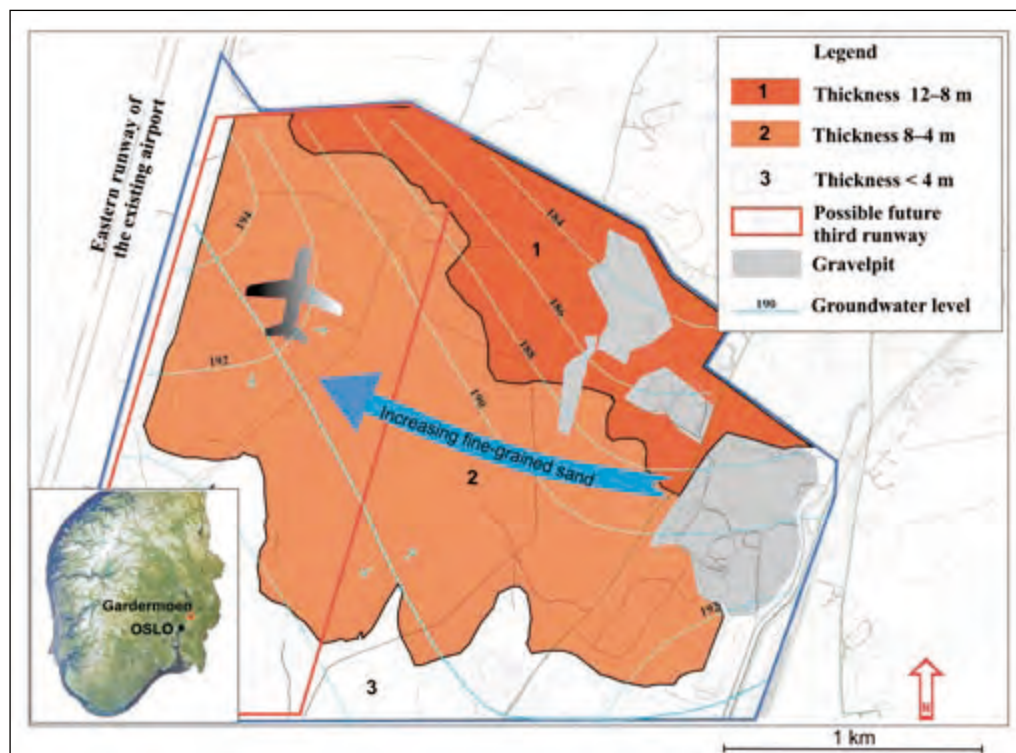


Figure 1. Variation in thickness in the investigated part of the Gardermoen sand and gravel deposit.

to such resources. Hence, there has been and will continue to be a need to optimise land-use planning in the area.

NGU has been involved in planning the future extraction of the most important part of the deposit before, during and after the construction of the airport (Wolden 2002). Fundamental tools in this work have been the existing geological map of the Quaternary deposits of the area (Longva 1987, Østmo and Olsen 1978) and comprehension of the land-forming geological processes in this area. Glaciofluvial processes have transported the sand and gravel in this deposit from its origin in Gudbrandsdalen (Østmo 1977). The deposit consists of 50% Precambrian rocks with the rest being Eocambrian sandstone and quartzite. Usually, these are regarded as strong rocks, which will meet the mechanical standards for use as aggregate in both concrete and asphalt. This assumption has been confirmed by mechanical tests. Investigation of the grain size, rock types and mineral content of the sand and gravel has also been important for identifying potential confines in the use of the material as aggregate.

In addition to quantity, knowledge about the thickness of the deposit is also important to ensure optimum utilisation of the resource. During extraction, it is vital that there is enough material remaining above the groundwater level to maintain filter effects and avoid contamination of the groundwater. Seismic investigations and georadar surveys have been used in order to obtain information about the deposit thickness and the depth to groundwater. These methods provide important information about layers and structures as well as confirming the exact depth to groundwater. They can also be used to estimate the expected average grain size in the layers. Drilling, shaft digging and sampling have supported the interpretation of the geophysical methods. In addition, a grab-dredger for depth penetration has been used to gain visual estimates of both volume and quality of the deposit. The sound picture during drilling, velocity, flush pressure, and knocks are important for the interpretation of the georadar profiles.

The data were collected in small areas and were then extrapolated to estimate the thickness together with the groundwater level of the deposit (Figure 1). Subsequently, this will be utilised in the municipal development plans to ensure that the right quality aggregate is produced for use in the correct areas. For instance, one alternative for a planned third runway is located in an area with fine-grained sand, which is normally only used

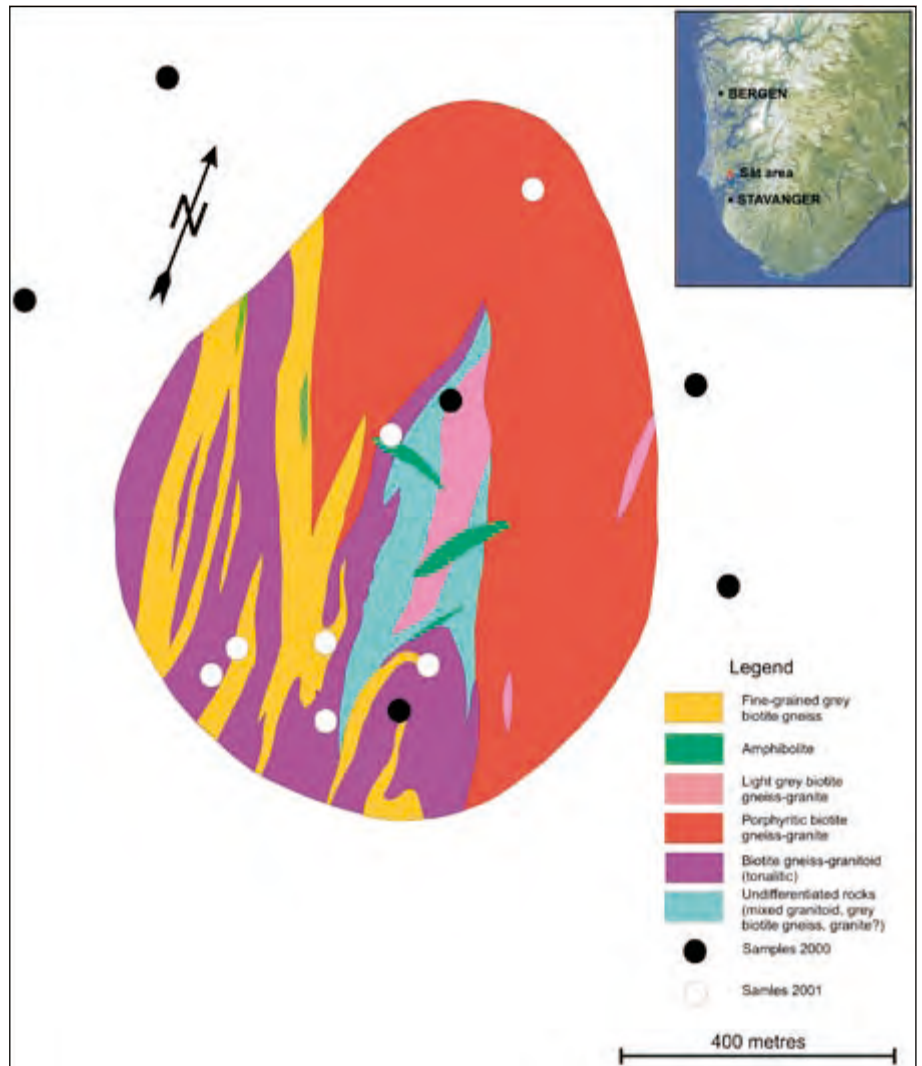


Figure 2. Geological map covering the potential extraction area of Sât (Marker and Erichsen 2002).

for filling compound (Figure 1). The thickest part and the best quality of the material are available at the northeastern part of the investigated area of the deposit. This area has therefore been earmarked for future aggregate production.

Hard-rock aggregate—Sât

The Sât site is located in Tysvær municipality, Rogaland county, in southwest Norway (Figure 2). The operator of a nearby existing quarry, where most of the production is exported, wanted to increase the reserves by establishing a new extraction area for hard-rock aggregates. The area was preliminary examined by sampling of material for mechanical testing in 2000 (Holm 2000). The samples were collected without any detailed references to the bedrock geology other than a regional geological map in 1:250,000 scale. Among various mechanical test methods indicating rock properties, the Los Angeles value was considered to be most relevant for potential export of the aggregates. Many samples showed Los Angeles values greater than 20 (Figure 3), which the operator believed was too high for exporting high-quality material to the European market.

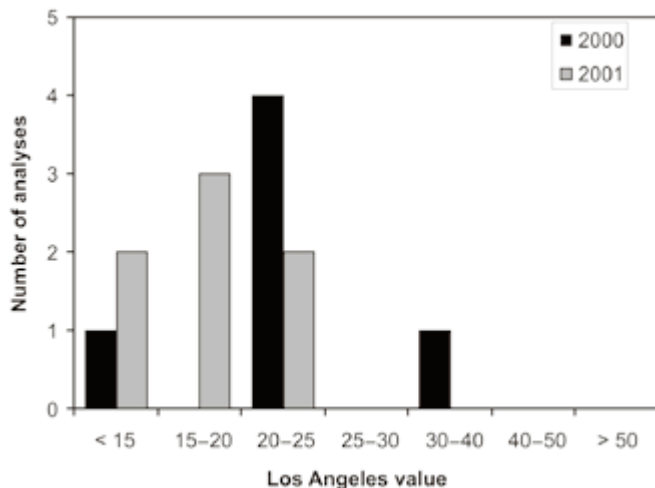


Figure 3. Variation in the Los Angeles value for samples collected in 2000 and 2001 from the potential extraction area of Sât (Marker and Erichsen 2002).

Despite the negative results, the operator still considered the area to be of interest and wanted to map the area geologically in detail before any final decision was made. The mapping (Marker and Erichsen 2002) showed that the Sât area is much more complex than previously imagined (Figure 2). Formerly, porphyritic biotite gneiss-granite was known to form the north-eastern half of the prospect. In addition to this, the new investigation indicated that the southwestern half consists of veined, fine-grained grey gneisses, which are intruded by porphyritic to even-grained, grey biotite granitoid gneisses. The two rock types occur in roughly even proportions. The different types of biotite gneiss-granites and gneiss-granitoids are generally well foliated to mylonitic, which give a textural variation in addition to a compositional variation. Based on the new geological information, further mechanical sampling was carried out in 2001, however, this time with more promising results (Figure 3).

The Los Angeles values for the porphyritic biotite gneiss-granite are on average similar to those for the Espevik gneiss-

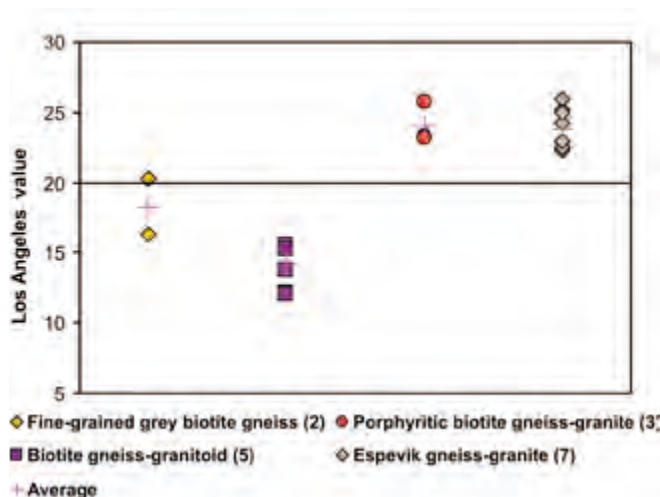


Figure 4. Variation in the Los Angeles value for different rock types (Marker and Erichsen 2002).

granite (Figure 4), where the existing quarry is located. The rock types within the southwestern half of the prospect, mainly fine-grained grey gneisses and grey biotite gneiss-granitoids, show much better results for the Los Angeles test. The conclusion from the new sampling and mechanical testing based on the geological map was that the rocks in the Sât prospect are a significant resource, which satisfied the requirements for the producer.

Mechanical properties

Various test methods are used to determine the mechanical quality of aggregate in Norway. The Norwegian impact test (Statens vegvesen 1997a, kapittel 14.451), the Los Angeles test (Norwegian Standard, NS-EN 1097-2) and the Nordic abrasion test (Norwegian Standard, NS-EN 1097-9), measure how much fines are produced, the Norwegian abrasion test (Statens vegvesen 1997b, kapittel 14.454) measures the resistance against wearing, while the polishing test (Norwegian Standard, NS-EN 1097-8) measures the polishing. Except for the polishing test, the quality improves when the value of the test result decreases.

Hard-rock aggregates and sand/gravel are used separately or in a mixture depending on their different properties, especially due to mechanical homogeneity and shape, which can be favourable for specific applications. Different aspects for the two types of raw material define the quality of the material where the geological genetic history and other geological parameters play an important role. They are therefore discussed separately.

Sand and gravel

The quality of sand and gravel varies both within and between deposits. The distinguishable difference that separates sand and gravel from hard rock is mainly the heterogeneity of the material. Especially gravel may contain several types of rock, both weak and strong. The sand and gravel deposits commonly mirror the bedrock. Areas containing weak rocks usually result in deposits that have weak material strength.

In the middle part of Norway, weak Cambro-Silurian rocks like phyllite, schist, greywacke and greenstone are abundant. In the western part of Norway, the bedrock typically consists of stronger Precambrian gneisses of variable composition. Analyses from the Database for sand, gravel and hard-rock aggregates at NGU show that the average value for the Norwegian impact test, the Nordic abrasion test and Los Angeles test is better (lower number) in the western part of Norway than in the middle part (Table 1).

The transport distance and how much the material is processed by water will also influence the material quality. In general, alluvial deposits (Table 2) have better mechanical and abrasive properties than glaciofluvial deposits (Table 1) and tills. Water has washed and worn weaker particles of alluvial deposits, and the grains obtain a rounder shape.

Table 1. Analyses of glaciofluvial deposits. Average values.

Glaciofluvial deposits	Norwegian impact value (n)	Nordic abrasion value (n)	Los Angeles value (n)
Mid-Norway	50.5 (77)	19.0 (29)	28.8 (12)
Western Norway	46.2 (123)	13.5 (27)	26.0 (22)

n = number of analyses

Table 2. Analyses of alluvial deposits. Average values.

Alluvial deposits	Norwegian impact value (n)	Nordic abrasion value (n)	Los Angeles value (n)
Mid-Norway	46.9 (8)	15.1 (3)	24.3 (2)
Western Norway	45.4 (10)	– (0)	30.3 (2)

n = number of analyses

Glaciofluvial deposits may have very short transport distances so angular and flaky grains normally will dominate the material. Then, if the source material is weak, there is a large possibility that the resulting superficial deposits may not exhibit good quality.

Hard-rock aggregates

NGU's Database for hard-rock aggregates contains information from nearly 1500 sites in Norway and cover a wide spectrum of rock types that are assumed to be suitable as aggregate for building purposes. Most of them have been sampled and analysed for mechanical and physical properties (Table 3). Lithological identification is based on a simplified thin-section analysis (Norwegian Standard, NS-EN 932-3). The information from the database is used to evaluate the quality properties for the

rocks given by different mechanical test methods. The standard methods for testing mechanical properties used in Norway concerning requirements today are the Los Angeles test, the Nordic abrasion test and the polishing test. Earlier, there were requirements also to the Norwegian impact test and the Norwegian abrasion test. For the existing standard test methods, analyses from the database show a wide variation both within and between the different rock types (Figures 5a–c).

Strength tests

The strength of the aggregate can be measured by different test methods. Until recently, the Norwegian impact test was the standard test for measuring brittleness. This method is replaced by the Los Angeles test, which is the new European Standard test method for determination of resistance to fragmentation. NGU's data verify a satisfying correlation between the two methods (Figure 6a). The Norwegian impact value is defined as the amount of fines (< 8 mm) produced, while the Los Angeles value is measured with a 1.6 mm sieve. By instead using a 2 mm sieve for the Norwegian impact test (Norwegian impact value < 2 mm), the correlation coefficient increases from 0.90 to 0.96 (Figure 6b).

The different types of rock classified in Table 3 show a wide range in mechanical quality for both of the two mechanical strength tests (Figures 7a, b). The variation is large and overlapping between the main types of rock. On average, extrusive/hypabyssal rocks show the lowest values, i.e., best quality, followed by sedimentary, plutonic and metamorphic rocks. So far, it can be documented that grain size is the factor that has the largest influence on the strength of the rocks. Both the extrusive/hypabyssal and the sedimentary rocks are characterised by fine to medium grain size compared to the two other types (Figure 8). For the plutonic rocks, the effect of grain size on mechanical strength is obvious (Figures 9a, b), increasing grain size leading to increasing Norwegian impact value and Los

Table 3. Rock types analysed for mechanical and physical properties. For each type the number of samples is given in parentheses. Data from NGU's Database for hard-rock aggregates. Nomenclature according to Norwegian Standard, NS-EN 932-3.

Igneous		Sedimentary		Metamorphic
<i>Plutonic</i>	<i>Extrusive/Hypabyssal</i>	<i>Clastic</i>	<i>Chemical and biogenic</i>	Amphibolite (43)
Anorthosite (55)	Basalt (35)	Arkose (22)	Dolomite (1)	Banded gneiss (12)
Charnockite (3)	Greenstone (56)	Breccia (2)	Limestone (18)	Eclogite (30)
Diorite (21)	Rhyolite (50)	Greywacke (33)		Mica-gneiss (27)
Gabbro (282)	Tuff (1)	Conglomerate (9)		Gneiss (255)
Granite (140)	Diabase (11)	Sandstone (55)		Granitic gneiss (174)
Granodiorite (46)	Porphyry (19)			Hornfels (43)
Hyperite (7)	Rhomb porphyry (32)			Quartzite (48)
Larvikite (16)				Marble (9)
Mangerite (9)				Mylonite (64)
Monzonite (13)				Augen gneiss (29)
Norite (19)				
Pyroxenite (3)				
Syenite (24)				
Trondhjemite (76)				

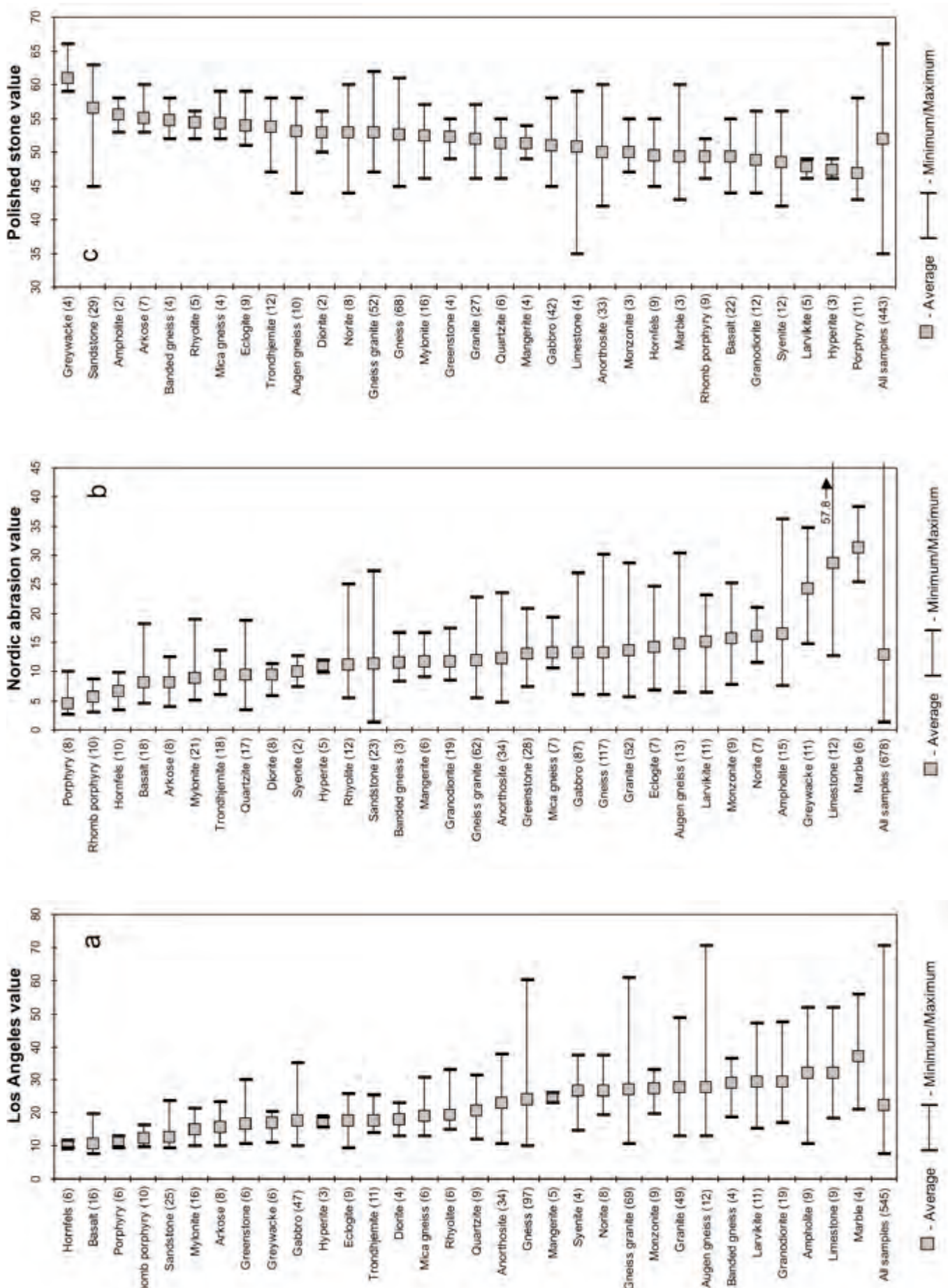


Figure 5. Variation in (a) the Los Angeles value, (b) the Nordic abrasion value, and (c) the polished stone value for different rocks. Number of analyses in parentheses.

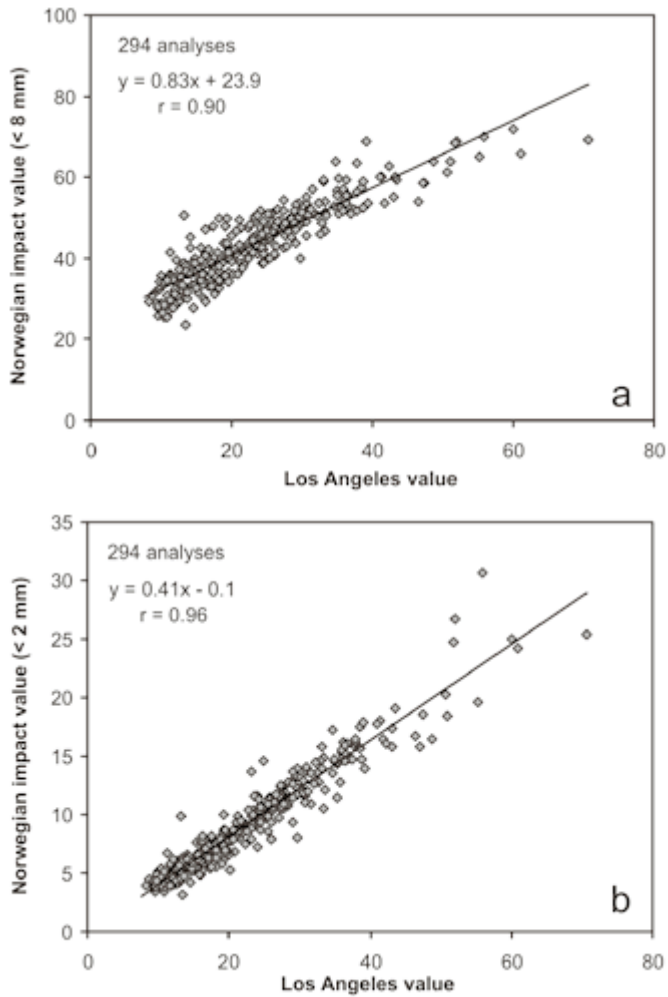


Figure 6. Los Angeles values versus Norwegian impact value (a) < 8 mm, (b) < 2 mm. Analyses from NGU's Database for hard-rock aggregates.

Anges value. For Norwegian basic igneous rocks, the same effect has been documented earlier (Brattli 1992).

Wearing tests

The Norwegian abrasion test was replaced by a new Nordic abrasion test, in accordance with the European Standardisation program for test methods. The methods are supposed to model the wearing due to the use of studded tires. Because the variation in the test results increases with higher values for the two parameters, the correlation between the test methods is not so obvious (Figure 10). Compared to the strength tests (Figures 6a, b), the two different wearing tests can therefore not reflect the actual same mechanical property.

The overlap between the main rock types is obvious also for the wearing tests (Figures 7c, d). For the Nordic abrasion test, extrusive/hypabyssal rocks give the lowest average values, similar to both the strength tests. The dominantly fine to medium grain size of extrusive/hypabyssal rocks (Figure 8) may be one reason for this observation. Despite the dominantly fine to medium grain size for the sedimentary rocks, they show the opposite to extrusive/hypabyssal rocks, on average the highest values for both

the tests, i.e., poorest quality (Figures 7c, d). Sedimentary rocks usually contain hard minerals like quartz and feldspar, but usually they also contain soft minerals like chlorite, mica and calcite. These minerals are known to be little resistant against wearing.

For plutonic rocks, the Nordic abrasion value gradually achieves lower values (i.e., better quality) with decreasing grain size (Figure 9c), similar to the strength tests (Figures 9a, b). Alteration effects, changing the mineral content of the rock, can also influence the abrasion value. Primary gabbro seems to have lower abrasion value than metagabbro (Figure 11). For the Norwegian abrasion value, some rocks (norite, diabase) show a strong positive trend with increasing pyroxene content, while for other rocks (eclogite) amphibole has a weak negative effect (Figure 12).

Polishing test

Sedimentary rocks have on average the highest polished stone value (PSV), i.e., best quality (Figure 7e), but the variation within each main rock type is large and overlapping between the different types. In connection to quality, the polishing effect seems to have an inverse correlation to the Nordic abrasion value. For sandstones, this relation is especially distinct (Figure 13). The same inverse relation has earlier been documented for arenaceous rocks (Hawkes and Hosking 1972). The polished stone value becomes higher for Devonian sandstones (Figure 14) when the amount of hard minerals (quartz, feldspar and epidote) decreases at the expense of increasing amount of soft minerals (chlorite, mica and calcite). Mohs' hardness scale is used to weight and calculate the amount of hard and soft minerals. For Devonian sandstones, it seems that the polishing test expresses the roughness of the surface of the test material. A good mixture between hard and soft minerals gives a rough surface, which reduces polishing.

Conclusions

Generally, it is difficult to obtain any precise accordance between mechanical properties and geological parameters. The rough estimate of the geological parameters, which has been used for NGU's data, can be one reason for this, but also great variation in the mechanical properties has influence. Often, the variation in mechanical properties is greater within a specific rock type than between different rock types. Due to this variation it is often just possible to gain rough trends and precise statistical conclusions cannot be drawn.

For sand and gravel deposits, both the bedrock source and the genetic history of the deposit critically influence the quality as aggregate. In general, alluvial deposits show better mechanical quality than glaciofluvial deposits.

Extrusive and hypabyssal rocks show best quality with regard to both strength and wearing. So far, grain size seems to be the most provable geological parameter influencing the quality of the aggregate. A rule of thumb is that the quality improves with decreasing grain size.

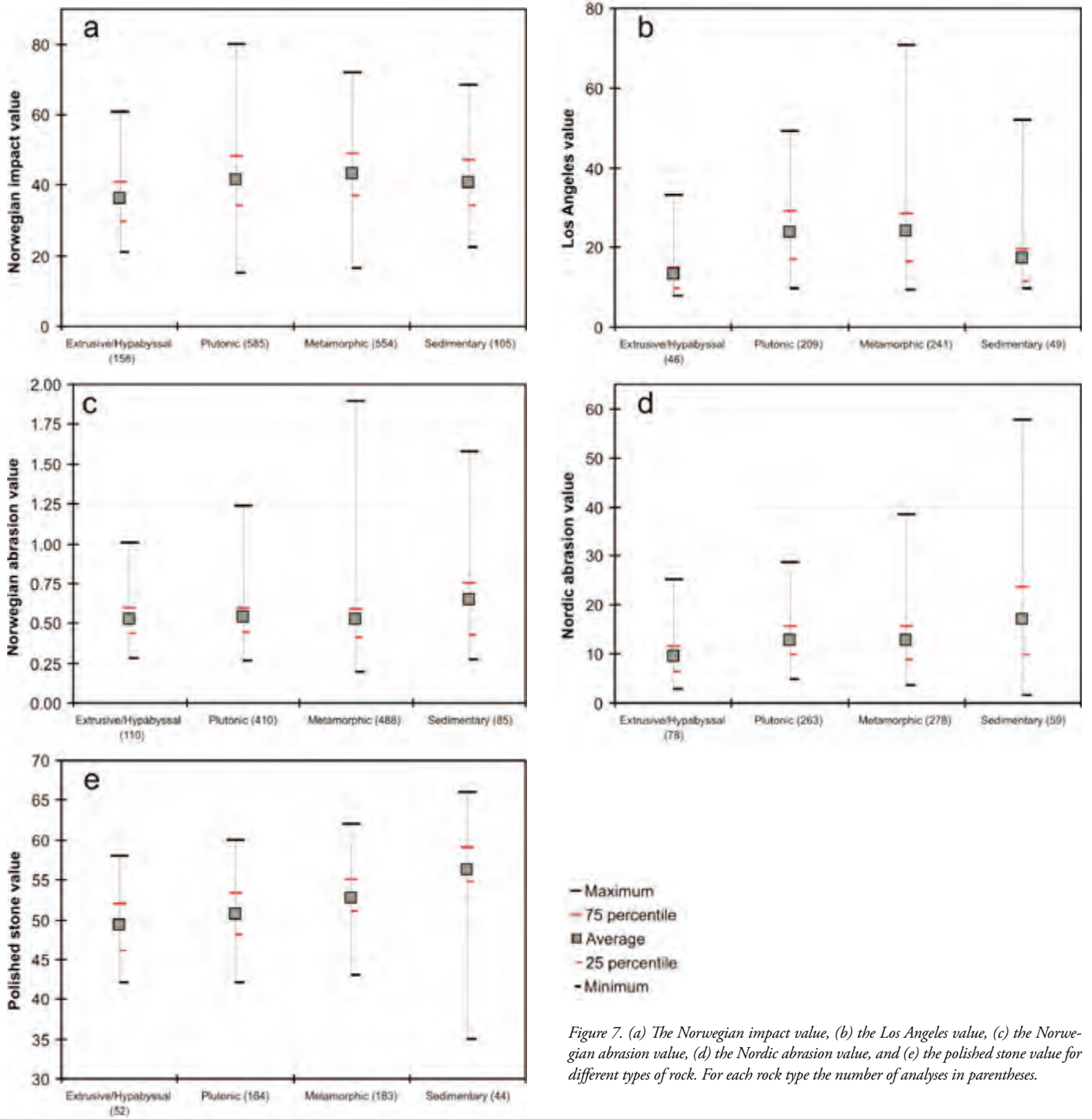


Figure 7. (a) The Norwegian impact value, (b) the Los Angeles value, (c) the Norwegian abrasion value, (d) the Nordic abrasion value, and (e) the polished stone value for different types of rock. For each rock type the number of analyses in parentheses.

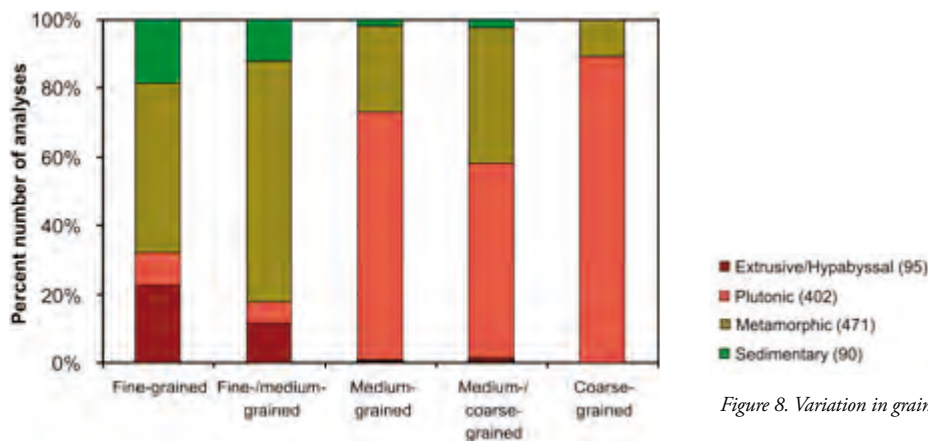


Figure 8. Variation in grain size for different types of rock.

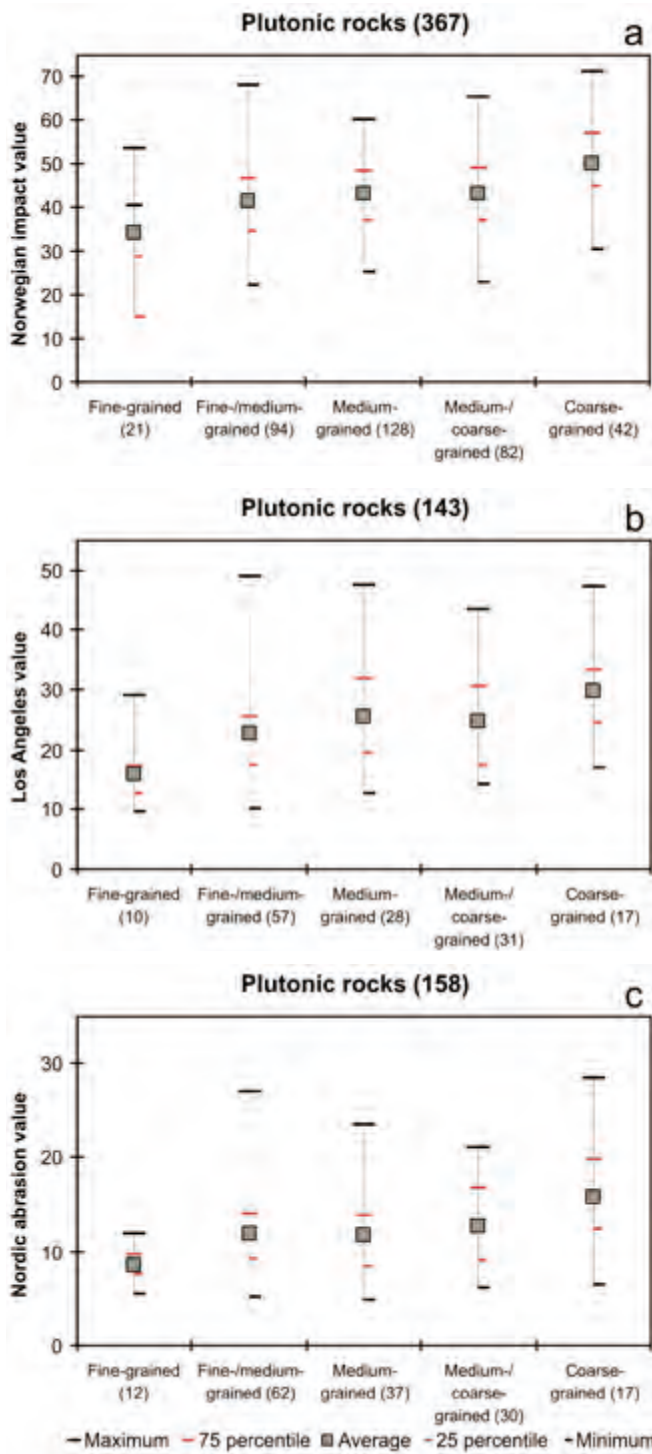


Figure 9. Variation in (a) the Norwegian impact value, (b) the Los Angeles value, and (c) the Nordic abrasion value with grain size for plutonic rocks. Number of analyses in parentheses.

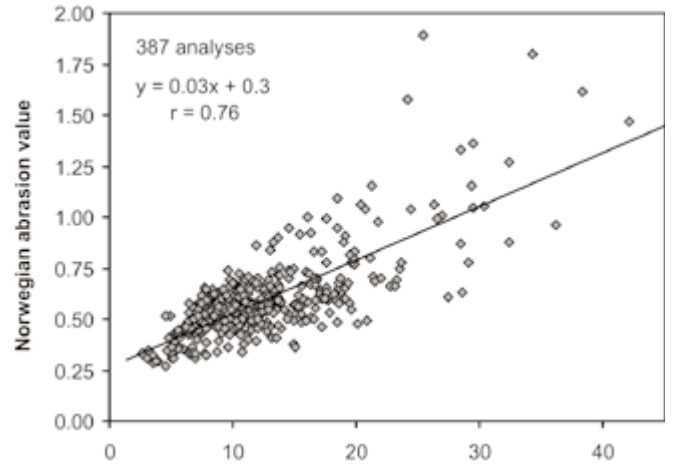


Figure 10. Nordic abrasion value vs. Norwegian abrasion value. Analyses from NGU's Database for hard-rock aggregates.

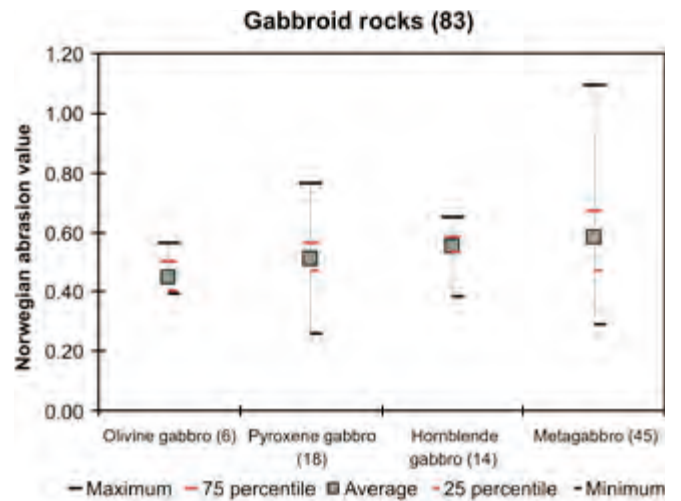


Figure 11. Effect of alteration on the Norwegian abrasion value for gabbroid rocks. Number of analyses in parentheses.

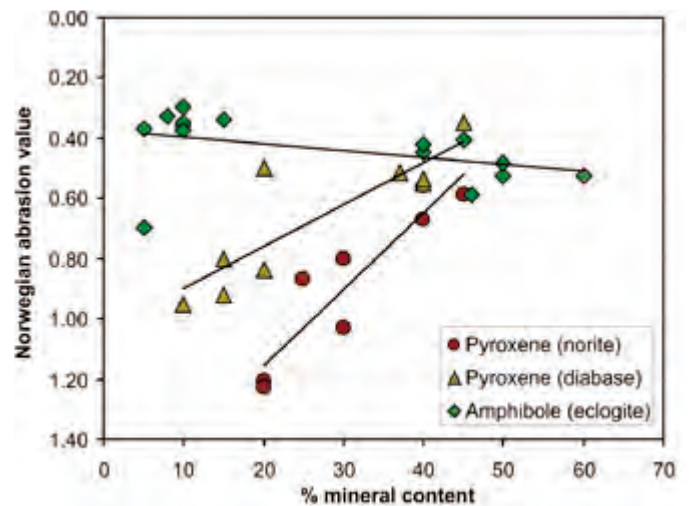


Figure 12. Variation in the Norwegian abrasion value depending on the mineral content for different rock types.

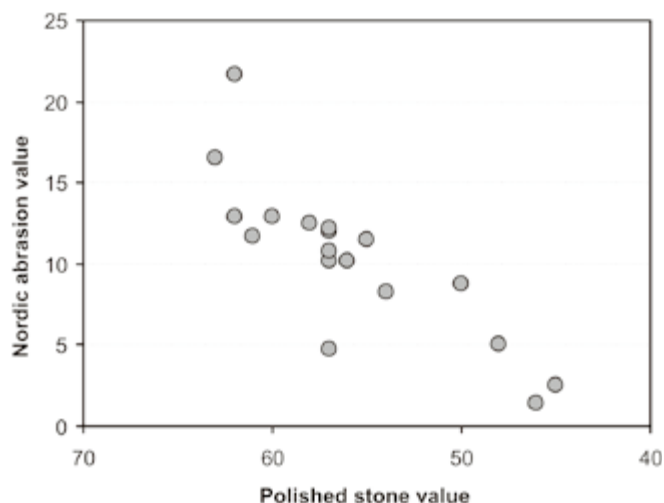


Figure 13. Polished stone values vs. Nordic abrasion value for sandstones.

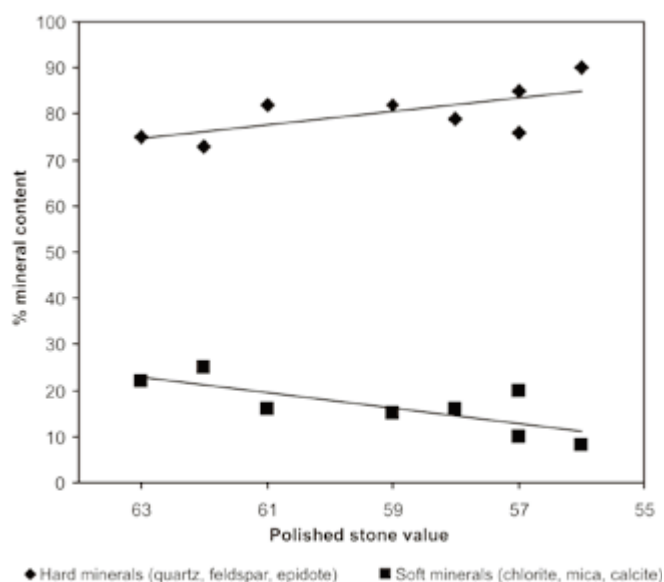


Figure 14. The variation in the polished stone value for Devonian sandstones depending on the mineral content.

Sedimentary rocks resist polishing best. Especially for Devonian sandstone, a suitable mix of hard and soft minerals increases the polishing resistance.

For sand and gravel deposits, different investigation methods are necessary to record both volume and the quality of the aggregate. A good documentation of the variation in the deposit, as shown for the Gardermoen superficial deposit, is fundamental for all sustainable planning.

For areas with a complex geology like Sât, it is crucial to have good geological control before sampling is carried out for examination of the mechanical properties.

Acknowledgements

The authors are grateful to Rolv Dahl and Berit Davies for constructive comments and correcting the English language of the

first draft of the manuscript. Mogens Marker is thanked for mapping the geology at the Sât prospect. Useful comments and corrections by Trond Slagstad and the reviewers, Lars Persson and Jean Côté are gratefully acknowledged.

References

- Brattli, B. (1992) The influence of geological factors on the mechanical properties of basic igneous rocks used as road surface aggregates. *Engineering Geology*, **33**, 31–41.
- Hawkes, J.R. and Hosking, J.R. (1972) British arenaceous rocks for skid-resistant road surfacings. *Report LR 488, Road Research Laboratory, Crowthorne*, 40 pp.
- Holm, J.V. (2000) Nytt uttaksområde Sâta—Geologiske undersøkelser. Felt- og laboratorieundersøkelser. *Noteby. Oppdrag/rapportnr. 101046-2*.
- Longva, O. (1987) Ullensaker, 1915 II. Beskrivelse til det kvartærgeologiske kartet, scale 1:50,000. *NGU Skrifter*, **76**, 39 pp.
- Lundqvist, S. and Göransson, M. (2001) Evaluation and interpretation of microscopic parameters vs. mechanical properties of Precambrian rocks from the Stockholm region, Sweden. In Stamatakis, M., Georgali, B., Fragoulis, D. and Toumbakari, E.E. (eds) *Proceedings of the 8th Euroseminar on Microscopy Applied to Building Materials, Athens, Greece*, pp. 13–20.
- Marker, M. and Erichsen, E. (2002) Geological and mechanical investigation of the Sât extraction prospect for hard rock aggregates in Espevik, Rogaland. *NGU Report 2002.007*, 31 pp.
- Neeb, P.-R. (2008) Norway's coastal aggregates. Export in 2007 and potential. *NGU Report 2008.044*, 30 pp.
- Norwegian Standard (NS-EN 932-3) Tests for general properties of aggregates. Part 3: Procedure and terminology for simplified petrographic description.
- Norwegian Standard (NS-EN 1097-2) Tests for mechanical and physical properties of aggregates. Part 2: Methods for the determination of resistance to fragmentation.
- Norwegian Standard (NS-EN 1097-8) Tests for mechanical and physical properties of aggregates. Part 8: Determination of the polished stone value.
- Norwegian Standard (NS-EN 1097-9) Tests for mechanical and physical properties of aggregates. Part 9: Determination of the resistance to wear by abrasion from studded tyres: Nordic test.
- Statens vegvesen (1997a) Håndbok 014—Laboratorieundersøkelser, kapittel 14.451 Flisighet og sprøhet.
- Statens vegvesen (1997b) Håndbok 014—Laboratorieundersøkelser, kapittel 14.454 Abrasjonsmetoden.
- Wolden, K. (2002) Undersøkelse av sand- og grusressursene på Gardermoen, Ullensaker kommune. *NGU rapport 2002.030*, 15 pp.
- Østmo, S.R. (1977) Rapport vedrørende kvartærgeologisk kartlegging med vekt på registrering og undersøkelse av sand- og grusforekomster i Ullensaker kommune, Akershus fylke. *NGU rapport nr. O-75045*, 102 pp.
- Østmo, S.R. and Olsen, K.S. (1978) Nannestad, Quaternary geology map 1915 III, scale 1:50,000. *Norges geologiske undersøkelse*.

From Hyllestad to Selbu: Norwegian millstone quarrying through 1300 years

Tor Grenne¹, Tom Heldal¹, Gurli B. Meyer¹ and Elizabeth G. Bloxam²

¹Geological Survey of Norway (NGU), 7491 Trondheim, Norway.

²Institute of Archaeology, University College London, 31–34 Gordon Square, London WC1H 0PY, England, UK.

E-mail: tor.grenne@ngu.no

‘Industrial-scale’ millstone production in Norway dates back to at least AD 700. Recent detailed mapping in the Hyllestad and Selbu areas has identified extensive quarry landscapes, which together demonstrate the development in ‘industrial scale’ millstone production over a period of 13 centuries. Based on geological characteristics, traces of quarrying techniques and archaeological dating, it is possible to relate different stages within this history to technological development, population change, market demands and other influences from the surrounding society. Production at Hyllestad, which dominated the Norwegian millstone market from the pre-Viking Age, was based on carving of relatively soft but massive garnet-kyanite-muscovite schist directly from the bedrock in shallow quarries, a technique that was essentially similar to Iron Age soapstone extraction. A change to a more centralised and technologically advanced production in larger and deeper quarries occurred in the 12th century, possibly introduced by professional stonemasons connected to the establishment of monasteries and churches. A marked decline in activity at Hyllestad after the High Middle Ages was followed by the rise of millstone production at Selbu in the 16th century, based on wedging of more easily cleavable staurolite-biotite schist. It is likely that this dramatic change in market dominance was influenced by the partial collapse of social and trade structures following the Black Death and recurrent plague outbreaks throughout the late 14th and early 15th centuries, when the millstone trade was practically in ruins due to the small population size and the market was left open for ‘newcomers’ when population and trade recovered in the 16th century. Equally important was the increasing demand for larger and more durable millstones caused by the gradual change from querns to water mills and from farm mills to village mills and commercial trade mills, a demand that could readily be met by the geological conditions that existed in the Selbu area.

Introduction

Millstone quarries are distributed throughout Norway and each quarry area produced stones that had specific usage attributes. Through history, the significance of the different qualities—and hence the demand for millstones from the different areas—varied with developments in milling technology as well as regional and temporal changes in the grain types produced. In addition, the overall production of millstone was strongly related to population development, because grain has always been a fundamental part of our diet.



Figure 1. Locations of major millstone-quarry areas in Norway.

Also significant for millstone demand was technological development. In Scandinavia, the rotating hand querns gradually took over from the traditional saddle querns in the Roman and Germanic Iron Age¹, and by the beginning of the Viking Age hand querns were fairly standardised with a stone diameter of 35–60 cm and a thickness of 10–20 cm of the upper stone ('runner') (Carelli and Kresten 1997).

Several authors have addressed the question of when water mills were introduced in Norway (Statens Kornforretning 1934, Grieg 1960, Gulbrandsen 1969, Carelli and Kresten 1997,

Baug 2002). Baug (2002) suggested that in Hyllestad the production of stones for water mills was established in the Early Middle Ages, which is also supported by archaeological records from Lejre, near Roskilde in Denmark (Carelli and Kresten 1997). However, according to Baug (2002) it is not unlikely that water millstones were produced in Hyllestad already in the late Viking Age. Note that in English literature the terms 'quern' and 'mill' generally refer to hand-driven and water-driven types, respectively. The Norwegian equivalent of the word quern—kvern—traditionally also included certain water-driven constructions, like those colloquially referred to as 'Norse Mills' ('kall-kvern' in Norwegian). For simplicity, in the following we will use 'mill' and 'millstone' both for hand-turned and for water-driven types. The size of the millstones in all types of early, essentially farm-based, water-driven mills was between 60 and 120 cm (Baug 2002), i.e., in general significantly larger than hand millstones.

Medieval laws and tax systems urged farmers to bring their grist to larger village mills, which led to a demand for larger and more durable millstones. Professional millers are first mentioned in King Magnus Lagabøte's (meaning Law Mender) Municipal Law of 1276 (see Grieg 1960). Commercial trade mills were established after the 18th century and gradually replaced most of the farm and village mills, further increasing the demand for large and durable millstones. More advanced industrialisation towards the end of the 19th century included artificial millstones and roller mills, and by the early 20th century production of natural millstones came to an end (Statens Kornforretning 1934).

Norwegian millstone-quarry landscapes

For more than one and a half millennia, good raw materials for the manufacturing of rotating millstones has been sought after and quarried in Norway, leaving traces in the landscape of one of the longest-lasting extractive industries in the country. Certain mica schists that had a knobby surface due to the presence of garnet or staurolite porphyroblasts² proved to be of particularly good quality and resulted in huge quarry landscapes, each of them active for many centuries. Five such quarry landscapes stand out as particularly important production sites, including the two case studies presented in the present paper—the Hyllestad and the Selbu quarry landscapes (Figure 1).

Production in Hyllestad dates back at least to the 8th century (Germanic Iron Age) and peaked in the Early to High Middle Ages (12th to 14th century) (Baug 2002). The decline in production in Hyllestad was followed by a rise in production at Selbu in the 16th century (Friis 1632), after which time the

¹ Historical time periods according to Scandinavian subdivision; i.e., Pre-Roman Iron Age: 500 BC–AD 0; Roman Iron Age: AD 0–400; Germanic Iron Age: AD 400–800; Viking Age: AD 800–1050; Early Middle Ages: AD 1050–1200; High Middle Ages: AD 1200–1400; Late Middle Ages: AD 1400–1536.

² *Porphyroblast* is a geological term for a relatively large crystal that is surrounded by a finer-grained matrix, formed by recrystallisation of the rock during metamorphism.

Selbu millstones totally controlled the Norwegian market for nearly 400 years (Statens Kornforretning 1934). Together, these quarry landscapes provide insight into a continuous, more than 1300-year history of technological progress and the role of early industry in the developing community.

Even though millstone production has been a very important industry over a long period, research on the subject is limited. One reason may be the lack of historical sources connected to the stone-extraction industries in general, in contrast to the post-medieval mining of metal ore deposits. The only exception is Selbu, where there are significant amounts of written records from the 19th and early 20th century quarrying, some of which were collected and published by Rolseth (1947). This unique material from Selbu provides important insight into the later stages of millstone production. Due to the historical records, interest and knowledge of the site have been kept alive in the local community in Selbu. This knowledge was an essential argument for the archaeological excavations of old quarry settlements that were threatened by flooding from a planned power plant reservoir in the 1970s (Alsvik et al. 1981).

In Hyllestad, historical records are almost completely absent. However, interest in the site has gradually grown in the community over the last decades, resulting in several locally based books and brief accounts (e.g., Rønneseth 1977, Thue 2000, Waage 2005, see also reports from Hyllestadseminaret 2004 and 2005 at <http://kvernstein.no/>). Some knowledge of the latest quarrying was achieved through interviews with elderly people (see http://www.nrk.no/nyheter/distrikt/nrk_sogn_og_fjordane/fylkesleksikon/1682747.html) who still remembered the millstone production. Archaeological excavations carried out by Irene Baug in her M.Sc. work provided the first evidence of Viking Age quarrying (see Baug 2002).

Based on present knowledge, Selbu and Hyllestad were by far the largest of the Norwegian millstone producers, and in both areas their significance as cultural heritage sites has stimulated new research that is still in progress. In contrast, little research has been done on the other quarry landscapes. A limited archaeological rescue excavation was recently carried out in a quarry site at Saltdalen, giving early 11th century radiocarbon dates (Helberg 2007). The site has also been partially mapped by Titland (2003, see also http://www.saltdal.kommune.no/Kvernsteinsbruddene_i_Saltdal). For other sites shown in Figure 1, work is limited to short accounts, for example in annuals of local history groups (e.g., Brekken 1980, Sognnes 1980, Monssen 1997, Krokvik 1999).

Also, the use and distribution of millstones from different sources is largely unknown, and provenance studies of ancient millstones found in archaeological contexts throughout Norway remain to be done. One exception is a study carried out by Carelli and Kresten (1997) providing evidence for the extensive use of Hyllestad millstones in southwest Sweden and Denmark in the Viking Age and Middle Ages. Another exception is a governmental registration of all mills in Norway in 1919, which showed that at that time Selbu millstones were used in 89% of

Norwegian mills (Statens Kornforretning 1934).

A study of millstones from the Iron Age farm at Ullandhaug near Stavanger (Figure 1), dating from AD 350 to 550, was carried out by Dahl (1986). Interestingly, rotating hand millstones found in the settlement seem to have been used contemporaneously with the 'old fashioned' saddle quern, and the site may represent the oldest use of rotating mills in Norway. Apparently, only gneiss and other local rocks were used (Dahl 1986), none of them resembling the rocks from the major millstone-production areas. A brief inspection of artefacts at the Archaeological museum in Stavanger by two of the present authors (TH and GBM) in January 2007, suggests that these millstones were made largely from local boulders. Thus, the millstones at Ullandhaug seem to represent the early precursor to the more standardised millstone production starting a few hundred years later.

Hyllestad

Previous research and historical sources

Millstone quarrying has made a significant impact on the landscape in Hyllestad and must have been an important part of the community's identity over hundreds of years. Nevertheless, this activity became absent in the collective memory of the community in an amazingly short period of time. Ottar Rønneseth (1968) 'rediscovered' the millstone quarries and understood their significance in the 1960s. After shipwrecks had been localised along the west coast of Norway with cargos of millstones from Hyllestad (Figure 2) (Hansen 1991), marine archaeology was carried out along Åfjorden in Hyllestad (Figure 3). This led to the discovery of several harbours where the stones had been loaded onto boats (Hansen 1997).

A provenance study by Carelli and Kresten (1997) demonstrated that Hyllestad millstones were widely distributed in settlements from the late Viking Age and early medieval times in Denmark and south Sweden. Specifically, they were



Figure 2. Hyllestad millstones found in a shipwreck. Whetstones (in the background) were placed in-between the millstone cargo for support during transport.



Figure 3. Map of the Hyllestad area showing distribution of quarries and names of the quarry landscapes.

predominant among the early medieval millstones used in the town of Lund in southern Sweden (Danish until 1658). Excavations in Hyllestad suggest that the earliest quarrying dates back to at least AD 700, with a peak between the 12th and 14th century and only minor extractions thereafter (Baug 2002).

At some stage after the Middle Ages, the production techniques changed from carving the millstones directly from the bedrock, to using wedges and, later, black powder for the primary extraction of blocks. Quarries near Rønset (Figure 4), where powder was evidently used, were abandoned in 1750 (Rønneseth 1968) and denote that blasting techniques were introduced already in the first half of the 18th century. Quarrying with powder continued in Hyllestad until 1930, when the last millstone was made.

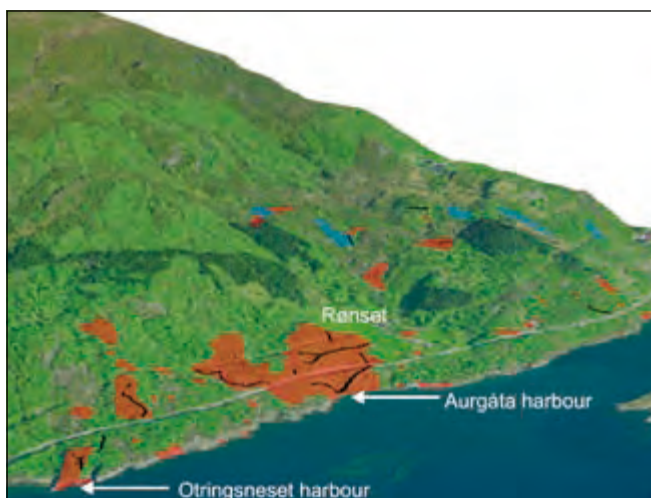


Figure 4. Perspective model of the Rønset quarry area, Hyllestad (Rønset farm is seen in the centre of the image). Red colour: quarries where millstones have been carved directly from bedrock, blue colour: quarries where blasting was applied for primary extraction. Black lines are ancient quarry roads and tracks.

One of the important milestones in Hyllestad millstone production was the introduction of water mills in Norway. Baug (2002) dates the first production of water millstones (60 to 120 cm in diameter) to around AD 1100. Before that, only hand millstones (35 to 60 cm) were produced. However, production of hand millstones continued also after water mills were introduced and probably remained an important product for a long time.

Not only millstones were produced in Hyllestad in the Middle Ages, but also several of the large stone crosses from the 11th century found at various locations along the west coast of Norway (Baug 2002). The schist from Hyllestad was also used for grave slabs and a range of domestic purposes. Traces of such non-millstone production are seen in several of the millstone quarries (Figure 5).

Since 1995, efforts in the local community along with multi-disciplinary research (see Heldal and Bloxam 2007 and reports from Hyllestadseminaret 2004 and 2005 at <http://kvernstein.no/>) have contributed in re-establishing Hyllestad as a ‘millstone community’ and an outdoor museum (‘The Millstone Park’), and several successful educational and promotional activities have put the site on the tourist map.

The quarry landscape

The quarry landscape is named after the municipality of Hyllestad, situated in the western part of Sogn og Fjordane county. Most of the quarries are found on the slopes above the fjord Åfjorden, less than 1 km from the sea (Figure 3) (Heldal and Bloxam 2007). Approximately 300 individual quarries and 70 trial extractions have been recorded in the survey. The highest concentrations of quarries are found in the southern part of the area, at Myklebust, Rønset and Berge. In these areas, numerous quarries occur side by side and even on top of each other. They are connected by roads and tracks to several harbours where the



Figure 5. Carved quarry face, Hyllestad, after extraction of large rectangular slabs, probably grave-slabs.



Figure 6. Example of prospecting site, Hyllestad, with traces after trial extraction of hand millstones.

millstones were loaded onto ships. Outside these core areas, only small and scattered millstone quarries are found. In addition to the numerous quarries, there are many prospecting sites showing evidence of limited test carving (Figure 6).

The *Myklebust area* is the southernmost and perhaps largest production site. All the quarries display evidence of carving of millstones directly from the bedrock. In the lowland around the Millstone Park there are numerous quarries worked only for hand millstones, together with deeper quarries where both hand millstones and water millstones were extracted. Similar quarry landscapes are probably buried under recent buildings and constructions of the Hyllestad community. Radiocarbon dating of charcoal from a quarry in the Millstone Park indicates that production took place from the Viking Age to the Late Middle Ages (Baug 2002). Further uphill on the northern side of the valley there are also numerous deep quarries.

Just to the north of the Myklebust area, a group of small and scattered quarries are situated on top of a hilly plateau near the *Sæsol farm* (Figure 3). Most of these quarries produced only hand millstones. One of them gave a calibrated radiocarbon date of AD 715–890, thus being one of the oldest recorded quarries in Hyllestad (Baug 2002). A few attempts at millstone production with powder blasting in later stages never developed to anything sizeable. In the northern part of the Sæsol area, along the Stigedalen valley, the mica schists and quarries can be followed down towards the fjord where ancient harbour facilities have been found.

The *Berge area*, north of Sæsol, contains some traces of early quarrying activity (assumed Viking Age and Middle Ages, Heldal and Bloxam 2007), particularly along the fjord. Further uphill, there are large quarries from the later period situated in a harder variety of the mica schist. The number of quarries increases towards the north in the *Rønset area* (Figure

4), which is the largest and most significant quarry area along with the Myklebust area. Numerous quarries partly overlap each other and display intensive quarrying during several periods, particularly the Viking Age and Middle Ages (Baug 2002, Heldal and Bloxam 2007). There are also some quarry pits in scree. These pits may represent remains of a very early phase of quarrying, exploiting single blocks of suitable size for the production of hand millstones only.

North of Rønset, there are several small quarry areas scattered over a wide area. Most significant is the *Sorbøvåg* quarries, the majority of which are covered by agricultural land. Several small and more remote quarries are situated at *Gil*, *Borsholmen*, *Sandal* and *Rutle*, all of them probably dating from the Middle Ages (Heldal and Bloxam 2007).

Geology and millstone characteristics

In Hyllestad, millstone quarrying has targeted a specific variety of garnet-kyanite mica schist within the *Hyllestad complex*, a unit of high-pressure metasedimentary rocks (Chauvet et al. 1992) along Åfjorden in Hyllestad. The Hyllestad complex is correlated with other aluminous pelitic units within the Lower or Middle Allochthon of the Norwegian Caledonides (Chauvet and Dallmeyer 1992, Tillung 1999). The main metamorphic assemblage and cleavage³ of the rocks were formed during the Scandian orogeny at crustal depths of ca. 50 km (Hacker et al. 2003). Subsequently, the complex underwent deformation and retrograde metamorphism at lower pressures and temperatures during late-orogenic extension along the Nordfjord–Sogn Detachment Zone (Hacker et al. 2003).

The Hyllestad millstone schist is composed predominantly of coarse-grained aggregates of muscovite alternating with quartz-rich laminae, garnet porphyroblasts ranging from 2 to 8 mm, and kyanite porphyroblasts up to 2 cm long (Figures 7 and

³ *Cleavage* is used in this paper as a general term for the rock properties resulting from a foliated or schistose texture with planar or near-planar arrangement of mica (muscovite or biotite).



Figure 7. Close-up of weathered surface of garnet-kyanite-muscovite schist (coarse-grained variety) from the Hyllestad millstone quarries.

8). Minor amounts of staurolite and retrograde chloritoid are also common. The presence of kyanite is generally considered a diagnostic feature of the Hyllestad millstones (Carelli and Kresten 1997, Baug 2002). Clearly, the size and distribution of garnet were important measures of quality, and there are many examples of quarrying that ended when it reached garnet-poor zones or zones with garnet that was too large. The zones of optimal quality apparently represent strongly folded layers and display very complex distribution patterns, embedded in heterogeneous mica schist with layers of quartzite, semipelite and ferruginous schist.

Roughly speaking, two subtypes of good-quality mica schist are recognised. In most of the area the schist is highly micaceous and 'soft', containing large flakes of mica in a quartz-poor matrix (Figure 8a). This subtype was the target for quarrying when millstones were carved directly from the bedrock (see below), particularly in the Myklebust area where it is very abundant. In the eastern part of the area, especially between Rønset and Sæsøl, the schist is more quartz-rich and contains smaller amounts and finer flakes of mica (Figure 8b). This subtype appears much harder to carve and seems to have been exploited only in later periods, when wedging and blasting became the primary extraction techniques.

It is likely that this selective quarrying was partly a consequence of the harder mica schist being more suitable for blasting, but there may also be quality measures linked to this change of source. The garnet in the mica-rich schist bears signs of strong deformation, such as rounding, cracking and chloritisation (Figures 8a, c). Thus, they are poorly attached to the enveloping, large mica aggregates of the matrix. In contrast, garnet in the quartz-rich schist is less cracked and more euhedral. It is likely that this difference was significant for the grinding properties and durability of the millstones, because the garnet of the 'soft' variety might loosen from the millstone. Yet, the mica-rich schist was easier to carve and was preferred until the use of black powder made it equally easy to quarry the quartz-rich schist.

In addition to the mineralogy, structural features such as folding, shear zones and brittle fractures have been important for the location and productivity of the quarries. For example, a small group of quarries just north of the Myklebust area are small and scattered due to the structural complexity; only small 'pockets' of proper schist have escaped the intense folding and shearing that was detrimental to millstone quality. In general, areas displaying little folding of the cleavage planes and wide spacing of brittle fractures were favourable for obtaining large blocks with uniform and straight cleavage planes.

In some areas, widely spaced brittle fractures define natural limits for extraction areas within individual quarries. Locally, a low inclination of the cleavage plane made it feasible to establish deep, efficient quarries in the hillside, such as in the northern part of the Myklebust area. In the southern part of the Hyllestad area, the primary cleavage is partly overprinted by subhorizontal shear zones (Figure 8c) probably related to late-orogenic extension (Chauvet et al. 1992, Hacker et al. 2003). Locally, this provided an alternative orientation for millstone extraction (Figure 9), but it could also cause high waste ratios due to cracking along either the primary or the secondary cleavage.

Quarrying primarily targeted areas where the combined geological conditions were most favourable for extraction. This can partly explain the large concentration of quarrying activity at Rønset and Myklebust. However, the near absence of exploitation in qualitatively similar areas further north (Heldal and Bloxam 2007) also points at other mechanisms, i.e., land use and ownership, as the driving force for quarrying.

Selbu

Historical records

The earliest reference to millstone quarrying in Selbu is a travelogue from 1591–1592 by the clergyman Peder Claussøn Friis, who claimed that in this area there were "produced millstones of better quality than anywhere else in the kingdom and that the stones were widely distributed in the country" (Friis 1632). This implies that the Selbu millstones were already well established on the market and that the production history may be extended back to at least the middle of the 16th century.

The first reference to black powder used in the Selbu quarries is from 1734 (Haarstad 1972), about 60 years after it was introduced in the Røros copper mines some 70 km to the south. The millstone quarries are also mentioned in an account of a journey through the area in 1773 by the historian Gerhard Schøning (1778), who noted that quarrying took place after the farm work season was finished by the end of September until close to Christmas. Court records show that quarrying rights were heritable and often held by different farms (Haarstad 1972). An indication of production rates is known from a statement signed by 286 farmers and peasants that had quarrying rights in the year 1800, when it was agreed that annual production must be limited to an equivalent of three medium-size millstone pairs

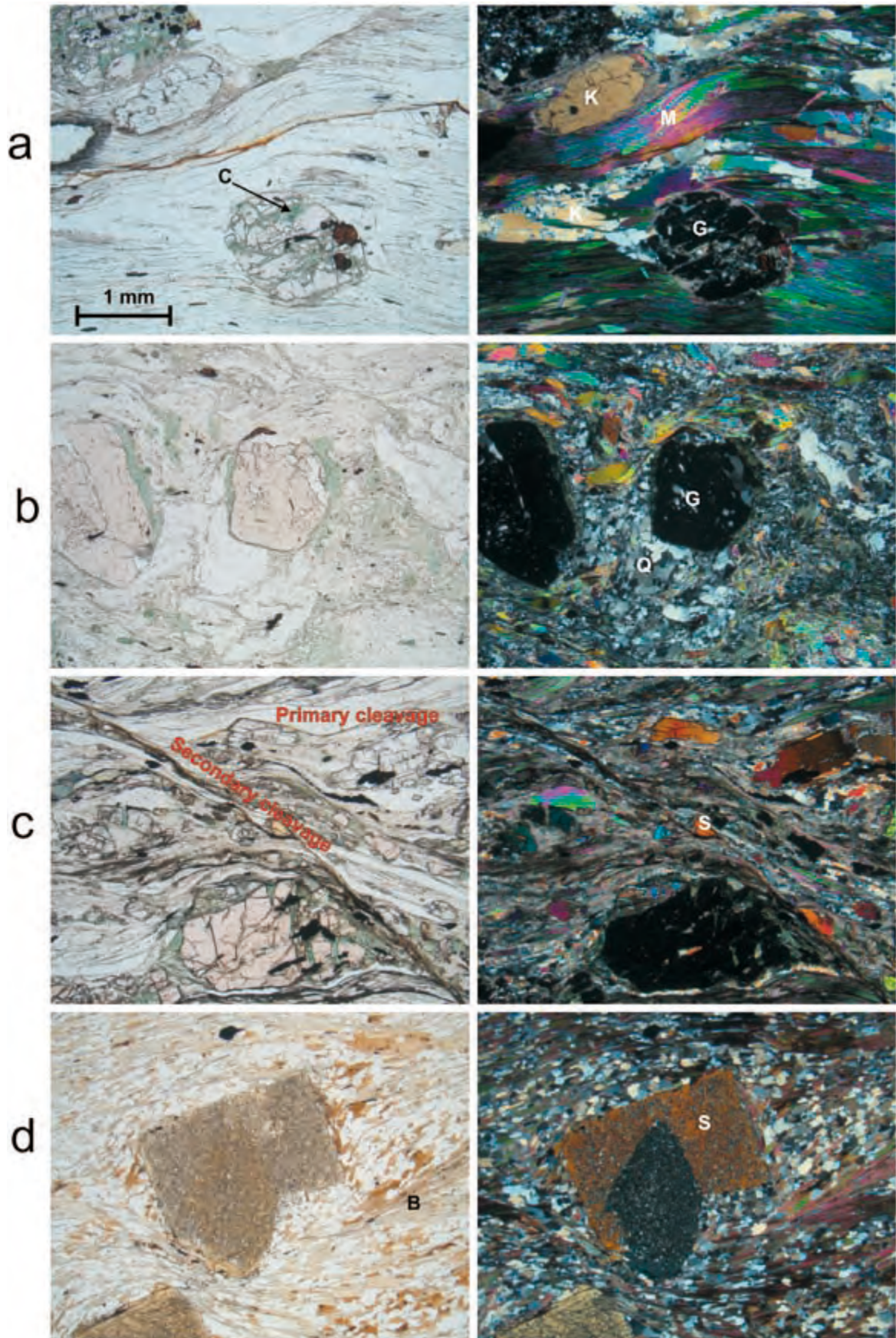


Figure 8. Photomicrographs, plane-polarised light (left) and cross-polarised light (right). (a) Mica-rich, 'soft' type millstone, Hyllestad, showing coarse-grained muscovite aggregates and rounded/cracked garnet porphyroblasts that are partly altered to chlorite. (b) Quartz-rich, harder type of Hyllestad millstone schist containing more euhedral garnet and finer-grained matrix with less mica. (c) Primary and secondary cleavage in Hyllestad millstone schist. (d) Selbu millstone schist displaying euhedral staurolite porphyroblasts set in a fine-grained biotite-quartz matrix. K: kyanite, M: muscovite, G: garnet, C: chlorite, Q: quartz, S: staurolite, B: biotite. Scale bar in (a) applies to all the photomicrographs.



Figure 9. Two directions of splitting of millstones, Hyllestad. 1) Splitting along the primary cleavage. 2) Splitting along the secondary cleavage.

for farmers and one pair for peasants. A comprehensive report on technical and economic aspects of the millstone production was written by the Commissioner of Mines, H.C. Strøm, who investigated the quarries in 1817 (Strøm 1820).

A change from small-scale quarrying to increased industrialisation is seen after the 1840s, just after the onset of the Industrial Revolution in urban parts of Norway. The change was partly incited by the central authorities (Department of the Interior) due to a need for more organised and efficient operations of the important millstone production. The Selbu merchant Frederik Birch took a leading role in this development when he bought up major parts of several quarries and introduced new equipment and techniques. Much of the documentation from this period, including records of stories told by quarrymen, was compiled by Rolseth (1947) some 30 years after the last quarry closed down. According to these records, the quarrying period generally stretched from autumn through to March, and the millstones were horse-sledged to the village, usually in April (Rolseth 1947).

Records of production rates exist for certain periods and were regular after 1867, when an official millstone register was established. A report from the County Governor for 1846–1850 indicates that about 250 quarrymen provided a total of 600 millstone pairs annually (Adresseavisen, 15 March 1856), but the true yield was considered to be higher than that declared by the quarry proprietors. The last decades of the century saw a gradual decline in production, ranging approximately from 225 millstone pairs (1869) to 80 (1883), due to competition from imported German millstones and increasing use of artificial millstones and roller mills. Quarrying came to a complete end in 1914.

According to the geologist and geographer Amund Helland, millstone quarrying in Selbu was highly peculiar compared to mining and stone extraction elsewhere in Norway (Helland 1901). This was not only by virtue of the remote location and extremely difficult working conditions, but also the quarrying terminology and law practice that had developed over the cen-

uries that was distinctly different from official mining legislation.

The quarry landscape

The Selbu area has about 1000 large and small quarries situated along a relatively narrow, ca. 30 km long ‘millstone zone’ (Figure 10). The majority of quarries were located in a remote mountainous terrain above the tree line, far from harbours and more than 15 km from the nearest road or permanent settlement. Quarries, traces of working techniques and remains of cabins and other infrastructure are well preserved and can easily be studied in this barren landscape. Combined with

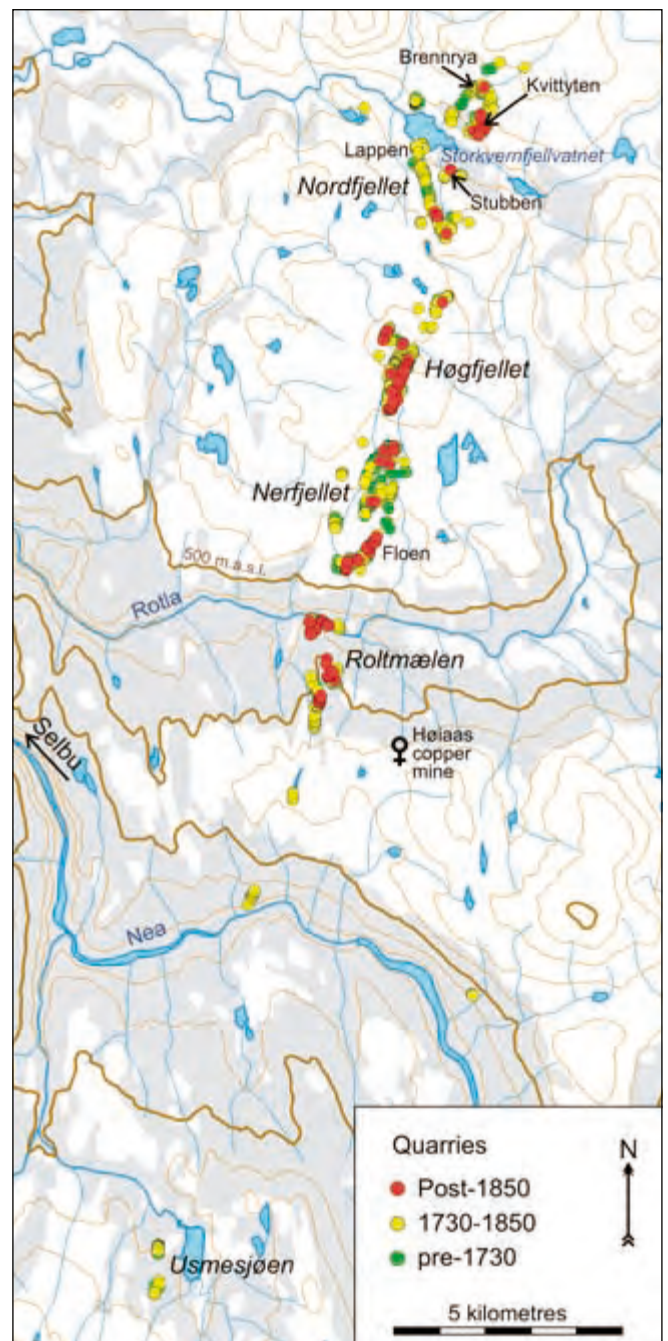


Figure 10. Selbu map showing the distribution of quarries from different periods and names of the quarry landscapes. Contour interval 100 m.

historical sources on major new developments in the quarrying activity, such as the initial use of powder, the shift from only autumn-season to full winter-season work, and documented technological achievements during the later 'industrialised' period, our recent field studies have served to distinguish different periods in the quarrying history. The millstone zone can be subdivided into five main quarry landscapes, from north to south: the Nordfjellet, Høgfjellet, Nerfjellet, Roltmælen, and Usmesjøen areas (Figure 10); the first three are by far the most important.

The most remote landscape, *Nordfjellet*, comprises several quarry areas around the lake Storkvern fjellvatnet, many of which show evidence of activity through all periods of quarrying history. *Kvittyten* and *Stubben* are young, large quarries surrounded by clusters of small, old quarries. *Kvittyten* is the largest single quarry of the Selbu area, measuring ca. 30 x 30 m with a depth of more than 15 m. Both quarries have remains of large cabins typical of the late period, built for 10–15 quarrymen and located close to the quarry in places where the snow would drift away. By contrast, the areas of *Brennrya* and *Lappen* (Figure 10) are dominated by older, small quarries where associated cabins were located mostly close to running water in places sheltered from the wind. Altogether, ca. 100 cabin ruins of this type have been found around the lake Storkvern fjellvatnet; each cabin was apparently meant for only two or three men and commonly built side by side (Alsvik et al. 1981). Trial excavations of six ruins by Alsvik et al. (1981) indicated that they were used after AD 1700.

Høgfjellet comprises several quarry areas that are internally fairly homogeneous with respect to morphology and quarrying history, while local overlapping relationships provide evidence of relative chronologies. An eastern zone displays almost only young (post-1850) and large workings that merge to form a more than 400 m long and 10 m wide trench-like quarry (Figure 11) with associated remains of large cabins. A few tens of metres to the west is an array of smaller, intermediate-age quarries with related intermediate-size house ruins, and 200 m farther west another series of intermediate-age to relatively young quarries. To the southwest is an area of numerous small, old quarries together with remains of small cabins and primitive shelters (Figure 12). An intermediate-age quarry area is located to the northwest, almost on the top of the mountain Høgfjellet in extremely barren and exposed terrain.

The *Nerfjellet* landscape shows traces of old activity variably preserved among scattered quarries of later age. Much of the area is relatively flat bog-land and the old quarries are typically filled with water (Figure 13). The majority of quarries are found in three separate zones that are oriented SW–NE in an *en echelon* manner. The southern area (*Floen*) is largest in terms of production, including several trench-like quarries of relatively late age that are 40–110 m long and 5–15 m wide.

Roltmælen is a group of relatively small quarry areas stretching southwards from the river Rotla. Most of the workings are intermediate in age, but there are also a number of relatively



Figure 11. Northeastern part of the Høgfjellet quarry landscape, Selbu, viewed towards the north. The most recent (post-1850) activity produced a deep, trench-like, continuous array of quarries (right), with waste and working areas irregularly spread on the right side. An earlier quarrying phase in the same zone is represented by large, flat-topped working areas and waste piles on the opposite (left) side of the trench. Farther left is an array of even older and smaller quarries with associated small, flat-topped working areas on their left side. A restored cabin from the most recent quarrying activity is seen in the background.

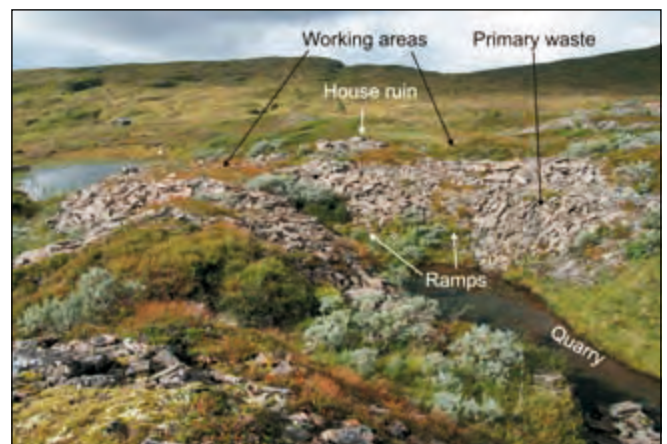


Figure 12. Area with small, old quarries in the southwestern part of the Høgfjellet quarry landscape, Selbu, viewed towards the west. The shallow, water-filled quarry in the foreground is partly filled with primary waste rock. Gently inclined ramps lead from the quarry to flat-topped working areas. A small house ruin is situated on an old part of the working area.

small, young quarries. The *Usmesjøen* landscape south of the Nea valley is comparable to Roltmælen, except that little or no evidence exists for late activity. According to B. Flakne (in Rolseth 1947), the quarrying at Usmesjøen took place mainly in the 18th century.

Geology and millstone characteristics

The Selbu millstone quarries are located in the eastern part of the Gula Complex, a medium- to high-grade metamorphic unit within the Trondheim Nappe Complex of the Norwegian Caledonides (Wolff 1989, Hacker and Gans 2005). This part



Figure 13. Water-filled old quarries typical of the Nerfjellet quarry landscape, Selbu, surrounded along their edges by waste heaps that are completely overgrown.



Figure 14. Close-up of slab from a quarry in the northwestern part of Hogfjellet, Selbu, showing a cleavage plane with lineation marked by a characteristically undulating surface. The slab was loosened along the primary cleavage using chisels and pick-axe (note tool marks) on a free 'cross-fracture' plane marked on the photo. The left side of the slab was broken along the lineation as discussed in the text.

of the Gula Complex is characterised by metasedimentary rocks, including calcareous metasandstone, calc-silicate schist, thin marble layers, and semipelitic biotite schist with varying proportions of garnet and staurolite (Olesen et al. 1973).

The 'millstone zone' is characterised by relatively homogeneous staurolite-biotite schist with a thickness of several metres, in some cases up to 20 m. Local heterogeneities include irregular bodies of milky quartz and boudins of variably skarnified marble layers. Staurolite typically forms euhedral porphyroblasts that are mostly 2–5 mm across, in a fine-grained (< 1 mm) matrix of biotite and quartz (Figure 8d). The staurolite is commonly twinned with crosses at 60°, and is strongly poikiloblastic with very fine-grained inclusions of quartz. Garnet is generally a subordinate or minor phase, forming < 1 mm euhedral porphyroblasts of clear, brownish-red almandine; garnet-biotite schist without staurolite has been observed in only two small quarries. Kyanite is a common, but minor, constituent, and small amounts of sillimanite and andalusite are found in places.

The rocks are affected by polyphase deformation, with two phases of early isoclinal folding superimposed by later open folding, which in some areas resulted in a complex pattern of several subparallel millstone zones. They typically display a primary cleavage striking approximately N–S with steep westerly dips, and a secondary cleavage striking SSE–NNW with moderate westerly dips. The two cleavage planes are defined by characteristically sigmoid-shaped biotite aggregates that probably represent an S–C tectonic fabric. The intersection of the cleavage planes defines a lineation that plunges SSW and is recognised on the surface of split millstone slabs as a 5–10 mm-scale undulation of the matrix biotite (Figure 14).

The tectonic fabric is variably developed, resulting in different cleavage and lineation characteristics that were significant for quarrying. Most of the quarries display a well-developed

primary cleavage that facilitated easy wedging and production of millstones with a cleavage-parallel grinding surface. Also, thin but extensive fractures across the cleavage were important for quarrying (Figure 15). These 'cross-fractures' are oriented E–W with moderate to steep northerly dips and are spaced at intervals of less than one metre to tens of metres.

On weathered and worn rock surfaces the staurolite and garnet stick out from the softer and less resistant micaceous matrix, leading to a characteristic knobby surface (Figure 16). The quarrymen distinguished between millstone varieties with 'ståltyt' ('steel knobbles') and 'bruntyt' ('brown knobbles'), which were the old terms for staurolite and garnet, respectively. In places, staurolite is variably replaced by a fine-grained aggregate of muscovite, especially along rims of the porphyroblasts, and this retrograde metamorphism may be accompanied by partial chloritisation of the matrix biotite. The whitish mica aggregates were referred to as 'kvit-tyt' ('white knobbles') and were considered to have a detrimental effect on the millstone quality. Also the size and distribution of staurolite and garnet were important for quality, and different varieties were demanded by different markets to suit the various requirements for grinding properties (Rolseth 1947). According to the Commissioner of Mines, H.C. Strøm (1820), the hard porphyroblasts in the softer matrix allowed a simple 'sharpening' of the millstone using only sand for roughing of worn grinding surfaces.

Also the cleavage characteristics were significant for grinding properties. Rolseth (1947) claims that millstones with the grinding surface oblique to the cleavage plane were highly valued, supposedly due to their better grinding or 'self-sharpening' properties. Such millstones (called 'tvihaus' in the old quarrying terminology) were produced if the secondary cleavage was well developed; however, extensive production was restricted by the high risk of failure along the secondary cleavage during wedging.

Quarrying techniques

In both Selbu and Hyllestad, the millstones were formed by carving and hewing using picks or hammer and chisel, and the same basic principle was used throughout the history of millstone extraction. The main difference is seen in the primary production of blocks from the bedrock and in the size and shape of the final millstones. In the following, we distinguish between four extraction techniques: loose-block quarrying, carving of millstones directly from the bedrock, wedging of slabs from the bedrock, and blasting combined with wedging.

Loose-block quarrying

A few quarries in Hyllestad show evidence of quarrying based on the collection of suitable loose blocks for making hand millstones. The quarries appear as circular depressions in scree deposits, enveloped by piles of unusable talus blocks, broken millstones and waste from carving. This type of ad hoc exploitation is an anomaly compared to the other quarries, suggesting quarrying for local domestic use rather than manufacturing of standardised millstones for trade. Although it cannot be ruled out that such exploitation may have occurred during different stages of the production history in the area, there is a possibility that these quarries are the remains of the earliest millstone quarrying activity in Hyllestad.

In the Selbu area, this type of exploitation is very limited, probably due to the near absence of talus containing appropriate rocks. Carving of millstones from small erratic blocks is observed locally along the stream Rensbekken, near Brennrya in the most remote quarry landscape (Nordfjellet, Figure 10), but the age is unknown.

Direct carving

Direct carving from bedrock is used in the majority of the Hyllestad quarries. After making a circular groove on the primary



Figure 16. Close-up of weathered surface of typical staurolite-biotite schist from the Selbu millstone quarries.

cleavage surface (or more rarely on the secondary cleavage) outlining the shape of the millstone, a channel was carved by a pick or a pointed chisel (Figure 17). The millstone was loosened along its base by striking a pointed chisel repeatedly along its perimeter until a crack was created parallel to the cleavage plane. Smoothing of surfaces and carving of the centre hole ('eye') in the millstone was carried out in the quarry, while final fitting of the millstone pair was probably carried out at the site where it was used (Hansen 1991, Baug 2002). This view is supported by cargos of unfinished millstones found in shipwrecks and in medieval contexts in the city of Bergen.

Even though the basic principle of this extraction technique seems to remain the same from the earliest known quarries in Hyllestad throughout the Middle Ages, there are some important differences between the quarries that have chronological implications (Figure 18). In many of the quarries, extraction took place one layer at a time, leaving laterally consistent quarry



Figure 15. Intermediate-age quarry in the Hogfjellet area, viewed towards the north-east. See text for the significance of cleavage planes, lamination and cross fractures for quarrying.

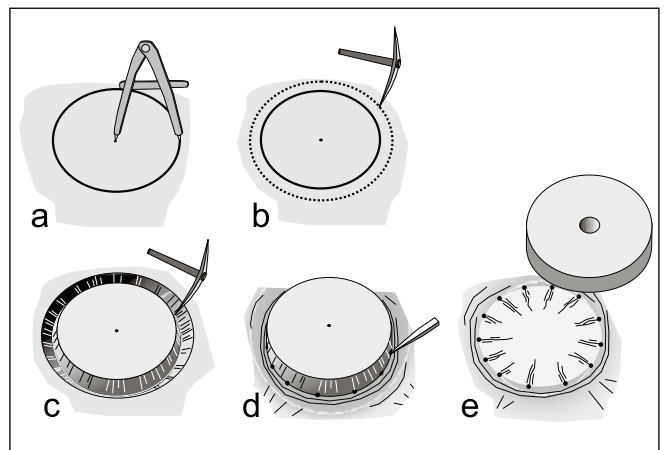


Figure 17. Schematic illustration of millstone carving directly from the bedrock. (a) Measuring and making circular groove; (b-c) carving of channel around the planned millstone; (d) splitting the millstone from the bedrock with a pointed chisel; (e) loosening of millstone with carved centre hole.

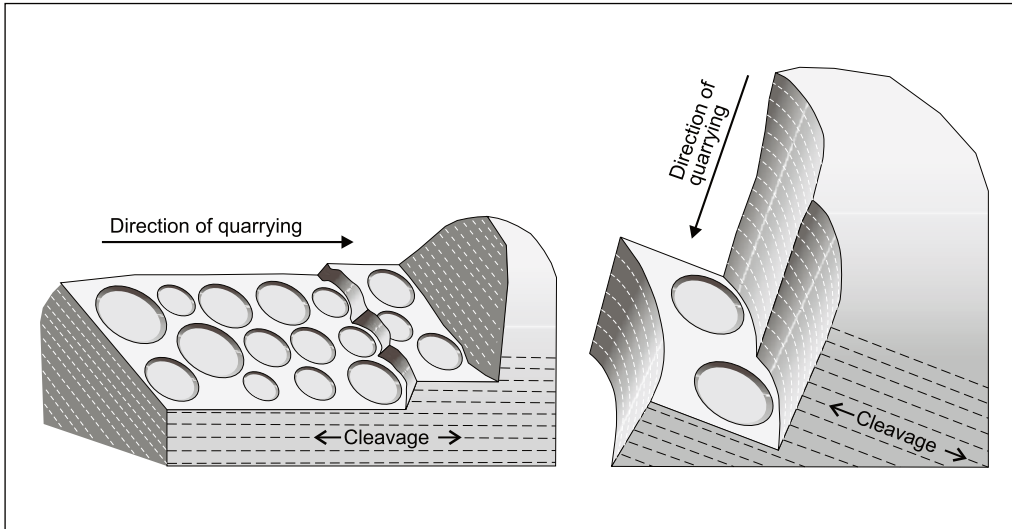


Figure 18. Schematic illustration of the two subtypes of quarries worked by carving directly from the bedrock in Hyllestad. Left: quarrying layer by layer along the cleavage plane. Right: 'coin pile' quarry involving deep extraction.



Figure 19. Shallow quarry established in layers along the cleavage plane, Sesol area, Hyllestad.



Figure 20. Typical marks after extraction of hand millstones by carving directly from the bedrock, Myklebust area, Hyllestad.

floors along the cleavage plane with the circular marks from millstone extraction occurring side by side (Figure 19). Some of the oldest dated quarries display such morphology, such as one at Sæsøl from the pre-Viking to Viking Period (Baug 2002). This first subtype of direct-carving quarries, which produced predominantly hand millstones (Figure 20), is widely distributed throughout the Hyllestad area.

A second subtype of carved quarries is characterised by deeper extraction in taller steps. The millstones were quarried in piles, each one under another ('coin piles' as described by Baug 2002), leaving tall quarry faces perpendicular to the cleavage (Figure 21). The change in extraction method towards deeper (and more efficient?) quarries seems to be associated with the period after water millstones were introduced in Norway, which most likely happened at about AD 1100 (Baug 2002).

The second subtype of carved quarries is confined to only two quarry areas, namely Rønset and Myklebust (Figure 3). Thus, the development in quarrying in Hyllestad seems to have moved from widely distributed quarries of the first subtype during the Viking Age and Early Middle Ages, to more concentrated extraction in deeper and more efficient quarries at some stage in the 12th century. Some quarries display an early phase of layer-wise quarrying of hand millstones (first subtype), and a later phase with deeper quarrying of water millstones and hand millstones. At Otringneset (Figure 3), such multi-period quarrying is confirmed by radiocarbon dating (Baug 2002).

Pre-powder wedging

In contrast to Hyllestad, practically all primary extraction in Selbu was done by wedging or chiselling along the cleavage plane. The most primitive and least labour-intensive technique depended heavily on the presence of a well-developed cleavage, combined with one or more free faces and fractures or other weak structures that facilitated easy loosening of slabs. Examples of this are seen on the west side of small hillocks or narrow, E-W-oriented 'whaleback' ridges, where slabs of appropriate



Figure 21. Deep extraction of millstones on top of each other, Hyllestad. Unfinished water millstone is seen at the bottom.

thickness (10–20 cm) were loosened along the west-dipping cleavage plane (Figure 22).

More extensively worked pre-powder quarries can be up to 20 m wide and more than 30 m long, but the majority are significantly smaller. Their depth rarely exceeds 2 m. The exact shape and size is often difficult to estimate, because in many cases the quarries are highly overgrown and filled with water and are not easily discernable from the undisturbed landscape. Moreover, much of the waste was disposed of in previously worked parts of many quarries (Figure 12), leaving quarry landscapes characterised by innumerable small pits and waste mounds that together may comprise one coherent quarry. There are no existing records of extraction methods in these old quarries, however, on the basis of quarry morphology and a limited number of exposed quarry walls the following quarrying pattern emerges:

Slabs were loosened along the steeply west-dipping cleavage by splitting with iron or possibly wooden wedges. Some of the pre-powder quarries reveal 10 x 6 cm wide and up to 19 cm deep wedge holes at 50 cm intervals (Figure 23). The size of the wedge holes and wide depressions hewn around each hole may indicate the use of wooden wedges. This would be consistent

with Rolseth's (1947) reference to findings of wedges made of juniper in an old water-filled quarry when it was reopened in 1818. In other quarries, narrow channels, a few centimetres deep and wide, were hewn to weaken the rock along appropriate cleavage planes, usually combined with hewing of small holes at close intervals for the subsequent use of chisels or iron wedges.

The presence of appropriately spaced north-dipping 'cross fractures' (cf., Figure 15) was apparently crucial, providing a practically free surface on the lower south side of each slab. Loosening of the lower north side of the slabs was controlled by the minimal mechanical strength in a plane across the slab and parallel to the south-plunging lineation fabric (Figure 24), commonly referred to as 'grain' in dimension-stone quarrying terminology. The structurally controlled working of slabs in most cases facilitated quarrying from west to east, followed by a stepwise extension and deepening of the quarry southwards along the millstone zone. A common reflection of this technique is a triangular or trapezoidal quarry morphology.



Figure 22. Primitive extraction of millstone slabs from the Brennråa area in the Nordfjellet quarry landscape, Selbu. Three slabs are variably loosened from a small cliff by cutting grooves along the primary cleavage.



Figure 23. Large and deep wedge holes with shallow depressions around each hole, possibly for the use of wooden wedges. Pre-powder quarry in the Nerfjellet quarry landscape, Selbu.

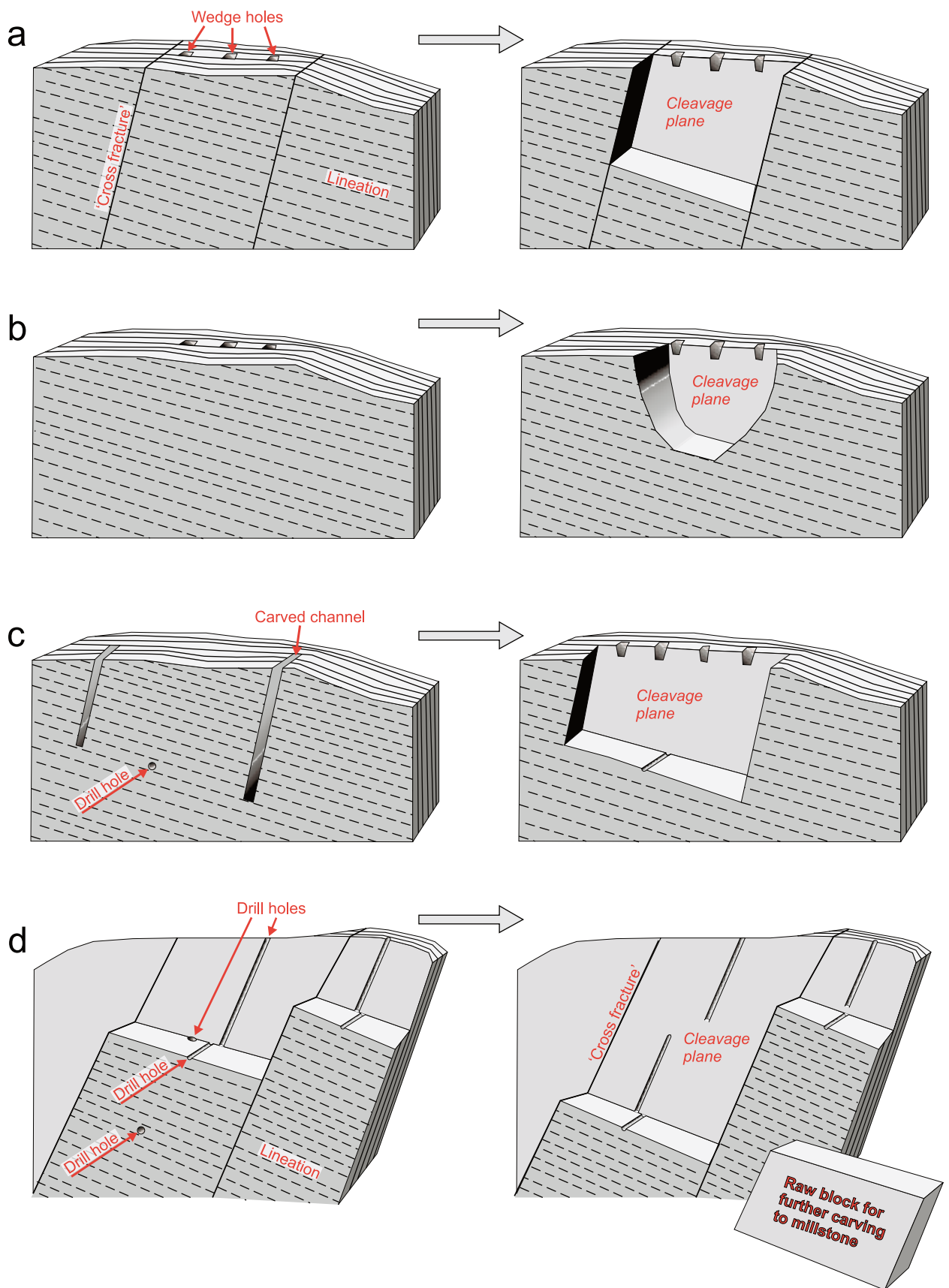


Figure 24. Schematic illustration of quarrying in the Selbu area. (a) Pre-powder wedging of slabs along the cleavage, using 'cross fracture' for loosening the millstone slabs. (b) Pre-powder wedging of slabs along the cleavage in rare cases where cross fractures are absent. (c) Wedging of slabs along the cleavage combined with drilling/blasting across the cleavage; carving of 10–20 cm deep V-shaped channels on the cleavage plane in the absence of cross fractures. (d) Drilling/blasting both across and along the cleavage plane with extraction of thick blocks that were subsequently split into slabs.

The primary waste from slab extraction was thrown out to form a mound along the edge of the pit, or was left behind in previously worked parts of the quarry (Figure 12). Suitable slabs were mostly removed from the quarry along a gently inclined ramp up to a wide, semicircular, flat-topped working area (Figure 12) where the actual millstone hewing took place.

In Hyllestad, we have observed only one quarry in which primary blocks have been extracted from the bedrock by the use of wedging alone. Here, the cleavage is slightly inclined and favourable for wedging along the cleavage planes at small steps in the surface. Small grooves in the split surface suggest that wedging was done by flat, thin chisels.

Blasting

In Selbu, the adoption of black powder for quarrying, apparently from the early 18th century onwards, led to a progressive development rather than a sudden changeover in techniques. This is reflected in a gradual change in quarry morphology and tool marks, from relatively small quarries similar to those of the pre-powder period with evidence of only limited blasting, to large quarries (Figure 25) with very abundant drill holes from the latest period of millstone production. Parallel with this change to larger and deeper quarries was a gradual adoption of more advanced technical equipment for transportation of rock slabs and for emptying the seasonally water-filled quarries (Rolseth 1947).

Throughout this period, quarrying was based on easy splitting of slabs or thicker blocks along cleavage planes, coupled with loosening along the steeply north-dipping 'cross fractures' like in the pre-powder period (Figure 24). In a few quarries, especially in the Rotla-Flora area (Figure 10), an absence of appropriately spaced cross fractures was compensated by carving 10–20 cm-deep V-shaped channels along the cleavage plane. Initially, powder was only used to break the base of the slabs across the primary cleavage (Figure 24), while wedging was still used



Figure 25. Westerly view of the large Raudhammeren quarry, from the latest period of quarrying in Selbu. Note the cross fractures that were appropriately spaced for production of large blocks. An open adit enters the quarry from near the lake. On top of the irregular waste heaps and working areas on the quarry margin, one can see three remains of timber capstans used to lift waste and blocks. An area with much older, pre-powder quarries is seen in the background to the right of the lake.

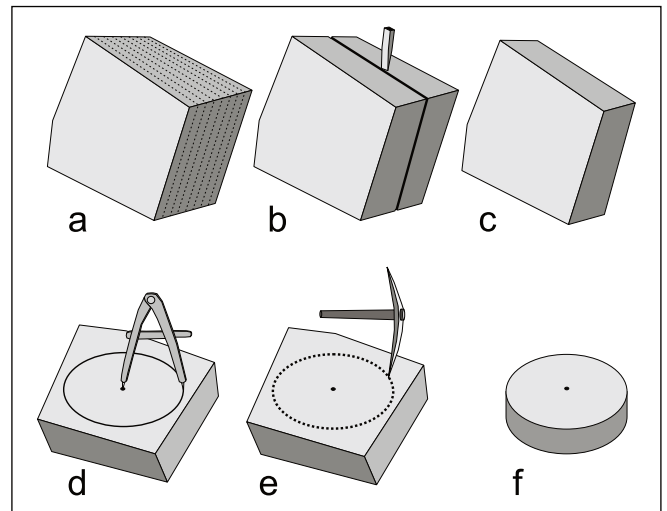


Figure 26. Schematic illustration of block splitting and carving of millstone in the Selbu quarries. (a–c) Splitting of a thick block into several slabs with a thickness appropriate for millstone hewing. (d–f) Marking and hewing of millstone from slab. Note that stages (a–c) are relevant only for the extraction of thick blocks in the latest quarries. See text for explanation.

for splitting along the cleavage plane. In later times, longer holes were drilled both along and across the cleavage plane (Figure 24) to produce blocks that were subsequently split into slabs with a thickness suitable for millstone hewing. Splitting of blocks was based on chiselling or wedging with iron tools (Figure 26), essentially similar to pre-powder techniques, except in the relatively young 'industrialised' quarries where arrays of short drill holes were used for wedging.

Hewing was also similar to the old technique, except for a general increase in millstone diameter from mostly ca. 50–100 cm in pre-powder quarries to ca. 80–140 cm in young quarries and a parallel increase in thickness of the lower stone from 10–12 cm to 12–20 cm and occasionally up to 33 cm (these ranges are based on remnants of flawed millstones left behind in the quarry areas and may not be truly representative of the production). If necessary, the split cleavage plane was trimmed by carving of parallel grooves, probably by a chisel or a pickaxe, before the intervening ridges were chopped off, as described by Strøm (1820). A metal-pointed compass was used to mark the millstone perimeter at an appropriate diameter (Figure 26), and the vertical sides of the stone were carved through the slab with a pickaxe or a chisel (Figure 27).

The topside of the runner (upper) stone was typically trimmed to a bell-shaped, double-curved, form (Figure 28) that seems to be characteristic of the Selbu millstones. The centre hole of the upper stone was occasionally carved at the quarry site, but in most cases this was part of the final preparation that was done after the stones had been carried to the village of Selbu (Rolseth 1947).

As long as quarrying was limited to the autumn season, working areas had a flat-topped semicircular shape like in the pre-powder quarries, although they grew significantly larger because



Figure 27. Marks after a compass used to outline a planned millstone in Selbu. Carving of the millstone side was finished almost through the slab before it continued along the rest of the compass markings.



Figure 28. Characteristically bell-shaped upper millstone ('runner') from the blasting period in Selbu. Behind the millstone there are several slabs that were placed edgewise on the working area, ready for millstone hewing.



Figure 29. Entrance of a Selbu quarry worked through the winter, showing primary waste that was sledged on the snow and disposed along ridges extending out from the quarry. Nordfjellet quarry landscape.

of all the primary waste that had to be removed from the deep pits. Only in the relatively late quarries, which were worked also during the winter, did the working area and waste heaps change significantly. In some of these quarries, the coarse primary waste created by blasting was sledged on the snow and was disposed of along ridges extending out from the quarry (Figure 29, see also Figure 11). Elsewhere, man-driven timber capstans were used to lift the coarse waste and the blocks for production, leaving disorderly-shaped waste heaps and intervening working areas along the quarry margins. The deepest and most industrialised quarries from this period were established in sloping terrain where the construction of open adits allowed efficient water drainage as well as transport of waste and blocks in wagons.

In Hyllestad, only 18 of the known quarries were worked by powder blasting. The majority are located in the Berge–Rønset area, while a few small quarries are found at Sæsøl, Hatlem and Bjørkåsen. Black powder was detonated in short drill holes, and well-fitted blocks were worked to millstones. This type of quarrying probably never achieved the efficiency seen in Selbu due to more folding of the cleavage planes, poorer splitting properties and a less favourable relationship between cleavage and topography.

Hyllestad vs. Selbu—the significance of geology

The suitability of rocks to be used for grain milling depends on a range of factors. Hardness is required for durability and to avoid excessive rock powder in the flour. According to the Norwegian Commissioner of Mines, H.C. Strøm (1820), millstone qualities were also strongly dependent on their ability to maintain good grinding properties without frequent roughening of the grinding surfaces. On this basis, Strøm divided millstones into three quality categories:

(1) Millstones that required no surface dressing. This type included the vesicular basalts from Mayen in Germany. Millstone types with apparently similar properties were the porous, but tough siliceous gritstones from Derbyshire in England and the world-famous siliceous limestone from La Ferté-sous-Jouarre in France.

(2) Millstones where intermittent grinding with sand was sufficient. Strøm (1820) claimed that the Selbu millstones belonged to this group; it is also likely that Hyllestad millstones would be included, in view of their similar mixture of hard porphyroblasts in a softer micaceous matrix.

(3) Millstones that required periodical hewing of furrows to maintain the cutting surface. In this category, Strøm (1820) included various granites and sandstones.

In Norway, focus was put on porphyroblastic mica schist already in the early days of standardised production of millstones. Obviously, the occurrence of evenly distributed porphyroblasts of hard minerals in a softer matrix must have been a well-known measure of quality. Nevertheless, there were differences between

the Norwegian millstone mica schists that may have been significant for their grinding and maintenance properties.

It is noteworthy that the garnet porphyroblasts in Hyllestad, particularly in the micaceous and ‘soft’ schist variety, are commonly cracked, altered and rounded, and enveloped by mica aggregates so that they would be expected to easily fall out. The Selbu schist is strikingly different. Here, staurolite porphyroblasts are euhedral and commonly twinned, the matrix is finer grained and the mica is more evenly distributed. Furthermore, the porphyroblasts are more firmly attached to the matrix due to abundant intergrowths and less post-porphyroblast deformation. Consequently, the Selbu millstones may have been more durable and had better grinding properties than the soft variety of the Hyllestad schist.

While the differences in mineralogy and texture may have contributed to Selbu’s total dominance in the market during the latest periods of Norwegian millstone production, production feasibility must also have been significant. Clearly, Hyllestad had a great advantage in terms of accessibility and transport by virtue of a mild climate and proximity to harbours and permanent settlements, in contrast to the very remote Selbu area with its tough climate during most of the year. Other millstone-quarry sites in Norway, such as Salten, Brønnøy and Vågå, also held this logistical advantage (Figure 1), and may alone explain why there was apparently no production in Selbu in the early days of Norwegian millstone quarrying. In spite of this, Selbu took over and dominated the market by the end of the 16th century or somewhat earlier, even if there is nothing to suggest that the Selbu quarry areas had become comparatively more favourable from a logistical point of view.

The Selbu millstone lithology must have been known already in the Middle Ages, because the mountainous regions of central Norway had long been extensively used and explored by hunters, shepherds and travellers. Moreover, extensive exploitation of usable rocks, such as soapstone for the production of pots, already took place in the Pre-Roman Iron Age and the Viking Age in equally remote areas across the region (e.g., Skjølsvold 1969). Thus, it is unlikely that the shift in market dominance resulted from a late discovery of the millstone resources in Selbu.

Nor is it likely that the shift in market dominance was provoked by different suitability for blasting. Certainly, the combination of cleavage, lineation and ‘cross fractures’ in Selbu was ideal for extracting rectangular blocks with minimum effort, in contrast to Hyllestad where geological structures were less favourable for blasting and gave much more unpredictable results with a higher proportion of waste. However, while this may have strengthened Selbu’s dominance in the period characterised by blasting, it does not explain why Selbu took over already in the 16th century, well before powder was introduced in millstone quarrying.

A possible clue to the enigma may be found in different geological conditions of significance for quarrying. In the early days of millstone quarrying, the main prerequisite from a quarrying point of view was that the rocks were easy to carve. In Hyllestad, the type of mica schist targeted in the carving

periods is relatively soft due to a high content of mica and was thus feasible for carving. While the Selbu rocks may have been equally easy to carve and apparently gave more durable millstones, their main advantage over Hyllestad was a much better cleavability. Combined with the abundant ‘cross fractures’ that were in many areas appropriately spaced for the preferred millstone dimensions, this obviously was in favour of Selbu when the markets demanded larger millstones in response to the shift from hand mills to gradually larger water mills. With this in mind, it is interesting to note that when the production techniques in Hyllestad shifted towards blasting, a different quality of schist was targeted, namely a more quartz-rich type with euhedral garnet and finer-grained mica. This development may have been forced by better blasting properties in the harder, quartz-rich variety, but it may also represent an attempt at adapting to new market demands for larger and mechanically stronger millstones like those produced in Selbu.

Millstone-quarrying development and society

The Hyllestad schist seems to have been in the game almost as long as organised millstone production has taken place in Norway. Around AD 700, carving of millstones directly from bedrock took place even in more remote parts of the Hyllestad quarry landscape (Baug 2002). This is only 200–300 years after the first significant evidence of rotating hand mills used in Norway (i.e., Ullandhaug Iron Age farm), where non-standardised millstones were apparently produced from suitable local stones. Thus, it is likely that the early, standardised production in Hyllestad represents some of the earliest organised millstone quarrying.

The early quarrying technique applied in Hyllestad is represented mostly in small but numerous quarries that are widely distributed across the area. This might indicate a decentralised organisation of production. The carving technique was basically similar to that used for the contemporaneous extensive extraction of soapstone for various types of pots and cooking vessels, the latter having roots in comparable quarrying techniques in the Early Iron Age. The quarrying remained largely unchanged until production of water millstones began in the early 12th century (Baug 2002). At this stage, the quarries turned deeper and larger, and at the same time the activity was apparently concentrated in the Rønset and Myklebust areas. Both the technique itself and the concentration of the activity indicate a more centrally organised quarrying.

The shift in quarrying technique may be partly explained by increased efficiency, i.e., larger work force and higher output per square metre in the deeper quarries. However, it is also noteworthy that the shift temporally coincides with a widespread exploitation of building stone for the construction of churches and monasteries. The medieval quarrying of building stone represents an important introduction of new methods of

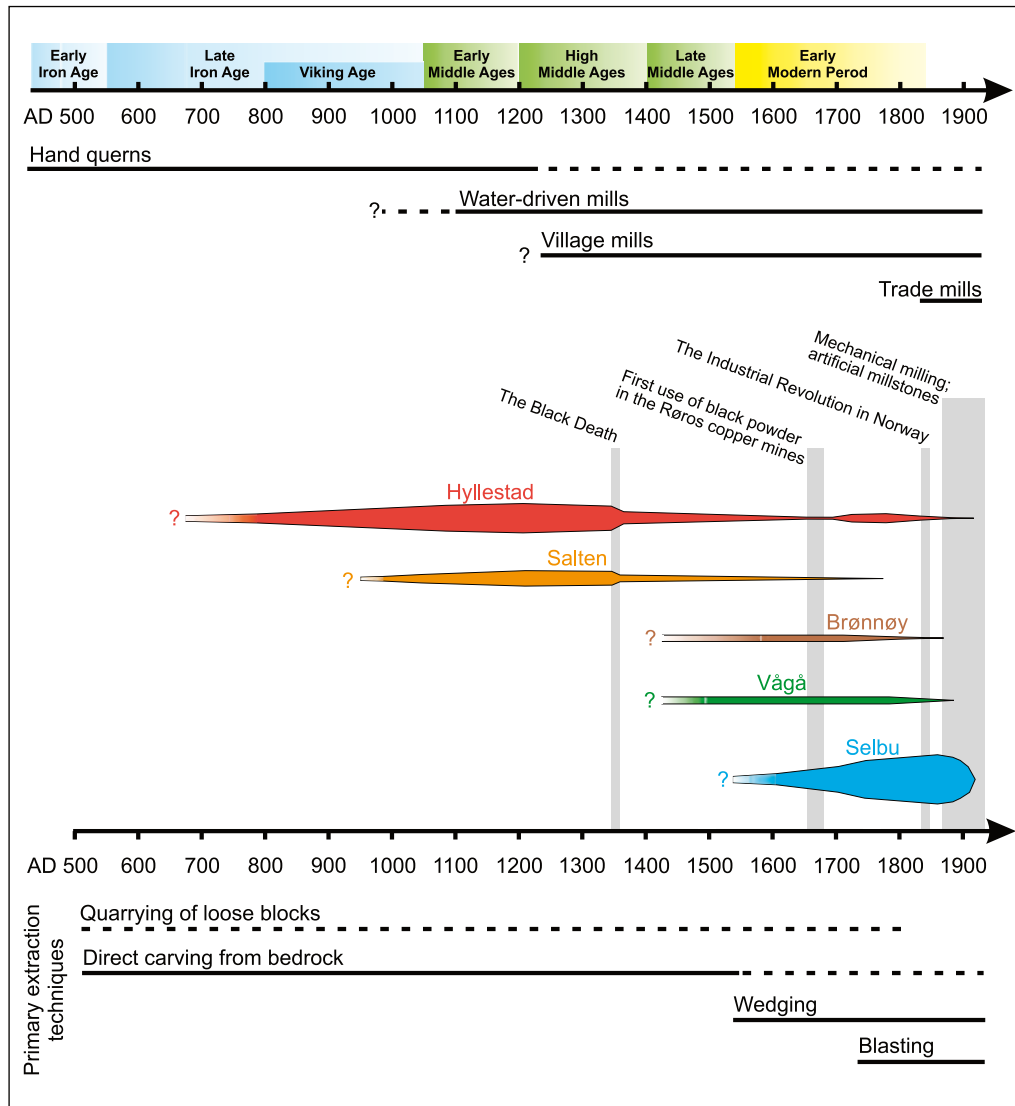


Figure 30. Time line showing the development of the major millstone-quarry areas, together with related technological and historical events in Norway. See discussion in the text for details. Figure based on data from Baug (2002), Berg (1998), Brekken (1980), Carelli and Kresten (1997), Friis (1632), Grieg (1960), Gulbrandsen (1969), Helberg (2007), Krokvik (1999), Monssen (1997), Rolseth (1947), Schøning (1778), Sognes (1980), Statens Kornforretning (1934), Trones (2003) and Tønnesson (1997).

extraction, aided by foreign stonemasons (Storemyr and Heldal 2002). The planning and organisation of the later medieval millstone quarries in Hyllestad bear strong similarities to some of the large building-stone quarries and may have been inspired from this activity. This specifically applies to deep extraction in tall steps. We know that the Munkeliv Abbey took over land in Hyllestad at about the early 12th century (Baug 2002), including some of the most important millstone-quarry areas. As the monasteries were important users of building stone and may have been directly involved in the exploitation of such quarries themselves, it is reasonable to assume that the knowledge of building-stone production had some impact also on millstone-quarry technology and organisation.

The production of water millstones and hand millstones during the Middle Ages represents the peak of the Hyllestad millstone industry, both with respect to volume and distribution of the products (Carelli and Kresten 1997, Baug 2002). This period was followed by a decline in quarrying activity during the Late Middle Ages. Post-medieval quarrying techniques parallel

those of the Selbu area, but production never reached the previous levels and was negligible compared to Selbu (Figure 30).

A major shift in primary extraction technique came with the use of wedging in Selbu, apparently in the 16th century, followed by further development of wedging combined with blasting techniques. At least in Selbu, blasting led to highly efficient quarrying, but the question remains as to why the principal change in extraction method, from primary carving to wedging, occurred well before powder was introduced in quarrying early in the 18th century.

Laws and taxes urged farmers to bring their grist to larger village mills already from medieval times. Together with the general technological development, this led to a demand for larger and more durable millstones. Although it is likely that the coinciding shifts in quarrying techniques and quarry areas were at least to some extent influenced by the increasing usage of large millstones, which were easier to produce in Selbu due to different geological conditions, as discussed above, additional factors may have served to strengthen the development. The

Selbu quarries are located in a mountainous region far from permanent settlements and harbours, and in traditional ways of thinking production took place ‘against all odds’. On the other hand, the Selbu quarries were closer to important grain producing areas in central and eastern Norway, which may have been a driving force for building market power. Such a scenario is particularly relevant for the rise of Selbu quarrying in the 16th century, when the Norwegian population started to increase after the catastrophic decline following the Black Death in 1349–50 and recurrent serious outbreaks of the plague until the first half of the 15th century (Figure 30). Even if the old quarrying skills were not necessarily lost, the small population through this period may have reduced or practically ruined the trade of millstone that was previously dominated by Hyllestad, leaving the market open for new entrepreneurs when population and trade recovered.

Another aspect of the Selbu quarries is its location in the important copper province of central Norway. New mining technology was introduced to Norway in the 16th century when the Danish–Norwegian King Christian III (Norwegian reign 1536–59) summoned Saxonian mine officials to help with copper exploration and mining. The first direct evidence of copper mining in Selbu is from 1713, when the Høiaas mine (‘Gammelgruva’) was opened for production and was worked intermittently until 1764 (Rolseth 1945). The mine was located only a few kilometres from the millstone zone (Figure 10), and many of the farmers involved in millstone quarrying were also periodically involved in mining. Thus, it is likely that knowledge of mining technology disseminated to the millstone quarries earlier and faster than in Hyllestad. Moreover, historical records indicate that copper exploration in the region began already in the 16th century (Rolseth 1945). A letter from Archbishop Erik Walkendorf of Nidaros, written in 1516, refers to copper findings by Swedish miners at a distance from Trondheim that fits with the Høiaas mine in Selbu or ores in the Meråker area just to the north. This implies that the area may have benefited from the influence of new mining technology at a very early stage after the late-medieval recession.

Concluding remarks

The Hyllestad and Selbu quarry areas define huge ‘industrial landscapes’, which are testament to acquisition of stone resources over hundreds of years. Starting at least 1300 years ago, large-scale millstone production in Hyllestad saw a gradual development of technology from ancient hewing techniques, similar to those used for soapstone extraction since the Early Iron Age, to the more centralised and technologically advanced exploitation that may have been initially introduced by professional stonemasons related to the establishment of monasteries during the early 12th century. The decline in millstone production in Hyllestad after the High Middle Ages and the rise of Selbu as the dominant producer from the 16th century, coincided with a major

technological shift to wedging, later combined with blasting, as the primary extraction technique (Figure 30).

It is likely that such a dramatic change in market dominance was significantly influenced by the breakdown of social and trade structures following the Black Death and recurrent plague outbreaks through the late 14th and early 15th century, leaving the market open for ‘newcomers’ when population and trade was recovering in the 16th century. Yet equally important was the increasing demand for larger millstones caused by the gradual change from hand querns to water mills, and from farm mills to village mills (Figure 30). These changes in demand favoured the geological conditions in Selbu, the properties of which consequently necessitated different extraction techniques.

Geological surveys are obviously crucial in multidisciplinary studies of such landscapes. For instance, knowledge of the exploitation of geological resources through history provides insight into developments in stone-working skills and the transfer of technology across regions, which again adds important information about social contexts. Moreover, geological studies of ancient quarries are essential in provenance studies of archaeological stone artefacts, which is a powerful tool in the understanding of trade routes and relations between countries and regions.

The knowledge gained from this study opens new challenges and possibilities. On the one hand, it points to the need for heritage management systems capable of dealing with ancient industrial landscapes, and on the other, it is significant for the historical identity of local communities and is essential in the development of geotourism. The Hyllestad and Selbu quarry landscapes are extensive and well preserved and clearly have a potential for arousing interest on an international scale as ‘windows’ into mankind’s utilisation of geological resources.

Acknowledgements

We are grateful to Irene Baug, Torbjørn Løland, Finn B. Førsund and Bjarne Akse for sharing their knowledge of the Hyllestad area, and to Ola A. Hårstad, Knut Stomsvik and Rut Langbrekke Nilsen for discussions on various aspects of the Selbu quarries. Ane Engvik is thanked for valuable comments on the structural and metamorphic geology. The enthusiasm and interest of the Hyllestad and Selbu municipalities have been crucial for the implementation of the studies and is greatly acknowledged. Thanks are also extended to Leif Furuhaug (NGU) for help with mapping and preparation of figures, and to Astrid Waage (Hyllestad), Per Morten Storhaug and Sverre Selboe (Selbu) for logistical support. Øystein J. Jansen and Peter Kresten are thanked for their thorough and constructive reviews of the manuscript. The present paper is a result of ongoing multidisciplinary research in Hyllestad and Selbu, funded by NGU, the Directorate for Cultural Heritage, the Directorate for Nature Management, the Sør-Trøndelag County Council and the Hyllestad municipality.

References

- Alsvik, E., Sognnes, K. and Stalsberg, A. (1981) Kulturhistoriske undersøkelser ved Store Kvern fjellvatn, Selbu, Sør-Trøndelag 1978. Det Kongelige Norske Videnskabers Selskab, Museet. *Rapport Arkeologisk serie 1981*, Trondheim, 146 pp.
- Baug, I. (2002) Kvernsteinsbrota i Hyllestad. Arkeologiske punktundersøkingar i steinbrotsområdet i Hyllestad i Sogn og Fjordane. *Norsk Bergverksmuseums skriftserie*, **22**, 113 pp.
- Berg, B.I. (1998) *Gruveteknikk ved Kongsberg Solvverk 1623–1914*. Centre for technology and society, Norwegian University of science and technology, Norway, *Report 37*, 586 pp.
- Brekken, J. (1980) Tolstadkvernberget og andre kvernsteinbrot i Vågå og Sel. *Årbok for Gudbrandsdalen 1980*, pp. 78–83.
- Carelli, P. and Kresten, P. (1997) Give us this day our daily bread. A study of Late Viking Age and Medieval Quernstones in South Scandinavia. *Acta Archaeologica*, **68**, 109–137.
- Chauvet, A. and Dallmeyer, R.D. (1992) $^{40}\text{Ar}/^{39}\text{Ar}$ mineral dates related to the Devonian extension in the southwestern Scandinavian Caledonides. *Tectonophysics*, **210**, 155–177.
- Chauvet, A., Kienast, J.R., Pinarion, J.L. and Brunel, M. (1992) Petrological constraints and PT path of Devonian collapse tectonics within the Scandinavian mountain belt (Western Gneiss Region, Norway). *Journal of the Geological Society, London*, **149**, 383–400.
- Dahl, J.M. (1986) Kvernsteinene på Ullandhaug. *Frå haug ok heidni*, **1**, 4–7.
- Friis, P.C. (1632) *Norriges oc Omliggende Øers sandfærdige Beskriffuelse*. København, 185 pp.
- Grieg, S. (1960) Kvern kall og mølle. *Volund, Norsk Teknisk Museums tidsskrift 1960*, 9–45.
- Gulbrandsen, G. (1969) Kornmaling gjennom tiderne. *Volund, Norsk Teknisk Museums tidsskrift 1968*, 9–156.
- Haarstad, K. (1972) *Selbu i fortid og nåtid*, Volume 1. Aktietrykkeriet in Trondheim, 405 pp.
- Hacker, B.R. and Gans, B.G. (2005) Continental collisions and the creation of ultrahigh-pressure terranes: Petrology and thermochronology of nappes in the central Scandinavian Caledonides. *GSA Bulletin*, **117**, 117–134.
- Hacker, B.R., Andersen, T.B., Root, D.B., Mehl, L., Mattinson, J.M. and Wooden, J.L. (2003) Exhumation of high-pressure rocks beneath the Solund Basin, Western Gneiss Region of Norway. *Journal of Metamorphic Geology*, **21**, 613–629.
- Hansen, A.M. (1991) Kverna som maler på havets bunn. Et kvernsteinsfunn i Alverstraumen, Lindås i Hordaland. *Sjøfartshistorisk årbok 1991*, pp. 195–215.
- Hansen, A.M. (1997) Maritime perspektiv på kvernsteinsproduksjonen i Hyllestad. Arkeologi og kystkultur, 25 and 26 October 1997, Sunnmøre Museum, Ålesund, Proceedings, Sørheim, H. (ed.), pp. 58–63.
- Helberg, B.H. (2007) Rapport vedrørende overvåking av inngrep i kvernsteinsbrudd i damområdet for Saksenvik kraftverk, Saksenvik i Saltdal Kommune, Nordland. *Unpublished report*, Tromsø, 9 pp.
- Heldal, T. and Bloxam, E.G. (2007) Kartlegging og karakterisering av kvernsteinsbruddene i Hyllestad. *NGU Rapport 2007.079*, 120 pp.
- Helland, A. (1901) *Bergverksdrift og Stenbrydning i Norge*. John Griegs Forlag, Bergen, 116 pp.
- Krokvik, O. (1999) Kvernsteindrif. *Blad av Brønnøy Historie 1999*, 26–30.
- Monssen, J.D. (1997) Kvernfloget. *Saltdalsboka*, Saltdal kommune, pp. 17–18.
- Olesen, N.Ø., Hansen, E.S., Kristensen, L.H. and Thyrsted, T. (1973) A preliminary account on the geology of the Selbu–Tydal Area, the Trondheim Region, Central Norwegian Caledonides. *Leids Geologische Mededelingen*, **49**, 259–276.
- Rolseth, P.O. (1945) *Selbo Kobberverk*. Selbu og Tydals Historielag, 188 pp.
- Rolseth, P.O. (1947) *Kvern fjellet*. Selbu og Tydals Historielag, 275 pp.
- Rønneseth, O. (1968) Das Zentrum der ältesten Mühlsteinindustrie in Norwegen. In Haarnagel, C.W. and Raddatz, K. (eds.) *Studien zur europäischen Vor- und Frühgeschichte*, Karl Wachholtz Verlag, Neumünster, pp. 241–252.
- Rønneseth, O. (1977) Kvernsteinsbrota ved Åfjorden. *Sogeskrift frå Hyllestad*, hefte 2.
- Schønning, G. (1778) *Reise giennem en deel af Norge 1773–1775*. Det Kongelige Norske Videnskabers Selskab i Trondheim i anledning af dets 150-Aars Jubilæum, 1920. Trondhjem, A/S Adresseavisens bogtrykkeri, 333 pp.
- Skjølsvold, A. (1969) Et keltertids klebersteinsbrudd fra Kvikne. *Viking*, **33**, 201–238.
- Sognnes, K. (1980) Kvernsteinsdrifta i Monsholet. *Årbok for Helgeland 1980*, 171–176.
- Statens Kornforretning (1934) *Norske mylnor og kvernar*. Bind I–II, H. Aschehoug and Co., Oslo, 556 pp.
- Storemyr, P. and Heldal, T. (2002) Soapstone production through Norwegian history: geology, properties, quarrying and use. In Herrman, J.J., Herz, N. and Newman, R. (eds.) *Asmosia 5—Interdisciplinary studies on ancient stone*. Proceedings of the Fifth International Conference of the Association for the Study of Marble and Other Stones in Antiquity, Museum of Fine Arts, June 1998, Boston, Archetype Publications, London, pp. 359–369.
- Strøm, H.C. (1820) Beretning om Qværnsteinsbruddene i Sælboe. *Budstikken*, issue 59–66.
- Thue, J.B. (2000) Livets steinar: produksjon og eksport av kvernstein frå Hyllestad i mellomalderen. *Skald*, Leikanger, 79 pp.
- Tilling, M. (1999) *Structural and metamorphic development of the Hyllestad-Lifjorden Area, Western Norway*. Cand. Scient. thesis, University of Bergen, 264 pp.
- Titland, H.P. (2003) Kvernsteinsbruddene i Saltdal. *Saltdalsboka 2002/2003*, Saltdal kommune, pp. 35–43.
- Trones, J.I. (2003) Om bergverksdrift fra middelalderen og muligens tidligere. *Saltdalsboka 2002/2003*, Saltdal kommune, pp. 44–47.
- Tønnesson, K. (1997) *Spor i tid. Norge for 1850*. H. Aschehoug and Co. (W. Nygaard), Oslo, 223 pp.
- Waage, A. (2005) Kvernsteinsdrifta i Hyllestad—eit nyoppdaga kapittel av norsk bergverkssoge. *Fortidsvern*, **30**, 28–29.
- Wolff, F.C. (1989) Trondheim, bedrock geology map, scale 1:250,000, *Norges geologiske undersøkelse*.

Groundwater monitoring and modelling from an archaeological perspective: possibilities and challenges

Hans de Beer¹ and Henning Matthiesen²

¹*Geological Survey of Norway (NGU), 7491 Trondheim, Norway.*

²*National Museum of Denmark, Copenhagen, Denmark.*

E-mail: hans.debeer@ngu.no

Since 2002, an intensive monitoring scheme at the World Heritage site of Bryggen in Bergen, western Norway, has shown damaging settling rates caused by deterioration of underlying cultural deposits. Monitoring focuses on both chemistry and quantity of groundwater and soil moisture content in the saturated and unsaturated zone. Continuous logging of piezometric head, oxygen and soil moisture content and chemical analyses of water and soil samples are key elements. The monitoring includes registration of movement rates for buildings and soil surface, field measurements and archaeological recording in small excavations, as well as studies of archaeological and modern materials in the subsoil. The results have given good insight into the preservation conditions, with focus on deterioration rates. Groundwater monitoring and chemical analyses reveal a dynamic flow regime under the thick, organic cultural deposits of the site. The flow regime is controlled by interaction of tidal fluctuations, urban drainage systems, natural and urban stratigraphy and bedrock hydraulic features. The documented preservation conditions within the cultural deposits as well as oxygen and moisture-content fluctuations in the unsaturated zone have a significant correlation with the different groundwater flow dynamics found throughout the site. It is demonstrated that groundwater and soil-moisture monitoring, combined with 3D transient modelling are potentially effective routines to improve the understanding of preservation conditions in complex archaeological surroundings and, therefore, protection of archaeological deposits in situ.

Introduction

Preservation conditions of archaeological remains preserved in situ are dependent on both the natural environment and changes to this environment caused by urban development, agriculture or climate changes (Holden et al. 2006). Most variables influencing the preservation conditions are closely related to the presence or absence of groundwater. Absence of water leads to increased flux of oxygen into the deposits and increased deterioration of archaeological materials. Therefore, to better understand the preservation conditions and eventually design measures to protect archaeological deposits, it is necessary for any archaeological site to be placed within its wider natural environment, and to thoroughly understand the natural hydrogeological balance and possible changes that are being forced upon it by nature or human activities.

In situ preservation is often preferred to excavation as a sensible way to manage non-renewable archaeological resources (Valetta Treaty 1992). The idea is to leave some undisturbed archaeological remains as research material for future generations of archaeologists, who will probably have better methods and who will certainly ask different questions than today. Also, constraints on museum space, and conservation and curation costs, limit excavation. In situ preservation is, however, only a viable strategy if the archaeological deposits are lying in a steady, balanced environment, with no or only insignificant decay going on (Corfield et al. 1998, Nixon 2004). As groundwater is a major factor, monitoring of the piezometric head and chemical analysis of groundwater and soil pore water are included in many monitoring projects of archaeological deposits. However, only few attempts exist to combine dynamic hydrogeological and geochemical data in an integral interpretation focused on preservation conditions. A first attempt to compare the chemical analyses from Bryggen in Bergen, western Norway, with monitoring data from Parliament Street in York, Tower of London, and leachate from landfill sites was made by Matthiesen (2008).

Monitoring of the preservation conditions in the archaeological deposits at the World Heritage Site Bryggen in Bergen has been ongoing since 2002. The monitoring covers both the saturated and unsaturated zone and includes detailed chemical analysis of water and soil samples, continuous logging of piezometric head, oxygen and soil moisture content, measurements of movement rates for buildings and soil surface (Jensen et al. 2004), field measurements in test pits, as well as studies of archaeological material and modern samples left in the soil for a few years. It has been found that preservation conditions within the 0.02 km² study area vary considerably, from excellent to very poor preservation conditions, as well as intermediate zones with less ideal preservation conditions (Matthiesen et al. 2007).

This paper will focus on the underlying causes of these conditions, by linking integrated hydrological investigations such as high-resolution groundwater monitoring, modelling

and chemical analysis to archaeological investigations. We will test the following hypotheses:

H1. A combined hydrological and archaeological approach leads to a more fundamental understanding and thus improved protection of the archaeological site in situ.

H2. A combined hydrological and archaeological approach improves identification of archaeological deposits at risk.

Site description

History

Bryggen in Bergen, with its traditional timber buildings, is one of the oldest trading ports in northern Europe, and one of the Hanseatic Leagues' four overseas offices. The current buildings are from 1702, but have a pre-Hanseatic building structure dating back to the 11th century (Figure 1). A historical map showing important (former) hydrogeological features such as drainage patterns, former coastline and catchment areas during the Middle Ages is shown in Figure 2.



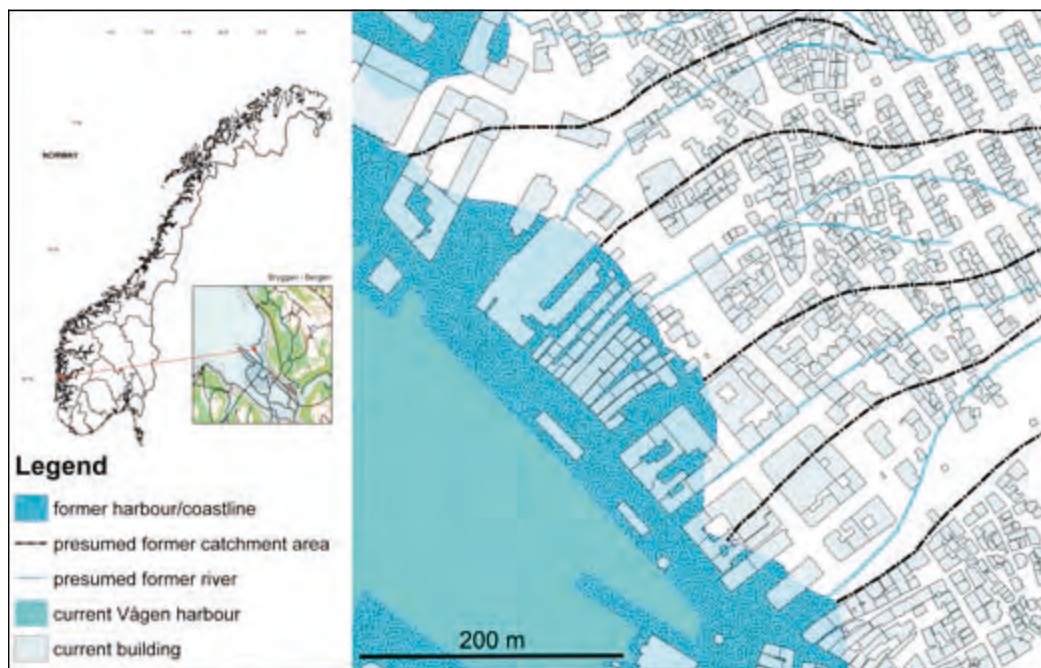
Figure 1. Traditional timber buildings of Bryggen, interconnected in long rows with narrow straits in-between.

In 1955, a large fire destroyed about a third of Bryggen's buildings, on the western side of the study area. Extensive archaeological excavations took place in the period from 1955 to 1968 by A.E. Herteig (Herteig 1985). In 1979, Bryggen was included in the World Heritage list based on the selection criterion "to bear a unique or at least exceptional testimony to a cultural tradition or to a civilization which is living or which has disappeared" (Unesco 2008). The total system comprising the World Heritage Site Bryggen, including underground archaeological remains plus 61 buildings, i.e., from the underlying bedrock to the rooftops, is to be considered a single cultural monument.

After Herteig's archaeological excavations were completed in 1968, a hotel with underground parking lot was constructed in 1979 at the former excavation area, west of the remaining part of Bryggen.

Low phreatic levels and increased flux of oxygen in the

Figure 2. Index map and historic map showing important hydrogeological features such as former natural drainage patterns, coastline and catchment areas during the Middle Ages (modified after Department of History, University of Bergen).



subsurface, leading to decomposition of organic material and settling, currently threaten World Heritage Site Bryggen. A large restoration project is running from 2001 to 2021, covering all the buildings and their foundations. The strategic project aims to bring Bryggen to a state of repair that is in accordance with the status as a World Heritage Site, and where only regular maintenance is necessary. More details on the history of Bryggen are given in Christensson et al. (2004).

Archaeology

Below the buildings lie cultural deposits covering the entire span of Bryggen's history. The excavations in 1955–1968 revealed an excellent state of preservation and a huge amount of information in the deposits (Herteig 1969). It has been, and will be, of great importance to understand the different ways in which the cultural layers were deposited, and to interpret the varying relationships between layers and constructions (Myrvoll et al. 1983, Christensson et al. 2004). At Bryggen, the cultural deposits with their 'cargo' of constructions and artefacts add up to a thickness exceeding 8 m in places, with 10 or more separate building phases one on top of the other. A 'typical' sequence consists of layers with high organic content interspersed with fire-layers, the latter being the remains of many fires that struck Bergen in medieval and later times. The deposits are highly organic, with loss on ignition values of 10–70% in most layers and water contents commonly over 100% (weight to dry weight). The deposits constitute approximately 100,000 m³. Soil samples from the current monitoring project show that the state of preservation is still good in most of the area, with a few exceptions (Dunlop 2007). The current policy for Bryggen is to not excavate but leave as much as possible for future generations. This requires the survival of all the evidence

preserved in the cultural deposits through the maintenance of the physical, chemical and hydrogeological conditions that resulted in its preservation.

Hydrogeology

The hydrogeological situation of the site is characterised by Bryggen's position along the Vågen harbour, just beneath a mountain slope. The regional groundwater level is topographically induced, representing a subdued print of the topography with a regional groundwater flow towards Vågen. The regional phreatic level and hydraulic heads in deeper geological formations depend on the amount of precipitation, the infiltration capacity and the hydraulic characteristics of the underlying sediments, cultural deposits and bedrock.

Bryggen is located on a geological formation called the 'Bergen Arc', consisting of greenstones, phyllites and gneisses with a low primary hydraulic conductivity. During the construction of a railway tunnel to the northeast of Bryggen, high water bearing features such as zones of weakened bedrock, open faults and joints were mapped. Under the World Heritage Site, the bedrock surface occurs at about 12 m below sea level, rising gradually to about 2 m below sea level at the northeastern side of Bryggen. Old beach sands and underlying moraines cover the bedrock, representing the old coastline before the current quay was constructed. The wooden buildings were originally built on the beach along the coastline. After a fire, new buildings were constructed on top of the old foundations.

Although the regional groundwater flow is generally in a southwestern direction towards the harbour, local phreatic level, hydraulic head and chemistry are influenced by a complex interaction of multiple factors: (a) Precipitation and evaporation, influenced by buildings and terrain surface such as

pavements and vegetation. Mean annual precipitation is 2250 mm, while mean annual evaporation is about 450 mm (source: Norwegian Meteorological Institute, Penman estimate). Terrain surface varies from cobbles, wood planking, asphalt to grassland. (b) Local variations in hydraulic properties such as natural alternation of sand, silt and clay, bedrock fractures, filling materials and trenches, causing heterogeneity or anisotropy of the hydraulic permeability. Water-bearing fractures have earlier been identified and mapped during tunnel construction in the direct vicinity of Bryggen. Archaeological investigations describe a large heterogeneity in filling materials and trenches, often constructed for dewatering the former tenements. (c) Tidal variations and salt-water intrusion, tidal variation being up to 2 m, while seawater intrusion and flooding with a mixture of seawater and rainwater causes a complex density-dependent flow system at the front of Bryggen (Golmen 2005). (d) Groundwater-regulating systems such as drainage, but also (unwanted) leakages in sewage and storm-water runoff pipes. According to the authorities, no known significant leakages in the domestic water-supply system exist. Diffuse leakages, damaged storm-water runoff pipes and wrong jointing of pipes are well known, but unquantifiable phenomena at Bryggen. (e) Underground infrastructure such as sheet piling and cellars. A sheet piling exists around the underground parking of the hotel on the former excavation site west of Bryggen, as well as around Bryggen's museum northwest of the hotel.

A simplified section is shown in Figure 3.

Methodology

Introduction

Holden et al. (2006) demonstrated from a research review on hydrological controls of waterlogged archaeological deposits, that both the quantity and quality of data on preservation status, as well as hydrological and chemical parameters collected during routine archaeological surveys, need to be improved. Any activity that changes either source pathways or the dominant

water input may have an impact not just because of changes to the water table, but also because of changes to water chemistry. In order to understand the preservation potential fully, it is necessary to move away from studying the archaeological site as an isolated unit, since factors some distance away from the site of interest can be important for determining preservation (Holden et al. 2006). The methodology used at Bryggen follows this recommendation by using regional and local groundwater modelling parallel to field investigations, chemical analyses and monitoring.

Low phreatic levels and increased flux of oxygen in the subsurface, leading to decomposition of organic material and settling, currently threaten Bryggen. In order to better understand the water balance and factors influencing the phreatic levels at Bryggen, numerical modelling has been used parallel to field monitoring and laboratory analyses. The use of groundwater modelling in addition to 'traditional' monitoring efforts enables continuous adjustment and improvement of the monitoring strategy, thereby improving both the understanding of the hydrogeological system as well as giving feedback to the numerical model describing the system more adequately. Ultimately, the numerical model can then be used as a tool to predict changes in hydraulic head and phreatic levels as a consequence of natural or human changes forced upon it.

The field monitoring covers both the saturated and unsaturated zone and includes detailed chemical analysis of water and soil samples, continuous logging of piezometric levels, oxygen and soil moisture content, measurements of movement rates for buildings and soil surface, field measurements in test pits, as well as studies of archaeological material.

Numerical modelling

To improve the understanding of the hydrological system and the factors influencing the phreatic levels at Bryggen, a numerical groundwater model was constructed (de Beer et al. 2007). As with all hydrogeological model formulations, a model is a simplification of reality and inherently includes a number of errors. These errors are related to conceptualisation and descrip-

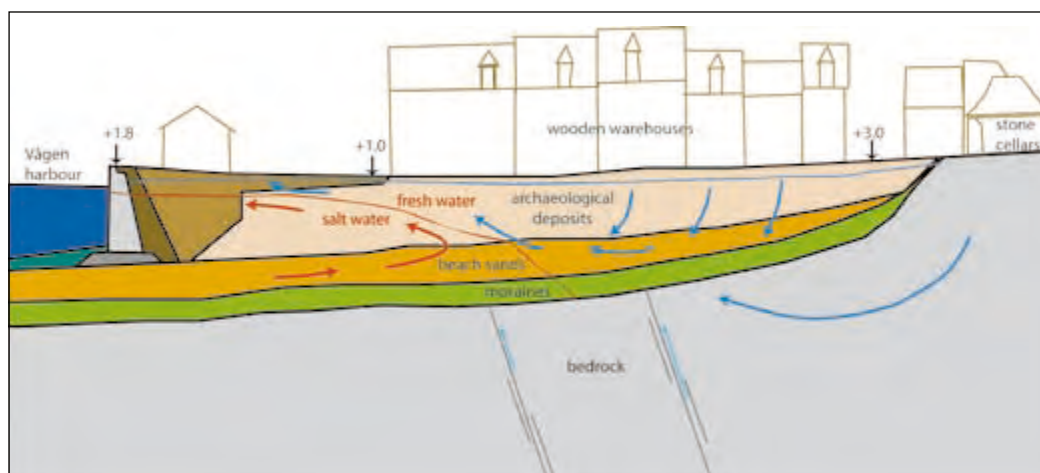
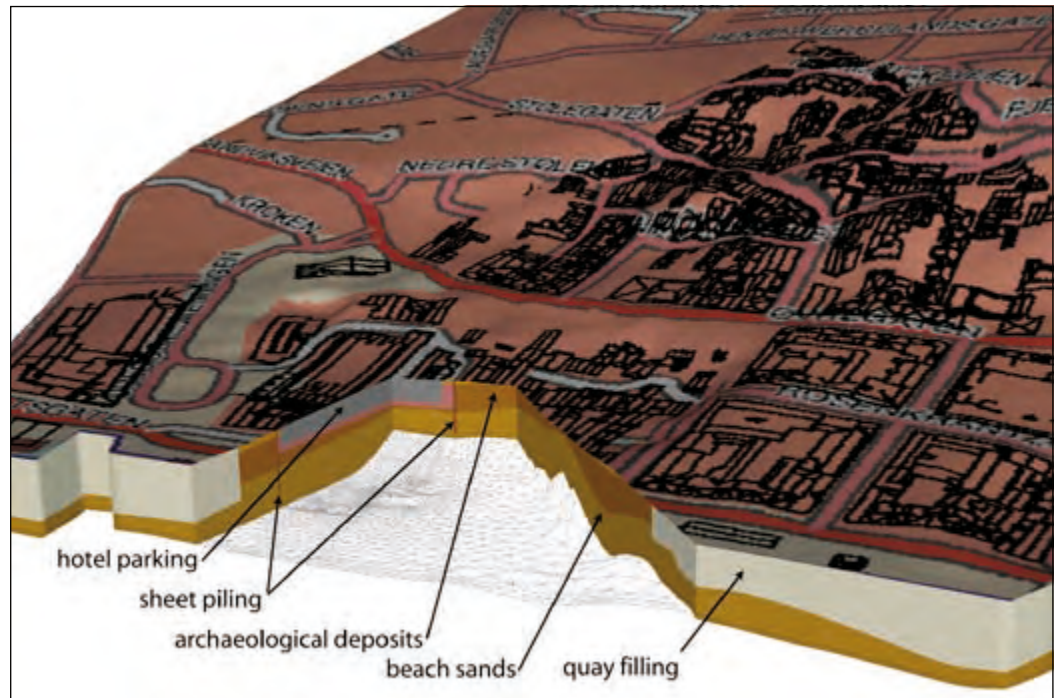


Figure 3. Model section from the rear of the old wooden settlement to the modern quay front (modified and extended after E. Mørk, Stiftelsen Bryggen).

Figure 4. 3D block diagram of the topographical layers included in the groundwater model, showing schematisation of archaeological deposits, quay front and bedrock level.



tion of processes and interactions, estimates of parameter values, initial and boundary conditions, spatial and temporal variability and system stresses (Bierkens et al. 2006). In order to increase the usefulness of predictive simulations, it is necessary to reduce the uncertainties by indicating and quantifying the reliability of the results by verification against monitoring values. However, also early conceptual or intermediate (steady state) modelling stages provide valuable information and understanding of the hydrological system facilitating improvement of the monitoring program.

The finite element model code Feflow[®]5.3 (Diersch 2007) was used to simulate groundwater flow at Bryggen. Feflow[®] models flow, contaminant mass and heat-transport processes as coupled or separate phenomena. It is based on the physical conservation principles for mass, chemical species, linear momentum and energy in a transient and three-dimensional numerical analysis. For detailed description on the numerical calculations is referred to Diersch et al. (2007).

The model code has been chosen because of its ability to simulate fully three-dimensional transient groundwater flow, including density-driven flow (salt/fresh-water interaction and temperature effects), 3D anisotropy and flow within the unsaturated zone. Because the code is based on the finite element method, it provides an extremely flexible grid generation that is advantageous for use in urban areas with man-made structures such as sheet piling and drainage systems. In the unsaturated zone, insufficient soil-moisture measurements at various depths are currently available to adequately simulate unsaturated flow. The first slice in the model simulates a 'free' phreatic level and therefore changes its vertical position in time.

The chosen model area encloses the catchment area in which the study area is located. It extends from the Vågen harbour

towards the topographically higher area of Fløyfjellet, behind Bryggen. Based on borehole descriptions, geological mapping, archaeological descriptions and construction drawings, a numerical model was constructed using 10 model layers with their estimated hydrogeological properties. The model layers were constructed using a digital terrain model, spatially interpreted borehole data and known construction depths for buildings.

A block diagram illustrating the schematised hydrogeological layering in the upper 5 layers of the numerical model is shown in Figure 4. The model consists of 158,200 6-noded triangular prisms, with a total of 88,572 nodes. The model mesh has been strongly refined along sheet piling and drainage systems. Boundary conditions have been applied along the harbour (tidal variations, salt water), top layer (daily precipitation) and known drainage systems (drainage level).

The hydraulic properties used prior to verification against monitoring values, are based on literature values, borehole descriptions and grain-size analyses. Parameter values were changed stepwise in a procedure of sensitivity analysis, steady-state calibration and subsequent transient calibration against registered piezometric levels, tidal variations and daily precipitation measurements (weather station 50540, Bergen-Florida).

For natural sediments, a range of applicable hydrogeological parameter values such as permeability, storativity and porosity exists, based on literature values, grain-size analyses or pumping tests. The hydraulic properties of an extremely heterogeneous archaeological deposit can only be deduced indirectly from groundwater-pressure measurements above, inside and below the deposit, in addition to a spatial distribution good enough to reflect effects of horizontal heterogeneity. However, a good description

of the archaeological materials themselves, such as configuration and layering, together with a detailed description of the non-archaeological matrix between the archaeological artefacts, will give a qualitative indication of the hydrogeological behaviour to be expected. In the case of Bryggen, detailed knowledge about the configuration and layering of the archaeological structures has been gathered during archaeological excavations. One of the key features is horizontal layering of wooden elements together with known dewatering structures in and around the buried foundations. In model terms this is interpreted as a form of anisotropy, with a higher horizontal permeability than a vertical permeability and possible existence of preferential flow paths. Experiences with dewatering during excavation suggest relatively homogeneous, low permeability of the deposits. These qualitative data were used during calibration of the numerical model, in combination with monitored piezometric levels.

Field monitoring and laboratory analyses

In 2001–2005, a network of 14 observation wells (MB1 to MB14) was installed at selected locations within the archaeological deposits (Figure 5). One observation well (MB11) was installed in modern fill and archaeological and natural deposits about 150 m northeast (uphill) of Bryggen. Observation well MB11 was located further away from Bryggen in order to obtain undisturbed background data on the phreatic groundwater level, possibly reflecting the recharge pressure towards Bryggen. No other regional observation wells currently exist, which thus limits the interpretation of the regional groundwater flow system.

After a first (steady state) modelling study of the site, another 8 observation wells (MB16 to MB23) were installed in

2005–2006 (Figure 5). In order to place the site within its wider hydrological context, these observation wells were installed at specific locations within and outside the actual heritage site and at specific depths to determine vertical groundwater flow and chemistry changes. MB18 to MB22 are observation wells with a filter placed in the centre of the archaeological deposits, at depths of 6 to 7 m below the current terrain surface. MB23 and MB17 have their filter placed under the archaeological deposits, within the old sea bottom at a depth of approximately 11 to 12 m below the terrain surface (10 m below sea level). MB16 is located inside the hotel area, with a filter placed in remains of the archaeological deposits. MB15 is not yet installed.

When referring to ‘sea level’, the average sea level is referred to. At Bryggen, the average sea level is 1 cm above the national reference level NN1954.

All observation wells were measured manually with a monthly interval during the period 2001–2004. From December 15, 2006, 10 selected observation wells are equipped with data loggers (type Mini-Diver®, Van Essen) registering both piezometric level and temperature on an hourly basis. One data logger for registration of barometric pressure is installed in MB22 to compensate the other series for barometric variations. Sampling of groundwater in MB1–MB14 took place a couple of weeks after installation of each well, and for all wells simultaneously in June 2005. Further information on sampling method and detailed chemical analyses are given in Matthiesen (2008). On April 27, 2007, another 9 selected wells were sampled and analysed for major ions, pH, alkalinity and conductivity. In addition, pH and conductivity have been measured in the field for these 9 wells. An OTD-Diver® (Van

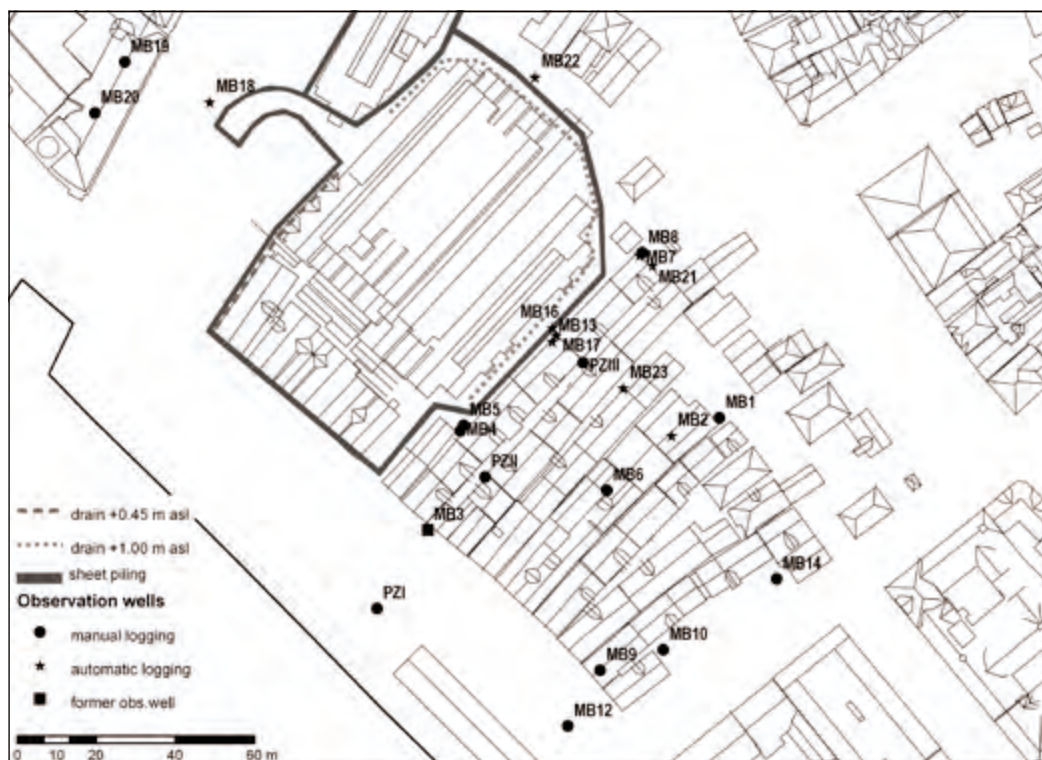


Figure 5. Situation overview with monitoring wells, drainage system and sheet piling.

Essen) was used for continuous logging of oxygen, temperature and piezometric level subsequently in MB1, 2, 3, 5, 6 and 7. A description of the method and detailed discussion of the results are given in Matthiesen (2008). At MB17, grain-size analyses have been performed on a depth-integrated soil sample from the old sea-bottom sand below the archaeological layers, at a depth of 10.6 to 11.4 m below the terrain surface. All analyses took place at accredited laboratories.

After a rough water-balance calculation performed with the numerical model, the drainage system under the current hotel was inspected on January 27, 2006. The discharge volume was measured and drainage water was sampled and analysed on major ions, pH, alkalinity, conductivity, turbidity and colour.

Results

Logger data and temporal variation

Groundwater monitoring results from observation wells MB13, MB22 and MB23 are shown in Figure 6 as representative examples for the groundwater behaviour at Bryggen. Relative variations in observation wells MB2 and MB18 were similar to MB13, MB7 gave the same response as MB22, while MB17 reflected a comparable result to MB23. Daily precipitation is shown for comparison. All piezometric levels have been corrected for atmospheric pressure variations.

The results from the groundwater loggers (Figure 6) show three distinct characteristics for both the local hydrological system at Bryggen as well as the influence of the wider hydrogeological situation:

1. At the rear side of Bryggen (upstream), a slow recession curve indicating a large aquifer system characterises the hydrological system. Observation wells MB7 and MB22 show groundwater variations on the order of 1 m during the measurement period, with an expected base flow level of around 0.5 m after a month with no precipitation.
2. Within the archaeological deposits, a strong correlation exists between the average observed tidal fluctuation in the Vågen harbour and the piezometric level. Piezometric levels are only indirectly influenced by precipitation due to the varying inflow from the recharge area and varying in- and outflow to and from the harbour. From March 21 to April 4, 2007, a rising groundwater trend in the observation wells within the archaeological deposits (MB2, MB13 and MB18) was observed, while there was no precipitation. Until April 9, there was no significant precipitation directly influencing the piezometric levels within the deposits. This groundwater rise coincided with a rise of the daily averaged tidal variations (see Figure 7).
3. Observation wells MB17 and MB23 show a rapid response with a delay of 2 hours with respect to the observed tidal fluctuation in the Vågen harbour. However, the amplitude of the groundwater variation is 90% damped in comparison with the observed tidal fluctuation, unless the observed sea

level is higher than about 0.40 m above the average sea level (see Figures 8 and 9). At sea levels higher than 0.40 m, the piezometric levels are nearly equal to the tidal level. For comparison, the average high water level is 0.45 m above NN1954.

The measured hydraulic heads in the old beach sands under the archaeological deposits (MB17 and MB23) are permanently lower than the measured phreatic levels within the archaeological layers at Bryggen. Groundwater flow within the archaeological deposits is thus downward towards the underlying beach sands. The average head difference at MB2 is 70 cm, reduced to an average of 15 cm at MB13 (Bugården) due to a lowered phreatic level. The average horizontal groundwater flow direction is southwards to the Vågen harbour and partly westwards to the hotel area west of Bryggen. Figure 10 shows the general groundwater flow pattern for both phreatic groundwater and the underlying beach sands as simulated by the groundwater model.

Registered groundwater temperatures from December 15, 2006 to April 25, 2007 in all wells equipped with data loggers vary from 10°C to 14°C. MB11 and MB21 showed relatively low temperatures with respect to the average groundwater temperature. For comparison, the mean annual temperature in Bergen is 7.6°C.

Chemical analyses of groundwater

Matthiesen (2008) describes and discusses the results of chemical analyses of groundwater from 14 observation wells using an extended groundwater-analysis package covering 17 different chemical species. All 14 observation wells have filter positions within archaeological deposits. Correlations between chemical species show that even if the deposits are heterogeneous, the groundwater chemistry is not completely random across the site. A relatively simple model for the groundwater chemistry at Bryggen is presented and used to characterise areas with very good preservation conditions, and areas with more questionable conditions (Matthiesen 2008). A summary of the major ions is presented in Table 1 and graphically in Figure 11 along with new data from chemical analyses performed in 2007. These new data include chemical analyses of groundwater from observation wells below the archaeological deposits (MB17 and MB23) and from a location where archaeological deposits have been removed by excavation (MB22). Table 1 also includes results of chemical analyses of sampled water from the groundwater drainage system under the current hotel area.

Estimate of saturated hydraulic conductivity

During the installation of observation well MB17, a depth-integrated soil sample was taken from the sands below the archaeological deposits. A grain-size analysis was performed in order to obtain a better description of the material and an estimate of the saturated hydraulic conductivity. The grain-size distribution reflects a typical depositional environment of a beach zone, with a relative enrichment of both fine

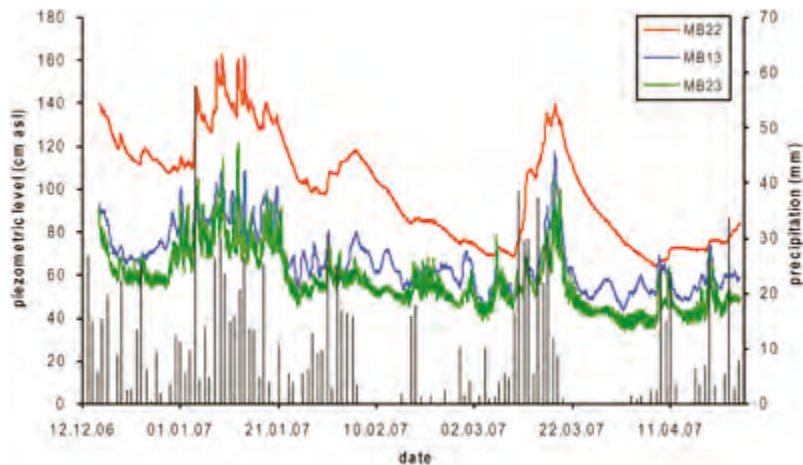


Figure 6. Representative hydraulic heads behind Bryggen (MB22), within archaeological deposits (MB13) and below archaeological deposits (MB23). Vertical lines represent precipitation.

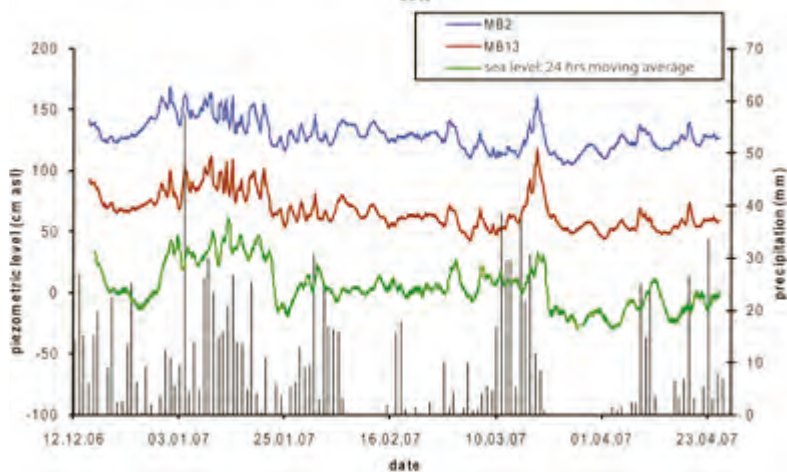


Figure 7. Comparison of 24 hours moving-average sea level with the piezometric level at MB2 and MB 13 (within archaeological deposits). Vertical lines represent precipitation.

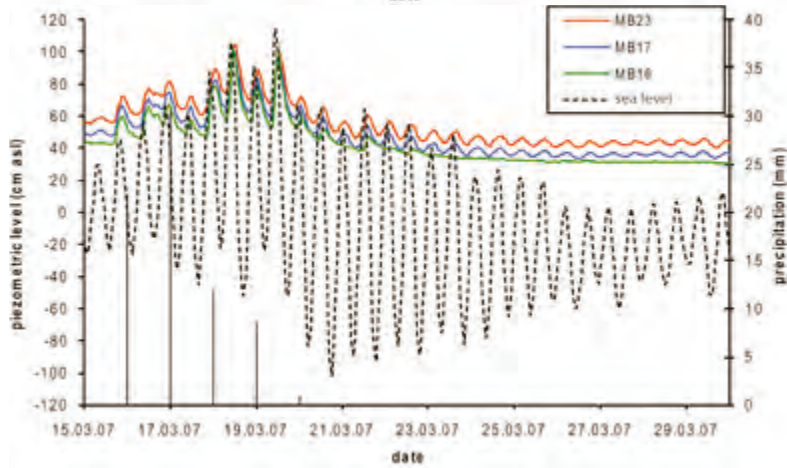


Figure 8. Tidal fluctuations below the archaeological deposits. Vertical lines represent precipitation.

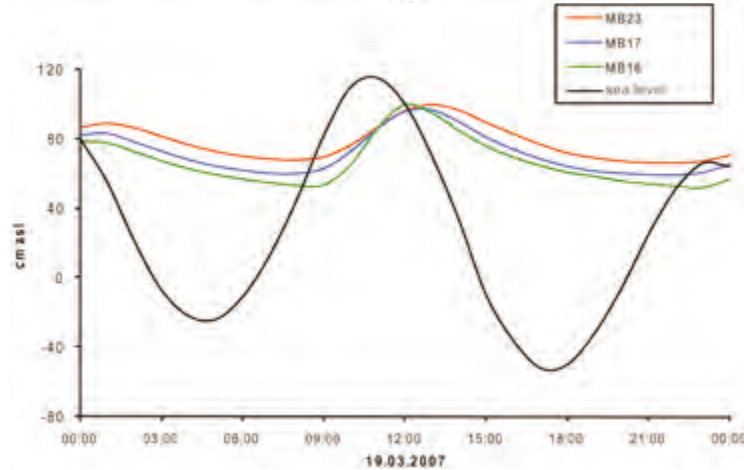


Figure 9. Time delay and damping of sea-level fluctuations to piezometric levels in MB16, MB17 and MB23.

Figure 10. Steady-state simulated phreatic level within the archaeological deposits and the hydraulic (pressure) head in the beach sediments below the archaeological deposits. Arrows indicate general horizontal flow direction.



Table 1. Major ions from analyses of groundwater sampled on the 9th of June, 2005 (Matthiesen 2008). *Sampled on the 25th of April, 2007 (NGU). **Sampled on the 27th of January, 2006 (Multiconsult). All results are in mg l⁻¹ except alkalinity, pH and electrical conductivity (EC). Sulphate is given as mg SO₄ l⁻¹. Molar weights of the different species are given in the second row, to allow easy calculation of the content to mmol l⁻¹.

<i>g mol⁻¹</i>	Na ⁺	K ⁺	Ca ²⁺	Mg ²⁺	Fe ²⁺	Cl ⁻	SO ₄ ²⁻	Alkalinity (meq l ⁻¹)	pH	EC (mS m ⁻¹)
	22.99	39.10	40.08	24.31	55.85	35.45	96.06			
MB1	140	9.7	21	6	24	120	2.6	4.9	7.1	85
MB2	410	26	130	24	1	470	4.5	13.1	6.9	250
MB2*	405	30	114	27	0.16	438	4.4	11.0	6.3	238
MB3	840	38	110	44	0.79	950	9.2	16.1	7.1	540
MB4	230	13	70	12	11	150	<0.5	7.4	7.0	160
MB5	4.6	1.8	9.3	<1	0.11	2.6	10	0.5	7.2	9
MB5*	7.1	1.38	7.9	1	0.01	8.3	3.4	0.5	6.9	10
MB6	790	42	110	43	1.6	1200	7	14.5	7.0	480
MB7	42	7.8	78	10	1.1	63	2.9	4.5	7.6	64
MB9	2700	86	150	250	1.8	4600	400	10.7	7.7	1400
MB10	760	39	200	30	3.1	2000	2	20.7	7.2	750
MB11	68	5.5	79	4	0.02	150	29	2.3	7.6	81
MB11*	14	1.8	23	1	0.012	13.4	5.5	0.8	7.0	16
MB12	410	40	300	60	1.2	710	16	23.4	7.0	420
MB13	110	13	88	14	3.3	130	2.3	11.9	7.2	150
MB13*	155	18	110	18	0.056	147	1.5	12.4	6.4	168
MB14	73	73	170	200	2.3	83	3.4	10.7	7.4	120
MB16*	382	26	206	52	0.274	627	20.5	12.9	6.4	188
MB17*	58	11	108	8	0.014	64.4	0.6	7.4	7.0	93
MB18*	43	13	191	22	19.3	62.3	1.9	10.5	6.4	120
MB22*	19	5.4	61	5	0.076	38.1	24.4	3.1	6.5	51
MB23*	164	22	242	20	0.046	126	2.8	14.3	6.6	66
drain**	202	15	80	22	0.008	318	38.2	4.0	7.2	146

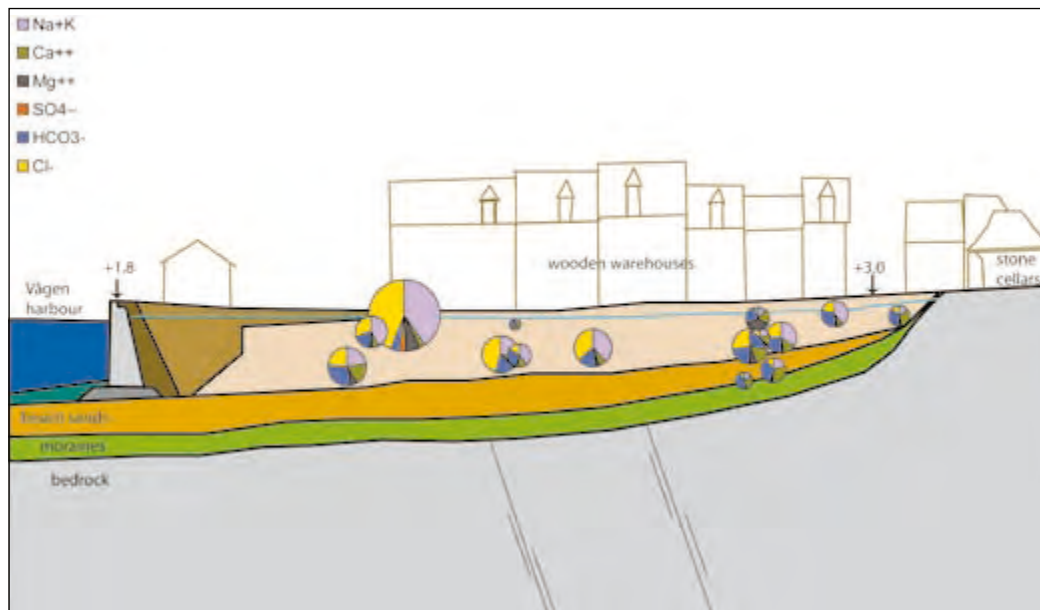


Figure 11. Graphical presentation of major ions in groundwater samples at monitoring wells, sampled in 2005 and 2007. See also Table 1. The left side of each circle represents the anions, while the right side represents the cations (in meq l⁻¹). HCO₃⁻ is estimated from the alkalinity. The area of the circle is proportional to the total amount of dissolved ions. MB11 is outside this picture, and MB8 is not represented as it was dry at the time of sampling.

(< 0.1 mm, $d_{10} = 0.054$ mm) and very coarse (> 5 mm, $d_{60} = 2$ mm) fractions due to washing out by wave activity. Based on a review of empirical formulae to estimate the saturated hydraulic conductivity (Odong 2007) from grain-size analyses, estimates on this highly bimodal, sorted sample are not applicable. We thus have to rely on in situ field testing, groundwater monitoring and model calibration.

Based on the depositional environment, a layering with coarser and finer fractions is expected, probably causing a significantly higher (semi-horizontal) hydraulic conductivity than empirically estimated by grain-size analysis of a depth-integrated sample. Pumping of observation well MB17 and MB23 during sampling indicates a significantly higher saturated hydraulic conductivity in the beach sediments below the archaeological layers than in the archaeological layers themselves. The rapid response of the piezometric pressure to tidal pressure variations (Figures 8 and 9) is a strong indication of a high-permeable deposit. Transient model calibration (ongoing) based on the measured piezometric monitoring indicates a saturated hydraulic conductivity of about $3.4 \times 10^{-4} \text{ m s}^{-1}$, compared to 2×10^{-7} to $8 \times 10^{-7} \text{ m s}^{-1}$ for the archaeological deposits.

Groundwater model calibration

In Figure 10, representative model results are shown for the spatial groundwater variation. Transient model calibration is ongoing and is not discussed in this article. See de Beer (2005) for further details on boundary conditions and steady-state calibration.

Discussion

Groundwater: flow pattern and temporal variations

The hydrological regime within the archaeological deposits is

a result of the interaction of tidal fluctuations in the Vågen harbour and the groundwater flow towards the deposits from the recharge area behind Bryggen. Due to the relatively low hydraulic permeability of the archaeological materials, groundwater changes are slow and dependent on the average fluctuations of the boundary conditions around, above and below the deposits.

Observation wells MB16, MB17 and MB23 (MB17 and MB23 below archaeological deposits) show a clear gradient towards the drainage system under the hotel, west of Bryggen. Rapid reactions indicate a good hydraulic connection. The head difference between MB16 (inside area enclosed by sheet piling) and MB13 (just outside sheet piling), both installed within archaeological deposits, is approximately 20 cm, indicating a limited hydraulic resistance over the sheet piling. The dynamic response of MB16, 17 and 18 confirms this by a slightly increased delay in response from MB16 towards MB23 (Figure 9), reflecting the input of tidal pressure from the hotel area towards Bryggen. The average head differences, the dynamic response and the grain-size analysis from MB17 support the impression of a good hydraulic connection between the drained hotel area and Bryggen, with flow via the old beach sands under the sheet piling. Construction drawings of the hotel show that the sheet piling probably does not reach the bedrock level at the front of the hotel. Groundwater flow through the beach sediments to the drainage system is thus unobstructed.

It is expected that the hydraulic head under the hotel is nearly horizontal due to a thick layer of high-permeable, coarse gravel under the parking lot. The drain installed at 1 m above sea level (asl) at the north and east side of the hotel only occasionally discharges groundwater, which supports this assumption. MB16 can thus be regarded as representative for the piezometric level below the entire hotel. It shows the lowest registered piezometric levels of all measured observation wells.

MB22 shows significantly higher piezometric levels than MB16, but in dry periods the registered levels steadily lower towards the levels of MB16. It shows that the current hydrological balance is not favourable for maintaining high phreatic levels in the archaeological deposits.

It is expected that both the observed horizontal flow towards the Vågen harbour as well as the downward flow within the archaeological deposits will be disturbed by high salt concentrations along the front of Bryggen. Seawater intrusion acts as a barrier for groundwater flow due to its higher density. Analyses of 61 soil samples from the archaeological deposits show that the chloride contents at the quay front are up to 3 orders of magnitude higher than at the back of Bryggen. The analyses also showed that the maximum chloride contents at the quay front were found a few metres down in the deposits, and that the contents decreased at greater depths (Matthiesen et al. 2007). In a natural situation, one would expect an upward flow against the salt-water wedge with a higher fluid density. However, this is dependent on the permeability of the underlying beach sands, its hydraulic connection with the harbour, occasional flooding, and the horizontal flow pressure from the recharge area through the beach sands and possible fractures in the bedrock. Further investigations at the front of Bryggen are required to resolve this issue.

Correlation with chemical data

In order to fully understand the impact of the hydrogeological situation on the preservation conditions, an attempt is made to relate the hydrological measurements with chemical analyses of the groundwater. The chemical composition of groundwater is the combined result of the composition of water that enters the hydrogeological system and reactions with minerals present in sediments and rocks, as well as degradation of organic material and other elements that may modify the water composition (Appelo et al. 2005). A description of the chemical composition of the groundwater within the archaeological deposits under Bryggen has been reported and discussed in Matthiesen (2008), and is further elaborated here.

At MB5, results from an automated oxygen logger show a dynamic environment characterised by abrupt piezometric level fluctuations up to 60 cm, with a sharp increase in oxygen content and a drop of temperature at the depth of the sensor at 1.4 m below sea level (Matthiesen 2008). During installation of MB5, a 30 cm-thick layer of sand and gravel was reported, surrounded by more dense organic-rich soil layers. The archaeological records document that at around this location and on this depth, a contemporary wharf-front was located, presumably indicated by a row of piles (Herteig 1990). According to the archaeological descriptions, a public thoroughfare was present between Bugården and Bredsgården, with a stake-lined drain beneath a stone paving. The drain or sewage was stabilised by a filling of gravel and wood chips of variable thickness providing the bedding for the untrimmed paving stones (Figure 12). Although no hard evidence exists, as there was no excavation



Figure 12. Stake-lined drain filled with gravel and wood chips beneath stone paving in the Bugården thoroughfare (Herteig 1990).

down to a depth of 1.4 m below sea level at MB5, at least the presence of a possible higher permeable element supports the dynamic hydrological environment. Also, a barrier effect of the sheet piling cannot be discarded, where groundwater is 'forced' along preferential flow paths by the sheet piling.

A negative correlation between the alkalinity and the filter depth is presented in Matthiesen (2008), along with positive correlations between alkalinity, ammonium and calcium as well as between potassium and ammonium. The addition of new results for observation wells MB17, MB23 and the drainage water show the increasing alkalinity with depth as reported by Matthiesen (2008), but a clear breach in this trend is observed within the old beach sands, where alkalinity drops significantly. In Figure 13, the alkalinity vs. filter depth is plotted.

The correlation between the alkalinity and filter depth may stem from a vertical or horizontal flow of groundwater. An increasing alkalinity with depth due to a groundwater formation process where groundwater slowly percolates down through the soil layers, gradually picking up bicarbonate and other ions from decaying organic material or from dissolution of carbonates, is supported by the measurements of the piezometric

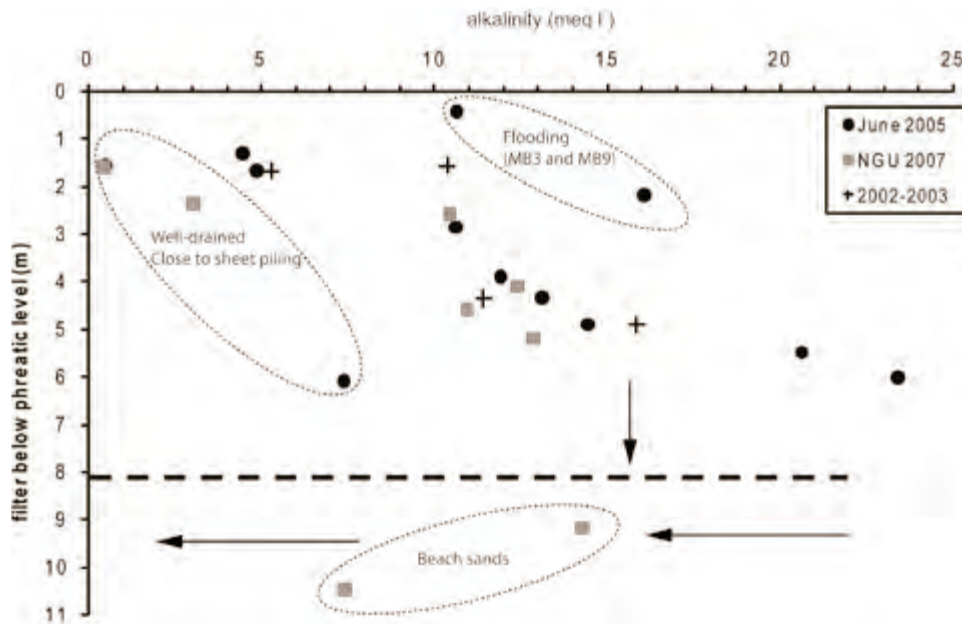


Figure 13. Alkalinity vs. filter depth below the phreatic level at each observation well at the time of sampling. Exceptions from the trend are indicated and general flow direction is shown with arrows.

heads at different depths. A downward groundwater flow exists. However, the alkalinity drops dramatically at depths under the archaeological deposits, indicating an abrupt change of the hydrological environment. Water with high alkalinity from the archaeological deposits is mixed with possibly younger, more diluted groundwater in the permeable beach sediments. Although carbonate is present in the beach sediments (shells), the groundwater does not reflect this by a further rise in alkalinity, possibly due to the highly dynamic environment with relatively short retention times. A similar plot of groundwater conductivity vs. depth gives the same results.

Matthiesen (2008) discerns three types of groundwater: (1) Seawater-influenced groundwater with a high content of Na^+ , Cl^- , Mg^{2+} , SO_4^{2-} and K^+ . (2) Slowly downward percolating groundwater, with high contents of reduced species as well as increasing HCO_3^- , NH_4^+ , Ca^{2+} and K^+ with depth. (3) Rainwater with some oxygen and nitrate, but overall a low concentration of ions. An additional, fourth type of groundwater, may be distinguished based on chemical analyses in MB17, MB23 and flow measurements: (4) Groundwater between the archaeological layers and the bedrock, influenced by upward flow from the bedrock and downward flow from the archaeological deposits. This mixed water type has a lower total amount of dissolved ions compared to 'type 1' and 'type 2', but relatively high HCO_3^- , Na^+ , Ca^{2+} and K^+ concentrations, possibly due to a more dynamic environment and short retention times.

Numerical model

Figure 10 shows the average simulated phreatic level within the archaeological deposits (blue contours) as well as the average hydraulic head in the underlying beach sediments at approximately 11 m below the terrain surface (red contours). Flowlines have been added to illustrate the general horizontal groundwater flow pattern. Comparison of the contours in both soil layers

shows downward flow under Bryggen. Under the southwestern part of the hotel area, an upward flow towards the drain system at 0.45 m asl is visible. However, due to the very high permeability and a hydraulic connection between the drainage system and the harbour, the vertical flow direction under the hotel area changes with the tide. When the tide is higher than 0.40 m asl, temporary infiltration from the drainage system occurs.

At the eastern part of Bryggen, calculated piezometric levels between the beach sediments and the archaeological deposits are almost equal, indicating a limited vertical flow. This is probably caused by a relatively high bedrock level in this area, acting as a barrier for vertical groundwater flow. From historical maps, the beach sediments are thin or even absent in the eastern area of Bryggen. A rock outcrop is present at the far northeastern side of the study area and no significant settling of the ground or buildings is currently measured, which supports this hypothesis.

The groundwater model simulates upward flow under the quay area due to salt-water intrusion. Fresh water from the archaeological deposits and the underlying beach sediments is pushed upwards against a salt-water wedge extending to the front buildings of Bryggen. Seawater intrusion thus forms a hydrological barrier for groundwater flow, which changes the water balance under Bryggen. A comparative model simulation with a fresh-water boundary condition instead of a salt-water boundary condition results in a significant decrease (around 50%) of the discharge volume from the drainage system under the hotel area. It must be stressed that these calculations are based on the assumed boundary condition that the Vågen harbour forms a hydrological barrier with salt water down to about 2 m below the harbour bottom. Depending on the permeability of the old beach sands, depth and permeability of the harbour bedding and the inland hydraulic head, freshwater outflow towards the Vågen harbour might occur via the beach

sediments and bedrock. An indication of this possible flow direction comes from soil and groundwater analyses at MB12 (Matthiesen 2006a, b), showing lower chloride concentrations at greater depths. A multilevel monitoring well, including the old beach sediments at the front of Bryggen, was installed in the autumn of 2007. This well should provide further evidence of the validity of the applied boundary condition.

The marked area in Figure 10 indicates bad preservation conditions due to a lowered phreatic level. This is observed and carefully registered in archaeological investigation samples taken during drilling of the observation wells (Christensson et al. 2007).

Conclusions and future work

Conclusions

Two hypotheses (H1 and H2) were tested:

H1. A combined hydrological and archaeological approach leads to a more fundamental understanding and thus improved protection of the archaeological site in situ. The use of 'traditional' groundwater monitoring and chemical analyses in combination with numerical groundwater modelling is a useful routine in increasing the understanding of the hydrological system of a complex archaeological site, such as Bryggen. The following conclusions could be drawn due to the combination of a hydrological, geochemical and archaeological approach:

- The phreatic level is the most important factor for preservation of organic material. Intensifying the monitoring frequency within the archaeological deposits to an hourly interval showed that the phreatic level strongly correlates to the average observed tidal fluctuation in the Vågen harbour. Precipitation has a minor, indirect effect on the phreatic level. Before the high frequency monitoring started in 2006, it was concluded that the phreatic level is steady and variations were related to precipitation, based on a monitoring interval of 2 months.
- Placing observation wells, monitoring hydraulic head and analysing groundwater at different locations outside and below the archaeological deposits themselves provided new information on possible threats to the archaeological layers to be preserved. A good hydraulic connection and relatively high saturated conductivities between the (earlier ignored) beach sediments below the archaeological deposits seem to have a major impact on the long-term phreatic levels. Although reaction time may be in terms of decades due to the very low saturated conductivity of the organic archaeological layers, a change in the water balance by extracting water from the underlying beach sediments (at a location not necessarily below Bryggen) will eventually cause a lowering of the phreatic level over a larger area if not compensated by additional inflow elsewhere.
- Numerical groundwater modelling provided a better understanding of the hydrological processes involved by

forcing us to look beyond the archaeological site to be preserved. It resulted in preliminary quantitative measures of the water balance at Bryggen. The groundwater model helped us to identify sensitive parameters that control the phreatic level and thus the preservation conditions. This knowledge is used to design measures for re-establishing the phreatic level at Bryggen and creating a stable water-balance condition. The groundwater model will be an important tool to design and evaluate technical measures involved to create a system in balance where further deterioration and settling is minimised.

Generally, from an archaeological perspective, the above-described approach results in identification of important factors influencing preservation conditions, specifically the phreatic level and the processes leading to the chemical composition of groundwater surrounding archaeological deposits. In situ preservation requires a thorough understanding of the regional and local hydrogeological system in order to assess possible protective measures and prevent actions leading to deterioration of archaeological material. An interdisciplinary approach combining hydrogeology, chemistry and archaeology is, therefore, necessary to obtain a full understanding of preservation conditions.

H2. A combined hydrological and archaeological approach improves identification of archaeological deposits at risk. The use of groundwater modelling in addition to 'traditional' monitoring efforts enables continuous adjustment and improvement of the monitoring strategy, which in turn improves the understanding of the hydrogeological system and gives feedback to the numerical model describing the system more adequately. The improved hydrogeological understanding of the site within its wider environment leads to identification of areas with unfavourable conditions for archaeological preservation, thus improving identification of archaeological deposits at risk.

Future work

Once transient calibration of the numerical groundwater model of Bryggen and surroundings is satisfactory, the model will also help to predict impacts of landscape and climate change. The urban landscape around Bryggen changes continuously with new buildings and infrastructure, renewal of drainage and sewage systems, changes of pavements and so on. Urban development has taken place since Bryggen was built and certainly has had its impact on the hydrological situation. The groundwater model facilitates us in simulating effects of those urban changes. Consequences of climate change, which may lead to increased precipitation and a sea-level rise, can be estimated with the groundwater model, resulting in valuable management information for in situ preservation of the archaeological deposits.

The current intensive monitoring program will be reduced to an effective, permanent monitoring scheme. Once detailed data analysis and hydrological modelling have clarified the underlying processes, the number of wells and the frequency of monitoring can be adjusted to a minimum level necessary

to provide essential information for preservation management. At complex sites, the use of groundwater modelling in addition to monitoring is a cost-effective alternative to simply gathering more monitoring data and waiting for a significant number of data to show a trend.

A future challenge will be a more quantitative approach by extending the numerical groundwater model with geochemical data. The hydrogeochemical model may then be used to quantify chemical changes in the groundwater that control preservation conditions. The unsaturated zone is of major importance for preservation conditions. An extension of the groundwater model to also include the unsaturated zone may, therefore, be a valuable improvement.

Since November 8, 2006, continuous logging of soil moisture content is carried out with 4 soil-moisture sensors at depths of 2.00, 2.45, 2.83 and 3.29 m asl, at a former small archaeological excavation between observation wells MB7 and MB21. A challenge will be to use these field data and obtain other suitable field data for calibrating soil water content and unsaturated flow.

The registered relatively high groundwater temperatures caused by urbanisation need to be further elaborated with regard to possible effects on preservation conditions. Understanding the above-mentioned processes will then allow for more generic risk-mapping tools to be developed

Acknowledgements

The monitoring at Bryggen is funded by the Directorate of Cultural Heritage in Norway. The support of all participants in the Bryggen Project is very much appreciated. We would like to thank Sylvi Gaut and Bjørn Frengstad for carefully reading the manuscript. The helpful comments of Mike Corfield and one anonymous reviewer are highly appreciated.

References

- Appelo, C.A.J. and Postma, D. (2005) *Geochemistry, groundwater and pollution*. 2nd edition, Balkema, Leiden, 649 pp.
- Beer, H. de (2005) Hydrogeologisk modellering Bryggen, Bergen: midlertidig rapport. *NGU Rapport 2005.080*, 44 pp.
- Beer, H., de, Christensson A., Jensen J.A. and Matthiesen, H. (2007) A numerical model to support archaeological preservation strategies. *Journal of Bio- and Archaeological Studies*. Proceedings from Preservation of Archaeological Remains in situ 3, Amsterdam, in press.
- Bierkens, M.F.P., Gehrels, J.C. and Kovar, K. (eds.) (2006) International Commission on Groundwater and TNO Built Environment and Geosciences 2006: *Calibration and reliability in groundwater modelling: from uncertainty to decision making*. IAHS Publication **304**, Wallingford, 316 pp.
- Christensson, A., Paszkowski, Z., Spriggs, J.A. and Verhoef, L. (2004) *Safeguarding historic waterfront sites. Bryggen in Bergen as a case study*. 1st edition. Stiftelsen Bryggen and Polyteknika Szczecinska, Bergen, Norway, 338 pp.
- Christensson, A., Dunlop, R., Beer, H. de, Jensen, J.A. and Matthiesen, H. (2007) The project "Safeguarding Historic Waterfronts - Bryggen in Bergen". *Journal of Bio- and Archaeological Studies*. Proceedings of Preserving Archaeological Remains in situ 3, Amsterdam, in press.
- Corfield, M., Hinton, P., Nixon, T. and Pollard, M. (1998) Preserving archaeological remains in situ. Proceedings of the conference 1st-3rd April, 1996. Museum of London Archaeology service, English Heritage, London.
- Diersch H.-J.G. (2007) FEFLOW Finite Element Subsurface Flow and Transport Simulation System, Reference Manual, version 5.3.
- Dunlop, R. (2007) Archaeological recording in connection with monitoring in Norway's medieval towns. *Journal of Bio- and Archaeological Studies*. Proceedings of Preserving Archaeological Remains in situ 3, Amsterdam, in press.
- Golmen, L.G. (2005) Bryggen in Bergen. Vassinntrengning i fundament og bolverk. Resultat av målinger vinteren/våren 2005. *Norwegian Institute for Water Research, Report 5047-2005*, 34 pp.
- Herteig, A.E. (1969) *Kongers havn og handels sete. Fra de arkeologiske undersøkelser på Bryggen i Bergen 1955-68*. Aschehoug, Oslo, 224 pp.
- Herteig, A.E. (1985) *The archaeological excavations at Bryggen, "the German wharf", in Bergen, 1955-68: excavation, stratigraphy, chronology, field-documentation*. The Bryggen Papers Main Series, Volume 1, Universitetsforlaget, 46 pp.
- Herteig, A.E. (1990) *The buildings at Bryggen: their topographical and chronological development*. Universitetsforlaget, Oslo, 151 pp.
- Holden, J., West, L.J., Howard, A.J., Maxfield, E., Panter, I. and Oxley, J. (2006) Hydrological controls of in situ preservation of waterlogged archaeological deposits. *Earth-Science Reviews*, **78**, 59-83.
- Jensen, J.A. and Stordal, A.D. (2004) Miljøovervåkningsprosjekt Bugården-Bryggen i Bergen, FoU-prosjekt. Grunnundersøkelser og setningsmålinger. *Multiconsult, avdeling Noteby Report 400962*, 15 pp.
- Matthiesen, H. (2006a) Composition of soil and groundwater at dipwells MB12, 10, 14 and 13 Bryggen, Bergen. National Museum of Denmark, Department of Conservation, Lyngby, *Report 12027-0004*, 37 pp. Available online from www.natmus.dk/sw8893.asp
- Matthiesen, H. (2006b) Groundwater composition at Bryggen in Bergen June 2005 - an evaluation of the use of water samples for monitoring preservation conditions. National Museum of Denmark, Department of Conservation, Lyngby, *Report 12027-0005*, 28 pp. Available online from www.natmus.dk/sw8893.asp
- Matthiesen, H. (2008) Detailed chemical analyses of groundwater as a tool for monitoring urban archaeological deposits: results

- from Bryggen in Bergen. *Journal of Archaeological Science*, **35**, 1378–1388.
- Matthiesen, H., Dunlop, R., Jensen, J.A., Beer, H. de, and Christensson, A. (2007) Monitoring of preservation conditions and evaluation of decay rates of urban deposits – results from the first five years of monitoring at Bryggen in Bergen. *Journal of Bio- and Archaeological Studies*. Proceedings of Preserving Archaeological Remains in Situ 3, Amsterdam, in press.
- Myrvoll, S., Golembnic, A. and Dunlop, A.R. (1983) The Finnegården project. Paper stencil, Riksantikvarens utgravningskontor, 1983.
- Nixon, T. (2004) Preserving archaeological remains in situ? Proceedings of the 2nd conference 12–14 September, 2001. Museum of London Archaeology service, pp. 254–260.
- Odong, J. (2007) Evaluation of empirical formulae for determination of hydraulic conductivity based on grains-size analysis. *Journal of American Science*, **3**, 54–60.
- Valetta Treaty (1992) European Convention on the Protection of the Archaeological Heritage (Revised). ETS no. 143.
- Unesco (2008) *Operational Guidelines for the Implementation of the World Heritage Convention*. Intergovernmental committee for the protection of the world cultural and natural heritage, World Heritage Centre. WHC 08/01, January 2008, 173 pp.

Global geochemical mapping and sediment-associated flux of major world rivers

Jim Bogen¹ and Rolf Tore Ottesen²

¹*Norwegian Water Resources and Energy Directorate (NVE), P.O. Box 5090, 0301 Oslo, Norway.*

²*Geological Survey of Norway (NGU), 7491 Trondheim, Norway.*

E-mail: jbo@nve.no

Paper previously published in Russian in N.I. Makkaveev memorial volume: R.S. Chalov, 'Makkaveevskie chteniya–2005', edited by Moscow University Publ. House, Moscow, 2006.

A global geochemical mapping project based on sampling of overbank sediments from rivers was established by the International Commission on Continental Erosion, ICCE, in 2001. Overbank sediments were introduced as a sample medium in geochemical mapping in 1989, and a number of papers on the geochemistry of overbank sediments have since been published. The present paper reviews main aspects of this literature, arriving at the following conclusions: Depth-integrated samples of overbank sediments reflect the composition of many current and past sediment sources upstream of the sampling point, contrary to active stream sediments which normally are recent deposits derived from a more restricted number of presently active sediment sources. Mapping the composition of recent and pre-industrial overbank sediments can therefore be used (1) in a characterisation of the present state of pollution, and (2) as a regional prospecting tool in natural as well as polluted environments. Human interference with rivers and the predicted climate change will affect the global sediment flux to the oceans.

Introduction

Available data concerning the spatial heterogeneity of the chemical composition of the Earth's surface and data concerning the flux of persistent organic pollutants and metals from land to the marine environment are incomplete. Overbank sediments have turned out to be an important medium for the construction of maps of geochemical elements in large regions (Ottesen et al. 1989). Widely spaced, global geochemical sampling of deposited sediments is crucial because it provides a practical way to relatively quickly obtain a consistent overview of the contemporary global distribution of elements (natural and anthropogenic) on the Earth's surface. Such data can be used for environmental and related human health studies and mineral exploration.

The traditional method in geochemical mapping has been to sample sediments from the bottom of small streams. It has been assumed that the composition of active sediments in the stream channel represents the geochemistry of the catchment area upstream of the sample site. However, the sediments in stream channels are often derived from sources of limited extent and may change with time (Ottesen et al. 1989). The assumption that active stream sediments may characterise the composition of whole drainage areas can, therefore, be questioned.

Ottesen et al. (1989) suggested that overbank sediments could be a more representative type of sample and demonstrated that this type of sediment was usable also in very large drainage basins. Overbank sediments are deposited by large-magnitude floods during conditions when a number of sediment sources are active and thus integrate material from a large area. They are available along rivers with variable water discharge. Older sediment deposits are often preserved, providing opportunities to detect natural and anthropogenic chemical signals from the past. Many papers have subsequently been published about the use of overbank sediment as a geochemical sampling medium (e.g., Leenaers 1989, Lewis and Macklin 1989, Edén and Björklund 1994, Macklin et al. 1994, Ridgway et al. 1995, Bølviken et al. 1996, 2004, Langedal 1996, 1997a, De Vos et al. 1996, Gäbler 1997, Swennen and Van der Sluys 1998, 2002, Swennen et al. 1998, Walling and He 1998, Xie and Hangxin 2001, Caritat et al. 2005). Based on the use of overbank sediments, Xie and Hangxin (2001) mapped China (9.5 million km²) with 529 sample localities. The authors concluded that a global reconnaissance study should use overbank sediments as a sample medium.

A river is a dynamic system where continuous erosion and sedimentation give rise to a redistribution of sediments and sediment-associated chemical elements. The use of overbank sediments is also important when the sedimentary dynamics of a river system have to be taken into account. Changes in the hydrological regime, or man-made changes in sediment sources or transport conditions, may thus affect the distribution of chemical elements within the drainage basin and the sediment delivery to the oceans. A large part of the sediment flux to the

oceans is delivered by a relatively small number of large rivers. A record of the changes in sediment supply due to natural or man-made changes in the sediment budget and the particle-associated flux of the world's major rivers, is thus of great importance.

In January 2001, the project 'Global geochemical mapping and sediment-associated flux of major world rivers' was established by the International Association of Hydrological Sciences/International Commission on Continental Erosion (IAHS/ICCE). It is the aim of this project to carry out a worldwide sampling programme based on overbank sediments to obtain a global geochemical map.

Formation of overbank sediments

Overbank sediments (also called alluvial soils, floodplain sediments or levee sediments) occur along rivers with variable water discharge. During floods, temporarily enhanced discharge may exceed the capacity of the channel (Figure 1a). Material in suspension will be transported and deposited onto floodplains and levees (Figure 1b). In most rivers, this process has taken place many times in the past.

Overbank deposits therefore consist of successive, nearly horizontal strata of young sediments overlying older sediments. A vertical section through such a deposit reflects the history of sedimentation back in time.

During floods, the great quantity of water activates many sediment sources in the drainage area, and the material in suspension will reflect the composition of these and earlier developed sources. This is why overbank sediments represent large parts of—or even complete—catchments.

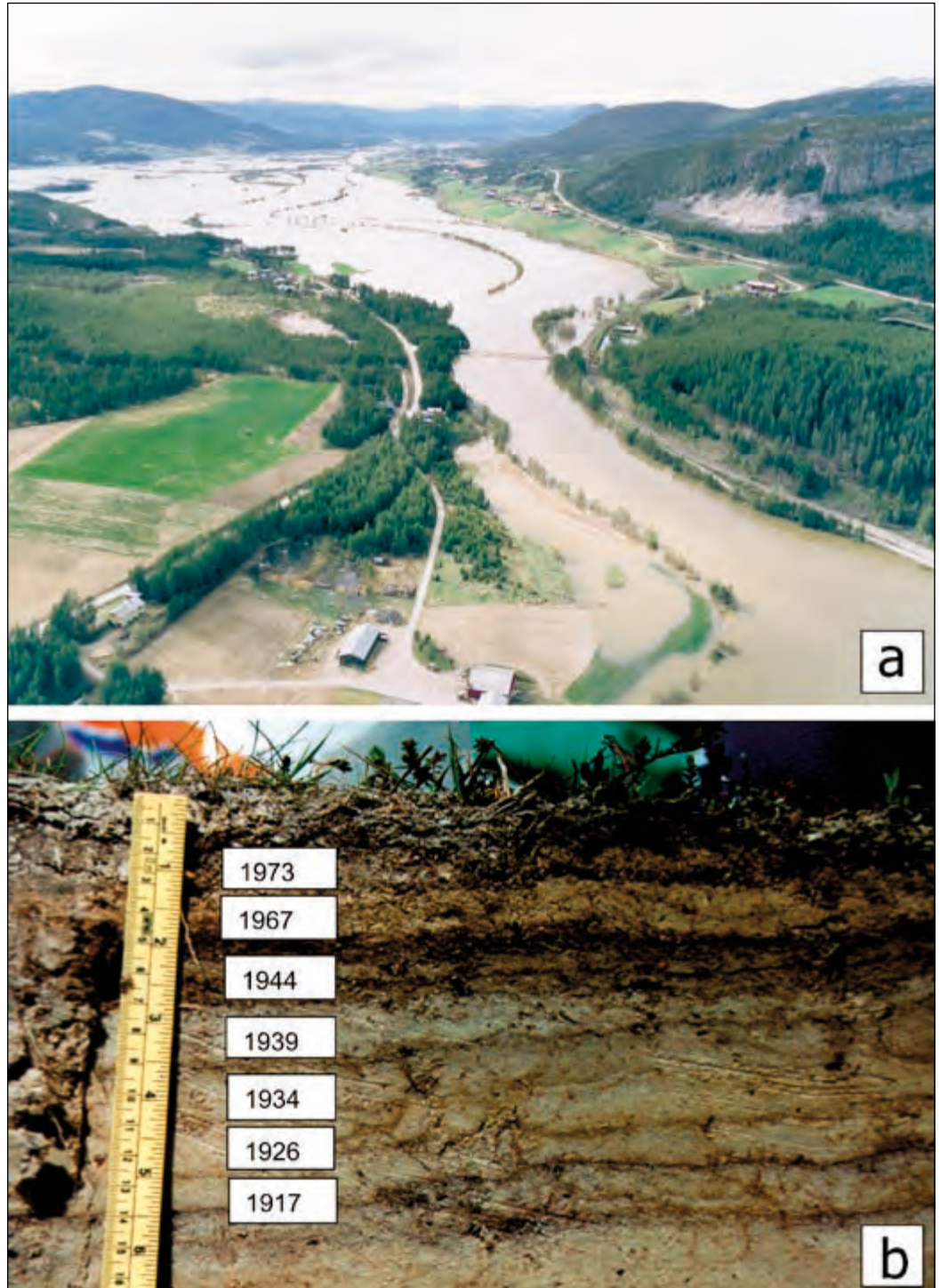
In some overbank deposits, the stratigraphy may be complex due to redeposition of material eroded from earlier-formed upstream deposits. Young sediments may then be intermixed with older sediments.

Properties of overbank sediments

Since overbank sediments normally consist of individual horizontal strata formed at different times, the variations in chemical composition and the corresponding sampling error will be greater in the vertical plane than in the horizontal direction.

In principle, vertical trends in the chemical composition of overbank sediments have two origins, namely variations in the composition of the original source material and alteration caused by the secondary migration of substances after deposition. Secondary migration is due to factors such as climate, pH, reduction/oxidation conditions, the amount and type of organic material, biological activity and time. In many climates, soil formation processes may need hundreds of years in order to develop significant vertical patterns. For overbank sediments, the available time interval is normally more restricted, as new layers of sediment are deposited on top of the older ones. Problems of

Figure 1. (a) Major flood in eastern Norway, and (b) a profile in the floodplain.



vertical migration are therefore expected to be less in overbank sediments than in other soils.

In Belgium, the Netherlands, Luxembourg and parts of Germany, 34 overbank sediment profiles located along the banks of meandering rivers have been studied (De Vos et al. 1996, Swennen and Van der Sluys 1998, 2002, Swennen et al. 1998). In 30 of these, pre-industrial sequences could be detected below polluted surface overbank deposits. Samples were collected at depth intervals of 10 cm and analysed for main and trace elements.

Three main groups of vertical distribution pattern were distinguished in the sections: (1) either low or high metal concentrations throughout the profile, thought to reflect high or low natural metal contents in the catchments, (2) no variations in grain size or lithology, but a gradual increase in heavy-metal concentrations towards the top of the profile, presumably caused by airborne pollution, and (3) abrupt changes in metal concentrations at certain depths and a corresponding change in lithology. These patterns are interpreted as being an effect of man-made discharges into the catchments and subsequent

fluvial dispersion of particle-bound pollution.

In a Norwegian study (Langedal 1996, 1997a, b, c), overbank-sediment profiles were sampled from the Knabeåna–Kvina drainage basin, which is influenced by Cu- and Mo-rich tailings from the now closed Knaben molybdenum mine. Along the rivers, pre-industrial overbank sediments were detected below the present inundation level in the bottom sections of 14 out of 18 profiles. The four atypical profiles are situated where lateral river migration has had an impact on the sedimentary environment, or where minor river regulations and influx of tailings have altered the original peat bog and lacustrine environments into floodplains. Most of the Knabeåna–Kvina profiles show high Cu and Mo contents in the upper part, while concentrations in the bottom section approach a lower, probably natural level similar to the recent natural sediments that overlie the present inundation zone of polluted sediments.

Edén and Björklund (1994) suspected downward percolation of long-range atmospheric pollution to be the cause of high Pb concentrations in the lower part of the overbank-sediment profiles in northern Europe. Acid rain and low buffer capacity in the sediments may have contributed to the migration. However, Ottesen et al. (2000) questioned this interpretation, claiming that the Pb enrichments are natural, on the basis of data published by Taylor and Heier (1958), which reveal high Pb contents in K-feldspar in this region.

In English and Welsh basins with old Pb/Zn-mines, the vertical distributions of Pb and Zn in dated overbank-sediment sequences were found to be closely related to the mining history, suggesting that no significant vertical migration of these metals had taken place after the sediments had been deposited (Macklin et al. 1994). Similarly, along the Rio Guanajuato and Rio Puerco rivers, Mexico, no vertical migration was seen for the elements As, Cr, Cu, Pb, Sn, and Zn (Ridgway et al. 1995).

In a study of 49 selected floodplains, Edén and Björklund (1994) found that the lateral variations within floodplains were insignificant in comparison with the between-floodplain variation (Table 1). Similar results were obtained by Chekushin et al. (1993) for the chemical composition of duplicate overbank-sediment samples from the border area of Finland, Norway and Russia.

Langedal (1997b) found that in floodplain surface sediments (0–25 cm depth) of the polluted Knabeåna river, the highest Cu and Mo concentrations are in samples proximal to the river or in floodplain depressions. Enrichment of metals in these parts of the floodplains may be an effect of differences in the timing of the sediment transport pulse, and the timing of floodplain inundation (Bradley 1984). In the proximal areas and the depressions, the suspended-sediment transport rates are often highest during the rising and peak stages. These are the first to be inundated and receive the largest load of particle-bound metals. Similar results were also found along the Geul river in Belgium by Leenaers (1989) and Swennen et al. (1994).

In both small and large catchments, the sampling error for natural overbank sediments within a floodplain is small

Table 1. Analysis of variance of the content of aqua regia-soluble chemical elements in widely spaced duplicate samples of overbank sediments taken at depth and near the surface in a 23,000 km² area in northern Europe. (From Edén and Björklund 1994).

Element	(1) %	(2) F	(3) F	(4) F
Al	2.2	14.5	6.1	4.2
Ba	6.0	14.7	5.6	5.4
Ca	1.8	73.0	15.3	15.3
Co	10.0	12.0	5.8	7.8
Cr	4.7	48.0	7.1	8.3
Cu	10.7	34.7	5.6	5.3
Fe	25.5	13.0	5.1	4.4
K	3.8	33.3	10.5	10.8
La	4.3	34.0	9.3	6.1
Mg	1.8	66.0	8.6	10.3
Mn	6.2	14.1	3.7	6.0
Na	7.3	4.2	5.6	4.6
Ni	10.1	26.0	7.3	7.9
P	4.0	25.0	6.3	8.9
Pb	21.7	5.5	3.9	4.1
Sr	5.0	47.2	8.2	8.3
Th	35.8	10.7	3.9	5.6
Ti	2.2	33.3	6.7	6.9
V	4.5	7.0	6.0	5.0
Zn	5.0	30.0	6.2	7.7
Critical F value at p=0.05		1.7	1.4	1.4
Number of pairs	36	36	116	116

(1)–(3) Samples at depth. (1) Combined sampling and analytical error. (2) Ratio between total variance and combined sampling and analytical variance. (3) Ratio of between-site variance and within-site lateral variance. (4) Ratio of between-site variance and within-site vertical variance.

in relation to variation between floodplains. This conclusion appears to be valid in most regions of the world for genuinely natural deposits and in situations where pristine sediments at depth are covered by polluted surface sediments.

Sampling of older terraces is appropriate in order to obtain pre-industrial material. Such sampling should be done above the present inundation zone to avoid material draped during recent floods. Along laterally stable river reaches, sampling in the bottom sections of the sediment profiles is adequate (Langedal 1997a, b). Sampling along meandering reaches, as suggested by Bogen et al. (1992), may also be a possibility if lateral migration is slow.

Pollution of overbank sediments may be of two types: (1) mine waste and other anthropogenic material may enter the stream from local sources and then be transported downstream, and (2) airborne contaminants originating from distant sources may reach the catchments (Langedal and Ottesen 1998). Situation (1) is often recognisable since the sources may be easily identified, but situation (2) can be more difficult to detect.

The selection of appropriate locations for sampling overbank sediments should be undertaken only by personnel trained in

sedimentology. If this prerequisite is fulfilled, subsequent high-quality chemical analysis of the samples will produce reliable data for most chemical elements.

Regional distribution of chemical elements in overbank sediments

Ottesen et al. (2000) published a geochemical atlas of Norway based on 700 floodplain sampling sites distributed across the country (300,000 km²). Each site represents a drainage area of 60–600 km². A vertical section through the sediments was cut with a spade, and a composite bulk sample 50–100 cm long was taken from the section excluding the upper 5–10 cm. After drying, the samples were sieved and the < 0.062 mm fraction analysed for the total contents (XRF) of 30 elements and determination of 29 elements in a nitric acid extract. Most elements show systematic patterns with great contrast. In some cases, these patterns agree with those of known geological structures, in others they indicate previously unknown structures.

Xiachu and Mingkai (1995) carried out a reconnaissance survey in a part (170,000 km²) of the Jiangxi Province of southern China in order to develop techniques for implementing ultra-low density sampling of overbank sediments for global geochemical mapping. Sampling sites (1 site per 1800 km²) were picked at the apexes of 94 drainage basins of between 100 and 800 km². It was concluded that floodplains with catchment areas of 100 to 800 km² do indeed provide suitable sampling stations for global geochemical mapping based on overbank sediments. Widely-spaced sampling of lower-layer overbank sediments was seen as a fast and cost-effective method for identifying geochemical provinces.

Xie and Hangxin (2001) collected 529 floodplain samples across the Republic of China (9,600,000 km²), each sample representing a drainage basin of between 1000 and 6000 km². It was concluded that the geochemical data generated from the widely-spaced sampling were strikingly similar to those generated by China's Regional Geochemical National Reconnaissance Program, which was based on more than 1 million samples of active stream sediments.

As a contribution to the Geochemical Atlas of Europe, 747 floodplain samples from all over Europe were collected and analysed for both major and trace elements (Figure 2, Salminen et al. 2005). Caritat et al. (2005) published a geochemical survey based on the contents of a wide range of chemical elements in overbank sediments from parts of Australia. All these projects demonstrate that the use of overbank-sediment samples in regional geochemical mapping is a very cost-effective method.

Flux of major world rivers

A comparison of the annual sediment transport in about 20 major rivers reveals that there is no direct relation between the volume of the sediment load and the size of the river basins (Table 2). However, it is indicated that a small number of rivers deliver a large share of the total sediment flux to the oceans. The combined sediment load of the 20 rivers constitutes nearly half of the estimated total global load of $13,500 \times 10^6 \text{ t yr}^{-1}$ that was given by Milliman and Meade (1983). Panin (2004) discussed the current estimates of global loads proposed over the last two decades and found that they all fall within the range of $13,500$ to $22,000 \times 10^6 \text{ t yr}^{-1}$.

Several of the rivers in Table 2, however, are severely affected by human activity. The most striking example is the Nile. The measured mean annual sediment load during the years 1902–63 was $160\text{--}178 \times 10^6 \text{ t yr}^{-1}$. After the construction of the Aswan dam in 1964, no sediment passed downstream. As a consequence, the delta receded and the delta rim is now situated about 5 km behind its most advanced position (Khafagy and Fanos 1993). The Mississippi is another example of a river where the sediment load has decreased because of reservoir sedimentation. The many reservoirs built on its tributaries reduced the transport from $400\text{--}500 \times 10^6 \text{ t yr}^{-1}$ to the present load of $230 \times 10^6 \text{ t yr}^{-1}$ given in Table 2.

Syvitski et al. (2005) estimated that 20% of the global load is deposited in reservoirs that were mainly constructed within the past 50 years. Sediment transport in the Yellow River has decreased because of reduced precipitation, increased water abstraction and sediment-control practices. During the years 1950–77, the river had a load of $1.6 \times 10^9 \text{ t yr}^{-1}$ (Milliman and Syvitski 1992). According to the Yellow River Commission, the mean transport rate in its lower part had decreased to $0.5 \times 10^9 \text{ t yr}^{-1}$ for the period 1989–2003.

Some of the rivers draining to the Arctic Ocean have also experienced large sediment-transport changes due to dam construction and other human impacts. Hasholt et al. (2005) gave a recent estimate of the total sediment transport to the Arctic Ocean and adjoining cold seas. By combining available monitoring data and estimates for ungauged areas, they estimated that the total sediment transport is within the range $325\text{--}885.1 \times 10^6 \text{ t yr}^{-1}$. Of this total, only a part can be considered as monitored, while the rest is based on different types of estimate, ranging from morphology- and process-based estimates to more empirically based estimates. The largest uncertainty is the contribution from glacier calving, which may be as large as $500 \times 10^6 \text{ t yr}^{-1}$.

The sum of the load carried by Russian rivers is also of considerable magnitude, with a total of $73 \times 10^6 \text{ t yr}^{-1}$. The water discharge of the Yenisey river ranks among the six largest in the world, averaging an annual total of 630 km^3 into the Arctic Ocean. Its sediment load is, however, relatively low. During the period 1941–56, the mean sediment load was measured at 13.2

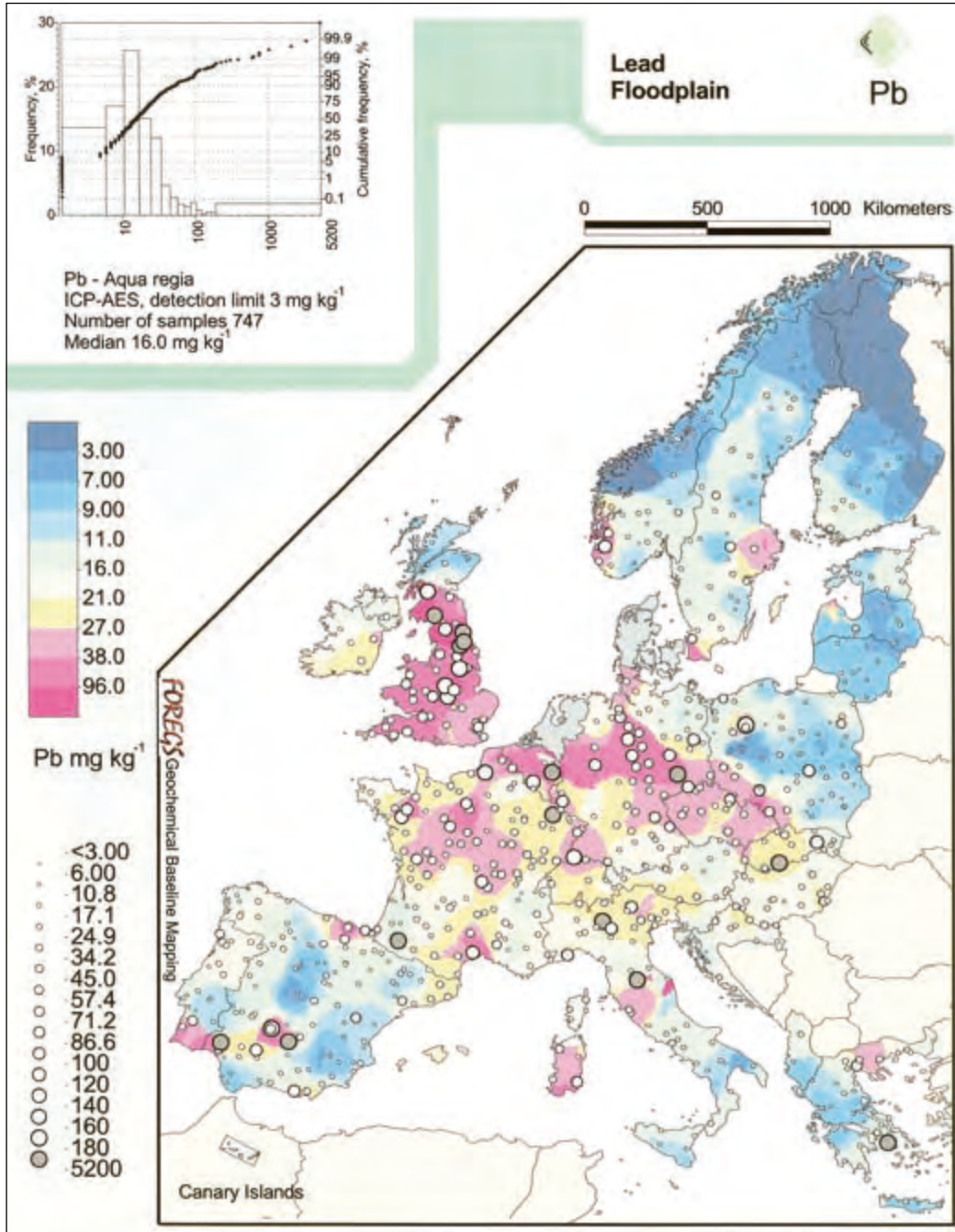


Figure 2. Geochemical distribution of lead in overbank-sediment samples from 747 localities in Europe. After Salminen et al. 2005.

$\times 10^6 \text{ t yr}^{-1}$ at the Igarka gauging station in the lower part of the river basin. After dams were constructed on the Yenesej and its tributary the Angara, the sediment load decreased to a mean of $4.2 \times 10^6 \text{ t yr}^{-1}$ (Bobrovitskaya et al. 1996). Observations of sediment transport in other Russian rivers draining to the Arctic Ocean are, according to Holmes et al. (2002): Lena $20.7 \times 10^6 \text{ t yr}^{-1}$ ($7.6\text{--}40.0 \times 10^6 \text{ t yr}^{-1}$), Ob $15.5 \times 10^6 \text{ t yr}^{-1}$ ($13.0\text{--}16.6 \times 10^6 \text{ t yr}^{-1}$), Kolyma $10.1 \times 10^6 \text{ t yr}^{-1}$ ($4.7\text{--}16.1 \times 10^6 \text{ t yr}^{-1}$), Pechora $9.4 \times 10^6 \text{ t yr}^{-1}$ ($6.5\text{--}13.5 \times 10^6 \text{ t yr}^{-1}$) and Severnaya Dvina $4.1 \times 10^6 \text{ t yr}^{-1}$ ($2.5\text{--}6.6 \times 10^6 \text{ t yr}^{-1}$).

The long-term sediment-transport monitoring programme of the river Kolyma in east Siberia, is a striking example where human impacts have increased the sediment load. Part of the

long-term record of water discharge and sediment load initiated in 1941 is shown in Figure 3. Although the mean annual water discharge has remained fairly constant, there has been a gradual increase in sediment yield since 1965. Among the anthropogenic factors affecting the sediment yield, gold mining is important because the surface soils are removed over large areas, thus producing conditions suitable for intensive erosion (Bobrovitskaya 1996).

The Kolyma case illustrates the way that analyses of overbank sediments may be used to obtain information of the present and past fluxes of geochemical elements. The upper sample represents the present conditions; dating the sedimentary sequence would help identify older overbank deposits representative of conditions

Table 2. The suspended-sediment flux of a selection of major rivers compared to the global total.

River	Area 10^3 km^2	Sed. load 10^6 t yr^{-1}
Amazon	7180	363
Mississippi	3221	230
Parana	890	90
Colorado	629	135
Congo	3822	65
Niger	430	40
Nile	2881	178
Yangtze	1980	486
Yellow river	745	1600
Indus	960	100
Ganges/Bhramaputra	1480	1670
Mekong	783	150
Irrawaddy	431	170
Flux to Arctic Ocean by major rivers, excluding calving		384
Sum		5661
Global total		13500

before modification by human impact. Since overbank sediments are deposited during major floods and represent conditions during which the main volume of sediments are transported, it may be possible to detect the long-term geochemical changes in the sediment load that is delivered to the oceans. The deltas of large rivers are often complex features, in which the sediments accumulated at the ocean margin throughout long periods. It may thus be easier to recognise the age of older sediments if the delta history is known at least as far back as the time when pristine conditions prevailed, perhaps 200 years before present or more.

The need for a global project

Present data on the chemical composition of the Earth's surface is limited to small, detailed studies in restricted areas. It is, however, necessary to map the global distribution of chemical elements to reveal large-scale patterns, both natural and anthropogenic. If one continued to use the present techniques and approach it would probably take several hundred years to complete the task. A wide-spaced sampling programme of overbank

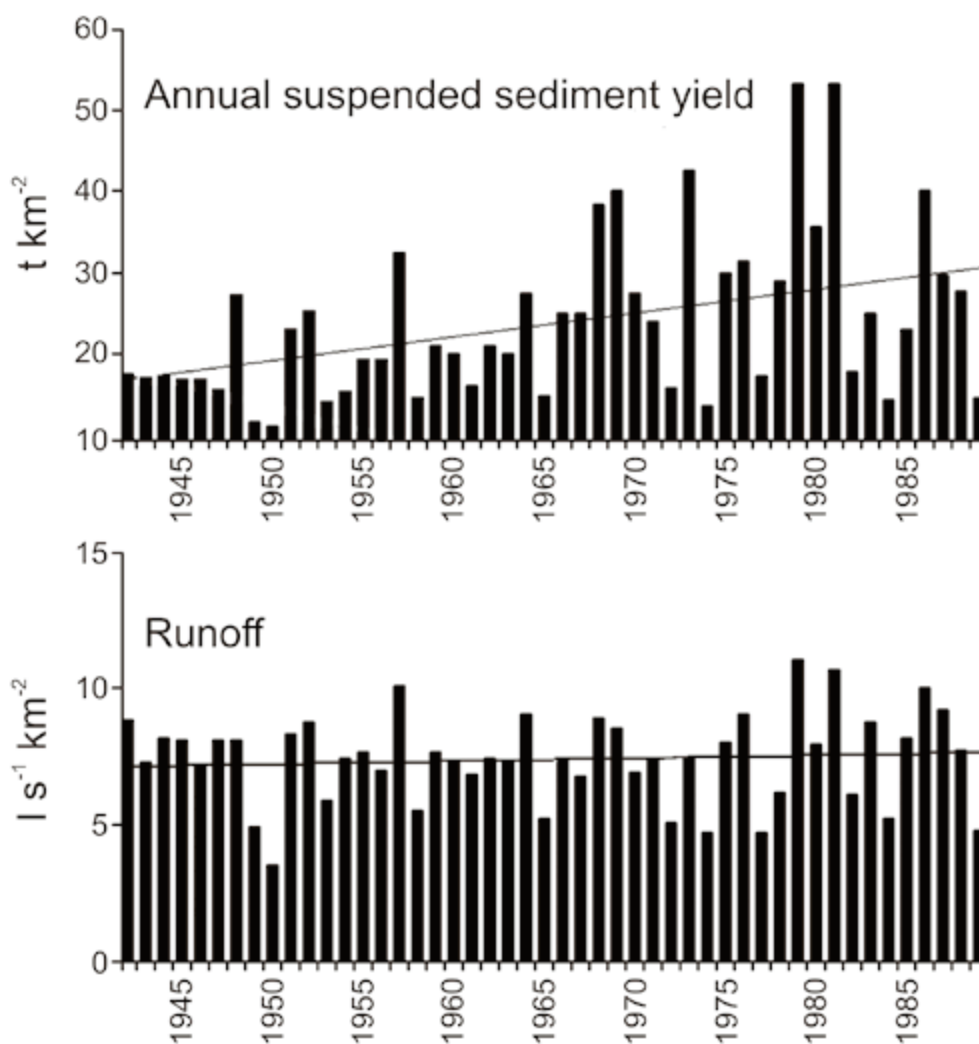


Figure 3. Sediment load and runoff in the Kolyma river in the period 1941–89. After Bobrovitskaya 1996.

sediments of rivers is the only practical way to obtain a global overview in a short time.

Such an overview is of practical importance in exploration for mineral resources. China has devised a mineral exploration strategy to rapidly assess the mineral-resource potential of a very large area by wide-spaced geochemical mapping followed by a progressive reduction of target areas by denser sampling (Xie and Hangxin 2001). The geochemical distribution of platinum in China was determined by analysing only 529 overbank-sediment samples. The most promising Pt target is a huge geochemical megaprovince covering an area of 700,000 km² in southwest China. Many Chinese exploration parties and foreign exploration companies have now commenced exploration activities. It is believed that similar megaprovinces will be found through a global mapping project.

In existing mining areas where river sediments are heavily polluted, it has previously been difficult to identify new mineral deposits. The application of pre-mining overbank-sediment data can successfully be used for prospecting in such areas.

Wide-spaced floodplain sampling is also a useful tool for environmental monitoring purposes, as demonstrated by the resultant mapped distribution of the ratio of Hg content in surface overbank sediments (present time) to Hg content in deep overbank sediments (historical time). It is obvious that Hg pollution in eastern China is serious (Xie and Hangxin 2001).

Other investigations have revealed that 30% of the floodplains in Europe are polluted, mainly by mine waste (Bølviken et al. 1996). A Pb map for overbank sediments in Europe is shown in Figure 2. Northern Germany, Belgium and England are particularly heavily polluted (Salminen et al. 2005).

A high natural content of a poisonous element can also represent a threat. An example is the high arsenic content of floodplain sediments in India and Bangladesh. Recent findings show that similar conditions may also exist elsewhere. This naturally high As content has resulted in hazardously high concentrations of arsenic in the groundwater used for drinking. Six million people in west Bengal use water with an unsafe arsenic level. Global geochemical mapping will reveal areas where the chemical quality of the groundwater should be investigated further. Rivers are large transporting systems that continuously redistribute and disperse the sediments in their catchments. Systematic mapping based on overbank-sediment samples may be used to identify source sediments and prevent further erosion of polluted deposits.

It is of great importance to know how future climate change will affect river systems. The globally averaged surface temperature is projected to increase by 1.4 to 5.8°C over the period 1990 to 2100. The water vapour concentration and precipitation are also projected to increase (World Meteorological Organization 2007). A probable result is that some permafrost will melt and more sediments will be released into river systems.

In Norway, for instance, model simulations carried out by RegClim (2005) predict an increase in total annual precipitation towards the year 2100. The increase will vary between 5% and

20% in different parts of the country and extreme rainstorm frequency will also increase.

Extreme floods have often been observed to cause erosion in deposits that are not exposed during floods of lower recurrence intervals. The 1995 flood in Norway was a large-magnitude flood of 100–200 year recurrence interval. During this event, the concentrations of particle-bound metals Cu, Zn, Cd and Pb increased considerably at a downstream monitoring station where the large river Glomma enters the sea. This increase in metal content is believed to be due to extensive erosion in the mining areas in the upper part of the catchment (Holtan and Holtan 1996, Bogen and Bønsnes 2000). The increased frequency of extreme situations will become a global phenomenon. Large-scale changes in water discharge and sediment load will in the long term affect the chemical composition of the oceans. Changes in sediment supply not only cause coastal retreat, but also greatly affect the benthic environment and coastal fisheries.

Conclusions

This paper discusses the use of overbank sediments from floodplains as a sampling medium to obtain large-scale geochemical maps. Low-density geochemical maps based on overbank sediments have been shown to give reproducible patterns that coincide with the patterns of high-density maps of the same areas.

Traditional prospecting methods based on active stream sediments involve sample collection without the use of skilled personnel. The appliance of overbank sediment samples is more costeffective, but requires knowledge of processes of erosion, transport and sedimentation within river basins. Such information adds another dimension to geochemical mapping. Knowledge of sedimentary dynamics makes it possible to reveal the historical development of a river system and record the associated changes in its chemistry.

Depth-integrated samples of overbank-sediments reflect the composition of many current and past sediment sources upstream of the sampling point, in contrast to active stream sediments which normally are recent deposits derived from a more restricted number of actively contributing sediment sources. In many regions, overbank sediments are more representative of drainage basins than active stream sediments and, consequently, can be used to disclose geochemical distribution patterns on a regional to continental scale by means of widely scattered sampling at low cost per unit area.

The stratigraphy of overbank sediments may in some cases be complicated. However, in flood plains or old terraces along laterally stable or slowly migrating channels, it is normally possible to obtain recent sediments near the surface and pre-industrial sediments at depth. Mapping the composition of recent and pre-industrial overbank sediments can, therefore, be used (1) in a characterisation of variations in the natural geochemical background as well as a documentation of the present state of pollution, and (2) as a regional prospecting tool

in natural as well as polluted environments.

Possible vertical movements of elements in overbank sediment strata have been reported, especially in some studies of relatively mobile elements (arsenic and cadmium) in non-calcareous areas heavily influenced by acid rain. However, the overall impression is that such migration is not a major problem in the use of overbank sediments in geochemical mapping.

Human interference with rivers and the predicted climate change will affect the global sediment flux to the oceans. Investigations of sediment sources and past changes in the particle-associated transport of chemical elements, documented by the sedimentary record, will be a valuable tool, which can contribute to a better understanding of future developments.

Acknowledgements

Two anonymous reviewers are thanked for comments that helped improve the paper.

References

- Bobrovitskaya, N. (1996) Long-term variations in mean erosion and sediment yield from the rivers of the former Soviet Union. In Walling, D.E. and Webb, B.W. (eds.) *Erosion and Sediment Yield: Global and Regional Perspectives*, International Association of Hydrological Sciences Publication, **236**, pp. 407–413.
- Bobrovitskaya, N., Zubkova, C. and Meade, R. (1996) Discharges and yields of suspended sediment in the Ob and Yenesej Rivers of Siberia. In Walling, D.E. and Webb, B.W. (eds.) *Erosion and Sediment Yield: Global and Regional Perspectives*, International Association of Hydrological Sciences Publication, **236**, pp. 115–124.
- Bogen, J. and Bønsnes, T.E. (2000) Miljøvirkninger av erosjon og sedimenttransport under flommer (Environmental impacts of erosion and sediment transport during floods). *HYDRA-report Mi 05, Norwegian Water Resources and Energy Directorate*, 48 pp.
- Bogen, J., Bølviken, B. and Ottesen, R.T. (1992) Environmental studies in Western Europe using overbank sediment. In *Erosion and Sediment Transport Monitoring Programmes in River Basins, Proceedings of the Oslo Symposium*, International Association of Hydrological Sciences Publication, **210**, pp. 317–325.
- Bradley, S.B. (1984) Flood effects on the transport of heavy metals. *International Journal of Environmental Studies*, **22**, 225–230.
- Bølviken, B., Bogen, J., Demetriades, A., De Vos, W., Ebbing, J., Hindel, R., Langedal, M., Locutura, J., O'Connor, P., Ottesen, R.T., Pulkkinen, E., Salminen, R., Schermann, O., Swennen, R., Van der Sluys, J. and Volden, T. (1996) Regional geochemical mapping of Western Europe towards the year 2000. *Journal of Geochemical Exploration*, **56**, 141–166.
- Bølviken, B., Bogen, J., Jartun, M., Langedal, M., Ottesen, R.T. and Volden, T. (2004) Overbank sediments: a natural bed blending sampling medium for large-scale geochemical mapping. *Chemometrics and Intelligent Laboratory Systems*, **74**, 183–199.
- Caritat, P., Lech, M., Jaireth, S., Pyke, J. and Lambert, I. (2005) Riverina geochemical survey a national first. *Geoscience Australia AUSGEO News*, **78**, 6 pp.
- Chekushin, V.A., Bogatyrev, I.V., Finne, T.E., Misund, A., Niskavaara, H., Pavlov, V.A., Volden, T. and Äyräs, M. (1993) Report on joint ecogeochemical mapping and monitoring in the scale of 1:1 million in the west Murmansk region and the contiguous areas in Finland and Norway. *NGU Report 1993.152*, 132 pp.
- De Vos, W., Ebbing, J., Hindel, R., Schalich, J., Swennen, R. and Van Keer, I. (1996) Geochemical mapping based on overbank sediments in the heavily industrialized border area of Belgium, Germany and the Netherlands. *Journal of Geochemical Exploration*, **56**, 91–104.
- Edén, P., and Björklund, A. (1994) Ultra-low density sampling of overbank sediment in Fennoscandia. *Journal of Geochemical Exploration*, **51**, 265–289.
- Gäbler, H.E. (1997) Mobility of heavy metals as a function of pH of samples from an overbank sediment profile contaminated by mining activities. *Journal of Geochemical Exploration*, **58**, 185–194.
- Hasholt, B., Bobrovitskaya, N., Bogen, J., McNamara, J., Mernild, S.H., Milbourn, D. and Walling, D.E. (2005) Sediment Transport to the Arctic Ocean and Adjoining Cold Oceans. *Nordic Hydrology*, **374**, 413–432.
- Holtan, H. and Holtan, G. (1996) Flommen på Østlandet mai/juni 1995. Effekten på vannkvaliteten i Glomma og Drammenselva (The flood in eastern Norway, May/June 1995. The impact on water quality in the rivers Glomma and Drammenselva). *Norwegian Institute for Water Research (NIVA) Report 3437-96*, 43 pp.
- Holmes, R.M., McClelland, J.W., Peterson, B.J., Shiklomanov, I.A., Shiklomanov, A.I., Zhulidov, A.V., Gordeev, V.V. and Bobrovitskaya, N. (2002) A circumpolar perspective on fluvial sediment flux to the Arctic ocean. *Global Biogeochemical Cycles*, **16**, 1–45.
- Khafagy, A.A. and Fanos, A.M. (1993) Impacts of irrigation control work on the Nile delta Coast. International Symposium on High Aswan dam, Cairo, Egyptian National Committee of Large Dams, pp. 306–325.
- Langedal, M. (1996) Temporal variations in the transport of mine tailings through the Knabeåna–Kvina river system, and into the Fedafjord, Norway. In Bøe, R. and Thorsnes, T. (eds.) *Marine geology in the Skagerak and Kattegat*, Geological Survey of Norway Bulletin, **430**, pp. 95–101.
- Langedal, M. (1997a) Dispersion of tailings in the Knabeåna–Kvina drainage basin, Norway; 1; Evaluation of overbank sediments as sampling medium for regional geochemical mapping. In Allan, R.J. and Salomons, W. (eds.) *Mining and metals in the environment*, Journal of Geochemical Exploration Special Issue, **58**, pp. 157–172.
- Langedal, M. (1997b) Dispersion of tailings in the Knabeåna–Kvina drainage basin, Norway; 2; Mobility of Cu and Mo in tailings-

- derived fluvial sediments. In Allan, R.J. and Salomons, W. (eds.) *Mining and metals in the environment*, Journal of Geochemical Exploration Special Issue, **58**, pp. 173–183.
- Langedal, M. (1997c) The influence of a large anthropogenic sediment source on the fluvial geomorphology of the Knabeåna–Kvina rivers, Norway. *Geomorphology*, **19**, 117–132.
- Langedal, M. and Ottesen, R.T. (1998) Airborne pollution of five drainage basins in eastern Finnmark, Norway; an evaluation of overbank sediments as sampling medium for environmental studies and geochemical mapping. *Water, Air and Soil Pollution*, **101**, 377–398.
- Leenaers, H. (1989) The transport of heavy metals during flood events in the polluted river Geul (The Netherlands). *Hydrological Processes*, **3**, 325–338.
- Lewis, J. and Macklin, M.G. (1989) Sediment transfer and transformation of an alluvial valley floor: The river south Tyne, Northumbria, U.K. *Earth surface processes and landforms*, **14**, 233–246.
- Macklin, M.G., Ridgway, J., Passmore, D.G. and Rumsby, B.T. (1994) The use of overbank sediment for geochemical mapping and contamination assessment: results from selected English and Welsh floodplains. *Applied geochemistry*, **9**, 689–700.
- Milliman, J.D. and Meade, R.H. (1983) World-wide delivery of river sediment to the oceans. *Journal of Geology*, **91**, 1–21.
- Milliman, J.D. and Syvitski, J.P.M. (1992) Geomorphic/tectonic control of sediment discharge to the ocean: The importance of small mountainous rivers. *Journal of Geology*, **100**, 525–544.
- Ottesen, R.T., Bogen, J., Bølviken, B. and Volden, T. (1989) Overbank sediment: a representative sampling medium for regional geochemical mapping. *Journal of Geochemical Exploration*, **32**, 257–277.
- Ottesen, R.T., Bogen, J., Bølviken, B., Volden, T. and Haugland, T. (2000) *Geochemical Atlas of Norway*. Geological Survey of Norway, Trondheim, 141 pp.
- Panin, A. (2004) Land–Ocean sediment transfer in Paleotimes, and implications for present-day natural fluvial fluxes. In Golosov, V., Belyaev, V. and Walling, D.E. (eds.) *Sediment transfer through the fluvial system*, International Association of Hydrological Sciences Publication, **288**, pp. 115–124.
- Ridgway, J., Flight, D.M.A., Martiny, B., Gomez-Caballero, A., Macias-Romo, C. and Grealley, K. (1995) Overbank sediments from central Mexico: an evaluation of their use in regional geochemical mapping and in studies of contamination from modern and historical mining. *Applied geochemistry*, **10**, 97–109.
- Reg Clim (2005) Regional Climate Development Under Global Warming. News Archive, <http://regclim.met.no/> (Norwegian Meteorological Institute).
- Salminen, R., Batista, M.J., Bidovec, M., Demetriades, A., De Vivo, B., De Vos, W., Duris, M., Gillucis, A., Gregorauskiene, V., Halamic, P., Heitzmann, P., Lima, A., Jordan, G., Klaver, G., Klein, P., Lis, J., Locutura, J., Marsina, K., Mazreku, A., O’Connor, P.J., Olsson, S.Å., Ottesen, R.T., Petersell, V., Plant, J.A., Reeder, S., Salpeteur, I., Sandström, H., Siewers, U., Stensfelt, A. and Tarvainen, T. (2005) *Geochemical Atlas of Europe*. Geological Survey of Finland, Espoo, 526 pp.
- Swennen, R. and Van der Sluys, J. (1998) Zn, Pb, Cu and As distribution patterns in overbank and medium-order stream sediment samples: their use in exploration and environmental geochemistry. *Journal of Geochemical Exploration*, **65**, 27–45.
- Swennen, R. and Van der Sluys, J. (2002) Anthropogenic impact on sediment composition and geochemistry in vertical overbank profiles of river alluvium from Belgium and Luxembourg. *Journal of Geochemical Exploration*, **75**, 93–105.
- Swennen, R., Van Keer, I. and De Vos, W. (1994) Heavy metal contamination in overbank sediments of the Geul river (East Belgium): Its relation to former Pb–Zn mining activities. *Environmental Geology*, **24**, 12–21.
- Swennen, R., Van der Sluys, J., Hindel, R. and Brusselmans, A. (1998) Geochemistry of overbank and high-order stream sediments in Belgium and Luxembourg: a way to assess environmental pollution. *Journal of Geochemical Exploration*, **62**, 67–79.
- Syvitski, J.P.M., Vörösmarty, C.J., Kettner, A.J. and Green, P. (2005) Impact of Humans on the Flux of Terrestrial Sediment to the Global Coastal Ocean. *Science*, **308**, 376–380.
- Taylor, S.R. and Heier, K.S. (1958) Alkali elements in potash feldspars from pre-Cambrium of Southern Norway. *Geochimica et Cosmochimica Acta*, **13**, 293–302.
- Walling, D.E. and He, Q. (1998) The spatial variability of overbank sedimentation on river floodplains. *Geomorphology*, **24**, 209–223.
- World Meteorological Organization (2007) *Climate Change 2006, The Scientific Basis. Contribution of Working Group I*. Cambridge University Press, Cambridge, 881 pp.
- Xiachu, S. and Mingcai, Y. (1995) Representativity of wide-spaced lower-layer overbank sediment geochemical sampling. *Journal of Geochemical Exploration*, **55**, 231–248.
- Xie, X. and Hangxin, C. (2001) Global geochemical mapping and its implementation in the Asia–Pacific Region. *Applied Geochemistry*, **16**, 1309–1321.

Ground-Source Heat Pumps and Underground Thermal Energy Storage— Energy for the future

**Kirsti Midttømme^{1,2}, David Banks^{3,4}, Randi Kalskin Ramstad^{1,5},
Ola M. Sæther¹ and Helge Skarphagen⁶**

¹Geological Survey of Norway (NGU), 7491 Trondheim, Norway.

²Norwegian Geotechnical Institute (NGI), Pb. 1230, Pirsenteret, 7462 Trondheim, Norway.

³Holymoor Consultancy, 8 Heaton Street, Chesterfield, Derbyshire, S40 3AQ, UK.

⁴Sir Joseph Swan Institute for Energy Research, Newcastle University, Newcastle-upon-Tyne, NE1 7RU, UK.

⁵Asplan Viak AS, Pb 6723, 7031 Trondheim, Norway.

⁶Norwegian Institute for Water Research (NIVA), 0349 Oslo, Norway.

E-mail: kirsti.midttomme@ngi.no

We need energy for space heating—but in most cases not where or when energy sources are available. Energy storage, which helps match energy supply and demand, has been practised for centuries, also in Norway. Energy storage systems will increase the potential of utilising renewable energy sources such as geothermal energy, solar heat and waste heat. The most frequently-used storage technology for heat and ‘coolth’ is Underground Thermal Energy Storage (UTES). The ground has proved to be an ideal medium for storing heat and cold in large quantities and over several seasons or years. UTES systems in the Nordic countries are mostly used in combination with Ground-Source Heat Pumps (GSHP). Several different UTES systems have been developed and tested. Two types of system, Aquifer (ATES) and Borehole (BTES) storage, have had a general commercial breakthrough in the last decades in the Nordic countries. Today, about 15,000 GSHP systems exist in Norway extracting about 1.5 TWh heat from the ground. About 280 of the Norwegian GSHP installations are medium- to large-scale systems (> 50 kW) for commercial/public buildings and for multi-family dwellings. The two largest closed-loop GSHP systems in Europe, using boreholes as ground heat exchangers, are located in Norway.

Introduction

We, especially here in chilly Norway, need energy for space heating, but, regrettably, most natural heat sources such as the sun, the air, and rivers are at their coldest when we most need their heat—in winter. Similarly, environmental heat sinks, e.g., the air and shallow surface waters, are at their warmest when we have most need for cooling. The use of rocks, sediments and groundwater in the subsurface as a huge Underground Thermal Energy Storage (UTES) system allows us to store surplus heat (regardless of whether it is solar in origin, radiogenic (geothermal), or simply waste summer heat from buildings) until a time when it is needed. In other words, the ground can be manipulated as a heat store; it can preserve summer heat until winter and winter cold until summer, allowing us to match supply and demand over at least a yearly cycle. The Ground-Source Heat Pump (GSHP) is the tool that we use to ‘pump’ surplus heat into the ground and to extract heat when we require it for space heating.

More than 80% of the world’s current energy resources are stored, in some form, in the subsurface (IEA 2007). Over millions of years of geological time, the geosphere has stored solar energy in the form of chemical potential energy (coal, oil, gas), and is also slowly releasing nuclear potential energy via decay of radionuclides (which manifests itself as a geothermal heat flux of several tens of mW m^{-2}). It is widely believed that the continuation of our modern, industrialised way of life will exhaust available oil and gas resources within a period of two centuries (Hahne and Benner 2000). Coal and oil-shale resources offer some potential to replace these, but with a world energy consumption that has increased 20-fold over the last century (Domanski 2003) and is increasing by 2.1% yearly (IEA 2006), these resources may also be regarded as finite over a similar time scale. Intriguingly, however, the amount of energy stored as carbon-based ‘fossil fuel’ is negligible compared to the amount of heat that is stored in the Earth.

The Earth’s total heat content is estimated to be about 10^{31} J and the current average global terrestrial heat-flux rate is 44 TW (1.4×10^{21} J yr^{-1} , Dickson and Fanelli 2004). Divided by the Earth’s surface area of 5×10^{14} m^2 , this results in an average geothermal heat flux of 88 mW m^{-2} . This flux of 1.4×10^{21} J yr^{-1} is almost three times the world’s primary energy-consumption rate (4.8×10^{20} J yr^{-1} in 2005, Bromley and Mongillo 2008).

It is not solely this geothermal heat flux that provides a potential alternative heat resource for mankind, however. The surficial portion of the crust is also able to absorb and store solar and atmospheric heat, acting effectively as a huge solar collector.

Figure 1. Norway’s first brochure for a ground-source heat pump from Normann Energiteknikk AS (today Normann Etek AS). It included an interview with Roger Jansen, one of the first people to install a GSHP in Norway. The picture to the right shows Roger Jansen and the heat pump 27 years later. The heat pump still works.

Ground-Source Heat Pumps (GSHP)

One might imagine, given the relatively low geothermal heat flux of 88 mW m^{-2} , that the practical use of geothermal energy is restricted to a few geologically anomalous areas with a very high heat flux (e.g., plate boundaries and volcanic areas). Fortunately, this is not the case. There exists a tool that enables us to extract low-temperature heat (at ‘normal’ Norwegian temperatures of $6\text{--}7^\circ\text{C}$) from the Earth’s subsurface store, to ‘concentrate’ that heat by compression, and to deliver it as space heating at a higher temperature. This tool is termed the Ground-Source Heat Pump (GSHP). It is based on the fluid compression–expansion cycle, well known from modern refrigerators, first proposed by Oliver Evans in 1805, and constructed by Jacob Perkins and John Hague around 1834 (see references in Banks 2008). It was, however, Lord Kelvin who first proposed using this cycle to artificially heat buildings (Thomson 1852), although his concept was based on using the heat pump to extract heat from outdoor air, rather than the ground.

The idea of using a heat pump to extract heat from the ground was patented by the Swiss Heinrich Zoelly in 1912 (Ball et al. 1983, Spitler 2005, Kelley 2006), and was being used (with rivers and groundwater from wells as a heat source) by the 1930s in America and Switzerland. The ‘closed-loop’ heat pump, where a carrier fluid or refrigerant is circulated through a loop of pipe in the subsurface to extract heat from rocks and sediments, was first constructed in 1945 by Robert C. Webber in Indianapolis, USA (IGSHPA 2006). He seems to have been inspired by his deep freeze, placing the condenser in his living room and an evaporator in a hole in the ground! It seems that the concept first arrived in Norway when Roger Jansen (Figure 1), Fredrikstad, and Per Stykket, Sørumsand, each installed 10–12 kW horizontal closed-loop systems in 1978 (see below).

Although the USA has over 50% of the current GSHP capacity installed worldwide today, the Scandinavian nations have amongst the highest numbers of GSHP systems per inhabitant. According to a global update given at the World Geothermal Congress in 2005, Sweden and Iceland are among the ‘top five’ nations for direct use of geothermal energy, while Denmark and Norway have experienced the largest increase in utilisation of ground-source heat during the past five years



(Lund et al. 2005). The total heat delivered by Norway’s GSHP installations is estimated to be 2.1 TWh per year. In Sweden, GSHP systems have become increasingly popular during the past four decades, and are now one of the most common heating systems, satisfying more than 15% (15 TWh) of the nation’s total space-heating demand. Several hundred larger UTES systems have been constructed and are currently in operation (Gehlin and Nordell 2006).

Ground-source heat pumps are now one of the fastest growing applications of renewable energy in the world, with annual increases of 10% in about thirty countries over the past ten years (Curtis et al. 2005). According to a Canadian study (Caneta Research 1999), GSHP systems potentially have a larger mitigating effect on greenhouse-gas emissions, and the resulting global-warming impact of buildings, than any other single technology available today.

Ground-source heat pumps in Norway

The first known GSHP systems in Norway were installed in 1978. Per Stykket in Sørumsand installed a heat pump with 500 m of shallowly-buried (0.8 m deep) horizontal pipe as a ground heat exchanger. The pipes were produced and installed by Kjell Nyen, and the heat pump was imported from Sweden. Another GSHP system with horizontal pipes as the ground heat

exchanger was installed by Einar Grønnevik for Roger Jansen’s house in Fredrikstad in the same year, and is still in operation.

Jens Sagen, a factory owner in Kristiansand, read about ground-source heat in the early 1980s. He contacted a consultant and they travelled together to Sweden to investigate this new ‘alternative’ energy technology (which had already gained considerable acceptance in Sweden). On their return, they constructed a 50 kW GSHP installation at Jens Sagen AS manufacturing company, based on heat extraction via six 115 m-deep closed-loop boreholes. This was commissioned in 1985. A high groundwater flow through the borehole array is claimed to have been significant in ensuring the system’s sustainability (transporting heat by advection with groundwater flow to the collector loops in the boreholes) and maintaining an acceptable temperature in the collector fluid.

Today, there are about 15,000 GSHP installations in Norway (Midttømme 2005). Statistics from NOVAP, the Norwegian heat-pump association, show a clear trend of increasing sales from 1992 to 2006 (Figure 2). Sales of air-sourced heat pumps (which have a lower capital cost, but which are somewhat less efficient than GSHP systems) are even more impressive—indeed, they accounted for around 95% of all heat-pump sales in Norway in the most recent years (Figure 3). The Norwegian state provided subsidies for all types of heat pump in 2003,

Figure 2. The sale of brine/water heat pumps (mainly GSHPs) in Norway in 1992–2006. Data from NOVAP, the Norwegian heat-pump association.

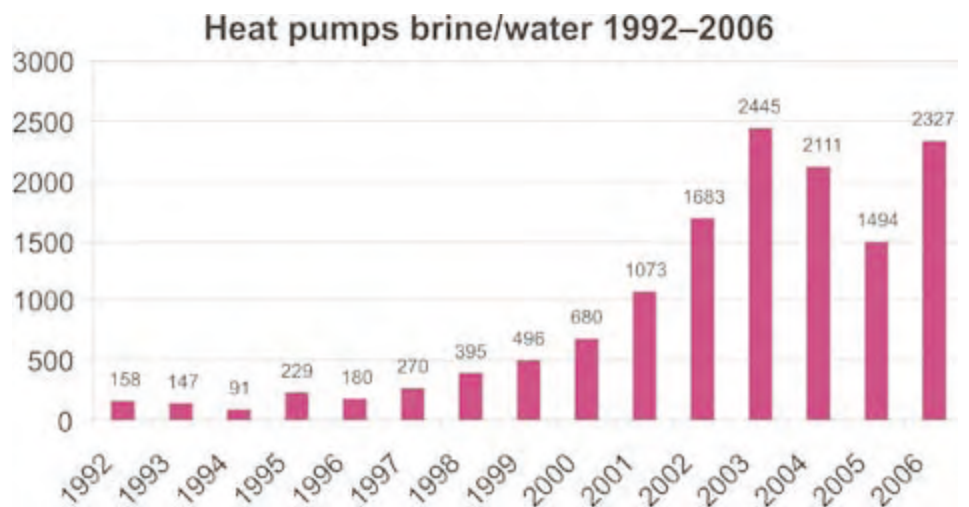
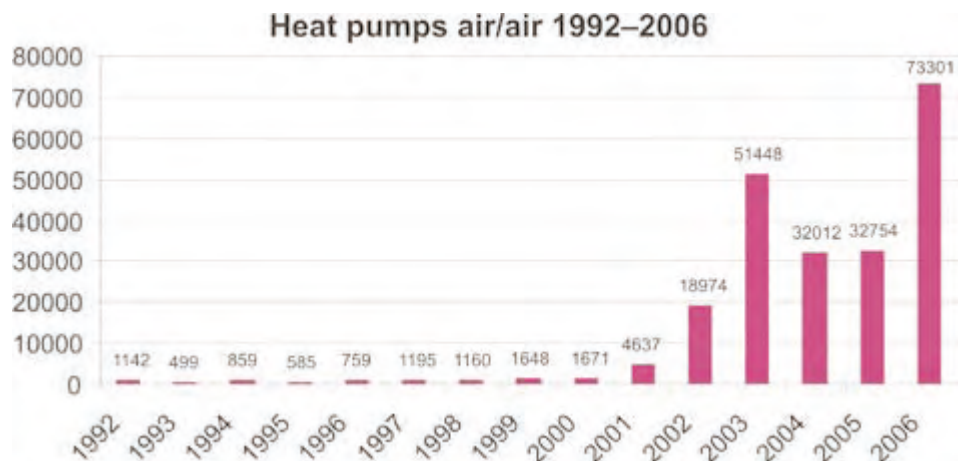


Figure 3. The sale of air/air heat pumps in Norway in 1992–2006. Data from NOVAP.



but only for ground-source heat pumps in 2006–2007, and the availability of these subsidies had a clear impact in terms of increased sales.

About 280 of the Norwegian GSHP installations are medium- to large-scale systems (heating power > 50 kW), for commercial/public buildings and for multi-family dwellings. The two largest closed-loop GSHP systems in Europe, using boreholes as ground heat exchangers, are located in Norway, at Nydalen Næringspark (Business Park) in Oslo and Akershus University Hospital in Lørenskog.

Underground Thermal Energy Storage (UTES) systems

The ground can, of course, be used not only as a heat source, but also as a heat sink for ‘waste’ heat. Thus, the ground can be used to provide either heating or cooling. Optimally, it can be used to provide a balanced combination of both heating and cooling, with surplus summer heat being stored in the ground for subsequent extraction in winter. Increasingly, larger buildings require some form of active cooling, even in the Nordic climate. In the summer, therefore, a heat pump can be designed to circulate a chilled fluid around a building. This chilled fluid effectively extracts heat from the building, which the heat pump transfers (via a ground heat exchanger) to the ground or to groundwater. In the winter, the direction of the heat pump is reversed, so that heat is extracted from the ground/groundwater and transferred to a warm space-heating fluid. The ground has now effectively become an Underground Thermal Energy Storage (UTES) system.

The concept of environmental thermal storage can be dated back to ancient civilizations. Harvesting of ice and snow from the mountains, and subsequent underground ‘cold storage’ during the spring and summer, is known from 350 years ago in Persia (Iran). Norway’s ‘ice-entrepreneurs’ (such as Johan Martin Dahll from Kragerø) (Figure 4) have even, during the last half of the 19th and early 20th century, exported Norwegian ice by ship to London to be stored underground in ‘ice wells’ along the Regent’s Canal (Banks 2008). The modern use of UTES applications commenced in China in the 1960s, where groundwater was initially extracted in large quantities to provide



Figure 4. Ice production from Nesodden. Ice from Norway was exported to Europe in the 1800s and early 1900s. Photo: courtesy of Nesodden Historielag, Nesoddens Historie, Bind 2.

industrial cooling. Such excessive extraction resulted in land subsidence, however. To rectify this situation, cold surface water was artificially injected into the aquifers and it was observed that the injected water maintained its cool temperature for a long period, making it an ideal source of industrial cooling (Morofsky 2007).

Several variants of UTES can be envisaged, although the two types that have been developed, tested and commercially operated in Norway are:

- Borehole Thermal Energy Storage (BTES), where no fluid is physically exchanged with the ground, but where the volumetric heat capacity of the rock alone is used to store heat.
- Aquifer Thermal Energy Storage (ATES), where heat transfer and storage is by warm or cold groundwater.

Borehole Thermal Energy Storage (BTES)

Sentermenigheten in Asker installed one of the first BTES schemes in Norway. Much of the installation work was performed by enthusiastic volunteers and, since the year 2000, the resulting BTES array of thirteen 130 m-deep boreholes has provided heating and cooling to the assembly building.

A new BTES system has recently been completed at Falstadsenteret, a 2850 m² historical museum in Levanger (Figure 5a). The heating and cooling scheme comprises a 130 kW heat pump (Figure 5b) and nine 180 m-deep closed-loop

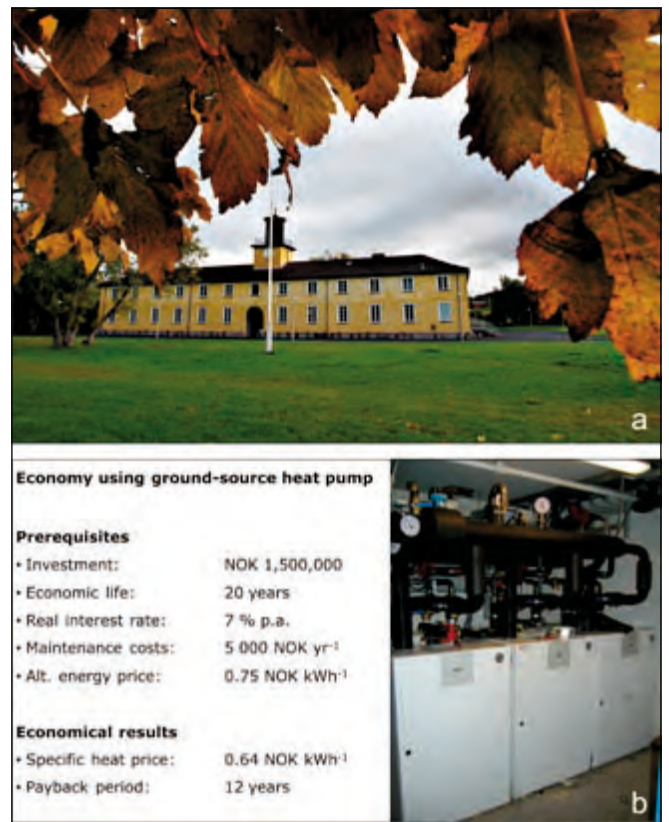


Figure 5. (a) Falstadsenteret, a 2850 m² historical museum in Levanger. Photo: Kjell A. Olsen, Adresseavisen. (b) The Falstadsenteret heat pump and economic considerations.

boreholes. The payback time for the extra capital costs of the ground-source system, compared to a conventional heating and cooling system, is estimated to be 12 years.

A BTES system comprising 220 boreholes of 200 m depth, drilled into dioritic rocks, will provide heating and cooling to the new Akershus University hospital. The hospital is under construction and will be fully operational in October 2008 (Stene et al. 2008). The BTES system became operational in May 2007, but a second phase of drilling is planned to provide an extension of the BTES scheme (making a total of up to 350 boreholes). It was originally planned to drill the boreholes close to the hospital, but seismic geophysical surveys and trial borings showed a high density of clay-filled fracture zones. This observation suggested that full-scale drilling would be difficult and expensive. The proposed BTES borehole array was thus relocated to a field about 300 m from the hospital. After drilling, the borehole heads will be completely underground and the farmer will continue to use the field to grow crops.

Aquifer Thermal Energy Storage (ATES)

In 1987, the first known ATES system in Norway was established in Seljord. A 10 m-deep well was drilled for heating and cooling of Seljord lysfabrikk (Dyrud 2008).

The largest UTES system in Norway is at Oslo's Gardermoen international airport. This ATES system has been in operation since the airport opened in 1998 and comprises an 8 MW heat-pump array, coupled to 18 wells of 45 m depth, 9 for extraction of groundwater and 9 for re-injection. The wells are sunk into the Øvre Romerike glaciofluvial sand and gravel aquifer. This system covers the total cooling needs of the airport, of which 25% (2.8 GWh yr⁻¹) is free cooling via direct heat exchange with cold groundwater, and 75% (8.5 GWh yr⁻¹) is active cooling via the use of the heat pumps. The annual heating provision is typically 11 GWh. There have been some problems with clogging of the groundwater loop, and the groundwater wells and heat exchangers require cleaning every few years. Because of a lack of knowledge of ATES systems in Norway, Dutch consultancies were hired to design the ATES system and GSHP installations. The total cost of the system was 17 million NOK and the payback time, compared to traditional heating and cooling systems, is estimated to be less than four years (Eggen and Vangsnes 2005).

Oslo Centre for Interdisciplinary Environmental and Social Research, a component of the Oslo Innovation Centre in Oslo, is a 13,500 m² office building with laboratories (Stene et al. 2008). An ATES system, extracting groundwater from the underlying limestone and shale rock, provides both heating and cooling to the building. A closed-loop BTES system was originally intended for the site, but extremely difficult ground conditions were encountered during initial drilling: namely, zones of remarkably high groundwater flow associated with a Permian syenite dyke structure several metres thick. It became clear that it would be both more feasible and cheaper to drill a small number of groundwater wells (using the dyke as an

aquifer) than a large number of closed-loop boreholes. Thus, a total of nine wells were drilled. These wells are typically located in extraction–injection pairs, one well drilled to 100 m depth and the second to 100–200 m depth. Using this arrangement, it is possible to access enough groundwater and rock volume to cover the seasonal cooling and heating demands of the building (Stene et al. 2008).

Conclusions

The idea of storing the Earth's natural heat or cold over the passage of several seasons has been practised in many countries for centuries. Norway even successfully exported its natural thermal resource (in the form of winter ice) to England during the late 19th and early 20th century. The concept of the heat pump is not new. It was invented 170 years ago and was first proposed for space heating of buildings some 150 years ago. Efficient GSHP technology has been utilised in Sweden for almost four decades and is now accepted as mainstream. Many other European nations (including both Norway and Great Britain), have been slow in taking up this technology due to a combination of factors, including cheap conventional energy (hydroelectric in Norway, coal and gas in the UK), lack of political will, and lack of awareness of the need to consider the impact of space heating on the national CO₂ budget.

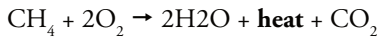
The theoretical framework for describing the flow and storage of heat in the ground is well known—much of it is based on the pioneering work of Horatio Scott Carslaw (Carslaw and Jaeger 1947). It transpires that the fundamental physics describing heat conduction in the ground is directly analogous to that used by hydrogeologists to describe groundwater flow (indeed, modern groundwater-flow theory is directly derived from heat-flow theory, Bredehoeft 2008).

GSHP and UTES can, of course, be seen as 'just another' alternative energy technology. It is probably more correct to regard them as complementary technologies, however. They are a means of utilising Norway's limited resources of hydroelectricity 300% more efficiently than would a conventional panel heater. Alternatively, they can be regarded as a means of avoiding future increased CO₂ emission from fossil fuels. They can also be coupled with other low-CO₂ energy technologies (wind turbines, solar thermal panels) to deliver integrated energy solutions. Unlike wind power and solar cells, however, ground-source heat is not vulnerable to the vagaries of the climate; the ground offers a huge thermal store that can bank heat energy in times of surplus and be drawn upon in times of need. It allows us to match heating and cooling demand with natural resources over a protracted period.

We would never think of producing our drinking water by burning hydrocarbons e.g., methane gas:



The hydrogeologist knows that we have abundant natural reserves of groundwater to draw upon. All we need to access them is a hole in the ground (a well) and a pump. In contrast, many nations have generated *heat* by burning fossil carbon:



even though we have abundant reserves of low-temperature ground-source heat in the rocks, sediments and groundwater beneath our feet. All we need to access this heat is a hole in the ground (a borehole or trench) and a heat pump! Why generate heat by burning fossil fuels, when we can use that energy many times more efficiently simply to pump natural ground-source heat into our homes?

Aknowledgements

Constructive reviews by Bo Nordell and Geir Eggen are greatly appreciated.

References

- Ball, D.A., Fischer, R.D., Talbert, S.G., Hodgett, D. and Auer, F. (1983) State-of-the-art survey of existing knowledge for the design of ground-source heat pump systems. *Battelle Columbus Laboratories Report ORNL/Sub 80-7800/2*, Columbus, Ohio, USA, 75 pp.
- Banks, D. (2008) *An Introduction to Thermogeology: Ground-Source Heating and Cooling*. Wiley/Blackwell, Oxford, 352 pp.
- Bredenhoft, J.D. (2008) An interview with C.V. Theis. *Hydrogeology Journal*, **16**, 5–9.
- Bromley, C.J. and Mongillo, M.A. (2008) Geothermal Energy from Fractured Reservoirs—Dealing with Induced Seismicity. *IEA Open Energy Technology Bulletin*, **48**, 7 pp.
- Caneta Research (1999) *Global Warming Impacts of Ground-Source Heat Pumps Compared to Other Heating and Cooling Systems*. Prepared for Renewable and Electrical Energy Division, Natural Resources Canada, 11 pp.
- Carslaw, H.S. and Jaeger, J.C. (1947) *Conduction of Heat in Solids*. Oxford University Press, London, 386 pp.
- Curtis R., Lund, J., Sanner, B., Rybach, L. and Hellström, G. (2005) Ground-Source Heat Pumps—Geothermal Energy for Anyone, Anywhere: Current Worldwide Activity. Proceedings World Geothermal Congress 2005, Antalya, Turkey, 24–29 April 2005, 9 pp.
- Dickson, M.H. and Fanelli, M. (2004) What is geothermal energy? Istituto di Geoscienze e Georisorse, CNR, Pisa, Italy. Available via the International Geothermal Association, <http://iga.igg.cnr.it/geo/geoenergy.php> (19 April 2008).
- Domanski R (2003) Energy Sources for XXI Century. Futurestock 2003, Proceedings 9th International Conferences on Thermal Energy Storage, Warsaw, Poland, pp. 13–32.
- Dyrud I.F. (2008) *Kartlegging av grunnvarmepotensialet i Seljord*. M.Sc. thesis, Høgskolen i Telemark, 105 pp.
- Eggen, G. and Vangsnes, G. (2005) Heat pump for district cooling and heating at Oslo Airport Gardermoen. Proceedings 8th IEA Heat Pump Conference, Las Vegas, Nevada, 30 May–2 June 2005, 7 pp.
- Gehlin, S. and Nordell, B. (2006) Promoting TES systems in Sweden. Ecostock 2006, 10th International Conference on Thermal Energy Storage, Richard Stockton College of New Jersey, 31 May–2 June 2006, 6 pp.
- Hahne, E.W.P. and Benner, M. (2000) Preface. In Benner, M. and Hahne, E.W.P. (eds.) *TERRASTOCK 2000*, 8th International Conference on Thermal Energy Storage. Proceedings, Volume 1, University of Stuttgart, Germany, 28th of August–1st September 2000, pp. *iv*.
- IEA (2006) *World Energy Outlook 2006*, International Energy Agency, 596 pp.
- IEA (2007) *Key World Energy Statistics*, International Energy Agency, 78 pp.
- IGSHPA (2006) Website of the International Ground-Source Heat Pump Association, http://www.igshpa.okstate.edu/about/about_us.htm (December 2006).
- Kelley, I. (2006) Ground-source heat pumps deliver both high efficiency and reliability—good news for both contractors and their customers. *Wisconsin Perspective*, September–October 2006, pp. 14–16.
- Lund, J.W., Freeston, D.H. and Boyd, T.L. (2005) Direct application of geothermal energy: 2005 Worldwide review, *Geothermics*, **34**, 691–727.
- Midttømme, K. (2005) Norway's Geothermal Energy Situation. Proceedings World Geothermal Congress 2005, Antalya, Turkey, 24–29 April 2005, 5 pp.
- Morofsky, E. (2007) History of Thermal Energy Storage. In Paksoy H.Ö. (ed.) *Thermal Energy Storage for Sustainable Energy Consumption: Fundamentals, Case Studies and Design*. Nato Science Series II, **234**, pp. 3–22.
- Spitler, J.D. (2005) Ground-source heat pump system research—past, present and future. *International Journal of HVAC & R Research*, **11**, 165–167.
- Stene, J., Midttømme, K., Skarphagen, H. and Borgnes, B.G. (2008) Design and Operation of Ground-Source Heat Pump Systems for Heating and Cooling of Non-Residential Buildings. 9th International IEA Heat Pump Conference, Zürich, Switzerland, 20–22 May 2008, accepted.
- Thomson, W. (1852) On the economy of heating or cooling of buildings by means of currents of air. *Proceedings of the Royal Philosophical Society Glasgow*, **3**, 269–272.

Factors influencing shallow (< 1000 m depth) temperatures and their significance for extraction of ground-source heat

Trond Slagstad¹, Kirsti Midttømme^{1,2}, Randi Kalskin Ramstad^{1,3} and Dag Slagstad⁴

¹Geological Survey of Norway (NGU), 7491 Trondheim, Norway.

²Norwegian Geotechnical Institute (NGI), Pb. 1230, Pircenteret, 7462 Trondheim, Norway.

³Asplan Viak AS, Pb 6723, 7031 Trondheim, Norway.

⁴SINTEF Fisheries and Aquaculture, 7465 Trondheim, Norway.

E-mail: trond.slagstad@ngu.no

The thermal structure of the shallow crust (defined here as < 1000 m depth) is sensitive to surface effects including geological variation (e.g., radiogenic heat production, terrestrial heat flow, thermal conductivity), terrain effects (e.g., topography, slope orientation), climatic conditions (e.g., palaeoclimatic history, mean annual surface temperatures) and human activity (e.g., farming, urbanisation). A number of quantitative models show that at shallow depths down to a few hundred metres, mean annual surface temperature is the main factor controlling subsurface temperature, whereas geological variation (heat flow, heat production, thermal conductivity) only becomes significant at depths of ca. 1000 m and greater. Ground-source heat for household heating is commonly extracted from shallow boreholes between 100 and 200 m deep; thus, at present, the effects of variation in heat flow and heat production are negligible, whereas thermal conductivity has some impact on the amount of heat that is extractable from the ground. Rather, one should focus on gathering information about thickness of overburden and hydrogeological activity, as well as reducing costs by developing cheaper, more efficient drilling techniques and heat pumps. With technological advances allowing affordable drilling to depths on the order of 1000 m, geological information will become increasingly more important.

Introduction

The thermal structure of the shallow continental crust (taken here as < 1000 m depth) is a function of heat flow from the Earth's interior, geological heterogeneity, surface effects (herein referred to as 'terrain effects', cf., Blackwell et al. 1980), surface temperatures and past climatic changes. The heat flowing from the Earth's interior is dominantly derived from radioactive decay of U, Th and K in the Earth's mantle and crust (Hofmeister and Criss 2005), and shallow geological effects include variation in radiogenic heat production and thermal conductivity, variable soil or till cover and hydrogeological activity. The main terrain effects are topographic relief, microclimatic variations from differences in vegetation cover, and varying solar influx as a function of slope orientation and slope angle (Blackwell et al. 1980). Long-term climatic variation (palaeoclimatic history), particularly in formerly glaciated areas, and mean annual surface temperature are important contributors to the shallow thermal structure (e.g., Clauser et al. 1997), and, in addition, human activity such as farming and urbanisation may locally change the thermal structure of the shallow crust (e.g., Taniguchi and Uemura 2005).

The purpose of this paper is to present generalised models that quantify the shallow thermal effects of some of the parameters mentioned above and discuss these in terms of utilisation of ground-source heat in houses and small buildings. We limit our discussion to variations in shallow radiogenic heat production and thermal conductivity, topographic relief, palaeoclimatic history and mean annual surface temperature—that is, factors related to conductive heat transfer. Convective heat transfer, in particular groundwater flow, is not discussed. The models and conclusions are based on and applicable to extraction of heat from crystalline bedrock in tectonically inactive areas, where conduction through a solid is the only means of heat transfer.

The modelling shows that although geological, terrain and palaeoclimatic factors contribute to the shallow thermal structure, their significance for extraction of ground-source heat is rather minor in the geological settings considered here (e.g., Scandinavia), and the main factor determining temperatures at shallow depths is the mean annual surface temperature.

Factors influencing shallow crustal temperature and heat flow

Below, we present 1D, 2D and 3D thermal models that address the geological, terrain and palaeoclimatic effects mentioned above. Ground-source heat is typically extracted from boreholes that are between 100 and 200 m deep; however, in the foreseeable future, drilling to 1000 m or deeper may become economically feasible. We therefore present modelled temperature and heat-flow data from depths of 100, 200 and 1000 m in the models and base our discussion on these. The models were developed

and run using the Comsol Multiphysics finite element method software (COMSOL AB Sweden, COMSOL Multiphysics v. 3.3a).

Radiogenic heat production

Variation in radiogenic heat production causes variation in heat flow and thus thermal gradient. These factors can be addressed by simple 1D calculations assuming a given, constant surface temperature (T_{sur} , °C), basal heat flux (Q_0 , mW m⁻²) and thermal conductivity (k , W m⁻¹ K⁻¹), and varying radiogenic heat production (A , μW m⁻³) or thickness of the heat producing layer (h , km) (Figure 1a). The steady-state heat flow (Q) and temperature (T) at depth (z , km), where z is positive upwards, can be derived from Fourier's law of heat conduction, slightly modified to also include internal heat sources (1):

$$-k \frac{dT}{dz} = Q_0 + A(z+h) \quad (1)$$

as

$$Q(z) = A(z+h) + Q_0 \quad (2)$$

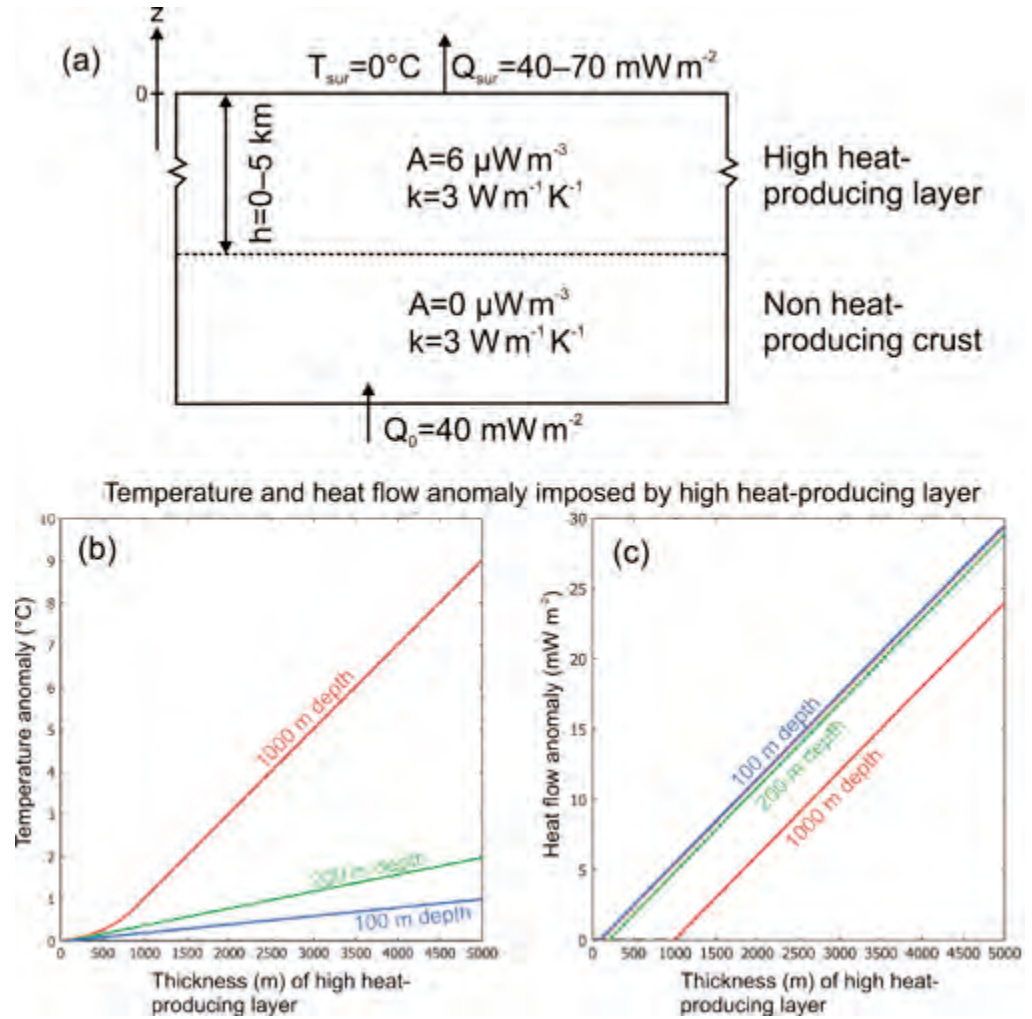
and

$$T(z) = T_{\text{sur}} - \frac{Q_0}{k} z - \frac{A}{2k} z^2 - \frac{A}{k} hz \quad (3)$$

In Norway, typical surface heat-flow (Q_{sur}) values range between 40 and 60 mW m⁻², but locally exceed 70 mW m⁻² in areas underlain by thick, high heat-producing granites (e.g., Grønlie et al. 1977, Heier and Grønlie 1977, see also discussion in Slagstad 2006). One such granite is the Iddefjord–Bohus granite in southeast Norway and southwest Sweden that ranges in thickness between ca. 1 and 5 km (Ramberg and Smithson 1973, Landström et al. 1980, Lind 1982), with an average heat-production rate of ca. 6 μW m⁻³ (Slagstad 2006, Slagstad in press). Here, we present the results of 1D calculations that quantify the thermal effects of a high heat-producing layer, like the Iddefjord–Bohus granite, ranging in thickness from 0 to 5 km with a heat production of 6 μW m⁻³, corresponding to a 30 mW m⁻² variation in surface heat flow. The top of the high heat-producing layer is kept at the surface, the surface temperature is constant at 0°C, and the basal heat flow is constant at 40 mW m⁻². The model geometry and parameters are shown in Figure 1a. Figures 1b and 1c show temperature and heat-flow anomalies, respectively, at 100, 200 and 1000 m depth as a function of the thickness of the high heat-producing layer. The temperature and heat-flow anomalies are calculated relative to the thermal structure of a similar model without a high heat-producing layer (i.e., $h = 0$).

At 100 and 200 m depth, the thermal anomaly imposed by a 5 km-thick, high heat-producing (6 μW m⁻³) layer is 1 and 2°C, respectively. This temperature anomaly corresponds to a 30 mW m⁻² increase in surface heat flow, which probably represents a maximum in terms of the variation one might expect in

Figure 1. (a) Model geometry and input parameters of a model investigating the significance of heat production on the near-surface thermal structure. (b) and (c) Temperature and heat flow anomalies, respectively, at 100, 200 and 1000 m depth, imposed by a high heat-producing layer, for example certain granite bodies, at the surface.



geologically stable areas. The results of the modelling thus show that the temperature in the uppermost few hundred metres is relatively insensitive to variations in heat production (and heat flow). At 1000 m depth, the thermal anomaly is 9°C for a 5 km-thick high heat-producing layer. The heat-flow anomaly increases linearly with increasing thickness of the heat-producing layer, reaching nearly 30 mW m^{-2} at 100 and 200 m depth when the layer is 5 km thick. At 1000 m depth, the anomaly is obviously smaller, but nevertheless significant, reaching nearly 25 mW m^{-2} for a 5 km-thick, high heat-producing layer.

Thermal conductivity and low-conductivity overburden

In contrast to variation in radiogenic heat production, variation in thermal conductivity only affects the thermal gradient but not the heat flow. Given no internal heat production (i.e., $Q_{sur} = Q_0$), Equation (3) can be reduced such that the temperature at a certain depth is expressed as:

$$T(z) = T_{sur} - \frac{Q_0}{k}z \quad (4)$$

Here, we consider the thermal effects of conductivities varying between 2 and $4\text{ W m}^{-1}\text{ K}^{-1}$, which covers most rock

types encountered in the continental crust (Clauser and Huenges 1995). Figure 2a shows how the temperature at 100, 200 and 1000 m depth varies with varying thermal conductivity given surface heat flows of $40, 50, 60$ and 70 mW m^{-2} . Because thermal gradient is inversely related to thermal conductivity, the temperature effect is proportional with increasing depth. This inverse relationship also means that temperatures at a particular depth converge with increasing conductivity. Thus, at 100 m depth, variation in thermal conductivity from 2 to $4\text{ W m}^{-1}\text{ K}^{-1}$ and surface heat flow between 40 and 70 mW m^{-2} amounts to ca. 2.5°C variation in temperature; at 200 m depth the corresponding value is ca. 5°C , and at 1000 m is ca. 25°C . Figure 2b shows calculated temperature anomalies relative to a model with thermal conductivity $3\text{ W m}^{-1}\text{ K}^{-1}$. For shallow depths (100 and 200 m), the temperature anomalies are small, on the order of 2 to 3°C , despite the relatively large variation in conductivity. At greater depths (1000 m), the temperature anomalies are naturally larger, on the order of $10-20^{\circ}\text{C}$. The temperature effects imposed by variations in conductivity are thus slightly higher than for variations in radiogenic heat production; however, at the shallow depths from which ground-source heat is normally extracted, the variation is at most a

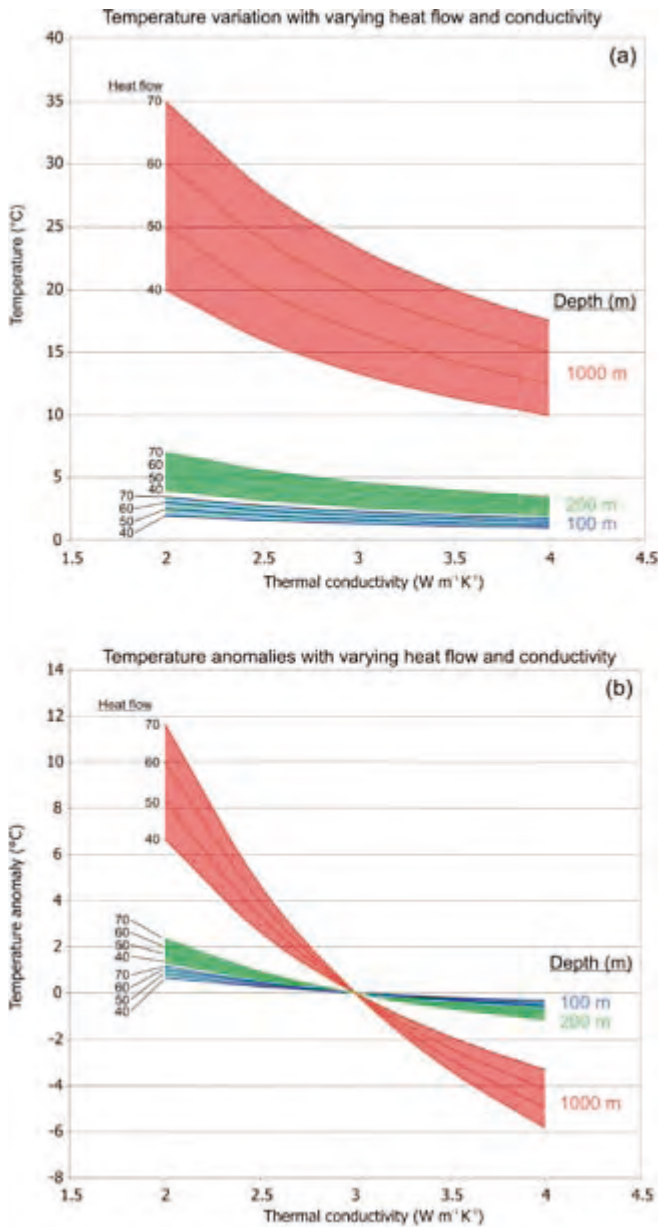


Figure 2. (a) Temperatures at 100, 200 and 1000 m depth with varying thermal conductivity given surface heat flows of 40, 50, 60 and 70 mW m⁻² and a surface temperature of 0°C. (b) Thermal anomalies calculated relative to a model with conductivity 3 W m⁻¹ K⁻¹, otherwise similar to (a).

few degrees, even when considering rather large variations in conductivity and heat flow. A downside is that the higher subsurface temperatures are attained at low conductivities that in turn reduce the amount of heat that is extractable from the ground (discussed further below).

Another factor related to thermal conductivity is the presence of overburden such as sand, clay and moraine. Such materials typically have thermal conductivities that are far lower than most rock types (Midttømme 1997), thereby acting as low-conductivity thermal blankets that will increase the subsurface temperature. In a two-layer model with overburden as the upper layer and bedrock as the lower layer, elevated temperatures attained due to high thermal gradients in the

upper, low-conductivity layer will propagate down through the lower layer. In most cases, thick accumulations of overburden are located in valleys, in which case lateral heat flow will limit the blanketing effect to rather shallow depths of a few hundred metres. The thermal effects of such a low-conductivity layer can easily be assessed by considering Equation (4), which, being a 1D equation, represents a maximum estimate of these effects by neglecting lateral heat flow.

Figure 3a shows temperature anomalies resulting from overburden of variable thickness (10, 50 and 100 m) as a function of thermal conductivity (0.5–1.5 W m⁻¹ K⁻¹) and heat flow (40–70 mW m⁻²). The anomalies are calculated by

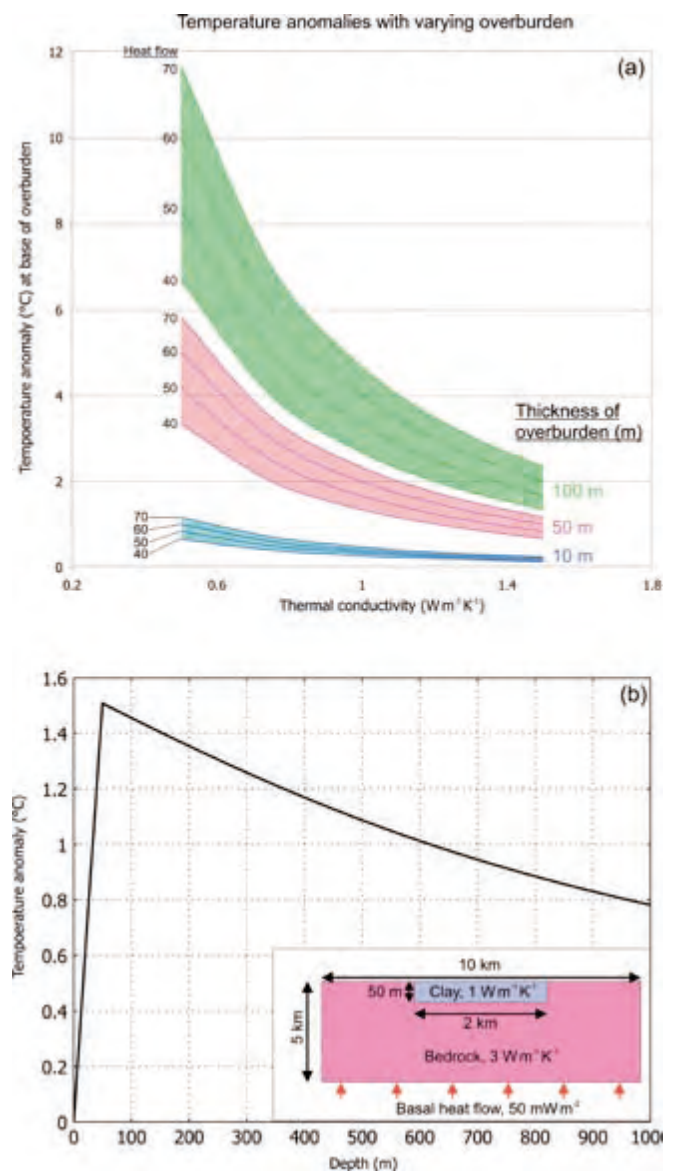


Figure 3. (a) Temperature anomalies at base of 10, 50 and 100 m-thick low-conductivity layers consisting of clay or other types of unconsolidated overburden for various heat flows and thermal conductivities. The temperature anomalies are calculated relative to the temperatures at 10, 50 and 100 m in bedrock with a thermal conductivity of 3 W m⁻¹ K⁻¹. (b) Temperature anomaly imposed by a 2 km-wide and 50 m-thick low-conductivity layer (1 W m⁻¹ K⁻¹) as a function of depth, given a heat flow of 50 mW m⁻². The inset shows the model setup (not to scale).

comparing the temperature at 10, 50 and 100 m depth (i.e., at the base of the low-conductivity layer) with the temperature at the same depth in exposed bedrock with a thermal conductivity of $3 \text{ W m}^{-1} \text{ K}^{-1}$. The depth of penetration of the thermal anomaly depends on the areal extent of the low-conductivity layer and distance to exposed bedrock acting as conduits for excess heat, but will even for relatively moderate extents of a few kilometres and thickness of a few tens of metres, penetrate to depths of several hundred metres. This is illustrated by the 2D model in Figure 3b, which shows temperature anomaly in the horizontal centre of the model as a function of depth imposed by a 2 km-wide and 50 m-thick low-conductivity layer ($1 \text{ W m}^{-1} \text{ K}^{-1}$) given a heat flow of 50 mW m^{-2} . The maximum anomaly at the base of the layer is slightly lower (0.2°C) than predicted from Figure 3a due to lateral heat flow, and tapers off with increasing depth. The modelling shows that very thick low-conductivity layers (at least 50 to 100 m) or with unrealistically low thermal conductivities are required to produce temperature anomalies of a few degrees. Although thick overburden has some impact on temperatures in the shallow crust, overburden requires that the borehole be cased, resulting in inflated drilling costs and discouraging the extraction of ground-source heat.

Topography

The most obvious topographic effects on subsurface temperatures are compressed isotherms (i.e., enhanced gradient) beneath topographic lows (referred to here as valleys), and drawn out isotherms (i.e., reduced gradient) beneath topographic highs (peaks). This relationship is illustrated in Figure 4, which shows temperature and heat flow in a 2D model with a sinusoidal topography with wavelength 10 km and amplitude 1000 m. The temperature at the model surface is 5°C at the valley floor and decreases upward by $6.5^\circ\text{C km}^{-1}$, equal to the atmosphere's lapse rate. The heat flow at the base of the model is 50 mW m^{-2} , and the model has an isotropic conductivity of $3 \text{ W m}^{-1} \text{ K}^{-1}$. The discussion on topographic effects below is based on this model.

Figures 5 and 6 show how modelled heat-flow and temperature anomalies (i.e., relative to a horizontal surface), respectively, at 100, 200 and 1000 m depth vary with amplitude (0–1500 m) and wavelength (3–15 km). The plots show that temperature and heat flow are reduced beneath peaks and increased beneath valleys, and that the topographic effect increases with increasing amplitude and decreasing wavelength (cf., Blackwell et al. 1980). Topography clearly has a significant effect on heat flow in the shallow crust, increasing or decreasing heat flow locally by up to several tens of mW m^{-2} . In contrast, temperatures at shallow depths (100 and 200 m) in areas with moderate topography are only weakly perturbed, whereas temperatures at greater depths are more strongly affected. This is analogous to the discussion above on the effect of variation in heat production, which can also be thought of as variation in heat flow: at shallow depths, even relatively large changes in heat flow, and thus thermal gradient, do not result in significant variation in temperature (this also follows from Equation 4). In

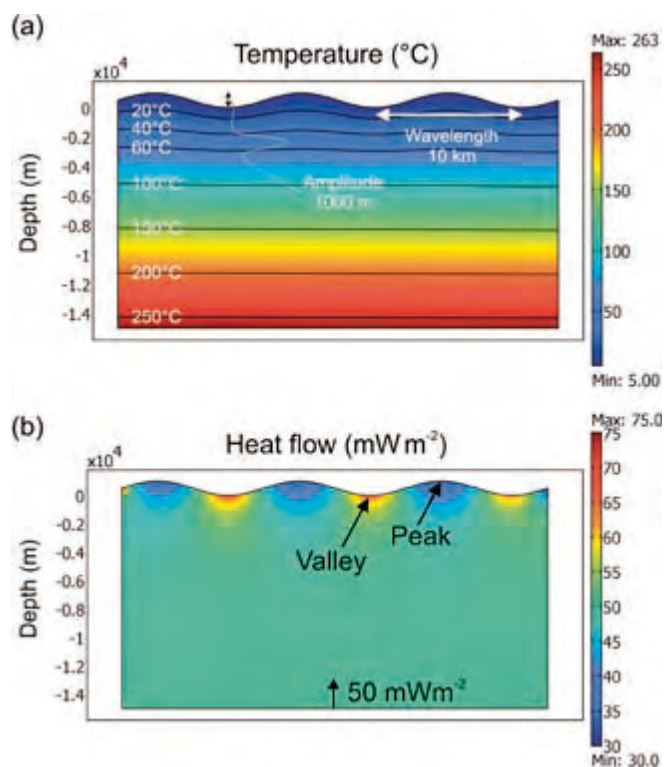


Figure 4. Thermal model illustrating how temperature (a) and heat flow (b) are affected by topography. The thermal parameters are: 5°C surface temperature, 50 mW m^{-2} basal heat flow, a conductivity of $3 \text{ W m}^{-1} \text{ K}^{-1}$, and no internal heat production.

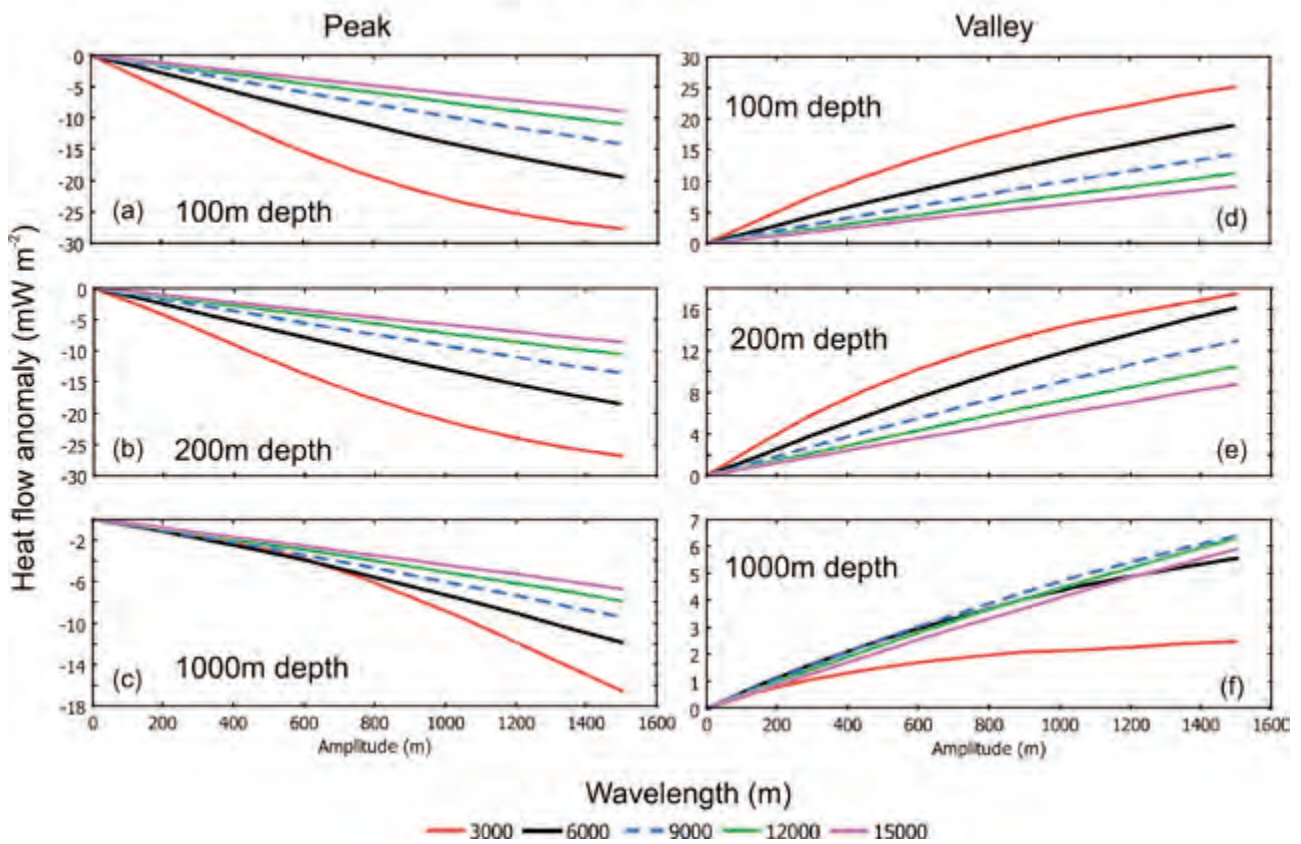
fact, the magnitudes of heat-flow and temperature anomalies relating to variation in heat production and topography are similar (cf., Figures 1, 5 and 6).

A perhaps surprising feature of the plots in Figures 5 and 6 is the fact that several of the lines for heat-flow and temperature anomalies at 1000 m depth cross each other. This may at first appear counter-intuitive, however, the reason this happens is that for a given wavelength, a point is reached where increasing the amplitude does not affect the subsurface thermal structure noticeably; this point is reached at greater amplitudes for greater wavelengths and/or shallower depths, hence the crossing lines. If the plots had been extended to greater amplitudes, similar effects would appear in the 100 and 200 m plots. Another way of looking at this is that as the walls of the peak–valley topography approach vertical (i.e., very high amplitude), the heat flow and temperature at a given depth will not change in response to further increases in amplitude, apart from the effect of the atmosphere's lapse rate. This relationship is illustrated and explained schematically in Figure 7.

Palaeoclimatic history

The effects of palaeoclimatic changes on subsurface temperature were recognised a long time ago (Anderson 1934, Benfield 1939). Each temperature perturbation at the surface propagates into the subsurface at a rate determined by the diffusivity of the rock, and the depth of penetration depends on both the amplitude and duration of the perturbation at the surface.

Topographic effect on heat flow



Topographic effect on temperature

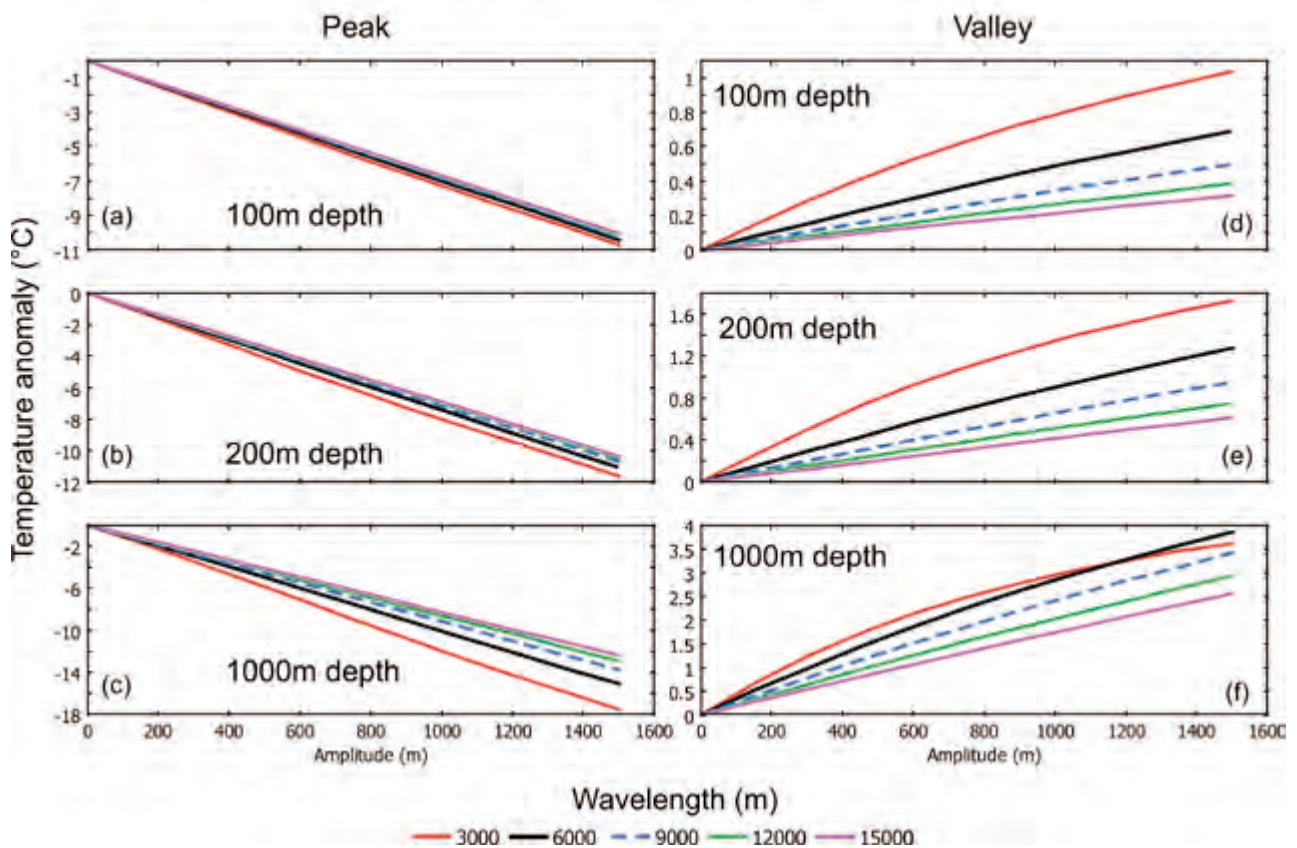


Figure 5. Influence of topography on heat flow at 100, 200 and 1000 m depth beneath a peak (a–c) and a valley (d–f). The heat-flow anomaly is calculated by subtracting the heat flow at a particular depth given a horizontal surface from the modelled heat flow at the same depth given a sinusoidal topography with a certain wavelength and amplitude. The amplitude varies between 0 and 1500 m, and the wavelength between 3 and 15 km. Thermal parameters as in Figure 4.

Roughly speaking, the effects of Pleistocene ice ages, which lasted several hundred thousand years, extend to depths of several kilometres, climatic changes during the Holocene extend to depths of several hundred metres to a few kilometres, and seasonal changes extend to depths of a few tens of metres. The amplitude of the perturbation varies inversely with the elapsed time since the perturbation, which means that the amplitude of a Holocene perturbation will be greater than the amplitude of a similar-magnitude Pleistocene event.

In order to assess the thermal significance of palaeoclimatic history we have calculated heat-flow and temperature effects at 100, 200 and 1000 m depth for three simple palaeoclimatic histories (Figure 8a): a ‘cold’ model in which the temperature is constant at -15°C between 30 and 20 ka, followed by a gradual warming to a present-day temperature of 5°C; a ‘warm’ model where the temperature is -1°C between 30 and 20 ka, followed by a gradual warming to a present-day temperature of 5°C; and a ‘tepid’ model which is similar to the ‘cold’ model except that the surface temperature rises to 5°C at 1 ka and remains at that temperature until the present day. The ‘cold’ model represents periglacial areas or areas beneath cold-based ice, whereas the ‘warm’ model represents areas beneath warm-based ice. The ‘tepid’ model is included to assess the rate of thermal recovery after a period of cold climatic conditions.

The modelling is based on a 2D model where temperature at the surface varies as a function of time and temperatures at depth are calculated by solving the time-dependent heat equation (5) using the finite element method.

$$\rho C_p \frac{\partial T}{\partial t} - \nabla \cdot (k \nabla T) = Q \quad (5)$$

where ρ is density, C_p is heat capacity and t is time. Thermal parameters are given in the caption to Figure 8.

Figure 8b shows the heat-flow anomalies (i.e., relative to steady-state conditions) at various depths at the end of the different palaeoclimatic histories (i.e., at present time). The anomaly imposed by the ‘cold’ model is as high as -50 mW m⁻² at 100 m depth, and decreases quite rapidly with increasing

Figure 6. Influence of topography on temperatures at 100, 200 and 1000 m depth beneath a peak (a–c) and a valley (d–f). The temperature anomaly is calculated by subtracting the temperature at a particular depth given a horizontal surface from the modelled temperature at the same depth given a sinusoidal topography with a certain wavelength and amplitude. The amplitude varies between 0 and 1500 m, and the wavelength between 3 and 15 km. Thermal parameters as in Figure 4.

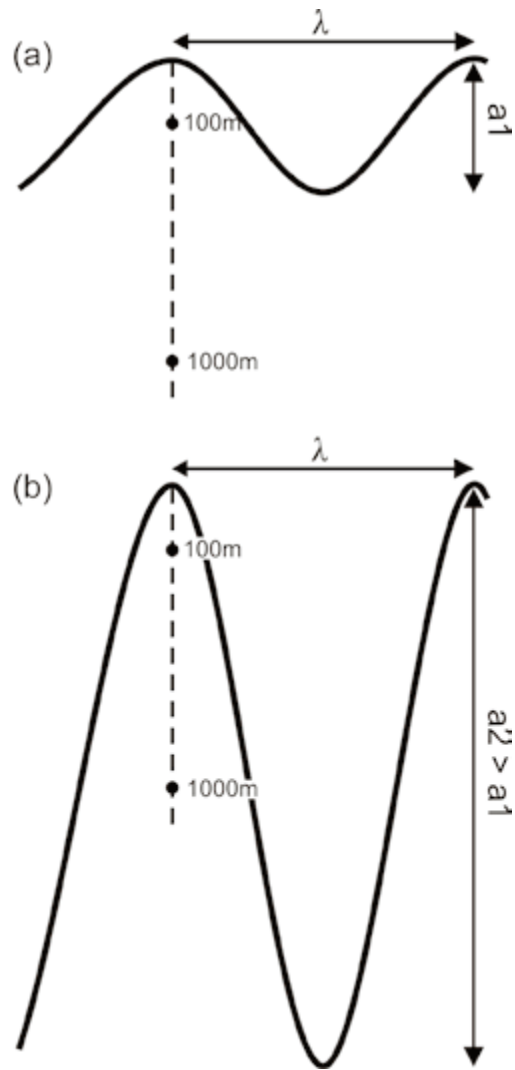


Figure 7. Illustration showing the relative topographic effect at 100 and 1000 m depth of varying amplitude (a_1 to a_2) for a constant wavelength (λ). (a) Topography with comparatively low amplitude (a_1), in which the topographic effect is relatively large at 100 m depth and significantly smaller at 1000 m depth. In (b) the wavelength is the same as in (a) but the amplitude is increased to ($a_2 > a_1$). In this case, topographic effects are significant at both depths, however, the relative increase in the topographic effect from (a) to (b) will be greater at 1000 m depth than at 100 m depth.

depth. The ‘warm’ model produces heat-flow anomalies up to -20 mW m⁻², whereas the ‘tepid’ model is intermediate between the two. Temperatures (Figure 8c) are similarly affected; the ‘cold’ model produces temperature anomalies of -2 and -3.5°C at 100 and 200 m depth, respectively, and as much as -7°C at 1000 m depth, whereas the ‘warm’ model yields temperature anomalies of -0.5, -1 and -2°C at 100, 200 and 1000 m depth, respectively. The ‘tepid’ model again yields intermediate results, with temperature anomalies of -1, -1.5 and -5°C at 100, 200 and 1000 m depth, respectively. These results show that the temperature effect of various palaeoclimatic histories can linger for a long time, particularly at depths greater than several

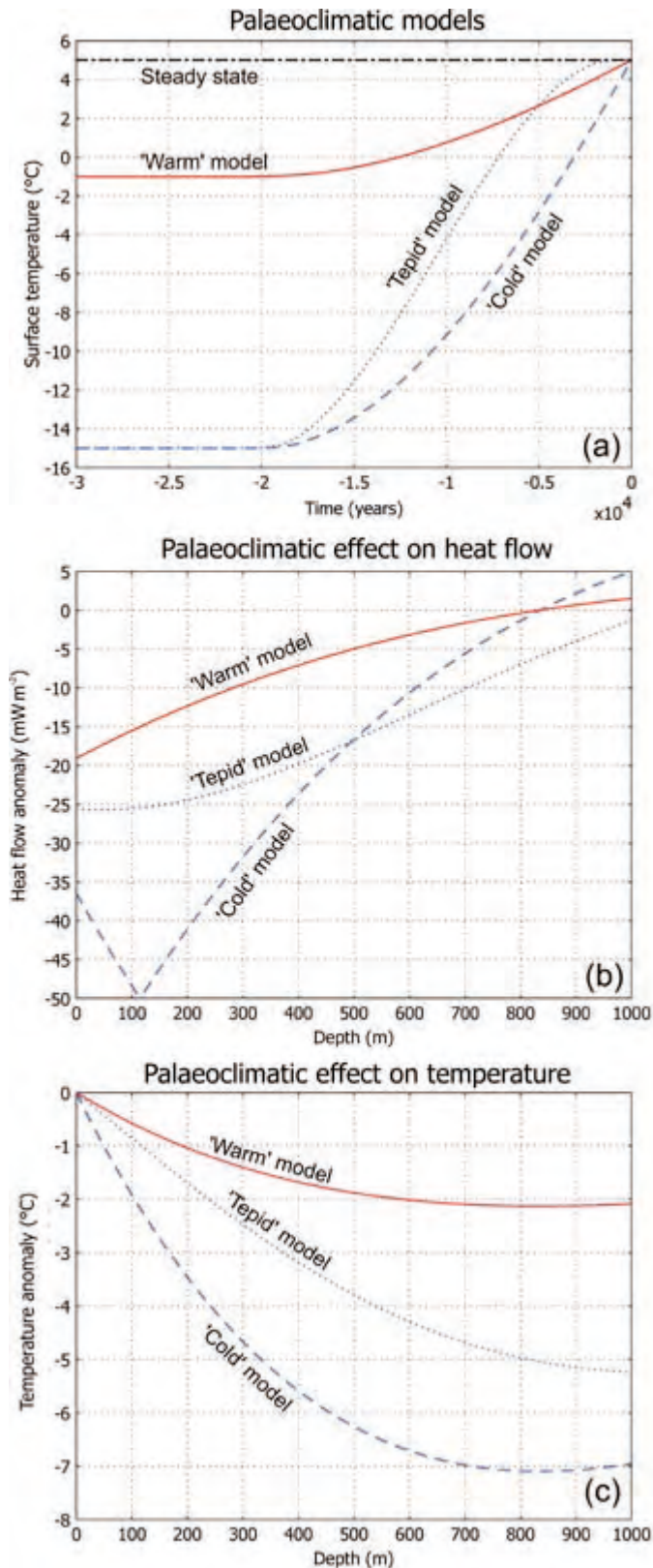


Figure 8. (a) Modelled 'warm', 'tepid' and 'cold' palaeoclimatic histories. The modelling assumes a constant heat flow of 50 mW m^{-2} , thermal conductivity of $3 \text{ W m}^{-1} \text{ K}^{-1}$, heat capacity of $850 \text{ J kg}^{-1} \text{ K}^{-1}$ and density of 2800 kg m^{-3} . The initial (i.e., prior to 30 ka) steady-state thermal conditions of the model are calculated for a surface temperature of 5°C . (b) Heat-flow anomalies in the uppermost 1000 m in response to the imposed palaeoclimatic histories. (c) Temperature anomalies in the uppermost 1000 m in response to the imposed palaeoclimatic histories. In both (a) and (b), the anomalies are calculated relative to the steady-state conditions.

hundred metres, but that in the uppermost few hundred metres temperatures will recover within a few thousand years

Mean annual surface temperature

When extraction of ground-source heat is considered, mean annual surface temperature is generally defined as the temperature in the ground, just below the surface, as opposed to the mean annual air temperature as defined by meteorological data. Although local effects such as type of vegetation cover, seasonal snow cover, slope angle and slope orientation may lead to deviations of up to several degrees (Blackwell et al. 1980, Lewis and Wang 1998), for the purpose of this paper they are considered equal. Figure 9a shows that mean annual surface temperatures in Scandinavia vary by ca. 10°C , from just below 0°C (Tveito et al. 2000).

From Equation (4) we see that in an area without topography, internal heat production and lateral variation in thermal conductivity (i.e., 1D conditions apply) there is a one-to-one correlation between surface temperature and the temperature at a certain depth. Although, clearly oversimplified, this relationship is, nevertheless, useful for considering the effects of varying surface temperatures at various depths. For example, given a heat flow of 60 mW m^{-2} and a thermal conductivity

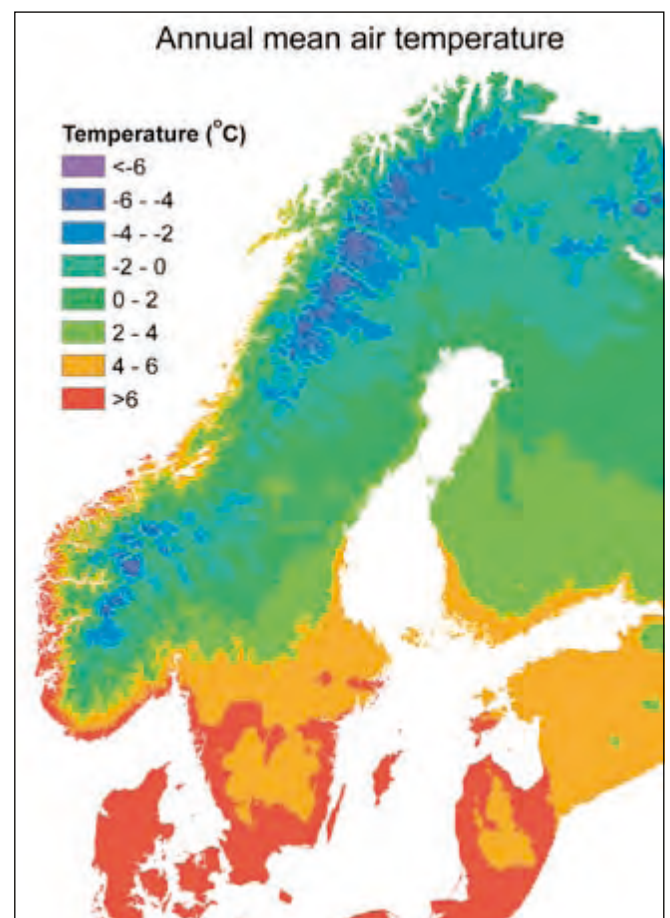


Figure 9. Mean annual air temperatures in Scandinavia. Data from the Norwegian Meteorological Institute (Tveito et al. 2000).

of $3 \text{ W m}^{-1} \text{ K}^{-1}$, surface temperatures of 0 and 10°C result in $2/12^\circ\text{C}$ at 100 m depth, $4/14^\circ\text{C}$ at 200 m depth and $20/30^\circ\text{C}$ at 1000 m depth. The relative temperature change at each depth resulting from this variation in surface temperature is 6-fold at 100 m depth, 3.5-fold at 200 m depth, and only 1.5-fold at 1000 m depth. Thus, as we intuitively expect, variations in surface temperature exert a major control on temperatures at 100 and 200 m, but relatively little at 1000 m depth. The effect of varying surface temperature (and other factors) on extraction of ground-source heat is discussed below.

Shallow thermal structure and significance for utilisation of ground-source heat

The results from the above modelling show that mean annual surface temperature is the main factor controlling the temperature at shallow depths down to a few hundred metres. In contrast, relatively large variation in factors such as heat production, thermal conductivity, low-conductivity overburden, topography and palaeoclimatic history cause variation in subsurface temperatures of at most a few degrees at these depths.

A misconception that is sometimes encountered is that high heat flow or radiogenic heat production are favourable because they help replenish heat extracted from the borehole. A simple exercise shows that this notion is unreasonable. If the temperature of the rocks in immediate vicinity of the borehole is reduced by 5°C as a result of heat extraction, whereas rocks 5 m away from the borehole remain unaffected, the lateral thermal gradient towards the borehole will be $1000^\circ\text{C km}^{-1}$. Given a thermal conductivity of $3 \text{ W m}^{-1} \text{ K}^{-1}$ this equates to a heat flow of 3000 mW m^{-2} , i.e., two orders of magnitude greater than the heat flow from the Earth's interior. Figure 10 shows the increase in temperature as a function of time at the basal surface as well as 50 and 100 m above the basal surface in a cubic thermal model with sides of 200 m. The heat flow is 50 mW m^{-2} across the basal surface and all other surfaces are thermally insulating. Even after 50 years, the temperature increases are $< 1^\circ\text{C}$; thus, over the life span of a ground-source heat facility or plant, terrestrial heat flow has a negligible effect. In practice, replenishment of heat takes place solely by lateral heat flow from the surrounding rock volume, whereas elevated, but nevertheless relatively miniscule, heat flow from the Earth's interior only serves to increase the ambient temperature.

Figure 11 shows the results of three models that calculate the energy output from boreholes of 100, 200 and 1000 m depth for different thermal conductivities, surface temperatures and heat flows. The model setup is shown in Figure 11a and consists of a 14 cm-diameter, water-filled borehole with a 5 cm-diameter, U-shaped collector pipe through which water, with an initial temperature of 0°C , is circulated at a rate of 0.8 l s^{-1} . Five cycles, each consisting of a 150-day circulation period followed by a 200-day recovery period with no circulation, are modelled. For each model, the net energy output is calculated at the outlet.

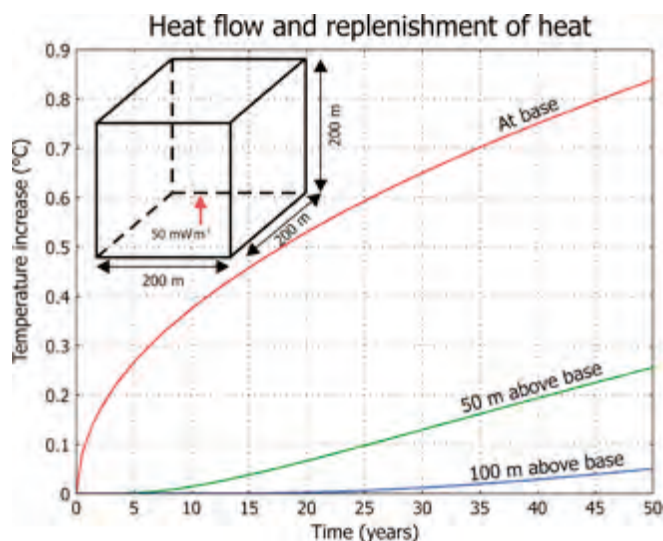


Figure 10. Cubic thermal model with sides of 200 m, thermal conductivity $3 \text{ W m}^{-1} \text{ K}^{-1}$, heat capacity of $850 \text{ J kg}^{-1} \text{ K}^{-1}$ and density of 2800 kg m^{-3} . The heat flux is 50 mW m^{-2} across the basal surface; all other surfaces are thermally insulating. The model is shown schematically in the inset figure. The plot shows temperature increase vs. time at 0, 50 and 100 m above the basal surface.

The main point of the modelling is to determine the effect of the factors discussed above on the amount of ground-source heat extractable from boreholes of a certain depth. The results are therefore plotted in lognormal time vs. effect diagrams, and only the magnitude variation is discussed rather than the absolute energy output.

Figures 11b, c show the results of varying thermal conductivity and heat flow, respectively. The heat-flow variation, in addition to heat flow from the Earth's interior, may also be taken to represent variation in heat production, topography and climatic variation. The figures show that the amount of heat extractable from shallow to deep boreholes depends mainly on depth and relatively little on thermal conductivity and heat flow. The effects of these parameters increase with increasing depth; e.g., varying the heat flow by a factor of 2, from 40 to 80 mW m^{-2} , has a negligible effect at 100 m depth, but increases the amount of extracted heat by a factor of ca. 1.5 at 1000 m depth. Figure 11d shows the results of varying the mean annual surface temperature from 0 to 10°C . It is immediately clear from the figure that varying the surface temperature has a profound effect on the amount of heat extractable at shallow depths (100 and 200 m), whereas the effect at 1000 m is significantly smaller and comparable to varying the thermal conductivity and heat flow.

This result shows that the heat extracted from boreholes only a few hundred metres deep is mainly derived from the surface, and that geological variation is relatively insignificant. It should be noted, however, that this conclusion is valid for long-term, low-load extraction of heat. If one were to extract heat at a significantly higher rate, thus lowering the temperature around the borehole to close to the temperature of the circulating fluid, the initial temperature would be relatively insignificant and thermal conductivity would be the limiting factor. The significance of various parameters is, therefore, highly model

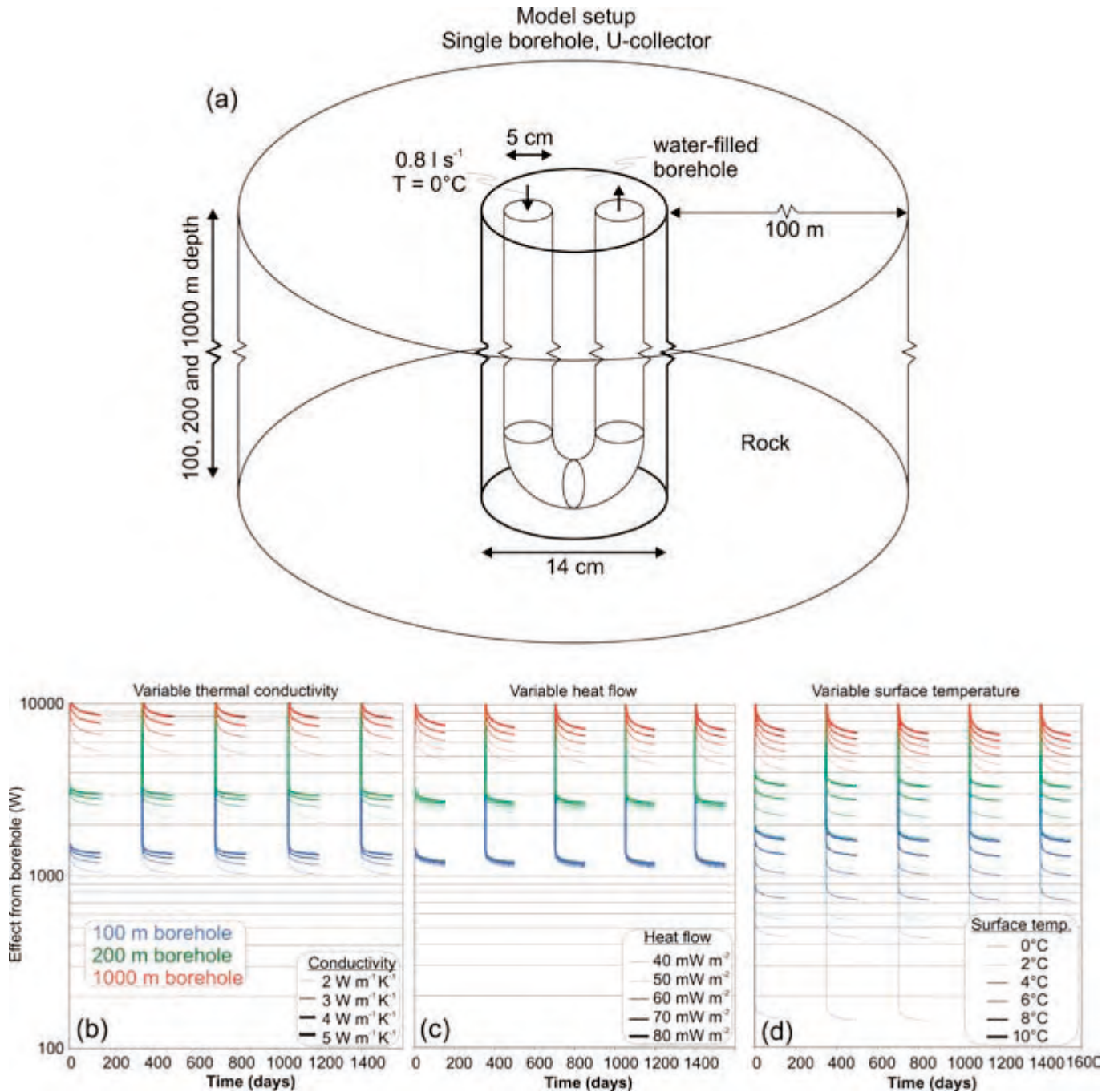


Figure 11. (a) Model setup used to determine the influence of thermal conductivity, heat flow and mean annual surface temperature on the amount of heat extractable from a borehole. The diagrams show the effects of varying (b) thermal conductivity, (c) heat flow and (d) surface temperature on the amount of heat extractable from boreholes of 100, 200 and 1000 m depth.

dependent. Other geological factors not considered here, in particular groundwater flow, may also be a significant factor locally.

Conclusions

At shallow crustal levels, i.e., down to a few hundred metres, mean annual surface temperature is the main controlling

factor on temperature. Other factors, including heat flow, heat production, thermal conductivity, low-conductivity overburden, topography and palaeoclimatic history play relatively minor roles. At greater depths, these factors progressively come into play and ultimately dominate.

Efficient use of ground-source heat is first and foremost a question of developing cheaper drilling techniques and more efficient heat pumps and heat exchangers. Other factors,

including geological information, play rather secondary roles. However, with the advent of cheaper, more efficient drilling techniques allowing deeper boreholes at an affordable price, geological knowledge will be highly valuable.

Acknowledgements

Christophe Pascal and Jan Steinar Rønning are thanked for critical comments that improved the paper. The work was supported by NGU project 277100, 'Efficient use of ground-source heat'.

References

- Anderson, E.M. (1934) Earth contraction and mountain building. *Beitrage zur Geophysik*, **42**, 133–159.
- Benfield, A.E. (1939) Terrestrial heat flow in Great Britain. *Proceedings of the Royal Society of London, Series A*, **173**, 474–502.
- Blackwell, D.D., Steele, J.L. and Brott, C.A. (1980) The terrain effect on terrestrial heat flow. *Journal of Geophysical Research*, **85**, 4757–4772.
- Clauser, C. and Huenges, E. (1995) Thermal conductivity of rocks and minerals. *Rock Physics and Phase Relations. A Handbook of Physical Constants. AGU Reference Shelf 3*, pp. 105–126.
- Clauser, C., Giese, P., Huenges, E., Kohl, T., Lehmann, H., Rybach, L., Šfanda, J., Wilhelm, H., Windloff, K. and Zoth, G. (1997) The thermal regime of the crystalline continental crust: Implications from the KTB. *Journal of Geophysical Research*, **102**, 18417–18441.
- Grønlie, G., Heier, K.S. and Swanberg, C.A. (1977) Terrestrial heat-flow determinations from Norway. *Norsk Geologisk Tidsskrift*, **57**, 153–162.
- Heier, K.S. and Grønlie, G. (1977) Heat flow–heat generation studies in Norway. In Saxena, S.K. and Bhattacharji, S. (eds.) *Energetics of Geological Processes*, Springer Verlag, New York, pp. 217–235.
- Hofmeister, A.M. and Criss, R.E. (2005) Earth's heat flux revised and linked to chemistry. *Tectonophysics*, **395**, 159–177.
- Landström, O., Larson, S.Å., Lind, G. and Malmqvist, D. (1980) Geothermal investigations in the Bohus granite area in southwestern Sweden. *Tectonophysics*, **64**, 131–162.
- Lewis, T.J. and Wang, K. (1998) Geothermal evidence for deforestation induced warming: Implications for the climatic impact of land development. *Geophysical Research Letters*, **25**, 535–538.
- Lind, G. (1982) *Gravity interpretation of the crust in south-western Sweden*. Ph.D. thesis, University of Göteborg/Chalmers University of Technology, Göteborg, 93 pp.
- Midttømme, K. (1997) *Thermal conductivity of sedimentary rocks—selected methodological, mineralogical and textural studies*. Ph.D. thesis, Norwegian University of Science and Technology, Trondheim, 146 pp.
- Ramberg, I. and Smithson, S. (1973) Geophysical interpretation of crustal structure along the southeastern coast of Norway and Skagerrak. *Geological Society of America Bulletin*, **86**, 769–774.
- Slagstad, T. (2006) Did hot, high heat-producing granites determine the location of the Oslo Rift? *Tectonophysics*, **412**, 105–119.
- Slagstad, T. (in press) Radiogenic heat production of Archaean to Permian geological provinces in Norway. *Norwegian Journal of Geology*.
- Taniguchi, M. and Uemura, T. (2005) Effects of urbanization and groundwater flow on the subsurface temperature in Osaka, Japan. *Physics of the Earth and Planetary Interiors*, **152**, 305–313.
- Tveito, O.E., Førland, E., Heino, R., Hanssen-Bauer, I., Alexandersson, H., Dahlström, B., Drebs, A., Kern-Hansen, C., Jónsson, T., Vaarby Laursen, E. and Westman, Y. (2000) Nordic temperature maps. *DNMI-Report 09/00 KLIMA*, 54 pp.

Sediment fluxes and sediment budget in Latnjavagge and the potential of applying unified methods for integrating investigations on sediment fluxes and budgets in cold-environment catchments

Achim A. Beylich^{1,2}

¹Geological Survey of Norway (NGU), Landscape and Climate group, 7491 Trondheim, Norway.

²Department of Geography, Norwegian University of Science and Technology (NTNU), Dragvoll, 7491 Trondheim, Norway.

E-mail: achim.beylich@ngu.no

This quantitative study on the Latnjavagge catchment (9 km²), located in the Abisko mountain area in northernmost Swedish Lapland, analyses recent gravitational and fluvial mass transfers in an Arctic-oceanic cold environment. By a combined recording of slope denudation and streamwork, information on (i) the absolute and relative importance of the different denudative processes for slope and valley formation, (ii) the temporal and spatial variability of the geomorphic processes, (iii) process intensities and frequencies, (iv) the geomorphic roles of an extreme rainfall event and a mega slush-flow event, (v) the sediment budget and (vi) recent trends of relief development is collected. Regarding annual mass transfers, fluvial transport in main channels dominates over slope processes. Fluvial solute transport is more important than fluvial sediment transport. Rock falls and boulder falls are most important at the slope systems, followed by chemical denudation, mechanical fluvial denudation, ground avalanches, creep and solifluction, slush flows, debris flows, translation slides and deflation. The intensity of the present-day processes is altogether low. Postglacial modification of the glacial relief is small. Because of the short time since the deglaciation (8000–10,000 yr) and the low intensity of the active geomorphic processes, there has been no adjustment of the Pleistocene glacial landforms to the surface processes, which have been operating until today under Holocene morphoclimates. The potential and expected benefit generated by coordinated data exchange and the unification of methods and techniques applied for long-term geomorphic-process monitoring/analysis, the quantitative investigation of storage elements and for quantitative sediment-budget studies in changing cold environments is discussed. Improved knowledge on mechanisms and controls of sedimentary transfer processes is of high significance to society, especially with respect to possible effects of land use, higher frequencies of floods and increased frequencies of hazards as caused by permafrost degradation and a higher frequency of extreme meteorological events.

Beylich, A.A. (2008) Sediment fluxes and sediment budget in Latnjavagge and the potential of applying unified methods for integrating investigations on sediment fluxes and budgets in cold-environment catchments. In Slagstad, T. (ed.) *Geology for Society*, Geological Survey of Norway Special Publication, **11**, pp. 111–130.

Introduction

There have been only a few truly quantitative–integrative investigations of sediment budgets and relief development in cold environments (e.g., Jäckli 1957, Rapp 1960, Barsch 1981, Beylich 1999, 2000a, 2008, Beylich et al. 2006a, b). Projected climate change will cause major changes in Earth-surface systems, with the most dramatic changes expected to occur in the high-latitude and high-altitude cold environments of the Earth. Geomorphic processes operating at the Earth's surface, transferring sediments and changing landforms, are highly dependent on climate, vegetation cover and human impact and will be significantly affected by climate change (e.g., Haeblerli and Beniston 1998, Lamoureux 1999, Slaymaker et al. 2003, Beylich et al. 2005a, b, 2006a).

Improved knowledge of mechanisms and controlling factors of sedimentary transfer processes is of high significance to society, particularly with respect to effects of land use, increased frequencies of floods and higher frequencies of hazards caused by possible permafrost degradation and a higher frequency of extreme meteorological events. In this context, it is a major challenge to develop a better understanding of the complex geoecosystems and the mechanisms and climatic controls of sedimentary transfer processes and sediment budgets in cold environments. A better knowledge of rates of sedimentary-transfer processes operating in present climates at the Earth's surface is needed to determine the consequences of predicted climate change and direct human impact. It is necessary to collect data from a wide range of different cold environments and to apply more standardised methods and approaches for future research on sediment fluxes and relationships between climate and sedimentary transfer processes (Beylich et al. 2006a, Beylich and Warburton 2007).

The investigation presented here is focused on quantifying rates of denudative processes, mass transfers and the sediment budget of a 9 km² catchment in an Arctic-oceanic cold environment with little human impact (Beylich 2002, Beylich et al. 2005a, 2006b). The presented process rates and mass transfers have been calculated after a seven-year investigation (1999–2006) carried out in the Latnjavagge catchment in northernmost Swedish Lapland. The collected data can be used for direct quantitative comparisons with other cold-environment catchments (Beylich 1999, 2000a, 2002, Beylich et al. 2006a). By a combined, quantitative recording of the relevant denudative slope processes and the stream-work information on the absolute and relative importance of the different denudative processes in Latnjavagge has been collected.

This kind of catchment-based quantitative study, using unified and simple (i.e., reliable and low-cost) geomorphic field methods and techniques, carried out in different cold environments, will help gain a better understanding of the internal differentiation of cold environments (Barsch 1984, 1986, Beylich 1999, 2000a, 2002, Beylich et al. 2006a, b, Beylich and Warburton 2007). Furthermore, information on

the controls of geomorphic processes, the quantitative role of extreme events for longer-term mass transfers and sediment budgets, the intensity of geomorphic processes, and the relative importance of different geomorphic processes for slope and valley formation and recent relief and landform development in cold environments will be improved. By coordinated comparisons of data sets collected in different cold-environment catchments, integrating investigations on effects of projected climate change and on relief and landform development in cold environments can be realised (Beylich 2000a, 2007, Beylich et al. 2006a, 2007, Beylich and Warburton 2007).

Study area

The Latnjavagge catchment (68°20'N, 18°30'E; 9 km²; 950–1440 m above sea level (asl)) is situated 15 km west of Abisko in the Abisko mountain area in northernmost Swedish Lapland (Figures 1 and 2). The Arctic-oceanic morphoclimate of Latnjavagge (Beylich 2003) is characterised by a mean annual temperature of -2.0°C (1993–2005) and a mean annual precipitation of 852 mm yr⁻¹ (1990–2005). July is the warmest month (mean 8.6°C). The coldest month is February (mean -9.4°C). About 2/3 of the annual precipitation is temporarily stored as snow during the winter. Snowmelt normally starts at the end of May/beginning of June. Stable freezing temperatures with little daily fluctuation at 10 cm above ground and autumn snow accumulation usually occur from September/October onwards. Regarding the summer months June–August, August



Figure 1. Location of the Latnjavagge catchment in northern Swedish Lapland.

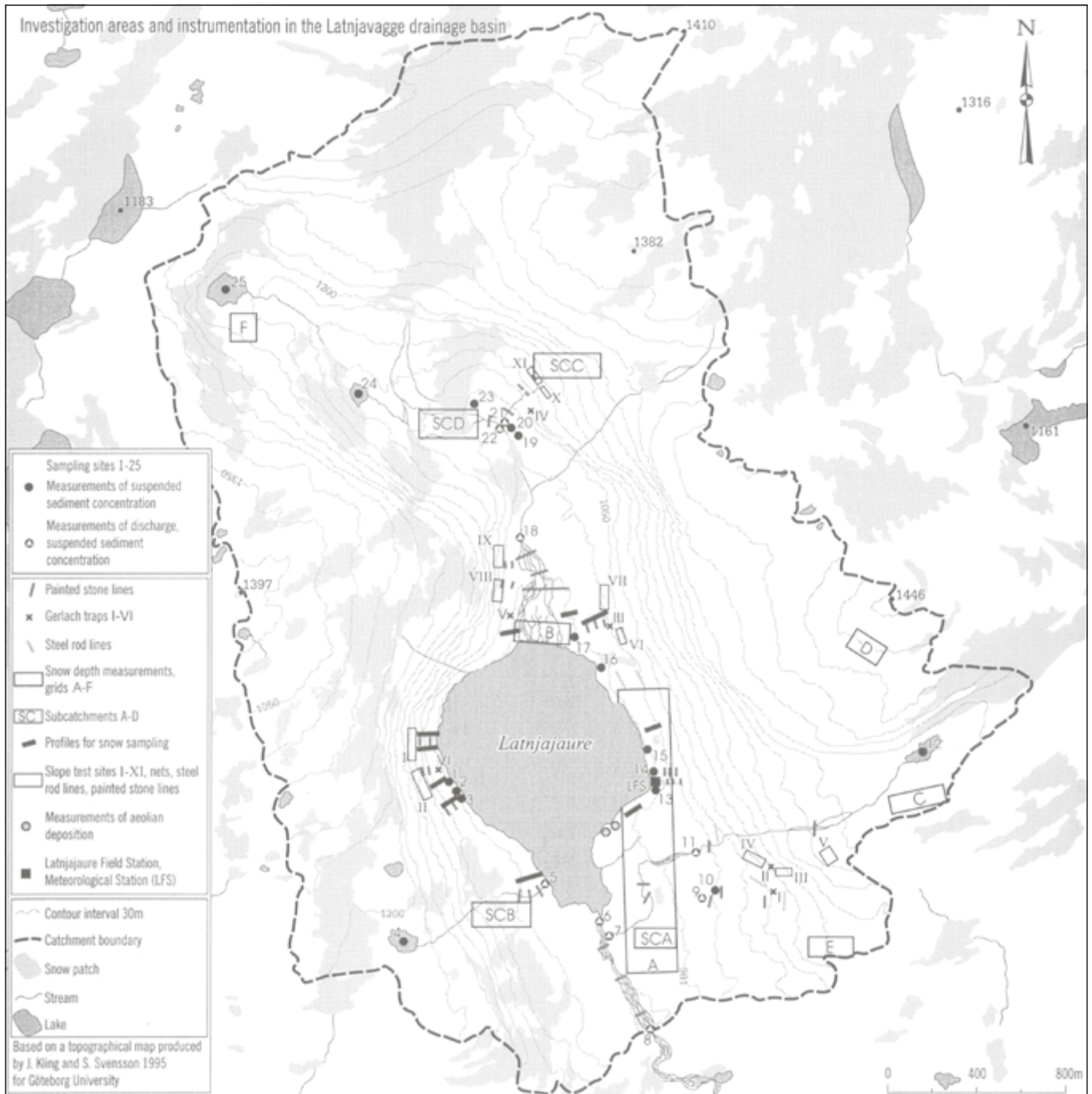


Figure 2. Investigation areas, test sites and instrumentation in Latnjavagge.

shows the highest mean precipitation (82 mm) and also the highest frequency of extreme rainfall events (Beylich 2003, Beylich and Gintz 2004). Precipitation from June to August accounts for about one quarter of the mean annual precipitation. The Latnjavagge catchment has an area of approximately 9 km², a length of 4.6 km, and elevation ranging from 950 to 1440 m asl. The bedrock is mainly composed of Cambro–Silurian mica-garnet schists and inclusions of marble (Kulling 1964, Beylich et al. 2004a). Intrusions of acidic granites can be found in the northern part of the valley. Regional deglaciation occurred about 8000–10,000 yr ago (André 1995). The catchment is

dominated by large and flat plateau areas at 1300 m asl, steep slopes that bound the glacially sculptured valley, and a flat valley floor situated between 950 and 1200 m asl (see Figure 2). The plateaux are best described as bare bedrock and boulder fields. The transition between slopes and plateaux is generally sharp, and the very steep, east-facing slope is covered by perennial snow and ice patches. The lower part of the valley floor is dominated by a lake, Latnjajure (0.73 km²), and a series of moraine ridges. Regolith thicknesses are shallow and reach locally only a few meters (Beylich et al. 2004b). The main present soils are regosols and lithosols. The catchment area belongs to the mid-

Alpine zone, with a continuous and closed vegetation cover up to 1300 m asl comprising dwarf shrub heaths and Alpine meadows and bogs. The exact distribution of permafrost is not directly known, but drilling outside the catchment at 1200 m asl suggests at least sporadic permafrost down to 80 m below the surface (see Kling 1996, Beylich et al. 2004b). There seems to be no ice-rich permafrost on the valley floor around 1000 m asl, nor on the lower parts of the gently-sloping, west-facing valley slope (Beylich et al. 2004b). Denudative slope processes include chemical weathering and denudation, mechanical weathering, rock falls, boulder falls, ground avalanches, debris flows, translation slides, creep processes, solifluction, ploughing boulders, and slope wash. Slush flows occur in certain areas of the valley and deflation is active where the vegetation cover is disturbed or lacking. In the channels, dissolved, suspended and bed load is transported. The hydrological regime is nival, with runoff limited to the period from the end of May until October/November (Beylich 2003). Direct human impact on the natural system is presently small and is limited to reindeer husbandry (extensive grazing), some hiking tourism and field research at the Latnjajaure Field Station (Beylich et al. 2005a).

Aims of this study

The aims of this study are to (i) analyse the rates and the spatio-temporal variability of denudative processes and sediment transfers within the Latnjavagge catchment; (ii) analyse the absolute and relative importance of the different denudative processes; (iii) quantify the current sediment budget for this catchment; (iv) analyse current trends of relief development in this Arctic-oceanic environment; (v) discuss the potential of coordinated data exchange and the unification of methods and techniques applied to long-term and quantitative sediment-budget studies in changing cold environments.

Approach and methods

Mapping

The geomorphological mapping (Figure 3) has been carried out by (i) studying stereo aerial photographs and (ii) mapping in field with a GPS, complemented by photo documentation. The mapped features were then transferred into a GIS (ArcView) where the rectified colour infrared (CIR) aerial photograph was available (Sandberg 2004, Beylich et al. 2006b).

Meteorological measurements and snow sampling

The Latnjajaure Field Station (68°20'N, 18°30'E; 981 m asl) is equipped with an automatic weather station, which has been in continuous operation since April 1992. The temperature sensors are installed in a standard Stevenson Screen at 2 m above ground. Ground temperature is monitored at different

depths. Daily precipitation has been measured since 1990 with a Hellmann-Totalisator (surface area 200 cm²) with wind shelter according to the SMHI (Swedish Meteorological and Hydrological Institute) standards with daily readings at 07.00 h Normal Time (see Molau 2001). Snow depth is monitored at different grids within the catchment (Figure 2). Snow cores of the complete vertical snow pack from the previous winter were taken in the beginning of the field seasons (May/June) along selected profiles (Figure 2) with a designed plastic tube (10 cm diameter). The snow cores were melted in buckets in the laboratory at the Latnjajaure Field Station. The water was then filtered with a pressure filter and ash-free filter papers (Munktells quantitative filter papers, OOH) to quantify total dissolved solids and the concentration of mineralogenic particles in the snow cores (Beylich et al. 2004a, 2006b).

Measurement of relevant denudative slope processes

A combination of monitoring, dating and mapping techniques, as well as further field observations and detailed photo documentation, were used to analyse relevant denudative slope processes in Latnjavagge. Eleven slope test sites (Slope Test Sites I–XI) within the 9 km² Latnjavagge catchment were selected after studying aerial photographs and after field work (Figure 2). The slope test sites differ with respect to exposition, elevation and local geographical setting and were selected to cover the different settings that can be found within the Latnjavagge catchment area. All slope test sites include a rock face, a talus cone and areas with slow mass movements (Figures 4a, b). The slope test sites were instrumented in September 1999 to monitor rock and boulder falls as well as creep processes. Additionally, ground avalanches, debris flows and slides, solifluction, ploughing boulders and slope wash were studied at other selected and adequate sites within the catchment (Figures 2 and 3). This paper presents data from seven years of process monitoring/investigations (1999–2006).

Rock falls and boulder falls at slope test sites

Rock and boulder falls were investigated at the eleven slope test sites by applying a combination of monitoring, dating and mapping techniques as well as a detailed photo documentation. The rock fall and boulder fall activity was not influenced by avalanche activity at the test sites. The denudative role of avalanches, with rock and boulder falls triggered by these avalanches, were studied separately at the steep east-facing valley slope (see below).

At each slope test site a 40 m² net (4 x 10 m, 1.5 cm mesh size) was installed with its longer side placed along the rock wall/face foot on the talus cone developed below clearly defined vertical or slightly overhanging rock walls/rock faces (Figure 5). The nets were efficient in collecting debris produced by mechanical weathering at the rock walls and transferred to the net by primary and secondary rock falls (Beylich 1999, 2000b). The collected debris was repeatedly quantified by weighing it with a portable field balance ((kg m⁻²), (kg m⁻² yr⁻¹)). Rock-wall

Figure 3. Geomorphological map of the Latnjavagge catchment.

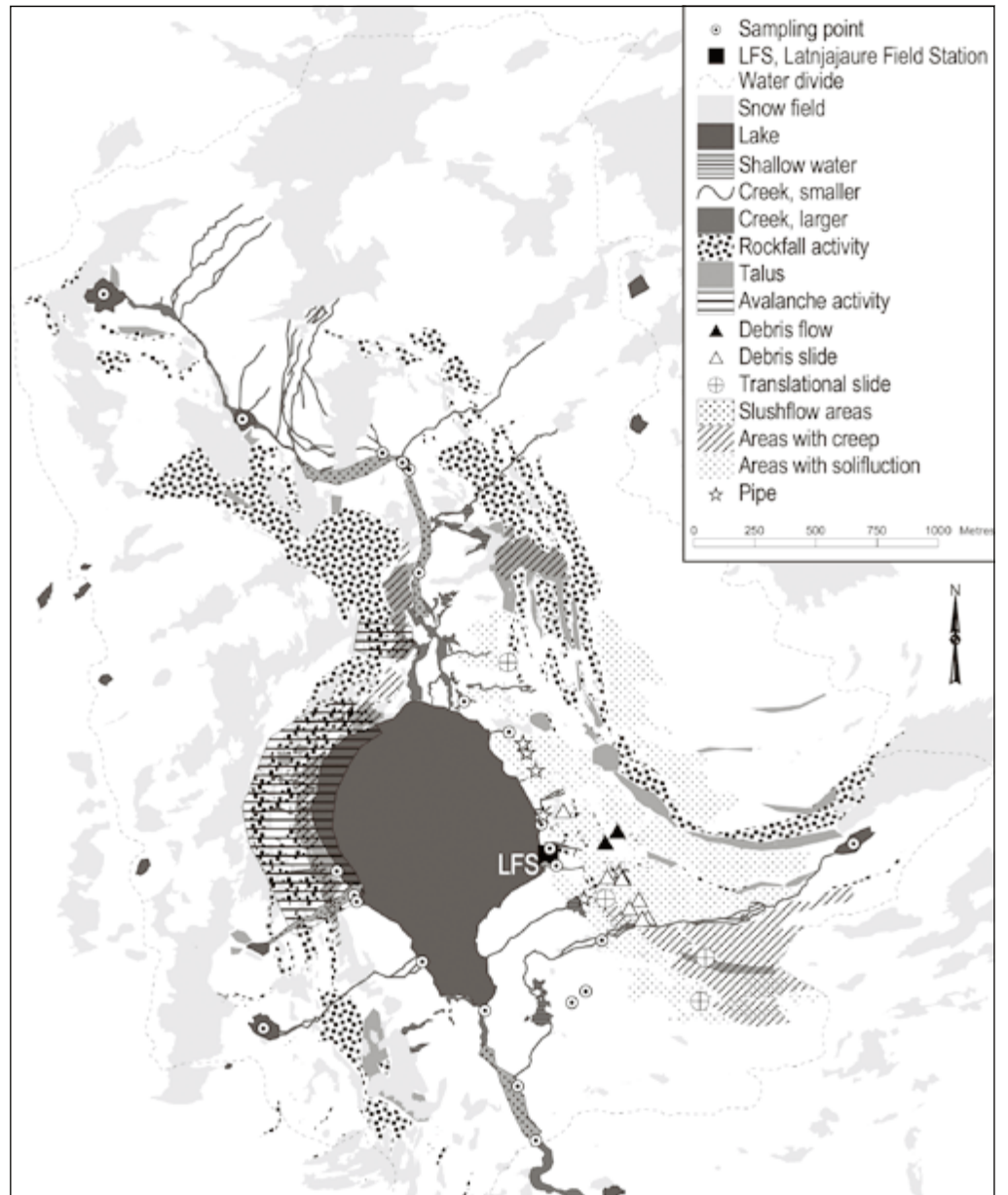


Figure 4. (a and b) Slope test site in Latnjavagge.



Figure 5. Net, which is collecting rock fall debris at a slope test site in Latnjavagge.

retreat (mm yr^{-1}) was calculated by measuring the surface area of the clearly defined and debris-supplying rock face and relating it to the mass of debris accumulated below the rock face, using an estimated mean rock density (based on field measurements) of 2.5 g cm^{-3} .



Figure 6. Painted rock face at a slope test site in Latnjavagge

The mass of accumulated debris smaller than ca. 1.0 cm in diameter was quantified with the help of painted rock faces (Figure 6). At each slope test site, two representative squares of 1 m^2 were painted in 1999 and repainted annually. Fine debris accumulated below the painted squares could be identified by the colour of the debris and the total mass of fine debris could be quantified by weighing the debris with a portable field balance. The total mass of fine debris could then be related to the defined source area of 1 m^2 rock surface.

Boulder falls were investigated at each slope test site by detecting, mapping, counting and measuring fresh boulders below the boulder-supplying rock walls. For detecting and mapping fresh boulder falls, a detailed photo documentation was carried out each field season taking photos from the ground as well as from boat (Latnajaure) and from helicopter. The boulder-size measurements (a-, b- and c-axis) were carried out in the field. In addition to the monitoring of boulder falls during the investigation period, older boulders located in the area of the slope test sites and at other selected sites within Latnjavagge could be dated using lichenometry (Sandberg 2004).

Avalanches

Avalanches occur in Latnjavagge during the early summer season, normally between the end of May and the middle of July, and are spatially restricted to the steep, east-facing valley slope in Latnjavagge (Beylich 2003) (Figure 7). Avalanches triggered at this valley slope cause rock and boulder falls at the extended rock faces of this slope and transfer newly triggered material as well as remobilised older material down slope. Total annual accumulations (t yr^{-1}) of inorganic material (including fine material, debris and boulders) by ground avalanches at the steep, east-facing slope were quantified during 2000–2006 by combining detailed sampling, measurement and weighing of newly deposited material at defined test fields with an estimate of the entire affected depositional area on the slope and a detailed photo documentation of the entire slope system. In total, forty test fields of 1 m^2 were installed and investigated

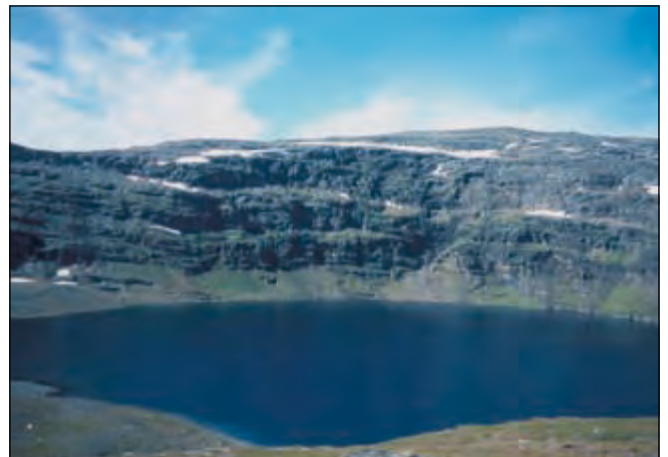


Figure 7. Steep, east-facing valley slope with ground-avalanche activity in early summer.

with ten test fields being oriented along each of four different longitudinal slope profiles (A–D). Newly accumulated and dried debris on the different test fields was weighted and fine material was sampled for the quantification of the inorganic mass (burning of the material for 12 h at 550°C). The mapping of the entire depositional area, as well as the detection and mapping of fresh boulder falls, were carried out each summer during the investigation period and were based on a detailed photo documentation with photos taken from the ground as well as from boat (Latnjajaure) and from helicopter. Fresh boulders were measured in the field (a-, b- and c-axis). By combining these different measurements, the total annual mass ($t\ yr^{-1}$) of deposited inorganic material was quantified. In addition, to this direct monitoring of mass transfers caused by ground avalanches, older boulders, which must have been deposited by earlier ground avalanches, were dated using lichenometry (Sandberg 2004).

Debris flows and slides

Debris flows and translation slides were investigated by annually repeated photo documentation of slope systems carried out from the ground, boat (Latnjajaure) and helicopter. Both new and older traces of debris flows and translation slides were mapped. Older debris flow traces were dated by estimating the age of pioneer vegetation newly growing on the debris flow traces (Sandberg and Molau, pers. comm.). Additionally, extended investigations and a detailed mapping of new debris flows and translation slides were carried out directly after the extreme rainfall event of July 20th–21st 2004 (Beylich and Sandberg 2005, Beylich et al. 2006b). The volumes of transferred material as well as the transfer distances were measured in the field.

Creep processes, solifluction and ploughing boulders

Creep processes and solifluction were analysed at all slope test sites by monitoring movements of painted stone-tracer lines and steel-rod lines (Figures 8 and 9). In addition, depth-integrating peg profiles were installed at each stone/rod line as well as at several other selected sites within the valley (Figure 10). Ploughing boulders were monitored by repeated annual measurements of boulder movements measuring the changing distances of the ploughing boulders from defined fixed points (rock outcrops).

At each slope test site, three stone lines with 30 painted stones at each line (A1–A30, B1–B30, C1–C30) were installed in late summer 1999. The stone lines were installed parallel and in different and clearly defined distances from the rock face of each slope test site. The horizontal distance between stones was 1 m. Downslope movements of all painted stones (90 stones per slope test site) were measured in each Arctic summer field season until 2006.

At each location where a painted stone was placed, a steel rod (1.0 cm diameter) was placed vertically 10 cm down into the ground. In total, 90 steel rods per slope test site were installed. Downslope movements of all steel rods were measured every



Figure 8. Monitoring of creep processes with painted stone-tracer lines and steel-rod lines at a talus cone/slope test site in Latnjavagge.



Figure 9. Monitoring of creep processes with painted stone lines and steel-rod lines at a slope test site in Latnjavagge.



Figure 10. Installation of depth-integrating peg profile at a solifluction lobe in Latnjavagge.

year, taking clearly defined and marked points at the stable rock faces as fixed points. Additional steel-rod lines were installed at three solifluction sheets as well as at four solifluction lobes within the valley. At each sheet/lobe, three lines with 15 steel-rods (A1–A15, B1–B15, C1–C15) were installed in the same way as at the eleven slope test sites.

At each of the in total 54 stone lines/steel-rod lines, one depth-integrating peg profile (composed of 17 pieces of 3 cm long plastic rods (1.5 cm diameter)) was installed vertically and 50 cm down into the ground (Figure 10). The downslope movements of the different plastic rod pieces were measured after the entire investigation period and after digging out holes next to the peg profiles.

Downslope movements of in total 45 ploughing boulders at the gently-sloping, west-facing valley slope were monitored by repeated measurements carried out at the end of each Arctic summer field season between 1999 and 2006. Measurements were conducted using a steel tape and two marked points at stable rock outcrops as fixed points for each boulder.

Chemical slope denudation

Chemical slope denudation was investigated by analysing water samples collected from small creeks and pipes on the slopes of Latnjavagge. Beylich et al. (2003, 2004a, b) published results from studies on water chemistry and its diversity in relation to local factors in the Latnjavagge catchment, including a detailed description of methods. Solute yields and chemical-denudation rates for the Latnjavagge catchment were calculated based on measurements of atmospheric solute inputs to the catchment, runoff and solute concentrations in main creeks (see below).

Slope wash

The importance of slope wash was estimated using six Gerlach traps, which were installed at different locations in Latnjavagge. A detailed study of suspended-sediment transport in small creeks draining slope systems, including a description of methods, is published in Beylich et al. (2006b).

Estimating the importance of deflation

The role of deflation was estimated by analysing sediment concentrations in snow cores collected along defined profiles within the valley (Beylich et al. 2006b) and by collecting aeolian deposits in two samplers installed close to the southern shoreline of Latnjajaure (Figure 2).

Quantifying mass transfers by slush flows

Mass transfers by slush flows were quantified by a mapping of slush-flow deposits and by estimating the transported volumes and masses as well as the transport distances (Beylich and Gintz 2004, Beylich et al. 2006b).

Monitoring runoff and fluvial transport

Discharge in channels was measured three times daily with an Ott-propeller C_2 (Ott GmbH & Co. KG, Kempten) immediately

prior to sampling of water (see Beylich 1999, Beylich et al. 2003). The installation of fixed gauge stations was not possible because of the characteristics of the channels (bedrock and/or blocks, shifting channels during snowmelt, high slush-flow frequency and destruction of installations).

Directly after each discharge measurement, vertically integrated water samples were taken with 1000 ml wide-necked polyethylene bottles. The samples were filtered in the laboratory of the Latnjajaure Field Station with a pressure filter and ash-free filter papers. After the field campaigns, the filter papers were burned (12 h, 550°C) to analyse the concentrations of mineralogenic suspended solids (mg l^{-1}). Daily discharge-weighted suspended-sediment concentrations were then calculated by interpolating the measurements (see Beylich 1999, Beylich et al. 2006b). The stability of creeks and channel stone pavements as well as the scale of bed-load transport was estimated using painted stone-tracer lines (Figure 11) at selected creeks and channel stretches (Figure 2). Fresh accumulations of debris/bed load were analysed by weighing of debris and by a detailed measurement of the volumes of fresh deposits (Beylich et al. 2006b). After each discharge measurement, surface-water electrical conductivity, corrected to 25°C, was measured using a portable conductivity meter (Cond 315i/SET, WTW Weilheim) and concentrations of total dissolved solids (mg l^{-1}) were calculated (Beylich et al. 2003).



Figure 11. Painted stone-tracer line in a creek in Latnjavagge.

Rates of denudative slope processes

Relevant denudative slope processes in Latnjavagge are rock falls and boulder falls, ground avalanches, debris flows, translation slides, creep processes and solifluction, ploughing boulders, chemical denudation, and slope wash.

Rock falls and boulder falls

Tables with masses of newly accumulated debris (kg m^{-2}) on nets installed below rock faces, corresponding annual rock wall-retreat

rates (mm) and mean annual rock wall-retreat rates (mm yr^{-1}) for the entire investigation period at the slope test sites I–XI are published in Beylich (2008). The mean annual rock wall-retreat rates vary between 0.096 mm yr^{-1} at the southwest-exposed slope test site IV and 0.363 mm yr^{-1} at the southwest-exposed slope test site V (Figure 2). The ratio of the largest recorded annual rate and the smallest annual rate is accordingly 3.8. The mean of all eleven recorded annual rock wall-retreat rates (1999–2006) is 0.216 mm yr^{-1} . Based on field observations, the main factors controlling the spatial variability of mechanical weathering at rock faces, rock falls and rock wall-retreat rates appear to be (i) the density of vertical and horizontal jointing of rock faces and (ii) the availability of moisture. Field observations also showed that daily freeze-thaw cycles, with minimum air temperatures around -10°C , trigger rock falls from snow-free but wet rock walls and rock ledges. Rock-fall activity is caused by both the annual freeze-thaw cycle and by daily freeze-thaw cycles and reaches its highest intensity in May and June. Strong wind gusts and heavy rainfall can trigger secondary rock falls also over the summer (Beylich 2003). On slopes without avalanche activity (see below) boulder falls were only observed in July and August, and were mainly caused by the delayed melting of ice developed in joints deeper within rock walls. These boulder falls were triggered by the annual freeze-thaw cycle (Beylich 2003) (Figure 12). The extreme rainfall event of July 2004 triggered secondary rock falls and some boulder falls (Beylich and Sandberg 2005). Single boulder falls can be triggered by direct human impact (Beylich et al. 2005a). The mean annual rock wall-retreat rate caused by boulder falls was calculated to be 0.197 mm yr^{-1} (Sandberg 2004).

Quantification of fine debris produced at painted rock walls at the eleven slope test sites showed little relevance, with a calculated mean annual rock wall-retreat rate (1999–2006) of 0.024 mm yr^{-1} .

With a given total surface area of 3.15 km^2 for rock walls and rock ledges in Latnjavagge (Molau pers. comm.) and a calculated mean annual rock wall-retreat rate of $(0.216 + 0.197 + 0.024)$



Figure 12. Fresh boulder fall in Latnjavagge.

0.437 mm yr^{-1} , the annual volume of material transferred by rock and boulder falls (excluding the rock falls and boulder falls which are triggered by avalanches at the steep and east-facing valley slope, see below) can be estimated to be on the scale of 1376.55 m^3 , or (given a mean density of 2.5 g cm^{-3}) 3441.38 t .

Avalanches

Detailed tables showing the total annual masses of inorganic material deposited by avalanches during the entire investigation period on talus cones of the steep and east-facing valley slope (Figure 7) are presented in Beylich (2008). The mean annual mass of deposited inorganic material is 69.3 t , which is composed of 57.3% boulders and 42.7% debris and finer material. The largest annual deposition occurred in 2000 (93.3 t) and the smallest in 2006 (43.3 t). Snow-rich winters lead to a higher frequency of avalanches in early summer (end of May until mid-July) and accordingly to larger amounts of deposited inorganic material than do snow-poor winters. The annual mass of accumulated boulders is higher than the annual mass of accumulated debris and finer material. Years with larger masses of accumulated boulders are also characterised by larger annual masses of accumulated debris and finer material.

Debris flows and slides

Debris flows and translation slides in Latnjavagge are triggered by heavy rainfall (Beylich 2003, Beylich and Gintz 2004, Beylich and Sandberg 2005). Annual mass transfers by debris flows and translation slides show a spatial variability within the Latnjavagge catchment. The mean annual mass transfers presented in Table 1 do not include the mass transfers, which were triggered by the extreme rainfall event of July 2004 (Beylich and Sandberg 2005). Comparison of the mean annual mass transfers published in Table 2 in Beylich and Sandberg (2005), with the mean annual mass transfers presented in Table 1 in this paper, reveals that the frequency and intensity of debris flows and translation slides have increased after the extreme rainfall event of July 2004. The increased frequency of debris flows is reflected in an increase in the mean annual mass transfer from 212 t m calculated for the period 2000–2004 to 279 t m quantified for the period 2000–2006. The increased frequency and intensity of translation slides is documented by an increase of the mean annual mass transfer from 2.5 t m calculated for 2000–2004 to 11 t m determined for 2000–2006. The higher frequency and intensity of debris flows and translation slides is a direct consequence of the destabilisation of slope systems and the disturbance of the vegetation cover in areas with debris flow and slide activity during the extreme event of July 2004 (Beylich and Sandberg 2005).

Creep processes, solifluction and ploughing boulders

Detailed tables with mean annual movement rates of stone-tracer lines as monitored at the eleven slope test sites over the investigation period within the Latnjavagge catchment are presented in Beylich (2008). Movements of painted stone

Table 1. Mean annual mass transfers by debris flows and translation slides (2000–2006) (excluding the extreme rainfall event of July 20th–21st, 2004).

Catchment area	Annual mass	Mean distance	Annual mass transfer	Annual mass	Mean distance	Annual mass transfer
	(t)	(m)	(t m)	(t)	(m)	(t m)
	Debris flows	Debris flows	Debris flows	Translational slides	Translational slides	Translational slides
SC D	0	-	0	0	-	0
SC C	0	-	0	0	-	0
Steep slope (between SC B & D)	1	14	14	1	5	5
Gentle slope (between SC A & C)	5	53	265	1	1	1
SC B	0	-	0	0	-	0
SC A	0	-	0	1	5	5
Entire catchment			279			11

tracers are mainly caused by ground avalanches, which are clearly reflected in significantly higher mean annual movement rates of entire stone-tracer lines at the slope test sites characterised by ground-avalanche activity in early summer (slope test sites I, II, VIII, IX) as compared to the slope test sites without avalanche activity (III–VII, X, XI) (Figures 2 and 3). This anticipates that ground avalanches cause, in addition to supplying and accumulating new material, a significant redistribution of older material on talus cones. The mean annual movement rates of entire stone-tracer lines at slope test sites with avalanche activity vary from 55.9 cm yr⁻¹ at slope test site VIII (stone-tracer line C) to 151.4 cm yr⁻¹ at slope test site II (stone-tracer line B). At the slope test sites without any avalanche activity, the mean annual movement rates of entire stone-tracer lines range from 0.7 cm yr⁻¹ at slope test site X (stone-tracer line C) to 3.7 cm yr⁻¹ at slope test site III (stone-tracer line C). Stone-tracer movements at slope test sites without avalanche activity are mainly triggered by rock falls.

Mean annual movement rates of entire steel-rod lines at the eleven slope test sites in Latnjavagge for the entire monitoring period are small and range from 1.7 mm yr⁻¹ at slope test site X (steel-rod lines B and C) to 5.1 mm yr⁻¹ at slope test site III (steel-rod lines A and C). The movement of the monitored 10 cm thick surface layer is mainly caused by the annual freeze-thaw cycle. Slope test site III shows clearly higher movement rates than the other slope test sites, which can be mainly explained by larger slope angle and lack of vegetation at slope test site III. The depth-integrating peg profiles document that the movements are shallow and reach only down to 25–30 cm depth at all slope test sites.

Measurements at solifluction lobes provided mean annual movement rates of entire steel-rod lines between 25 mm yr⁻¹ and 34 mm yr⁻¹, with a measured depth of movement of about 40–45 cm. The mean annual downslope movement rates of ploughing boulders for the investigation period range from 15 mm yr⁻¹ to 45 mm yr⁻¹, with a mean annual rate of 26 mm yr⁻¹ for all 45 monitored boulders (Beylich 2008).

Chemical slope denudation

Results from detailed investigations on atmospheric solute inputs, water chemistry, chemical slope denudation and its diversity in relation to local factors, ground frost, and regolith thickness are published in Beylich (2005) and Beylich et al. (2003, 2004a, b, 2005b). Rates of annual atmospheric solute inputs to the catchment, annual solute yields and chemical-denudation rates for the period 2000–2006, as well as mean annual values for the period 2000–2006, are presented in Tables 2 and 3. The mean annual atmospheric solute input in Latnjavagge is 4046.4 kg km⁻² yr⁻¹. The mean annual chemical-denudation rate is 1813 kg km⁻² yr⁻¹ at the inlet of Latnjajaure, 3951 kg km⁻² yr⁻¹ at the outlet of Latnjajaure and 4889 kg km⁻² yr⁻¹ at the outlet of the entire Latnjavagge catchment (see Figure 2). The investigation stresses the importance of spatial variability within even small catchments of homogeneous lithology as it demonstrates that solute concentrations from different sub-areas can differ significantly depending on exposure to radiation, duration of snow cover, frozen-ground conditions, regolith thickness, slope angle and vegetation cover (Beylich et al. 2003, 2004a, b).

Slope wash

Results from investigations on the spatio-temporal variability of fluvial sediment transfers based on analysis of suspended-sediment concentrations in small creeks draining the slope systems are published in Beylich et al. (2006b). The pattern of ice patches and larger snow fields within the valley, the steepness of creeks and the location of areas showing slush-flow activity are the major factors controlling spatial variability of mechanical fluvial denudation in the catchment. Slope wash occurring outside defined small creeks and from disturbed areas is minimal, which is due to the closed and stable vegetation cover and rhizosphere developed below 1300 m asl across the entire catchment (Molau et al. 2003). The material collected within the six Gerlach traps was minor and too little to quantify a reliable rate of slope wash.

Table 2. Annual atmospheric solute inputs in Latnjavagge (1999–2006).

Total period	Sub-period	Sampling	Number of samples	Concentration of diss. solids (mg l ⁻¹)	Total precipitation (mm)	Atmospheric solute input (kg km ⁻²)
01.10.1999 – 30.09.2000	01.10.1999 – 31.05.2000 01.06.2000 – 30.09.2000	Snow cores (taken in May/June) Precipitation (gauge at LFS)	60 66	Mean: 3.52 Max: 4.4 Min: 3.1 Mean: 6.15 Max: 13.8 Min: 1.5	764.6 304.8	2691.4 1874.5 Total: 4565.9
01.10.2000 – 30.09.2001	01.10.2000 – 31.05.2001 01.06.2001 – 30.09.2001	Snow cores (taken in May/June) Precipitation (gauge at LFS)	65 58	Mean: 3.64 Max: 4.3 Min: 3.2 Mean: 4.87 Max: 14.8 Min: 2.1	356.4 325.4	1297.3 1584.7 Total: 2882.0
01.10.2001 – 30.09.2002	01.10.2001 – 31.05.2002 01.06.2002 – 30.09.2002	Snow cores (taken in May/June) Precipitation (gauge at LFS)	25 -	Mean: 4.87 Max: 14.8 Min: 2.1 Mean: 5.51 (mean of 2000 and 2001)	748.2 296.2	2648.6 1632.1 Total: 4280.7
01.10.2002 – 30.09.2003	01.10.2002 – 31.05.2003 01.06.2003 – 30.09.2003	Snow cores (taken in May/June) Precipitation (gauge at LFS)	52 37	Mean: 3.58 Max: 4.3 Min: 3.1 Mean: 5.89 Max: 16.0 Min: 2.9	472.6 399.3	1691.9 2351.9 Total: 4043.8
01.10.2003 – 30.09.2004	01.10.2003 – 31.05.2004 01.06.2004 – 30.09.2004	Snow cores Precipitation	50 35	Mean: 3.56 Max: 5.0 Min: 3.1 Mean: 5.81 Max: 15.2 Min: 1.8	484.1 507.7	1723.4 2949.7 Total: 4673.1
01.10.2004 – 30.09.2005	01.10.2004 – 31.05.2005 01.06.2005 – 30.09.2005	Snow cores Precipitation	52 45	Mean: 3.56 Max: 5.0 Min: 3.1 Mean: 3.65 Max: 5.1 Min: 3.2	507.7 507.7	507.7 507.7 Total: 3985.1
01.10.2005 – 30.09.2006	01.10.2005 – 31.05.2006 01.06.2006 – 30.09.2006	Snow cores Precipitation	55 37	Mean: 3.59 Max: 5.1 Min: 3.0 Mean: 5.85 Max: 14.6 Min: 2.1	555.4 325.0	1993.9 1901.3 Total: 3895.2
01.10.1999 – 30.09.2006						Mean annual total input 4046.4

Abbreviation: LFS–Latnjajaure Field Station.

Deflation

Concentrations of inorganic solids in snow cores collected along different selected profiles within Latnjavagge (Figure 2) documented that deflation takes place to a certain degree in areas with destroyed, disturbed or stressed vegetation cover, especially if these areas show no closed snow cover in winter due to an aeolian redistribution of snow (Beylich 2003, Beylich et al. 2006b). Because of the obvious dominance of areas with closed and stable vegetation cover, the importance of deflation with respect to sediment transfers is altogether little in Latnjavagge. This is also underlined by very small (negligible) amounts of inorganic material collected in two samplers installed during each Arctic summer season (2000–2006) at the southern shoreline of the Latnjajaure.

Slush flows

Annual numbers of slush flows, the location of triggered slush flows within Latnjavagge, annually accumulated masses, transport distances and annual mass transfers by slush flows are discussed in detail in Beylich (2008). Triggering of slush flows is favoured in years that are characterised by significant snow melt periods during winter, which can lead to clearly defined ice layers within the winter snow pack (Molau pers. comm.). The years 2000–2002 as well as 2004 and 2005 were characterised by several small slush flows occurring in clearly defined areas within the catchment (Beylich et al. 2006b). There were no slush flows occurring in the years 2003 and 2006. In 1999, a mega slush-flow event was triggered in the upper valley by a melt-water outbreak from the uppermost small lake in Latnjavagge (Beylich et al. 2006b). This single mega slush-flow event caused a mass transfer of ca. 375,000 t m, with this mass transfer being 97 times higher than the mean annual total mass transfer as caused by more frequent smaller slush flows. Slush flows deliver fine and coarse material as well as large blocks. Aeolian, wash and fluvial processes transport part of the fine material further. In addition, the mega slush-flow event of 1999 removed the vegetation cover on several moraine ridges above the delta of Latnjajaure, which caused an increased intensity of deflation in the following years in these areas (Beylich et al. 2006b).

Fluvial transport

Fluvial solute transport, suspended-sediment transport, bed-load transport as well as yields of solutes and suspended sediments were quantified for the runoff seasons of 2000–2006 at the inlet and outlet of Latnjajaure and at the outlet of the entire Latnjavagge catchment. The extreme rainfall event of July 2004, with 58.4 mm of rain in 24 h and 71.7 mm of rain in 48 h, was excluded from the calculation of the mean annual transport rates and yields presented in Tables 3 and 4.

Fluvial solute transport

Fluvial solute transport and its spatio-temporal variability in Latnjavagge are discussed in detail in Beylich (2005) and Beylich et al. (2003, 2004a, b, 2005b). The mean annual chemical-denudation rate at the outlet of the entire Latnjavagge catchment (period 2000–2006) is 4889 kg km⁻² yr⁻¹ (Table 3). The mean annual discharge-weighted concentration of total dissolved solids shows only a minimum inter-annual variability, with a maximum of 12.16 mg l⁻¹ in 2003, a minimum of 11.92 mg l⁻¹ in 2000 and a mean annual of 12.04 mg l⁻¹ for the entire investigation period.

Fluvial suspended-sediment transport

Fluvial suspended-sediment transport and its spatio-temporal variability, the quantitative importance of snowmelt- and rainfall-generated runoff peaks for annual suspended-sediment transport, as well as the suspended-sediment transport during the extreme rainfall event of July 2004, are discussed in detail in Beylich and Gintz (2004), Beylich and Sandberg (2005), Beylich et al. (2005b) and Beylich et al. (2006b). The continuation of the monitoring programme after this event of July 2004, until the end of 2006, has revealed that the suspended-sediment transport at the inlet of Latnjajaure in 2005 was higher than in the years before (2000–2004) and in 2006, and accordingly clearly higher than the mean annual value calculated for the seven-year period 2000–2006 (excluding the extreme rainfall event of July 2004). Annual runoff, annual yields of suspended sediments and mean discharge-weighted suspended-sediment concentrations for the period 2000–2006, as well as the mean annual values for this seven-year period (excluding the rainfall event of July 2004) are shown for the measuring sites inlet Latnjajaure, outlet Latnjajaure and outlet entire Latnjavagge catchment in Table 3. The mean annual yield of suspended sediments is about 2.4 t km⁻² yr⁻¹ at the inlet of Latnjajaure, about 0.2 t km⁻² yr⁻¹ at the outlet of Latnjajaure, and about 0.6 t km⁻² yr⁻¹ at the outlet of the entire Latnjavagge catchment. During the extreme rainfall event of July 2004, the suspended-sediment transport at the inlet of Latnjajaure was 3.2 times higher than the mean annual suspended-sediment transport at this measuring site (Beylich and Sandberg 2005, Beylich et al., 2006b). The snowmelt- and rainfall-generated runoff peaks of the year 2005, as well as the snowmelt-generated peak runoff of the year 2006, show slightly higher suspended-sediment concentrations than hydrologically comparable seasonal peak-runoff events of the years before (Table 5). For the year 2005, this can be explained by the significantly higher intensity of slush flows and the higher mobility of channel debris pavements (see Table 4). In 2005 and 2006, the disturbance of the vegetation cover caused by debris flows and translation slides triggered during the extreme rainfall event of July 2004, is reflected by an increased intensity of slope wash (see Table 3). The significantly higher annual suspended-sediment transport in 2005 as compared to the years 2000–2004 and 2006, is caused by a combination of increased slush-flow activity, increased bed-load transport and debris-pavement mobility as well as increased slope wash.

Table 3. Annual suspended-sediment yields and annual chemical-denudation rates in Latnjavagge (2000–2006).

Field season	Catchment	Precipitation (mm)	Runoff (mm)	Yield of suspended solids (kg km ⁻²)	Mean weighted SSC (mg l ⁻¹)	Yield of dissolved solids (kg km ⁻²)	Mean weighted TDS (mg l ⁻¹)	Chemical denudation (kg km ⁻²)
2000	Latnjavagge	226	754	291	0.39	8985	11.92	
	Outlet lake		734	211	0.29	8165	11.12	
	Inlet lake		790	2587	3.28	6561	8.31	
2001	Latnjavagge	264	748	1259	1.68	9087	12.15	
	Outlet lake		754	252	0.33	8046	10.67	
	Inlet lake		748					
2002	Latnjavagge	158	648	674	1.04	7795	12.03	
	Outlet lake		650	202	0.31	7086	10.90	
	Inlet lake		654	2046	3.13	5143	7.86	
2003	Latnjavagge	175	663	603	0.91	8062	12.16	
	Outlet lake		670	194	0.29	7397	11.04	
	Inlet lake		676	2156	3.19	5340	7.90	
2004 (excluding the rare event July 20 th –21 st)	Latnjavagge	360	798	543	0.68	9602	12.03	
	Outlet lake		805	217	0.27	8050	10.00	
	Inlet lake		812	2599	3.20	6415	7.90	
2005	Latnjavagge	253	731	538	0.74	8772	12.00	
	Outlet lake		740	188	0.25	7992	10.80	
	Inlet lake		751	2704	3.60	5971	7.95	
2006	Latnjavagge	177	742	346	0.47	8910	12.01	
	Outlet lake		750	208	0.28	8175	10.90	
	Inlet lake		755	2310	3.06	5980	7.92	
Mean annual values for 2000–2006	Latnjavagge		742	626	0.84	8935	12.04	4889
	Outlet lake		742	214	0.29	7997	10.78	3951
	Inlet lake		742	2378	3.21	5859	7.90	1813

Abbreviations: TDS–total dissolved solids, SSC–suspended-sediment concentration.

Table 4. Annual bed-load transport in Latnjavagge (2000–2006).

Site	2000	2001	2002	2003	2004	2005	2006	Mean 2000–2006	Event July 20 th –21 st , 2004
Outlet SC A	0.00	0.00	0.00	0.00	0.00	0.00	0.00	0.00	0.00
Outlet SC B	0.05	0.03	0.04	0.03	0.05	0.10	0.01	0.04	0.34
Outlet SC C	0.09	0.08	0.08	0.07	0.08	0.16	0.04	0.09	0.93
Outlet SC D	7.0	4.6	3.7	4.1	7.2	9.8	3.2	5.66	42
Inlet Latnjajaure	8.2	5.3	7.1	6.0	7.3	14.9	5.1	7.7	55
Outlet Latnjajaure	0.0	0.0	0.0	0.0	0.0	0.0	0.0	0.0	0
Outlet Latnjavagge	1.5	0.7	1.0	0.7	1.1	1.8	0.3	1.0	11

Table 5. Suspended-sediment transport during snowmelt- and rainfall-generated peak runoff in Latnjavagge (2000–2006).

Field season	Runoff peak	Reason for runoff peak (kg km ⁻²)	Total yield during peak (kg km ⁻²)	% of total mean annual denudation (2378 kg km ⁻² yr ⁻¹)	Total runoff during peak (mm)	% of mean annual runoff (742 mm)	SSC max during peak (mg l ⁻¹)	SSC mean during peak (mg l ⁻¹)	% of total mean annual denudation (2378 kg km ⁻² yr ⁻¹)
2000	1	Snow melt	1864	78	163	22	43.40	11.44	
	2	Snow melt	412	17	211	28	6.75	1.95	
	3	Rain	113	5	66	9	2.20	1.71	100
2001	1	Snow melt	2064	87	388	52	16.20	5.32	87
2002	1	Snow melt	1820	77	334	45	18.23	5.45	
	2	Rain	49	2	31	4	1.80	1.58	79
2003	1	Snow melt	1902	80	376	51	23.20	5.06	80
2004	1	Snow melt	2008	84	352	47	26.05	5.71	
	2	Rain	7500	315	50	7	365	150	399
2005	1	Snow melt	2154	91	352	47	27.50	6.12	
	2	Rain	133	6	39	5	4.50	3.42	97
2006	1	Snow melt	2102	88	360	49	25.90	5.80	88

Abbreviation: SSC—suspended sediment concentration.

Fluvial bed-load transport

The mapped and quantified annual bed load is shown in Table 4. The mean annual bed-load transport during the period of 2000–2006 is about 1 t yr⁻¹ at the outlet of Latnjavagge and 7.7 t yr⁻¹ at the inlet of Latnjajaure. Most bed load (5.7 t yr⁻¹) is supplied by sub-catchment D (Figure 2) (Beylich et al. 2006b). The fluvial sediment transfers caused by the extreme rainfall event of July 2004 are discussed in detail in Beylich and Sandberg (2005) and Beylich et al. (2006b). The bed-load transport caused by this extreme event was 8.5 times higher than the mean annual transport at the outlet of sub-catchment B, 10.3 times higher than the mean annual transport at the outlet of sub-catchment C, 7.4 times higher than the mean annual transport at the outlet of sub-catchment D, 7.1 times higher than the mean annual transport at the inlet of Latnjajaure and 11 times higher than the mean annual transport at the outlet of the entire Latnjavagge catchment (Table 4). The continuation of the monitoring programme after the rainfall event of July 2004 until the end of 2006 has shown that a significant increase in the bed-load transport occurred at all monitoring sites with measurable bed-load transport (outlet sub-catchment B, outlet sub-catchment C, outlet sub-catchment D, inlet Latnjajaure, outlet Latnjavagge) in 2005. In the following year, clearly lower bed load-transport rates were measured and the quantified annual bed-load transport in 2006 was at all monitoring sites lower than the annual bed-load transport of the years 2000–2004 at these sites. The increased bed-load transport in 2005 can be explained by less stable channel debris pavements due to the removal of stable step-pool systems by high runoff caused by the extreme rainfall event of July 2004. In 2006, the channel pavements were characterised by the observed new formation of step-pool systems and by again clearly higher stability.

Mass transfers, sediment budget and trends of relief development

Relative importance of the different denudative processes

On the basis of the process rates calculated for Latnjavagge, the absolute and relative importance of present-day denudative processes in the entire catchment was estimated by a quantification of the mass transfers caused by the different processes. To allow direct comparison of the different processes, all mass transfers are shown as tonnes x meter per year (t m yr⁻¹), i.e., as the product of the annually transferred mass and the corresponding transport distance (see Jäckli 1957, Rapp 1960, Barsch 1981, Beylich 1999, 2000a). The mass transfers calculated for Latnjavagge are shown in Table 6. It should be stressed that these mass transfers are based on process studies and monitoring carried out with selected and simple (i.e., reliable and low-cost) methods over a seven-year period (1999–2006), and that the values shown in Table 6 ex-

Table 6. Annual mass transfers by the different denudative processes in Latnjavagge, based on field measurements carried out between 1999 and 2006.

	Process	Volume (m ³ yr ⁻¹)	Mass (t yr ⁻¹)	Area (km ²)	Mass/Area (t km ⁻² yr ⁻¹)	Average movement (m)	Mass transfer (t m yr ⁻¹)
Slope denudation	Rockfalls and boulder falls	1377	3441	3.15	1092	7.5	25,808
	Ground avalanches	28	69	0.02	3450	150	10350
	Debris flows	3	6	0.000016	375,000	47	279
	Translational slides	1.5	3	0.000022	136,364	3.7	11
	Creep and solifluction	840,000	1,680,000	2.8	600,000	0.003	5040
	Chemical denudation	22	44	9	4.9	500	22,000
	Mechanical fluvial denudation	10.5	21	9	2.4	500	10,500
	Deflation	little	little				
	Slush flows	12.2	30.4	0.000097	313,402	108.7	3305
Stream work	Solute transport	22	44	9	4.9	2300	101,200
	Suspended-sediment transport	10.5	21	9	2.4	1400	29,400
	Bed-load transport	3.1	7.7	0.04	192.5	250	1925

clude the geomorphic effects of the rare rainfall event of July 2004 (Beylich and Sandberg 2005) and of the mega slush-flow event of May 1999. The role of these extreme events is further discussed below. In computing the mass transfers caused by rock- and boulder falls, the following assumptions were made: a total debris-supplying rock-wall and rock-ledge surface of 3.15 km², a mean annual rock wall-retreat rate of 0.44 mm yr⁻¹, an average transport distance of 7.5 m and an average rock density of 2.5 g cm⁻³. Also, the material transported and deposited by ground avalanches was presumed to have an average density of 2.5 g cm⁻³. Calculating the mass transfer caused by creep and solifluction was led by the following assumptions: an affected surface of 2.8 km², an average movement rate of 0.003 m yr⁻¹ in a 0.3 m-thick layer, and an average material density of 2.0 g cm⁻³. In contrast to the other denudative processes, chemical denudation affects the total surface of the slope systems. The transport distance of 500 m is about half the medium distance between water divide and main channel.

The transport distance of 2300 m for fluvial solute transport is about half the medium distance between the water divide opposite to the outlet and the catchment outlet. Mass transfers by fluvial suspended-sediment transport and fluvial bed-load transport are based on an average movement of 1400 m for suspended sediments, which is about half the medium distance between the water divide and inlet Latnjajaure, and 250 m for bed load, based on monitoring of tracer movements. Fluvial solute transport clearly dominates over fluvial sediment transport.

Ranking the different processes according to their annual mass transfers shows that stream work dominates over slope denudation, with fluvial solute transport being clearly the most important process.

Ranking the different processes according to their annual mass transfers shows that rock falls plus boulder falls is the most important factor in slope denudation, followed by chemical denudation. As a result, according to their relative importance, the different processes can be ranked as follows: (1) Fluvial

solute transport, (2) Fluvial suspended-sediment transport plus fluvial bed-load transport, (3) Rock falls and boulder falls, (4) Chemical slope denudation, (5) Mechanical fluvial slope denudation, (6) Avalanches, (7) Creep and solifluction, (8) Slush flows, (9) Debris flows, (10) Translation slides, and (11) Deflation.

With respect to the temporal variability of process intensities and/or process frequencies, the main snow-melt period (late May–June/July), which is characterised by high runoff, increased fluvial transport, slush-flow activity, avalanches and rock and boulder falls, as well as August, which is the month showing the highest frequency of extreme rainfall events (Beylich 2003, Beylich and Gintz 2004) triggering debris flows, translation slides, secondary rock falls, boulder falls, peak runoff and increased fluvial transport, can be pointed out as periods with comparatively high activity of denudative processes. In comparison, the period from late October until early May is characterised by only very little (single avalanches) or no activity of denudative processes.

The importance of the July 2004 rainfall and May 1999 extreme slush-flow events

On July 20th–21st 2004, an extreme rainfall event, with 58.4 mm of rain in 24 h and 71.7 mm of rain in 48 h, as measured at the weather station of the Latnjajaure Field Station, occurred (Beylich and Sandberg 2005). This extreme rainfall event is considered a 'rare event' (Beylich 2003), which caused extreme peak runoff in the fluvial systems of the Abisko mountain area and significant damage to the road between Abisko and Kiruna (Beylich and Sandberg 2005). The rare rainfall event triggered high sediment transfers on the slopes and in the fluvial systems of the Latnjavagge drainage basin, and the quantified mass transfers at only one day during this extreme rainfall event exceeded the mean annual mass transfers calculated for the seven-year period 1999–2006 (and excluding the rare rainfall event of July 2004) by several times (see Beylich and Sandberg 2005, Beylich et al. 2006b). The rare rainfall event caused several debris flows,

translation slides, boulder falls, secondary rock falls, locally very high slope wash, bank erosion in creeks above the Latnjajure delta and high suspended-sediment and bed-load transport in creeks. Table 2 in Beylich and Sandberg (2005, page 415) provides mass transfers (t m) by debris flows, translation slides and fluvial debris transport in creeks and channels, which were caused in different parts of the Latnjavagge catchment by the July 2004 rainfall event. The mass transfers triggered by the rare event can be discussed in direct comparison with the mean annual mass transfers calculated for the period 1999–2006 (and excluding the extreme rainfall event) (see Table 1). The mass transfer by debris flows, which were triggered during the rare rainfall event, was 2030 t m in the entire Latnjavagge catchment, which is 7.3 times higher than the mean annual mass transfer by debris flows (279 t m). It has to be noted that the annual mass transfers by debris flows have clearly increased after the July 2004 event, which is also reflected in significantly higher mean annual mass transfer for the period 2000–2006 (279 t m) as compared to the mean annual mass transfer for the five-year period 2000–2004 (212 t m). The mass transfer by translation slides that were triggered during the rare event reached 2446 t m in the entire catchment, which is 222.4 times higher than the mean annual mass transfer by slides (11 t m). It is again necessary to stress that also the annual mass transfers caused by translation slides have clearly increased after the July 2004 rare rainfall event, which is documented by a significantly higher mean annual mass transfer for the seven-year period 2000–2006 (11 t m) as compared to the five-year period 2000–2004 (2.5 t m). The total mass transfer by fluvial debris transport in creeks and channels during the rare rainfall event was 7480 t m, which is 16.9 times higher than the corresponding mean annual mass transfer within the entire Latnjavagge catchment, quantified to be 444 t m for the period 2000–2004 (Beylich and Sandberg 2005).

During the rare event, the mass transfer by fluvial debris transport in creeks and channels (7480 t m) had clearly the highest relative importance, followed by mass transfers by slides (2446 t m) and debris flows (2030 t m). In comparison, the mean annual mass transfers (excluding the July 2004 event) again show a relative dominance of fluvial debris transport in creeks, but are followed by debris flows whereas translation slides are of only minor importance.

During the rare rainfall event, the mass transfers caused by debris flows, translation slides and fluvial debris transport, as well as suspended-sediment transport, were several times higher than the mean annual mass transfers.

The mega slush-flow event of May 1999 caused a mass transfer that was 97 times higher than the mean annual total mass transfer caused by several small slush flows between 2000 and 2006.

Both the rare rainfall event of July 2004 and the mega slush-flow event of May 1999 underline the high importance of rare events for the calculation of longer-term sediment budgets. Both rare events also reveal the difficulties of defining an adequate

length for monitoring programmes (Beylich and Sandberg 2005).

Comparing the results from Latnjavagge with data collected in other cold-environment catchments shows some similarities but also some significant differences to other areas. Rapp (1960) stressed in his seminal study of denudation and slope development in Kärkevagge, northernmost Swedish Lapland, the high importance of chemical weathering and denudation, and his work stands out as the study that opened awareness of chemical denudation in cold environments. His findings for Kärkevagge and a high relative importance of chemical weathering and denudation were confirmed by later investigations carried out in this valley (Dixon et al. 1995, 2001, 2005, 2008, Darmody et al. 2000, 2001, Campbell et al. 2001, 2002, Thorn et al. 2001, 2006) and have also been postulated for other cold environments (e.g., Semmel 1969, Lewkowicz 1983, Åkermann 1983, French 1996). In comparison and in accordance with findings in Latnjavagge, slope-wash processes are of only little importance in Kärkevagge (Rapp 1960, Strömquist and Rehn 1981). A significant difference between the mass transfers calculated for Latnjavagge and the mass transfers published by Rapp (1960) is the high importance of slides and debris flows in Kärkevagge. The high importance of slides and debris flows found by Rapp (1960) is based mainly on mass transfers which were triggered by a rare rainfall event with 107 mm in 24 h and 175 mm in 72 h in October 1959. This rare event occurred at the end of Rapp's nine-year investigation period (1952–1960) and the mean annual mass transfers caused by slides and debris flows as calculated by Rapp might actually be too high, given the long recurrence intervals of such rare rainfall events in northernmost Swedish Lapland (Beylich 1999, 2003, see also French 1996). The problem of defining an adequate length of monitoring programmes becomes, as in Latnjavagge with respect to the rare rainfall event of July 2004 and the mega slush-flow event of May 1999, again obvious (Beylich and Sandberg 2005).

Barsch (1981) found, in accordance with the results from Latnjavagge, a relative dominance of fluvial transport over slope processes for the Oobloyah Valley in northern Ellesmere Island (Northwest Territories, Canada). Rock falls and slope wash have the largest relative importance at the slope systems in this valley (Barsch 1981).

Beylich (1999, 2000a, b) pointed out that regarding annual mass transfers, fluvial transport dominates over slope processes in the very steep Austdalur catchment in east Iceland. Due to human impact and the connected disturbance and partly removal of the vegetation cover, fluvial sediment transport dominates over fluvial solute transport. At the slope systems, slope wash has, similar to the Oobloyah Valley in northern Ellesmere Island (Barsch 1981), but in clear contrast to Kärkevagge (Rapp 1960) and Latnjavagge, the largest relative importance and is followed by chemical denudation, ground avalanches, rock falls and boulder falls, creep processes, debris slides and flows, and deflation.

In all four study areas in sub-Arctic, oceanic east Iceland,

high-Arctic, continental northern Ellesmere Island, and sub-Arctic, oceanic to Arctic oceanic Swedish Lapland, the intensity of present-day denudative processes is altogether rather low, which is contrary to the earlier postulated (e.g., Tricart 1970, Büdel 1981) high intensity of geomorphic processes in cold environments.

Current trends of relief development

The combined analysis of the slope systems and channel systems, or of slope denudation and streamwork, respectively, allows statements on current trends of relief development in Latnjavagge. By the retreat of rock walls and rock ledges and the continued formation of talus cones located below the rock walls and rock ledges, slope processes cause a valley widening in Latnjavagge (Figure 13). The valley floor is characterised by a fluvial throughput of material above the delta of Latnjajaure (Figure 14), net accumulation of material in the delta of Latnjajaure and in the lake (Figure 13), and a moderate fluvial downcutting between the outlet of Latnjajaure and the outlet of the entire Latnjavagge catchment. Coupling between slope systems and fluvial systems exists only to a limited extent (i) via slush flows in defined areas within the valley, as well as (ii) via ground avalanches at a short main channel stretch directly above the delta of Latnjajaure (Figure 15) (see also Figures 2 and 3). Altogether, postglacial modification of the glacial relief is small (see also Figure 13). Due to the short time since the deglaciation (8000–10,000 yr ago) and the altogether low intensity of the active denudative surface processes, until today, there has been no adjustment of the Pleistocene glacial landforms to the geomorphic processes that have been operating until present under the Holocene morphoclimates.

Conclusions and prospect

By a combined, quantitative recording of the relevant denudative slope processes and stream work in the 9 km² Latnjavagge catchment in northernmost Swedish Lapland, information on the absolute and relative importance of the different denudative processes has been collected. The seven-year investigation period included a rare rainfall event, which caused major mass transfers within just two days, and considered also a mega slush-flow event with very large mass transfers in May 1999. The applied catchment-based approach (Beylich 1999, 2000a, 2002) seems to be effective for analysing the current sediment budget and recent trends of relief development in a selected cold environment with special features. More studies, carried out with unified, standardised and simple (i.e., reliable and low-cost) geomorphic field methods in cold-environment catchments having different morphoclimatic, vegetational, topographic, lithological/geological and tectonic features, will help gain a better understanding of the internal differentiation of cold environments (see Barsch 1984, 1986). Furthermore, more information on the control mechanisms of processes, the role



Figure 13. The Latnjavagge valley.



Figure 14. Main channel above the delta of Latnjajaure.



Figure 15. Main channel stretch with coupling above the delta of Latnjajaure and below the channel stretch shown in Figure 14.

of extreme events for mass transfers and sediment budgets, the intensity of processes, and the relative importance of different processes for slope and valley formation and recent relief development in different cold environments, can be collected. By coordinated comparisons of data sets collected in this way, in a larger number of different cold-environment catchments

of similar size (ca. 10–30 km²), larger, integrated studies on the effects of projected climate change and on relief and landform development in cold environments can be realised (Beylich 1999, 2000a, 2007, Beylich and Warburton 2007, Beylich et al. 2006a, 2007). Comparable data sets generated in other test catchments in high-latitude and high-altitude cold environments using methods and techniques that follow the guidelines and protocols provided in the SEDIFLUX Manual (Beylich and Warburton 2007) can be added to a metadata database developed within the global I.A.G./A.I.G. SEDIBUD programme (<http://www.geomorph.org/wg/wgsb.html>) (Beylich 2007, Beylich et al. 2007). The SEDIBUD metadata database will be used to model effects of projected climate change on solute fluxes, sediment fluxes and sediment budgets in sensitive and changing cold environments (Beylich 2007, 2008, Beylich and Warburton 2007, Beylich et al. 2007).

Improved knowledge on mechanisms and controlling factors of sedimentary transfer processes has high significance to society, particularly with respect to possible effects of predicted global climate change. The increased frequency of floods and hazards caused by a higher frequency of extreme meteorological events is a challenge for society and requires more detailed scientific knowledge on the natural systems and processes at the Earth's surface.

Acknowledgements

Research in Latnjavagge was funded by the German Exchange Service (DAAD) (1999–2001, grant to Achim A. Beylich), the German Science Foundation (DFG) (2002–2004, grant to Achim A. Beylich) and the Geological Survey of Norway (NGU) (since 2004). The logistic support and hospitality of the Abisko Scientific Research Station (ANS) and the Latnjajaure Field Station is greatly acknowledged. Special thanks go to Ulf Molau and his group from Gothenburg University for the fruitful collaboration at the field station and for data exchange and scientific discussions. Great thanks go to the following assistants: Karin Luthbom, Sarah Richardson, Timo Tapio, Jani Helin, Susan Wache, Olga Sandberg, Simone Lang, Anika Neubert. I would like to thank the two anonymous referees for their helpful, critical comments improving this paper.

References

- André, M.-F. (1995) Postglacial microweathering of granite roches moutonnees in Northern Scandinavia. In Slaymaker, O. (ed.) *Steepland Geomorphology*, Wiley, London, pp. 103–127.
- Barsch, D. (1981) Studien zur gegenwertigen Geomorphodynamik im Bereich der Oobloyah Bay, N-Ellesmere Island, N.W.T., Kanada. *Heidelberger Geographische Arbeiten*, **69**, 123–161.
- Barsch, D. (1984) Geomorphologische Untersuchungen zum periglazialen Milieu polarer Geosysteme. *Zeitschrift für Geomorphologie N.F., Supplementband*, **50**, 107–116.
- Barsch, D. (1986) Forschungen in Polargebieten. *Heidelberger Geowissenschaftliche Abhandlungen*, **6**, 33–50.
- Beylich, A.A. (1999) Hangdenudation und fluviale Prozesse in einem subarktisch-ozeanisch geprägten, permafrostfreien Periglazialgebiet mit pleistozäner Vergletscherungs-Prozessgeomorphologische Untersuchungen im Bergland der Austfiridir (Austdalur, Ost-Island). *Berichte aus der Geowissenschaft*, Aachen, 130 pp.
- Beylich, A.A. (2000a) Geomorphology, sediment budget, and relief development in Austdalur, Austfiridir, East Iceland. *Arctic, Antarctic, and Alpine Research*, **32**, 466–477.
- Beylich, A.A. (2000b) Untersuchungen zum gravitativen und fluvialen Stofftransfer in einem subarktisch-ozeanisch geprägten, permafrostfreien Periglazialgebiet mit pleistozäner Vergletscherung (Austdalur, Ost-Island). *Zeitschrift für Geomorphologie N.F., Supplementband*, **121**, 1–22.
- Beylich, A.A. (2002) Sediment budgets and relief development in present periglacial environments—a morphosystem analytical approach. *Hallesches Jahrbuch für Geowissenschaften*, **A 24**, 111–126.
- Beylich, A.A. (2003) Present morphoclimates and morphodynamics in Latnjavagge, the northern Swedish Lapland and Austdalur, East Iceland. *Jökull*, **52**, 33–54.
- Beylich, A.A. (2005) Intensity and spatio-temporal variability of chemical denudation in an Arctic-oceanic periglacial drainage basin in northernmost Swedish Lapland. *Nordic Hydrology*, **36**, 21–36.
- Beylich, A.A. (2007) Quantitative studies on sediment fluxes and sediment budgets in changing cold environments—potential and expected benefit of coordinated data exchange and the unification of methods. *Landform Analysis*, **5**, 9–10
- Beylich, A.A. (2008) Mass transfers, sediment budget and relief development in the Latnjavagge catchment, Arctic-oceanic Swedish Lapland. *Zeitschrift für Geomorphologie N.F., supplementary volume*, **52**, 149–197.
- Beylich, A.A. and Gintz, D. (2004) Effects of high-magnitude/low-frequency fluvial events generated by intense snowmelt or heavy rainfall in Arctic periglacial environments in northern Swedish Lapland and northern Siberia. *Geografiska Annaler*, **86A**, 11–29.
- Beylich, A.A. and Sandberg, O. (2005) Geomorphic effects of the extreme rainfall event of 20–21 July, 2004 in the Latnjavagge catchment, northern Swedish Lapland. *Geografiska Annaler*, **87A**, 409–419.
- Beylich, A.A. and Warburton, J. (eds.) (2007) Analysis of Source-to-Sink-Fluxes and Sediment Budgets in Changing High-Latitude and High-Altitude Cold Environments. SEDIFLUX Manual. First Edition. *NGU Report 2007.053*, 158 pp.
- Beylich, A.A., Kolstrup, E., Linde, N., Pedersen, L.B., Thyrted, T., Gintz, D. and Dynesius, L. (2003) Assessment of chemical denudation rates using hydrologic measurements, water chemistry analysis and electromagnetic geophysical data.

- Permafrost and Periglacial Processes*, **14**, 387–297.
- Beylich, A.A., Kolstrup, E., Thyrsted, T. and Gintz, D. (2004a) Water chemistry and its diversity in relation to local factors in the Latnjavagge drainage basin, Arctic-oceanic Swedish Lapland. *Geomorphology*, **58**, 125–143.
- Beylich, A.A., Kolstrup, E., Thyrsted, T., Linde, N., Pedersen, L.B. and Dynesius, L. (2004b) Chemical denudation in Arctic-alpine Latnjavagge (Swedish Lapland) in relation to regolith as assessed by radio magnetotelluric-geophysical profiles. *Geomorphology*, **57**, 303–319.
- Beylich, A.A., Lindblad, K. and Molau, U. (2005a) Direct human impacts on mechanical denudation in an Arctic-oceanic periglacial environment in northern Swedish Lapland (Abisko mountain area). *Zeitschrift für Geomorphologie N.F., supplementary volume*, **138**, 81–100.
- Beylich, A.A., Molau, U., Luthbom, K. and Gintz, D. (2005b) Rates of chemical and mechanical fluvial denudation in an Arctic-oceanic periglacial environment, Latnjavagge drainage basin, northernmost Swedish Lapland. *Arctic, Antarctic, and Alpine Research*, **37**, 75–87.
- Beylich, A.A., Etienne, S., Etzelmüller, B., Gordeev, V.V., Käyhkö, J., Rachold, V., Russell, A.J., Schmidt, K.-H., Sæmundsson, P., Tweed, F.S. and Warburton, J. (2006a) The European Science Foundation (ESF) Network SEDIFLUX—An introduction and overview. *Geomorphology*, **80**, 3–7.
- Beylich, A.A., Sandberg, O., Molau, U. and Wache, S. (2006b) Intensity and spatio-temporal variability of fluvial sediment transfers in an Arctic-oceanic periglacial environment in northernmost Swedish Lapland (Latnjavagge catchment). *Geomorphology*, **80**, 114–130.
- Beylich, A.A., Lamoureux, S.F. and Decaulne, A. (2007) Coordinated quantitative studies on sediment fluxes and sediment budgets in changing cold environments—Examples from three SEDIBUD key test areas in Canada, Iceland and Norway. *Landform Analysis*, **5**, 11–12.
- Büdel, J. (1981) *Klima-Geomorphologie*, 2. veränderte Auflage, Schweizerbart, Stuttgart, 304 pp.
- Campbell, S.W., Dixon, J.C., Darmody, R.G. and Thorn, C.E. (2001) Spatial variation of early season surface water chemistry in Kärkevagge, Swedish Lapland. *Geografiska Annaler*, **83A**, 169–178.
- Campbell, S.W., Dixon, J.C., Thorn, C.E. and Darmody, R.G. (2002) Chemical denudation rates in Kärkevagge, Swedish Lapland. *Geografiska Annaler*, **84A**, 179–185.
- Darmody, R.G., Thorn, C.E., Harder, R.L., Schlyter, J.P.L. and Dixon, J.C. (2000) Weathering implications of water chemistry in an Arctic-Alpine environment, northern Sweden. *Geomorphology*, **34**, 89–100.
- Darmody, R.G., Allen, C.E., Thorn, C.E. and Dixon, J.C. (2001) The poisonous rocks of Kärkevagge. *Geomorphology*, **41**, 53–62.
- Dixon, J.C., Darmody, R.G., Schlyter, P. and Thorn, C.E. (1995) Preliminary investigation of geochemical process responses to potential environmental change in Kärkevagge, Northern Scandinavia. *Geografiska Annaler*, **77A**, 259–267.
- Dixon, J.C., Thorn, C.E., Darmody, R.G. and Schlyter, P. (2001) Weathering rates of fine pebbles at the soil surface in Kärkevagge, Swedish Lapland. *Catena*, **45**, 273–286.
- Dixon, J.C., Campbell, S.W., Thorn, C.E. and Darmody, R.G. (2005) Incipient weathering rind development on introduced machine-polished granite discs in an Arctic alpine environment, northern Scandinavia. *Earth Surface Processes and Landforms*, **31**, 111–121.
- Dixon, J.C., Thorn, C.E. and Darmody, R.G. (2008) Spatial scale and chemical weathering in Kärkevagge: Influences on landscape evolution. *Zeitschrift für Geomorphologie N.F., supplementary volume*, **52**, 27–49.
- French, H.M. (1996) *The Periglacial Environment*, 2nd edition, Longman, London, 341 pp.
- Haeberli, W. and Beniston, M. (1998) Climate change and its impacts on glaciers and permafrost in the Alps. *Ambio*, **27**, 258–265.
- Jäckli, H. (1957) Gegenwartsgeologie des Bündnerischen Rheingebietes. *Beitrag zur Geologischen Karte der Schweiz, Geotechnische Serie*, **36**, 126 pp.
- Kling, J. (1996) *Sorted circles and polygons in northern Sweden, distribution and processes*. Ph.D. thesis, Department of Physical Geography, Gothenburg University, 28 pp.
- Kulling, O. (1964) Översikt över Norra Norrbottensfjällens Kaledonberggrund. *Sveriges Geologiska Undersökning, Serie Ba, Översiktskartor med beskrivningar*, **19**, 166 pp.
- Lamoureux, S.F. (1999) Spatial and interannual variations in sedimentation patterns recorded in nonglacial varved sediments from the Canadian high Arctic. *Journal of Paleolimnology*, **21**, 73–84.
- Lewkowicz, A.G. (1983) Erosion by overland flow, Central Banks Island, Western Canadian Arctic. Proceedings IV. International Conference on Permafrost, pp. 701–706.
- Molau, U. (2001) Tundra plant responses to experimental and natural temperature changes. *Memoirs of the National Institute of Polar Research Special Issue*, **54**, 445–466.
- Molau, U., Kling, J., Lindblad, K., Björk, R., Dänhardt, J. and Liess, A. (2003) A GIS assessment of alpine biodiversity at a range of scales. In Nagy, L., Grabherr, G., Körner, C. and Thompson, D.B.A. (eds.) *Alpine Biodiversity in Europe. Ecological Studies*, **167**, Springer, Berlin, pp. 121–129.
- Rapp, A. (1960) Recent development of mountain slopes in Kärkevagge and surroundings, Northern Scandinavia. *Geografiska Annaler*, **42**, 71–200.
- Sandberg, O. (2004) *Denudative slope processes in Latnjavagge, arctic-oceanic northernmost Swedish Lapland—a combination of mapping, dating and direct process measurement techniques*. B.Sc. thesis, Earth Science Centre Series B417, Gothenburg University, 33 pp.
- Semmel, A. (1969) Verwitterungs- und Abtragungerscheinungen in rezenten Periglazialgebieten (Lapland und Spitsbergen). *Würzburger Geographische Arbeiten*, **26**, 82 pp.
- Slaymaker, O., Souch, C., Menounos, B. and Filippelli, G. (2003) Advances in Holocene mountain geomorphology inspired by sediment budget methodology. *Geomorphology*, **55**, 305–316.

- Strömquist, L. and Rehn, J. (1981) Rainfall measurements, runoff and sediment transport in Karkevagge, Swedish Lapland. *Transactions, Japanese Geomorphological Union*, **2**, 211–222.
- Thorn, C.E., Darmody, R.G., Dixon, J.C. and Schlyter, P. (2001) The chemical weathering regime of Kärkevagge, arctic-alpine Sweden. *Geomorphology*, **41**, 37–52.
- Thorn, C.E., Dixon, J.C., Darmody, R.G. and Allen, C.E. (2006) Ten years (1994–2004) of 'potential' weathering in Kärkevagge, Swedish Lapland. *Earth Surface Processes and Landforms*, **31**, 992–1002.
- Tricart, J. (1970) *Geomorphology of cold environments*, McMillan St. Martin's Press, London, 320 pp.
- Åkermann, J.H. (1983) Notes on chemical weathering, Kap Linne, Spitsbergen. Proceedings IV. International Conference on Permafrost, pp. 10–15.

Airborne gamma-ray spectrometer mapping for relating indoor radon concentrations to geological parameters in the Fen region, southeast Norway

Björn Henning Heincke¹, Mark A. Smethurst¹, Arne Bjørlykke¹, Sven Dahlgren², Jan Steinar Rønning^{1,3} and John Olav Mogaard¹

¹Geological Survey of Norway (NGU), 7491 Trondheim, Norway.

²Geological advisor, Buskerud, Telemark and Vestfold, Fylkeshuset, 3126 Tønsberg, Norway.

³Norwegian University of Science and Technology (NTNU), 7491 Trondheim, Norway.

E-mail: bjorn.heincke@ngu.no

Extremely high thorium and considerable uranium concentrations are observed in carbonatite rocks of the Fen Complex—an alkaline intrusive complex in southern Norway. Since uranium-bearing bedrock and its weathering products are responsible for increased radon-222 concentrations in nearby dwellings, knowledge about the uranium concentrations of the individual rock types is important for evaluating the associated health risk. Earlier core-sample and ground-based scintillator measurements were limited in relating geological setting to indoor concentrations of radon-222 in such a region with very small-scale geological variations. We have performed airborne radiometric measurements over the entire Fen Complex and the nearby town of Ulefoss. The processed airborne data show that regions dominated by different carbonatite types vary significantly in mean thorium concentrations, but have similar uranium concentrations. Despite the complexity of the region, the obtained thorium/uranium ratios have proven to be a well-suited measure to distinguish regions that are dominated by specific carbonatite types. Furthermore, derived ground-concentration maps enable us to compare uranium ground concentrations directly with indoor radon concentrations of 139 individual dwellings in the Fen region. A positive correlation between local uranium concentrations and percentage of dwellings with indoor radon concentrations $> 200 \text{ Bq m}^{-3}$ was observed in regions where bedrock or its weathering material crops out. Similarly, high radon concentrations were observed for all carbonatites, indicating that the associated health hazard is largely independent of the dominant carbonatite type. In regions covered by clayey marine sediments, gamma radiation from bedrock is strongly attenuated. Also, indoor radon concentrations are predominantly low because radon transport is strongly limited by the low permeability of the marine sediments.

Heincke, B.H., Smethurst, M.A., Bjørlykke, A., Dahlgren, S., Rønning, J.S. and Mogaard, J.O. (2008) Airborne gamma-ray spectrometer mapping for relating indoor radon concentrations to geological parameters in the Fen region, southeast Norway. *In* Slagstad, T. (ed.) *Geology for Society*, Geological Survey of Norway Special Publication, **11**, pp. 131–143.

Introduction

The Fen Complex, an intrusive complex of alkaline rocks and carbonatites (carbonate rocks of magmatic origin), is located in Nome municipality, Telemark county, southeast Norway (Figure 1). The eastern parts of the complex are extremely rich in rare earth elements and the radioactive element thorium-232, and to a much lesser degree uranium-238 (Landreth 1979). Concentrations of thorium in this eastern part of the complex are so significant that Norway is considered to host one of the world's largest thorium deposits (OECD NEA and IAEA 2006).

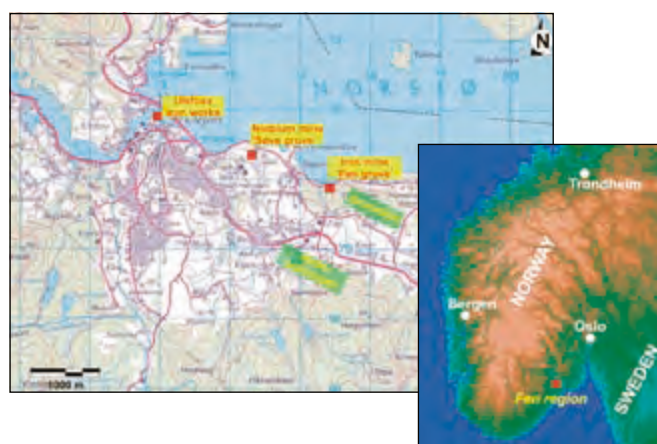


Figure 1. Map of the Fen region in the Telemark county (southern Norway). Locations of former mining-related activities are highlighted.

Health hazards associated with the daughter products of uranium and to a lesser extent thorium are of substantial interest for the residents in the Fen region (Sundal and Strand 2004). In particular, inhalation of radon-222 gas, a daughter of uranium, is considered as health risk. After smoking, long-term inhalation of radon is regarded as the second leading cause of lung cancer worldwide (e.g., ICRP 1981, Conrath and Kolb 1995, Strand et al. 2001, Argonne National Laboratory 2005) and is estimated to be responsible for about 280 cases of lung cancer in Norway each year (Smethurst et al. 2006). In a study from Sundal and Strand (2004), the average indoor radon level in the Fen region was determined to be 204 Bq m^{-3} and 37% of the investigated dwellings had radon levels above the intervention level of 200 Bq m^{-3} (see the Norwegian Radiation Protection Agency website at <http://www.nrpa.no>). This radon level is significantly above the average level in Norway of 88 Bq m^{-3} (Strand et al. 2001). Therefore, it is important to characterise in what way radon concentrations in dwellings vary with bedrock type and type of superficial deposits. With this knowledge, buildings with potential for elevated indoor radon concentrations and suitable, new residential areas can be located more easily.

Health hazards associated with the thorium daughter radon-220 are often neglected within buildings. Radon-220 is

short-lived (half-life of 55.6 s) and predominately decays before migrating into houses. In the Fen Complex, most dwellings—excluding houses containing building materials (slags) from the ancient Fen iron mines, which were located within the most thorium-enriched zones—show no increased radon-220 level (Stranden 1984, Stranden and Strand 1986). However, because thorium is far more abundant than uranium in the Fen region, outdoor dose rates (Stranden and Strand 1986) and in mines (Stranden 1985) are mostly dominated by thorium products, and the health hazard presented by radon-220 may potentially be hazardous in future mining activities (Solli et al. 1985).

The Fen Complex became famous in the geological community in 1921, after Brøgger published his classic work (Brøgger 1921). He discovered that carbonates in the Fen Complex were of magmatic origin, and became one of the first proponents of the existence of carbonate magmas. He introduced the term 'carbonatite' for carbonate rocks of apparent magmatic origin, and named rock types in this suite after localities in the Fen region. Since then, the Fen Complex has been investigated by many researchers due to its specific geology and resource potential. Sæther (1957), Barth and Ramberg (1966) and Heinrich (1966) described the general geology. Landreth (1979) summarised the results of an early joint-venture exploration programme evaluating the mineral potential of the region. Exposure-rate measurements in the Fen iron mines (Figure 1) in the 1950s showed that the Fen Complex included rocks with high thorium concentrations (Svinndal 1973). Svinndal (1973) determined thorium concentrations in samples taken along roads, paths and from boreholes and mine galleries in the late 1960s and early 1970s. Dahlgren (1983) published a map showing gamma-ray exposure rates 1 m above the ground over the Fen Complex around the nearby town of Ulefoss. Comparison with measurements on core samples showed that extremely high thorium concentrations, accompanied by elevated uranium concentrations in the carbonatites, were responsible for the high exposure rates. Between 1993 and 2000, indoor radon measurements were carried out in about 250 dwellings in Nome municipality by the company Labnett and the Norwegian Radiation Protection Authority. Sundal and Strand (2004) made a quantitative comparison between 95 of the indoor radon measurements, indoor dose-rate measurements and thorium, uranium and potassium concentrations in 38 rock samples from the nearby bedrock. On this basis, they discussed the influence of bedrock types and superficial deposits on indoor radon concentrations. A similar study based on indoor and outdoor dose-rate measurements in and around 22 dwellings, and investigation of 23 rock samples was published by Stranden and Strand (1986). Stranden (1985) made various radiometric investigations within and nearby the abandoned mines.

These earlier studies give an overview of the geological factors that influence health hazards associated with radon in the Fen region (Dahlgren 1983, Stranden 1984, Stranden and Strand 1986, Sundal and Strand 2004); however, uranium

and thorium concentrations obtained from rock-sample analyses are spot readings that may not reflect the average nuclide concentrations in geologically complex areas like the Fen region. This can lead to a reduced correlation between indoor radon concentrations and uranium concentrations in samples taken from the underlying bedrock. Ground-based scintillator measurements detected such local-scale variations in gamma-ray exposure rates (Dahlgren 1983). However, not all parts of the Fen Complex could be systematically surveyed using ground-level measurements due to high topographic relief, vegetation and limited accessibility of premises. In addition, gamma-ray exposure-rate measurements provide no information on the identities of the radionuclides present in the ground.

To account for these limitations, the Geological Survey of Norway carried out a helicopter-based gamma-ray spectrometer survey in October 2006 to map explicitly near-surface thorium, uranium and potassium concentrations in the Fen region. Because gamma-ray spectrometer measurements determine concentrations by integrating over finite surface areas, average near-surface concentrations of natural radionuclides are possibly better described by airborne spectrometry than by ground-based measurements. Furthermore, maps from detailed airborne surveying provide what is essentially 2D radionuclide coverage of a region and can be related to spatially varying geological phenomena like overburden and bedrock geology. In doing so, airborne surveying can further refine our understanding of the effects of geology on indoor radon concentrations (Smethurst et al. 2006, 2008, submitted).

Already, several other studies in Norway (Walker 1994, Smethurst et al. 2006, 2008, submitted), Canada (Doyle et al. 1990, Ford et al. 2000), Sweden (Åkerblom 1995) and the U.S. (Nielson et al. 1991) have demonstrated that uranium ground concentrations determined from airborne surveys provide a qualitative first-order approximation of regional variation in indoor radon levels under favourable geological conditions (e.g., regions where bedrock is exposed (Åkerblom 1995)). These studies emphasise that airborne data are only suited for identifying areas with an elevated likelihood of encountering high radon concentrations in dwellings. They cannot be used to identify individual dwellings with elevated radon concentrations because several other factors affect the actual indoor radon concentrations, like emanation coefficient, soil permeability, soil diffusivity, pressure conditions, wind, indoor–outdoor temperature differences, house construction and ventilation (e.g., Nazaroff 1992).

Geology

The Fen Complex has an irregular, oval-shaped surface structure of about 2.3 x 3.0 km (Figure 2a), and formed when alkaline magmas intruded Precambrian gneisses in the Late Neoproterozoic. The complex is dated by $^{40}\text{Ar}/^{39}\text{Ar}$, giving an average age

of 583 ± 15 Ma (Meert et al. 1998). Like other carbonatite areas in Scandinavia (Eckermann 1948, Paarma 1970, Puustinen 1971), the Fen Complex is related to crustal thinning during the break-up of Baltica from Laurentia (e.g., Meert et al. 1998, 2007). Today, only the feeder pipe is visible at the surface because the upper 1–2 km of the former volcanic edifice has been eroded away. Gravity modelling shows that the Fen Complex extends to at least 15 km depth (Ramberg 1973).

The principal types of carbonatite in the Fen Complex are søvite (a calcite carbonatite), rauhaugite (ankeritic or ferrodolomitic carbonatite) and rødberg (a hematite-carbonate rock). Steeply dipping iron-ore veins occur mainly in the hematite-rich rødberg (Svinndal 1973, Andersen 1984). Thorium concentrations are particularly high within the rødberg and ankerite carbonatite (rauhaugite) and associated iron-ore veins (Svinndal 1973, Dahlgren 1983).

An outer halo of fenite (100–400 m wide) surrounds most of the Fen Complex, but is best preserved along the western and southern margins. The fenites formed through alkali metasomatism of country gneisses in the contact zones with certain carbonatitic and alkali-silicate magmas. In this process, SiO_2 was replaced by Na_2O , K_2O and other constituents. In the Fen region, the fenite rocks grade into unaltered granitic gneisses with increasing distance from the carbonatite complex.

Basic alkaline silicate rocks of the ijolite and melteigite group (rocks consisting of nepheline and pyroxene) occur in the southwestern part of the complex. A minor area in the south-central part of the complex consists of vipetoite; a coarse-grained cumulate rock consisting of amphibole, pyroxene, phlogopite and apatite. Damtjernite, a porphyritic ultramafic lamprophyre with megacrysts of phlogopite, amphibole, pyroxene and olivine, occurs as minor bodies scattered within the Fen Complex (Bergstøl and Svinndal 1960, Dahlgren 1994).

Diatremes and dykes of damtjernite, and dykes of carbonatite and phonolite ('tinguaite') penetrate the Proterozoic basement surrounding the Fen Complex, and have been discovered up to 47 km from the complex (Dahlgren 1987, 1994).

The country rock in the Fen region is predominantly composed of medium-grained gneissic granite with interlayered units of mica schists, amphibolite and mica-rich gneisses.

The Fen region was located below sea level after the last glacial period and has risen about 140 m in the past 10,000 years (Bergstrøm 1984). Therefore, large parts of the Fen Complex are covered by post-glacial allochthonous marine silt and clay deposits (~60% of the surface area, Figure 2b) that can reach a thickness of several tens of metres (Bergstrøm 1984). In the Fen region, the bedrock or its weathering products only locally crop out at the surface. In the southern part of the region, the bedrock is partly covered by glacial moraine deposits (Figure 2b).

The Fen Complex has a rather interesting mining history. The Fen iron mines were operated between AD 1657 and 1927 in the eastern part of the Fen Complex, i.e., within the areas

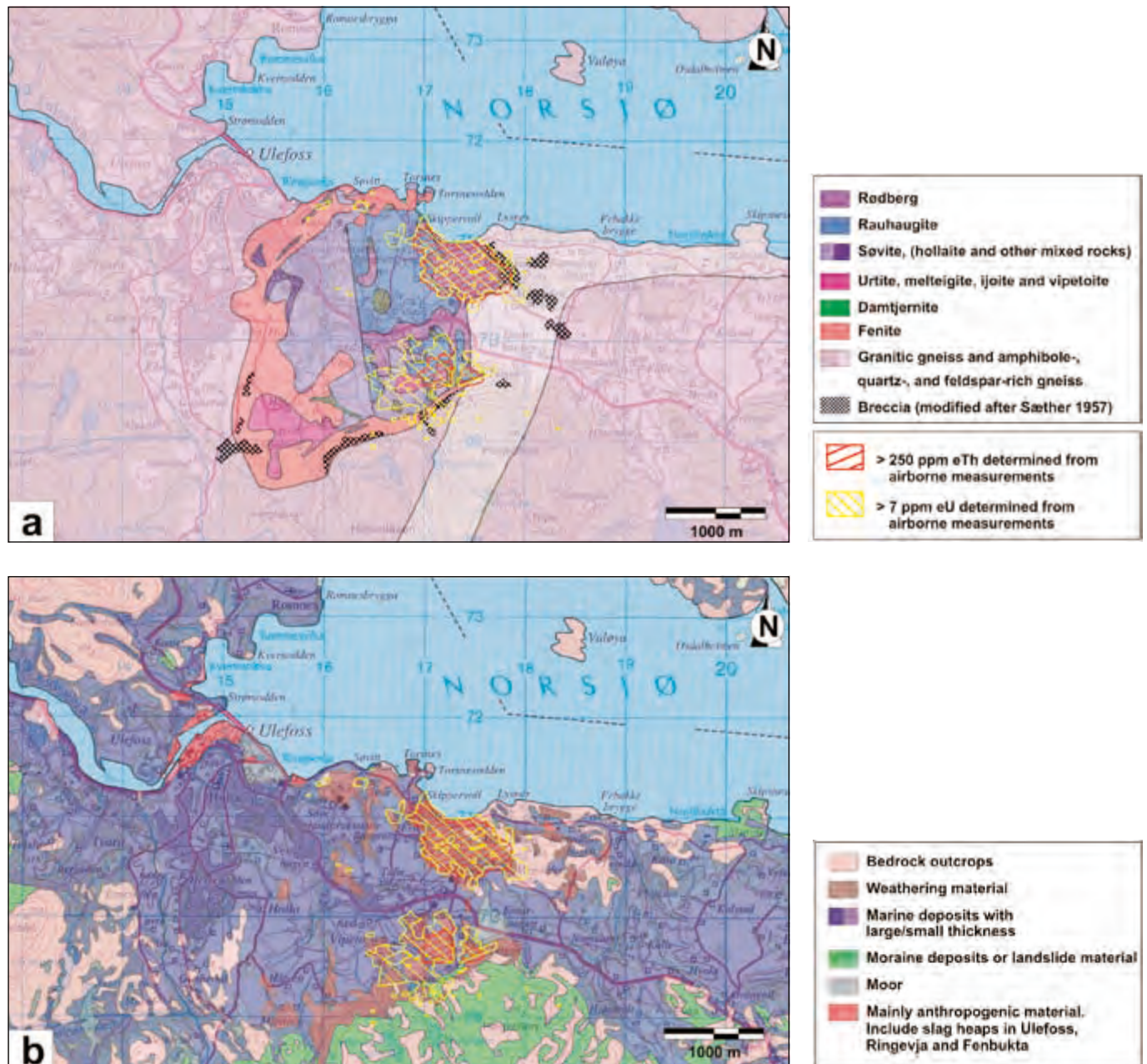


Figure 2. (a) Geological and (b) Quaternary map from the Fen region (modified after NGU database). Red and yellow lines highlight areas with high thorium ($> 250 \text{ ppm eTh}$) and significant uranium concentrations ($> 7 \text{ ppm eU}$) at the surface, respectively. The concentrations were derived from the airborne gamma-ray spectrometer data.

consisting of the high-Th rødberg rocks. Niobium and iron was exploited both in open pits and underground mines in the northwestern part of the complex, i.e., within the low-Th søvitic rocks (Bjørlykke and Svinndal 1960, Dahlgren 2005) (Figure 1). Over the centuries, material from the ancient Fen iron mines

was carried to the Ulefoss Iron Works, and cast-bricks made from slag during the iron ore melting were extensively used in the area for house construction (e.g., Ulefoss farm, Holden farm and Holla church, Dahlgren 1983, Stranden and Strand 1986, Dahlgren 2005).

Measurements and processing of radiometric data

Helicopter measurements were carried out using a 256-channel Exploranium GR820 gamma-ray spectrometer with sodium iodide detector packs with a total crystal volume of 20.9 l (16.7 l downward and 4.2 l upward directed). An area of about 20 km² over the Fen Complex and nearby town of Ulefoss was surveyed. To ensure a uniform and dense data coverage, the measurements were performed along parallel lines with a narrow line spacing of 50 m. The average flying altitude during the measurements was 45 m and an average speed of 70 km h⁻¹ resulted in measurement intervals of about 20 m. Referring to a formula given by Grasty (1987), we expect that about 80% of the gamma-ray counts for a single measurement come from an area on the ground with radius 90 m assuming a height of 45 m and no movements. With a line spacing of 50 m we can assume measurement overlap between adjacent flight lines and deduce that the airborne survey provides 2D data coverage of the region.

Processing of the airborne gamma-ray spectrometer data began with noise reduction of full-spectrum data using the NASVD method (Minty and Hovgaard 2002). Spectral windows were then live-time corrected and aircraft and cosmic background values removed (e.g., IAEA 2003). The spectral-ratio method of Minty (1998) was used to remove the effects of radon in the air below and around the helicopter. Window stripping was used to isolate count rates from the individual radionuclides K, U and Th (IAEA 2003). The topography in parts of the Fen region is rough (15–290 m above sea level), and stripped window count rates were corrected both for variations in ground clearance and ground geometry (Schwarz et al. 1992). Residual line-level errors—remaining inconsistencies between adjacent flight lines—were removed by passing a median filter over the data set (Mauring and Kihle 2006). Finally, radionuclide count rates were converted to ground element concentrations using calibration values derived from calibration pads at the Geological Survey of Norway in Trondheim. The processed data are shown in three maps: equivalent thorium concentration (eTh) in ppm in Figure 3a, equivalent uranium concentration (eU) in ppm in Figure 3b, and potassium concentration in % in Figure 3c.

Results and interpretation

Thorium and uranium concentrations vary strongly in the surveyed region (Figures 3a, b), reflecting the complex geology of the region (Figures 2a, b) and human activities like mining and ore smelting (generating spoil and slag heaps). Only a few decimetres of fine-grained marine sediments are enough to effectively shield gamma radiation emitted by underlying thorium- and uranium-bearing rocks. Consistent with this, areas of fine-grained marine deposits in the Fen area (Figure 2b) are marked by low concentrations of thorium (< 20 ppm eTh, Figure 3a)

and uranium (< 4 ppm eU, Figure 3b) on our maps.

Where rocks of the volcanic complex and their weathering products are at or near the land surface, we observe extremely high thorium concentrations (up to 1460 ppm eTh at Gruveåsen) and significant uranium concentrations (up to 27.3 ppm eU around Rullekollhaugen) (Figures 3a, b). Thorium-232 levels of other typical Nordic rock types are much lower, with a range of 0.5–350 Bq kg⁻¹, corresponding to ~ 0.12–88 ppm Th (Nordic 2000). Radium-226 levels above 150 Bq kg⁻¹, corresponding to ~ 12.2 ppm U, are observed in Norway, not only in carbonatites, but also alum shale and radium-rich granites (Nordic 2000). At first glance, a first-order correlation between thorium and uranium concentrations seems to exist in the carbonatites. However, we will see in the following discussion that the thorium/uranium ratio varies significantly between the different rock types.

In many parts of the surveyed region, human activities significantly affect thorium and uranium ground concentrations derived from the airborne data. In particular, thorium and uranium anomalies on the factory site of the Ulefoss mill (up to 111 ppm eTh and 5.2 ppm eU) are obviously caused by radioactivity from slagheap material (see Figures 1 and 3a, b). The natural uranium and thorium ground concentrations in this area are surely low. Moreover, two uranium anomalies on the premises of the Søve niobium mine area are associated with waste heaps (Dahlgren 2005). Additional excavations and heaps from mining activities and construction can disturb the original ground concentrations and accordingly can affect the estimates for thorium and uranium concentrations of individual rock types derived from airborne data.

Potassium concentrations in the Fen area are in the common range and reach 8.5% (Figure 3c). We want to remark that a distinct transition zone separates areas with larger (> 2.5%) and smaller (< 2%) potassium concentrations in the southeast and in the east of the surveyed region. This radiometric boundary coincides with the transition zone from the feldspar-rich gneissic county rocks and fenites (enriched in potassium by metasomatism) to potassium-poorer carbonatites in the Fen Complex. Analyses of rock samples, presented by Sundal and Strand (2004), also show that fenites have significantly higher potassium concentrations (~ 3.4%) than all kinds of carbonatites (< 1.5%).

Results of our airborne data are consistent with the ones of earlier ground-based exposure-rate measurements (Dahlgren 1983). (Dahlgren (1983) presented terrestrial gamma radiation in exposure rate ($\mu\text{R h}^{-1}$). However, today terrestrial gamma radiation is expressed in dose rate absorbed in air (nGy h^{-1}). To be consistent with the publication from Dahlgren (1983), we decided to use exposure rate $\mu\text{R h}^{-1}$ in this contribution. Conversion to SI-units is: $1 \mu\text{R h}^{-1} = 8.69 \text{ nGy h}^{-1}$ (IAEA 2003).) Although only the most inhabited areas were densely surveyed by Dahlgren (1983), the extrapolated extent of areas with exposure rates > 20 $\mu\text{R h}^{-1}$ resembles areas revealed by airborne surveying to have > 40 ppm Th and > 4 ppm U (Figures 3a, b). Moreover, areas with very high exposure rates of 100 μR

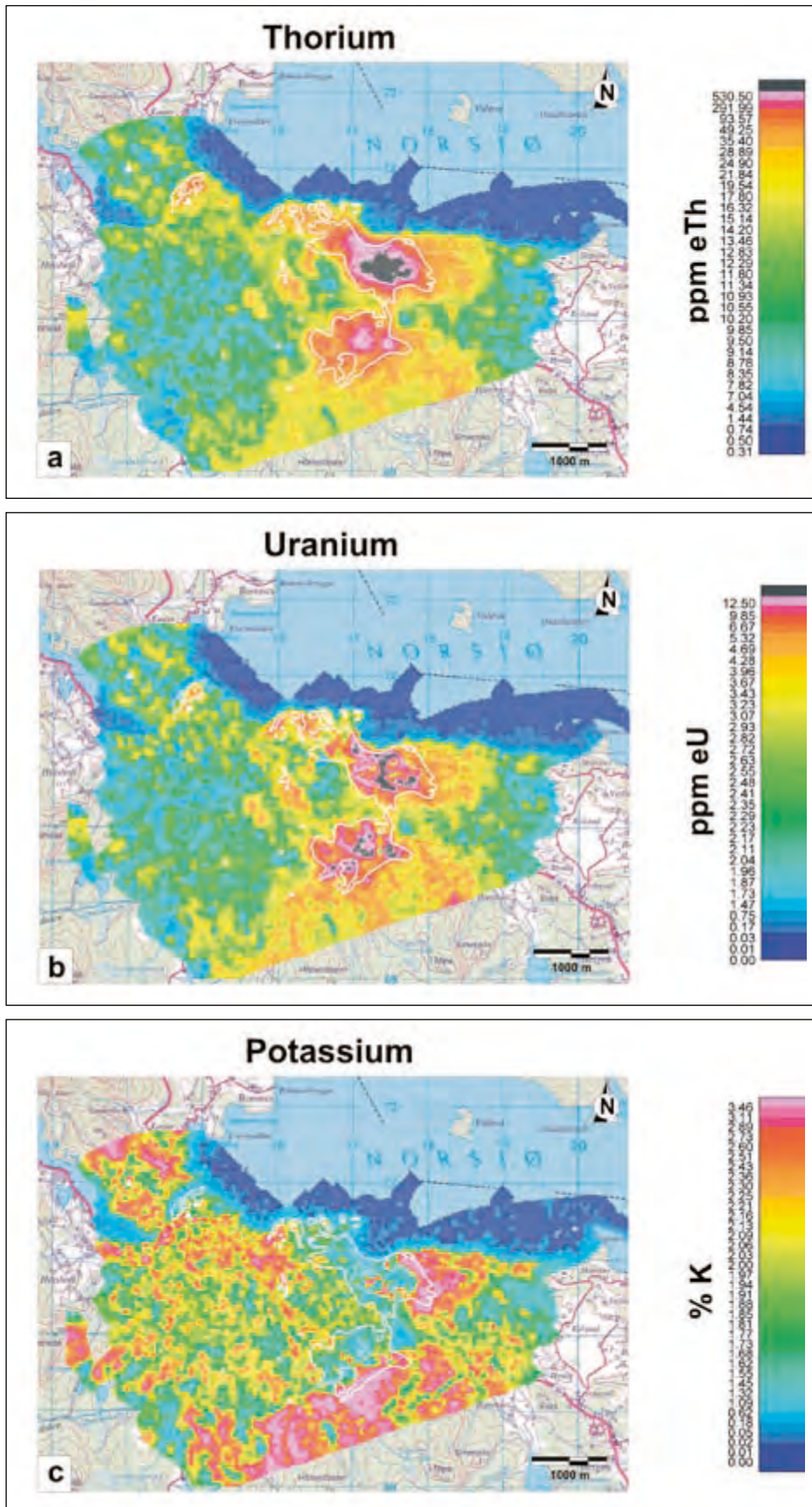


Figure 3. Ground concentrations of the natural radioactive elements (a) thorium, (b) uranium and (c) potassium, obtained from airborne gamma-ray spectrometer measurements are shown in three colour plots. Black colours in (a) and (b) indicate areas with more than 560 ppm eTh and 13 ppm eU, respectively. Continuous and dashed lines encompass areas with exposure rates of more than 20 and 100 $\mu\text{R h}^{-1}$ derived from ground-based scintillator measurements in the early 1980s (Dahlgren 1983). White triangles mark the locations of the farmyards Holden and Ulefoss. They are built up from blocks that were cast of slag from the Ulefoss Iron Works.

h^{-1} generally coincide with areas having thorium concentrations greater than 290 ppm. Concentrations of 4 ppm U, 40 ppm Th and 290 ppm Th are theoretically equivalent to exposure rates of 2.6, 11.48 and 83.23 $\mu\text{R h}^{-1}$, respectively, assuming radioactive equilibrium in the decay series (IAEA 1989). Considering an average potassium concentration of about 1.5% (see Figure 3c), corresponding to 2.26 $\mu\text{R h}^{-1}$, absolute values from the exposure-rate and airborne measurements are comparable.

Comparing results from airborne measurements and rock-sample analyses to quantify Th and U concentrations for different carbonatite types

Results from our airborne measurements and previous rock-sample analyses showed that high thorium concentrations are predominantly found within ankerite and hematite carbonatite rocks in the Fen region (see Table 1). Results from airborne measurements indicate highest thorium concentrations in the region around Gruveåsen, consisting mainly of rødberg carbonatites (183–1460 ppm eTh, Figure 3a). Significantly lower, but still very high thorium concentrations are observed in rødberg carbonatites around Rullekollhaugen and in rauhaugite carbonatites at various localities (33.4–586 and 17.7–545 ppm eTh, respectively). Lower, but still significant concentrations are observed in regions dominated by søvite carbonatites (10.3–150 ppm eTh, see Table 1 and Figure 4). In contrast to thorium concentrations, uranium concentrations derived from airborne measurements are relatively similar for the three carbonatite rock types. Mean values of 10.7, 9.1 and 7.1 ppm eU were obtained for rødberg, rauhaugite and søvite, respectively (see Table 1, Figures 3b and 4).

Results from various rock-sample analyses (Svinndal 1973, Dahlgren 1983, Stranden and Strand 1986, Sundal and Strand 2004) (Table 1) show the same order of decreasing thorium concentrations from rødberg through rauhaugite to søvite carbonatites in the Fen Complex. Except for søvite, mean thorium concentrations from different rock-sample analyses are in the same range (see Table 1). Thorium concentrations measured from rock samples are also in the same range as the concentrations determined from airborne investigations with the exception of rødberg around Gruveåsen. For Gruveåsen, rock-sample analyses by Dahlgren (1983) gave values of 560–3000 ppm Th, whereas the airborne investigation yielded 229–620 ppm eTh. Svinndal (1973) found that increasing concentrations of thorium from søvite to rødberg is very closely linked to the increasing hematite content. He reported highest thorium concentrations in core samples from a hematite-ore heap of the Fen iron mine (up to 4200 ppm) and from a 2 m-thick hematite vein within the rødberg carbonatites (2400–3100 ppm).

Uranium concentrations from different rock-sample investigations vary strongly between the carbonatite types. For example, søvite samples described by Stranden and Strand (1986) have a factor 15 (!) higher mean uranium concentrations than the ones from Sundal and Strand (2004) (Table 1). Referring to Sundal and Strand (2004), søvite is the carbonatite type with the lowest mean uranium concentrations, but Stranden and Strand (1986) present søvite as the carbonatite type with the highest mean uranium concentrations. In a similar way, rock-sample results from Stranden and Strand (1986) show that rødberg carbonatites have higher uranium concentrations than rauhaugite carbonatites, but results from Sundal and Strand

Table 1. Thorium- and uranium-concentrations for different rock types. Results from rock samples are taken from Dahlgren (1983), Stranden and Strand (1986) and Sundal and Strand (2004). For the airborne data, only regions where the bedrock or its weathering material is visible at the surface are considered to derive the thorium and uranium concentrations. Mean values are written in parentheses.

Rock type	Core samples										Airborne investigations		
	Thorium (ppm)					Uranium (ppm)					eTh	eU	n
	I	II ¹	n	III ¹	n	I	II ¹	n	III ¹	n			
Granitic gneiss	2.5–31.0	–	0	15.7–17 (16.5)	3	1.3–9.0	–	0	3.5–3.7 (3.6)	3	5.3–141.0 (28) ²	0.8–13.3 (3.8) ²	356
Fenite	~ 10	45.6	1	5–50 (32.5)	8	~ 2.5	0.6	1	3.3–6.5 (4.1)	8	8.2–44.2 (20)	1.7–7.8 (3.9)	148
Søvite	1–50	2.5–192 (76)	6	5–48 (20)	9	1–60	0.8–113 (25)	6	0.8–4.9 (1.6)	9	10.3–150 (56)	1.9–17.5 (7.1)	103
Rauhaugite	<2000	39–1724 (138)	4	72.5–232 (150)	9	–	1.6–23.4 (10.5)	4	3.3–24.4 (9.8)	9	17.7–545 (232)	2.1–22.6 (9.1)	137
Rødberg (Gruveåsen)	560– 3000	41–2950 (985)	12	97–1475 (775)	9	5–40	3.5–44.5 (12.9)	12	1.6–8.9 (5.7)	9	183–1460 (620)	1.8–25.1 (10.7)	259
Rødberg (Rullekoll- haugen)	160–330					3.5–20					33.4–586 (229)	4.0–27.3 (10.8)	25

¹ Stranden and Strand (1986) and Sundal and Strand (2004) presented activity concentrations in Bq kg^{-1} . Activity concentrations are converted to corresponding thorium, uranium and potassium concentrations (IAEA 2003).

² Gneiss on the Gruveåsen, in the vicinity of rødberg, are not considered here. References: I: Dahlgren (1983); II: Stranden and Strand (1986); III: Sundal and Strand (2004). n = number of samples. The number of samples from Dahlgren (1983) is unknown.

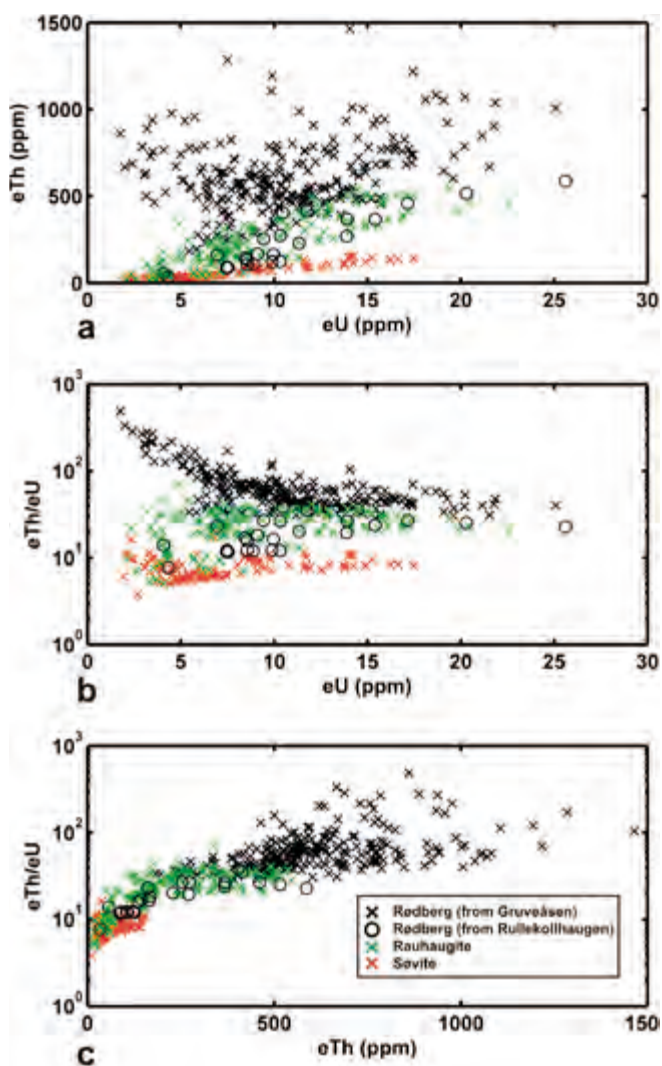


Figure 4. Relationships between (a) uranium and thorium concentrations, (b) thorium/uranium ratio and uranium concentration, and (c) thorium/uranium ratio and thorium concentration for different rock types. Each data point is related to the thorium and uranium ground concentrations from an individual airborne spectrometer measurement after processing. Only points in regions where bedrock or its weathering material is mapped at the surface are considered. Regions dominated by the carbonatites søvite and rauhaugite are marked with red and green crosses, respectively. Rødberg carbonatites from the Gruveåsen and close to the Rullekollhaugen are shown as black crosses and black circles, respectively.

(2004) show the opposite. Particularly in rock-sample analyses from Dahlgren (1983) and Stranden and Strand (1986), the obtained uranium concentrations vary a lot for individual carbonatite types.

These inconsistencies indicate the limitations of rock-sample investigations to provide 'average' uranium (and thorium) concentrations in the geologically very complex Fen region. It is difficult to classify carbonatites by uranium content and accordingly to assess their associated radon risk from analysis of individual samples. In contrast, concentrations obtained from airborne spectrometry represent an average property of the rocks within an area on the ground of some hundreds of square meters and thus lend themselves to establishing large-scale geochemical differences between rock types with complex internal variations.

Thorium/uranium ratios

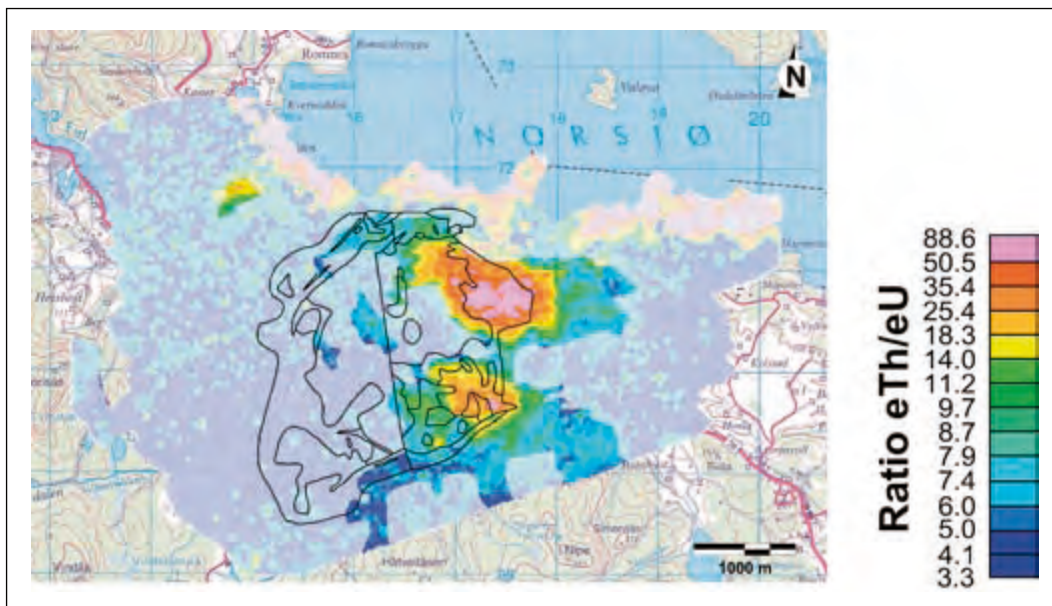
Although søvite, rauhaugite and rødberg have similar uranium concentrations (Figure 4), the ratio of thorium-to-uranium concentration is a very suitable parameter to distinguish the three carbonatite types. Except for rødberg-dominated rocks around Rullekollhaugen (thorium/uranium ratios of 10–30), rødberg-dominated rocks have clearly higher thorium/uranium ratios (> 25 around the Gruveåsen) than rauhaugite-dominated rocks (~ 10 – 30 west of Gruveåsen and around Rullekollhaugen). Areas dominated by søvite have significantly lower ratios (< 10), like in the central western part of the volcanic region and in Vipeto, southwest of Rullekollhaugen. Around Rullekollhaugen, the boundary between rauhaugite- and søvite-dominated areas coincides with a border that separates regions with higher (> 14) and lower (< 12) thorium/uranium ratios (see Figures 2a and 5). This is a remarkable correlation considering the limited spatial resolution of airborne investigations, the geological complexity of this area and the strong variation in uranium concentrations observed in the rock samples for each carbonatite type.

Different thorium/uranium ratios for the carbonatite types are in agreement with the outdoor gamma count rates measured by Stranden and Strand (1986). They noted that in rødberg-, rauhaugite- and søvite-dominated areas, 97%, 85% and 58%, respectively, of the total count rates originated from thorium. Similar uranium levels, but strongly varying thorium levels in søvite, rauhaugite and rødberg also explain Sundal and Strand's (2004) observation that there is only a weak correlation between indoor gamma dose rates and indoor radon concentrations in the Fen Complex. It is also consistent with geochemical mapping of stream sediments from Ryghaug (1986) that gave no indication of a correlation between thorium and uranium concentrations in the Fen Complex.

Our results are also in agreement with investigations from carbonatite complexes all over the world. Wolley and Kempe (1989) suggested average thorium/uranium ratios of 6, 7 and nearly 40 for calcio-, magnesio- and ferrocarnatites, respectively, based on investigations of various carbonatite complexes. Our ratios of 7.9, 25.5 and 54.7 for søvite (a calcite carbonatite), rauhaugite (ankeritic or ferrodolomitic carbonatite) and rødberg (a hematite carbonate rock), respectively, are in agreement with but slightly higher than the general ratios, possibly indicating weathering effects responsible for depletion of uranium relative to thorium. Andersen (1984) suggested that rødberg and the associated hematite-ore veins formed by secondary hydrothermal oxidation processes from the pre-existing rauhaugite. How such secondary processes can change actual uranium and thorium concentrations was not mentioned in this publication.

Most regions consisting of fenites and gneissic country rocks are characterised by low thorium/uranium ratios (< 12). However, east of the rødberg-dominated part of Gruveåsen, high thorium/uranium ratios are observed in gneiss as far as 250 m away from the carbonatite area. This compositional boundary is not a sharp one, but related to 'rødberg' veining

Figure 5. Ratios of thorium and uranium concentrations determined from airborne gamma-ray spectrometer data. To focus on regions whose ratios are not affected by sediment coverage, regions with low thorium and/or uranium concentration (threshold: $\text{ppm } e\text{Th} + 15 \times \text{ppm } e\text{U} < 70$) are covered with a semi-transparent mask. Boundaries of geological units (see Figure 2a) are indicated with black lines.



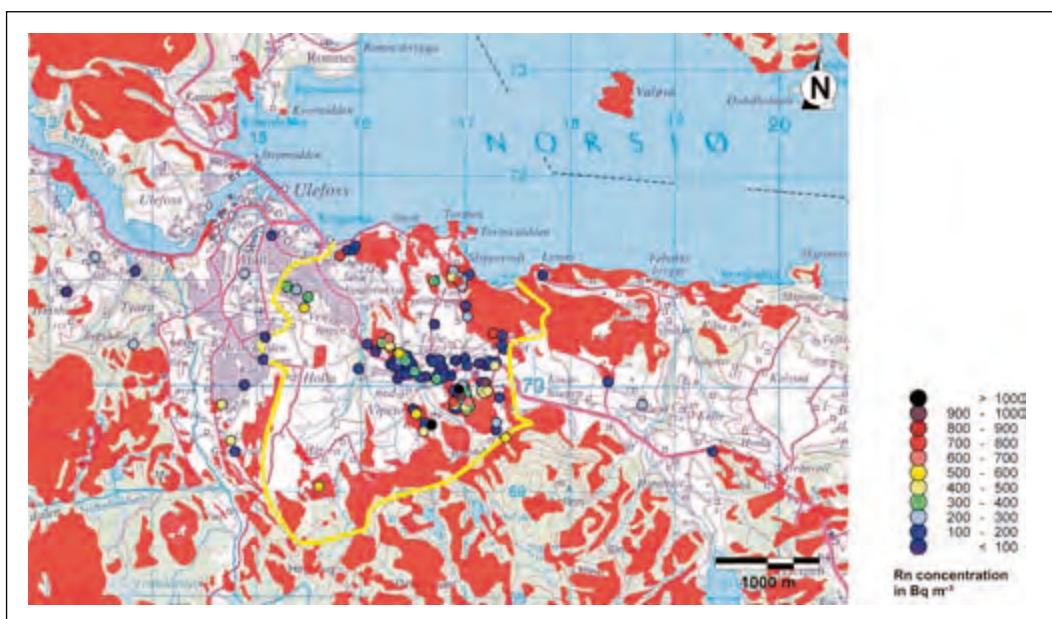
and carbonatite as matrix in brecciated gneiss (see Figure 2a) associated with ubiquitous secondary alteration (Andersen 1984). Areas dominated by damtjernite, vipeotite, urtite, iljoite and melteigite rocks are relatively small (Ramberg 1973) and their radionuclide concentrations are difficult to estimate from the airborne data. However, determination of low uranium and thorium ground concentrations in the southwestern part of the complex (see Figures 2a, b) suggest that iljoite-melteigite rocks are not enriched in natural radionuclides.

Relating uranium concentrations to indoor radon concentrations

Dense airborne surveying and accurate drift geology and bed-rock geology maps enable a detailed analysis of the relationship

between geology and indoor radon concentrations. For this purpose, we considered indoor radon concentrations measured by the Norwegian Radiation Protection Authority in 139 dwellings in Nome municipality (Figure 6). The indoor measurements were carried out with CR-39 etched track detectors (Sundal and Strand 2004). Since the radon diffusion half-time of the detector design is greater than a few minutes, measurements are considered to be insensitive to radon-220. The majority of indoor radon-concentration measurements were performed from February until May 2000 and the data were corrected for seasonal variations. One hundred and six of the indoor radon measurements were collected in 2000, and 33 were collected in the winter of 1996/97. Although two measurements were conducted in each dwelling (usually in the living room and in the

Figure 6. Indoor radon concentration in the Fen region. Coloured circles indicate locations of houses, for which results from indoor radon-concentration measurements are available. Red colours mark regions where either the bedrock or its weathering products crop out at the surface (see also Figure 2b). Yellow line sketches the extent of the volcanic region (see also Figure 2a). Results from indoor radon-concentration measurements based on material provided by Nome municipality.



bedroom nearest the ground), we consider here only the highest value. Because Nome municipality and its residents are generally aware that radon is associated with specific rock types in the Fen Complex, the majority of measurements are in dwellings standing on carbonatites (Figure 6). Thorium-/uranium-rich material from the Fen region was not used in the considered dwellings, and Sundal and Strand (2004) reported that building materials used for houses in the Fen region contain low levels of radioactivity. We had, unfortunately, no adequate data about the dwellings such that influence from building construction and ventilation could not be investigated. Radon from water supplies is not considered a dominant indoor radon source in the Fen region (Dahlgren 1983, Ryghaug 1984, Strandén 1985).

Average indoor radon concentrations in houses built on marine deposits are distinctly lower (mean value: 160 Bq m^{-3} ; 22% above 200 Bq m^{-3}) than in houses built directly on bedrock or its weathering products (mean value: 350 Bq m^{-3} ; 69% above 200 Bq m^{-3}) (Figures 6 and 7a). The marine sediments are mainly silts with significant clay contents of 19–20% (Bergstrøm 1984). Although fine-grained sediments may have a high radon emanation coefficient (e.g., Greeman and Rose 1996), their low permeability prohibits transport of the radon produced in them towards dwellings. Also, because clayey material is virtually impermeable, only a small portion, if any, of the radon gas emanating from bedrock beneath the clay layer is likely to reach the dwellings (Åkerblom 1986, Nazaroff 1992). This is unless a construction punctures the marine layer, exposing the structure to radon from deeper sources.

Although distinctly lower than on bedrock, the incidence of elevated radon levels in dwellings on the marine deposits is still high in the Fen region. These elevated radon levels could be caused by local variations in the nature of the substrate (e.g., higher portion of coarse-grained material) not evident in the generalised drift geology map, and/or the possible presence of radium-bearing soil in places. It is also possible that some spots in the clayey marine deposits with higher radium concentrations remain invisible to airborne spectrometry because clays' high moisture content leads to an increased attenuation of the radioactivity in the soil, thus underestimating the actual radioactive-element ground concentrations (Wilford et al. 1997). Finally, Åkerblom (1986), who described indoor radon risks in Sweden, emphasised that for all soil conditions there is a risk that indoor radon levels will exceed 200 Bq m^{-3} if sufficient quantities of soil gas leak into the house due to bad sealing.

In areas where the bedrock or its weathered products are exposed, radon concentrations in indoor air vary strongly ($10\text{--}1292 \text{ Bq m}^{-3}$; $\sigma = 271.7 \text{ Bq m}^{-3}$) and the percentage of dwellings with indoor radon concentrations above 200 Bq m^{-3} is 69%.

Only a very weak positive correlation is observed between indoor radon concentrations and uranium ground concentrations determined from the airborne data (see Figure 7a), consistent with observations from other studies (e.g., Smethurst et al. submitted). Locally, radon concentrations vary widely because indoor radon measurements are strongly influenced by the positions of the rooms that are measured, home construction methods, heating and ventilation solutions,

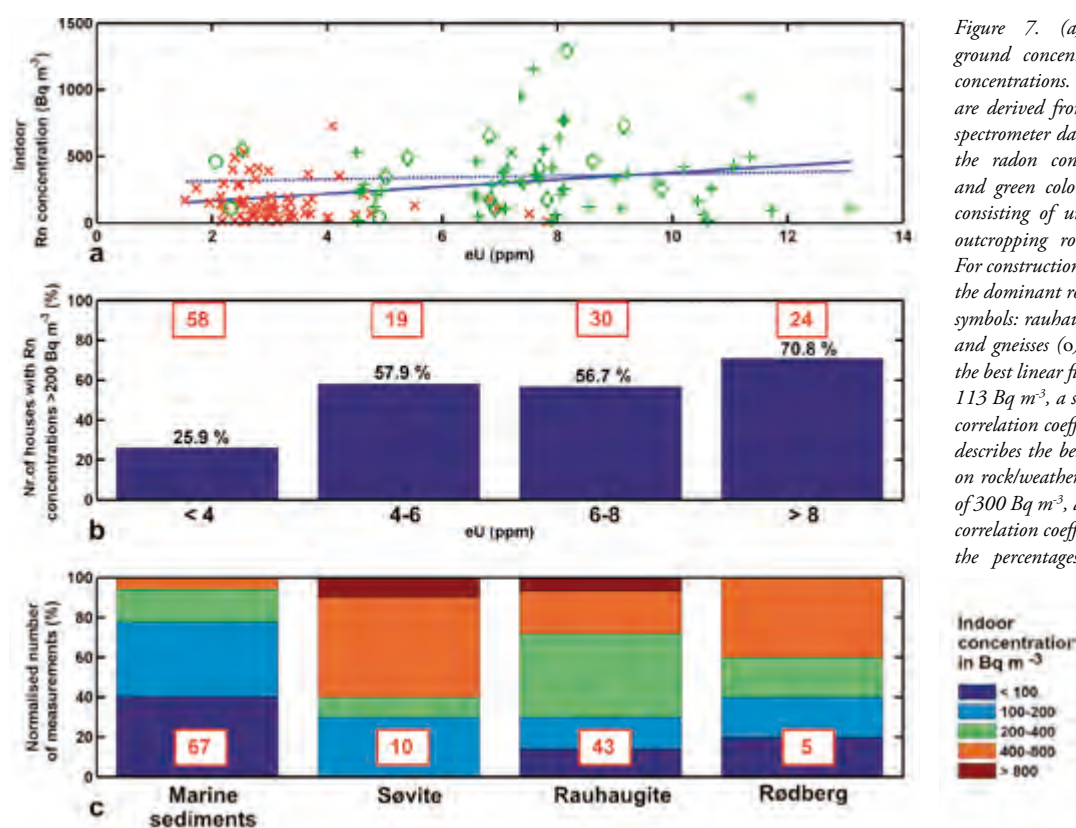


Figure 7. (a) Relationship between uranium ground concentrations and radon indoor activity concentrations. Uranium ground concentrations are derived from the processed airborne gamma-ray spectrometer data at the locations of houses in which the radon concentration was measured. The red and green colours indicate houses built on ground consisting of unconsolidated marine sediments and outcropping rock/weathering material, respectively. For constructions placed on rock/weathering material, the dominant rock types are distinguished by different symbols: rauhaugite/rødberg (+), søvite (◇), fenite (x) and gneisses (○). The blue, continuous line describes the best linear fit to all data. It has an axis intercept of 113 Bq m^{-3} , a slope of $26.4 \text{ Bq m}^{-3} \text{ ppm}$ and a linear correlation coefficient of 0.316. The blue, dashed line describes the best linear fit to data from houses built on rock/weathering material. It has an axis intercept of 300 Bq m^{-3} , a slope of $6.7 \text{ Bq m}^{-3} \text{ ppm}$ and a linear correlation coefficient of 0.47. (b) Histogram showing the percentages of dwellings with indoor radon concentrations $> 200 \text{ Bq m}^{-3}$ for different ranges of uranium ground concentrations. (c) Normalised histogram showing the indoor radon concentrations for marine sediments and different rock types cropping out at the surface. In (b) and (c), the corresponding number of measurements are plotted in the red boxes.

the presence of openings in the structure to the ground, local ground conditions, especially permeability in the ground, and local variation in radon emanation coefficients (e.g., Nazaroff 1992). This invariably complicates attempts to establish relationships between indoor radon concentrations and outdoor measurements made above the ground. Nevertheless, some studies (Ford et al. 2000, Smethurst et al. submitted) demonstrate that there can be a distinct correlation between uranium ground concentrations from airborne investigations and percentages of dwellings with indoor radon concentrations above a specific threshold. This kind of relationship also seems to hold for indoor radon and equivalent uranium measurements for the Fen region. The percentage of dwellings with indoor radon concentrations over 200 Bq m^{-3} are plotted against equivalent uranium concentrations, obtained from airborne measurements, in Figure 7b. The trend is less pronounced than observed in the studies of Ford et al. (2000) and Smethurst et al. (2006, 2008, submitted), presumably due to the lower number of indoor radon measurements available in the Fen region.

There is no clear relationship between indoor radon concentrations and different carbonatite types (see Figures 6 and 7c). This is to be expected because the airborne measurements indicate similar average uranium concentrations for the different carbonatite types. It seems that gneisses outside of the Fen Complex cause lower indoor radon concentrations than all carbonatite types. However, too few indoor measurements are available from the gneissic region to verify this observation.

Like us, Sundal and Strand (2004) observed fewer high radon concentrations in dwellings on marine deposits than on exposed bedrock (carbonatite)¹. Again, like us, they observed that radon levels are similar in dwellings on different carbonatite types and they suggested that high indoor radon concentrations were caused by søvite, rauhaugite and rødberg rocks in the building ground. They mentioned that uranium concentrations determined from their rock samples (see Table 1) may not be representative for søvite rocks because there is a contradiction of the low uranium concentrations in their rock samples and high indoor levels in the adjacent dwellings.

Conclusions

Airborne gamma-ray spectrometer measurements provided us with three maps showing ground concentrations of thorium-232, uranium-238 and potassium-40 in the Fen Complex and around the nearby town of Ulefoss. Extremely high thorium concentrations, and significant uranium concentrations, were observed in parts of the Fen Complex that were not covered by post-glacial marine sediments. The highest thorium concentra-

tions are found in the area around the Gruveåsen (up to 1460 ppm eTh). We observe very different thorium concentrations in the different carbonatite lithologies (mean values: 425 ppm eTh (rødberg), 232 ppm eTh (rauhaugite) and 56 ppm eTh (søvite)), but mean uranium concentrations are relatively similar (mean values: 10.7 ppm eU (rødberg), 9.1 ppm eU (rauhaugite) and 7.1 ppm eU (søvite)). Thorium/uranium ratios from our airborne data are suited for differentiating between the different carbonatites and can be used to refine and improve our knowledge of the spatial distribution of these lithologies.

Results from airborne investigations are in agreement with the results from former investigations (rock-sample studies and ground-based scintillator measurements). However, airborne investigations are less sensitive to small-scale variations in radionuclide concentration than rock-sample measurements, and probably better represent average concentrations for individual rock types in the complex Fen region.

Percentages of dwellings with indoor radon concentrations $> 200 \text{ Bq m}^{-3}$ correlate with increasing uranium ground concentrations in the Fen region. Where fine-grained, low-permeability marine sediments cover bedrock, uranium concentrations in the ground are low and high radon concentrations in indoor air are less common than in dwellings on other kinds of overburden or bedrock. Where bedrock and associated weathering products are exposed, different carbonatite types exhibit similar distributions of indoor radon concentrations. For all carbonatite types, dwellings were found that had very high indoor radon concentrations $> 700 \text{ Bq m}^{-3}$. In summary, elevated radon concentrations occur where carbonatites or their weathered products are close to the surface, and are equally associated with all types of carbonatite.

Acknowledgements

We thank John Peterson from the Argonne National Laboratory for his very helpful comments about the health risks of thorium and its decay products. Bjørn Ivar Rindstad (NGU) supported us with cartographical material. We thank Per Ryghaug and Håvard Gautneb (NGU) for helpful discussions about correlations of uranium and thorium concentrations in the Fen region, and Morten Rask Arnesen from Nome municipality for providing indoor radon measurements. Terje Strand of Oslo University supported us with important information about their radon measurements and the potential health risk related to radon-220 in the Fen region. The airborne gamma-ray survey was co-financed by Nome municipality and NGU. Agemar Siehl and an anonymous reviewer are thanked for comments that helped improve the paper.

¹ Sundal and Strand (2004) published results from 95 dwellings from the Fen region. It is quite likely that they partly used measurements from the same dwellings that we do. Accordingly, their and our data sets cannot be considered independent. Because information about the actual localities of investigated dwellings were not given in their publication, we did not use their data for relating uranium ground concentrations and indoor radon activities.

References

- Andersen, T. (1984) Secondary processes in carbonatites: petrology of 'rødberg' (hematite-calcite-dolomite carbonatite) in the Fen central complex, Telemark (South Norway). *Lithos*, **17**, 227–245.
- Argonne National Laboratory (2005) Human Health Fact Sheet. *Natural Decay Series: Radium*.
- Barth, T.F.W. and Ramberg, I.B. (1966) The Fen circular complex. In Tuttle, O.F. and Gittens, J. (eds.) *Carbonatites*, John Wiley and Sons, New York, pp. 225–257.
- Bergstøl, S. and Svinndal, S. (1960) The carbonatites and per-alkaline rocks of the Fen area. *Norges geologiske undersøkelse*, **208**, 99–105.
- Bergstrøm, B. (1984) Nordagutu. Beskrivelse til kvartærgeologisk kart. *NGU skrifter*, **57**, 44 pp.
- Bjørlykke, H. and Svinndal, S. (1960) Fen Region: Mining and exploration work. *Norges geologiske undersøkelse*, **208**, 105–110.
- Brøgger, W.C. (1921) Die Eruptivgesteine des Kristianiagebietes: IV. Das Fensgebiet im Telemark, Norwegen. *Det Norske Videnskaps-Akademi i Oslo, Skrifter. I. Mat.-Naturv. Klasse*, **1920**, **9**, 408 pp.
- Conrath, S.M. and Kolb, L. (1995) The health risk of radon. *Journal of Environmental Health*, **58**, 24–26.
- Dahlgren, S. (1983) Naturlig radioaktivitet i berggrunnen, gamma-strålingskart, Fensfeltet, Telemark, scale 1:10,000. *Prosjekt temakart, Telemark*.
- Dahlgren, S. (1987) *The satellitic intrusions in the Fen Carbonatite – Alkaline rock province, Telemark, Southeastern Norway*. PhD thesis, University of Oslo, 350 pp.
- Dahlgren, S. (1994) Late Proterozoic and Carboniferous ultramafic magmatism of carbonatitic affinity in southern Norway. *Lithos*, **31**, 141–154.
- Dahlgren, S. (2005) Miljøgeologisk undersøkelse av lavradioaktivt slagg fra ferroniobproduksjonen på Søve 1956–1965. *Regiongeologen for Buskerud, Telemark og Vestfold, Rapport nr.1*, 47 pp.
- Doyle, P.J., Grasty, R.L. and Charbonneau, B.W. (1990) Predicting geographic variations in indoor radon using airborne gamma-ray spectrometry. *Current Research, Part A, Geological Survey of Canada*, **90–1A**, 27–32.
- Eckermann, H. (1948) The alkaline district of Alnö island. *Sveriges Geologiska Undersökning, Serie Ca*, **36**, 9–36.
- Ford, K.L., Savard, M., Dessau, J.-C., Pellerin, E., Charbonneau, B.W. and Shives, R.B.K. (2000) The role of gamma-ray spectrometry in radon risk evaluation; a case history from Oka, Quebec. *Geoscience Canada*, **28**, 59–64.
- Greeman, D.J. and Rose, A.W. (1996) Factors controlling the emanation of radon and thoron in soils of the eastern U.S.A. *Chemical Geology*, **129**, 1–14.
- Grasty, R.L. (1987) The design, construction and application of gamma-ray spectrometer calibration pads–Thailand. *Geological Survey of Canada, Paper 87–10*, 34 pp.
- Heinrich, E.W. (1966) *The geology of carbonatites*, Rand McNally and Co., Chicago, 555 pp.
- IAEA (1989) Construction and Use of Calibration Facilities for Radiometric Field Equipment. *Technical Reports Series No. 309*, Vienna, Austria.
- IAEA (2003) Guidelines for radioelement mapping using gamma ray spectrometry data. *IAEA–TECDOC–1363*, Vienna, Austria. 173 pp.
- ICRP (1981) Limits for Inhalation of Radon Daughters by Workers. *International Commission on Radiological Protection (ICRP) Report No. 32*, 24 pp.
- Landreth, J.O. (1979) Mineral potential of the Fen Alkaline Complex. Ulefoss, Norway. *Bergvesenet Rapport BV 1332*, 30 pp.
- Mauring, E. and Kihle, O. (2006) Levelling aerogeophysical data using a moving differential median filter. *Geophysics*, **71**, L5–L11.
- Meert, J.G., Torsvik, T.H., Eide, E.A. and Dahlgren S. (1998) Tectonic Significance of the Fen Province, S. Norway: Constraints from Geochronology and Paleomagnetism. *The Journal of Geology*, **106**, 553–564.
- Meert, J.G., Walderhaug, H.J., Torsvik, T.H. and Hendriks, B.W.H. (2007) Age and paleomagnetic signature of the Alnö carbonatite complex (NE Sweden); additional controversy for the Neoproterozoic paleoposition of Baltica. *Precambrian Research*, **154**, 159–174.
- Minty, B.R.S. (1998) Multichannel models for the estimation of radon background in airborne gamma-ray spectrometry. *Geophysics*, **63**, 1986–1996.
- Minty, B.R.S. and Hovgaard, J. (2002) Reducing noise in gamma-ray spectrometry using spectral component analysis. *Exploration Geophysics*, **33**, 172–176.
- Nazaroff, W.W. (1992) Radon transport from soil to air. *Reviews of Geophysics*, **30**, 137–160.
- Nielson, D.L., Cui, P. and Ward, S.H. (1991) Gamma-Ray Spectrometry and Radon Emanometry in Environmental Geophysics. *Investigations in Geophysics*, **5**, 219–250.
- Nordic (2000) Naturally occurring radioactivity in the Nordic countries–recommendations. *The Radiation Protection Authorities, Denmark, Finland, Iceland, Norway and Sweden*, 80 pp. See also: <http://www.ssi.se/english/Flaggboken.pdf> (05.11.2007).
- OECD NEA and IAEA (2006) *Uranium 2005: Resources, Production and Demand*, OECD Publishing, 388 pp.
- Paarma, H. (1970) A new find of carbonatite in North Finland, the Sokli plug in Savukoski. *Lithos*, **3**, 129–133.
- Puustinen, K. (1971) Geology of the Siilinjärvi carbonatite complex, Eastern Finland. *Bulletin de la Commission geologique de Finlande*, **249**, 1–43.
- Ramberg, I.B. (1973) Gravity studies of the Fen Complex, Norway, and their petrological significance. *Contributions to Mineralogy and Petrology*, **38**, 115–134.
- Ryghaug, P. (1984) En uran-anomali i Telemark og dennes innvirkning på radon-innholdet i drikkevann. *Vann*, **2**, 172–181.
- Ryghaug, P. (1986) Stream-sediment geochemical survey of the Fen carbonatite/alkaline complex and surrounding areas. *Prospecting in Areas of Glaciated Terrain*, **7**, 187–200.

- Schwarz, G.F., Klingele, E.E. and Rybach, L. (1992) How to handle rugged topography in airborne gamma-ray spectrometry surveys. *First Break*, **10**, 11–17.
- Smethurst, M.A., Strand, T., Finne, T.E. and Sundal, A.V. (2006) Gammaspektrometriske flymålinger og radon: anvendelse av gammaspektrometriske fly- og helikoptermålinger til identifisering av radonutsatte områder—analyse basert på målinger på Østlandet *StrålevernRapport 2006:12*, 20 pp., Østerås: Statens strålevern.
- Smethurst, M.A., Sundal, A.V., Strand, T. and Bingen, B. (2008) Testing the performance of a recent radon-hazard evaluation in the municipality of Gran, eastern Norway. In Slagstad, T. (ed.) *Geology for Society*, Geological Survey of Norway Special Publication, **11**, in press.
- Smethurst, M.A., Strand, T., Sundal, A.V. and Rudjord, A.L. (submitted) A novel approach to radon-hazard mapping: Utilizing relationships between airborne gamma-ray spectrometer measurements and indoor radon concentrations. *Science of the Total Environment*.
- Solli, H.M., Andersen, A., Stranden, E. and Langård, S. (1985) Cancer incidence among workers at a niobium mine. *Scandinavian Journal of Work, Environment & Health*, **11**, 7–13.
- Strand, T., Ånestad, K., Ruden, L., Ramberg G.B., Jensen C.L., Wiig, A.H. and Thommesen G. (2001) Kartlegging av radon i 114 kommuner—Kort presentasjon av resultater. *StrålevernRapport 2001:6*, 14 pp., Østerås: Statens strålevern.
- Stranden, E. (1984) Thoron (^{220}Rn) daughter to radon (^{222}Rn) daughter ratios in thorium-rich areas. *Health Physics*, **47**, 784–785.
- Stranden, E. (1985) The radiological impact of mining in a Th-rich Norwegian area. *Health Physics*, **48**, 415–420.
- Stranden, E. and Strand, T. (1986) Natural gamma radiation in a Norwegian area rich in thorium. *Radiation Protection Dosimetry*, **16**, 325–328.
- Sundal, A.V. and Strand, T. (2004) Indoor gamma radiation and radon concentrations in a Norwegian carbonatite area. *Journal of Environmental Radioactivity*, **77**, 175–189.
- Svinndal, S. (1973) Thorium i Fensfeltet. *NGU Report 1162*, 28 pp.
- Sæther, E. (1957) The alkaline rock province of the Fen area in southern Norway. *Det Kongelige Norske Videnskabers Selskabs Skrifter*, **1**, 1–150.
- Walker, P. (1994) Airborne radon hazard mapping—Løten, Hedmark county, Norway. *NGU Report 1993.046*, 50 pp.
- Wilford, J.R., Bierwirth, P.N. and Craig, M.A. (1997) Application of airborne gamma-ray spectrometry in soil/regolith mapping and applied geomorphology. *AGSO—Journal of Australian Geology & Geophysics*, **17**, 201–216.
- Wolley, A.R. and Kempe, D.R.C. (1989) Carbonatites: Nomenclature, average chemical compositions and element distribution. In Bell, K. (ed.) *Carbonatites—Genesis and Evolution*, Unwin Hyman Ltd., London, pp. 1–14.
- Åkerblom, G. (1986) Investigations and mapping of radon risk areas. In Wolff, F.C. (ed.) *Geology for environmental planning*, Geological Survey of Norway Special Publication, **2**, 96–106.
- Åkerblom, G. (1995) The use of airborne radiometric and exploration survey data and techniques in radon risk mapping in Sweden. Application of uranium exploration data and techniques in environmental studies. *IAEA—Tecdoc*, **827**, 159–180.

Testing the performance of a recent radon-hazard evaluation in the municipality of Gran, eastern Norway

Mark A. Smethurst¹, Aud Venke Sundal², Terje Strand³ and Bernard Bingen¹

¹Geological Survey of Norway (NGU), 7491 Trondheim, Norway.

²Institute of Geography, University of Edinburgh, Drummond Street, Edinburgh EH8 9XP, UK.

³Department of Physics, University of Oslo, P.O. Box 1048 Blindern, 0316 Oslo, Norway.

E-mail: mark.smethurst@ngu.no

The Geological Survey of Norway and Norwegian Radiation Protection Authority have produced a new overview of radon hazard in the most densely populated part of Norway around the capital city, Oslo, and Oslofjord. We look closely at the performance of the radon-hazard evaluation within a rectangular area 520 km² in size centred on the municipality of Gran. The uranium-rich alum shale and superficial deposits associated with it are the principal sources of radon in the area. Small, isolated granite bodies and local, high-permeability glaciofluvial deposits are likely to contribute to elevated radon-hazard levels. The multidisciplinary hazard evaluation is based on direct measurements of radon in indoor air, bedrock geology, drift geology, and radon-daughter (bismuth) mapping using helicopter-borne instruments. Our testing of the hazard evaluation shows that combining signs of radon hazard from each of the data sets in the Gran region produces a liberal hazard map that encloses most of the known areas of severe radon contamination in dwellings, and reveals additional uninhabited areas where similar levels of contamination can be expected if those areas are taken into use for residential purposes without mitigating action. The hazard evaluation in the Gran area is 80.7% efficient in enclosing high indoor radon measurements in the high-hazard zone when this zone occupies 50% of the total geographic area. The probability of this distribution happening by chance is 0.054%. If the hazard prediction bore no relation to the actual distribution of high indoor radon measurements, the efficiency would be around 50%. The radon-hazard evaluation works well over the alum shale and should be used to improve the efficiency of indoor radon mapping programmes and develop strategies for the implementation of radon mitigation measures.

Smethurst, M.A., Sundal, A.V., Strand, T. and Bingen, B. (2008) Testing the performance of a recent radon-hazard evaluation in the municipality of Gran, eastern Norway. In Slagstad, T. (ed.) *Geology for Society*, Geological Survey of Norway Special Publication, 11, pp. 145–154.

Introduction

In Norway, long-term exposure to radon and its progenies are responsible for 14% of the new cases of lung cancer each year. This corresponds to nearly 300 cases per year. Given the generally poor prognosis for lung cancer, radon is likely to be responsible for as many deaths each year as occur on the roads of Norway. Furthermore, exposure to radon gas in the Norwegian population is increasing due to changes in the way we build houses and how we use the spaces within them (Strand et al. 2001, Strand et al. 2003).

Investigations have shown that the building substrate is the dominant source of radon in Norwegian dwellings (Stranden 1986). The geology of the area around Oslo is complex (Lutro and Nordgulen 2004), characterised by sharp transitions from uranium-rich rock types like alum shale and granite—traditionally associated with hazardous levels of radon in indoor air—to uranium-poor rock types like the majority of sedimentary rocks and mafic igneous rocks. The geological

complexity is increased by the presence of superficial deposits that vary widely in permeability from impermeable marine clay to highly permeable glaciofluvial sand and gravel. Permeability is a vital factor governing the transport of radon gas in the ground (Arvela et al. 1994, Sundal et al. 2004). The fact that geological factors influencing the production and transportation of radon gas vary dramatically in and around the capital city, dictates a need in society for geological information that can help identify the areas most likely to be affected by radon.

Smethurst et al. (2006) (also see Smethurst et al. submitted) assembled geological information for the area around Oslo and Oslofjord and interpreted it in terms of potential radon hazard as part of the Geological Survey of Norway's recent *geology in the Oslo region* (GEOS) initiative (Figure 1). Naturally, the Norwegian Radiation Protection Authority was an active participant in this part of the GEOS initiative. The data sets were (1) directly measured radon concentrations in indoor air (Strand et al. 2001, 2003), (2) digital bedrock geology (Lutro and Nordgulen 2004), (3) digital drift geology (Geological Survey of Norway), and (4) uranium concentrations in the ground from airborne geophysical surveying (Håbrekke 1982, Beard and Rønning 1997, Beard 1998, 1999, Mogaard 1998, 2001, Mogaard and Beard 2000, Beard and Mogaard 2001, Fugro 2003). Smethurst et al. (2006) interpreted each of them in terms of moderate and high radon hazard (Figure 2) and united these into a single hazard map (Figure 3). This is the map we will be testing in the present contribution.

We choose to test the hazard map in the Gran area marked by the black rectangle in Figure 1. We choose this area because it includes dramatic local variation in radon-hazard levels and is comparatively well covered by measurements of radon in indoor air. There are 549 measurements in all (Figure 4): 22% over 200 Bq m⁻³, 10% over 400 Bq m⁻³ and 3.5% over 1000 Bq m⁻³. The action level in Norway is 200 Bq m⁻³ (NRPA 2000).

Radon in indoor air

Annual average radon concentrations in indoor air (Strand et al. 2001, 2003) are unevenly distributed across the Gran area (Figure 4), reflecting the uneven distribution of dwellings and known locations of radon hot-spots. The colours of the symbols in Figure 4 clearly show that there are rapid transitions between areas where almost all measurements are over the action level and areas where almost all measurements are below it. Certainly within the tract Brandbu–Jaren–Gran, there are sufficient indoor measurements to create a good picture of radon-hazard hot-spots—without calling upon other data sets. The pattern between these towns and Jevnaker is less clear. There are no geo-referenced data around Grua so any potential radon hazards in this area remain undetected through this data set. The hazard evaluation scheme of Smethurst et al. (submitted) assigns high radon hazard to areas where 20% or more of the indoor radon measurements exceed the action level (Figure 2a).

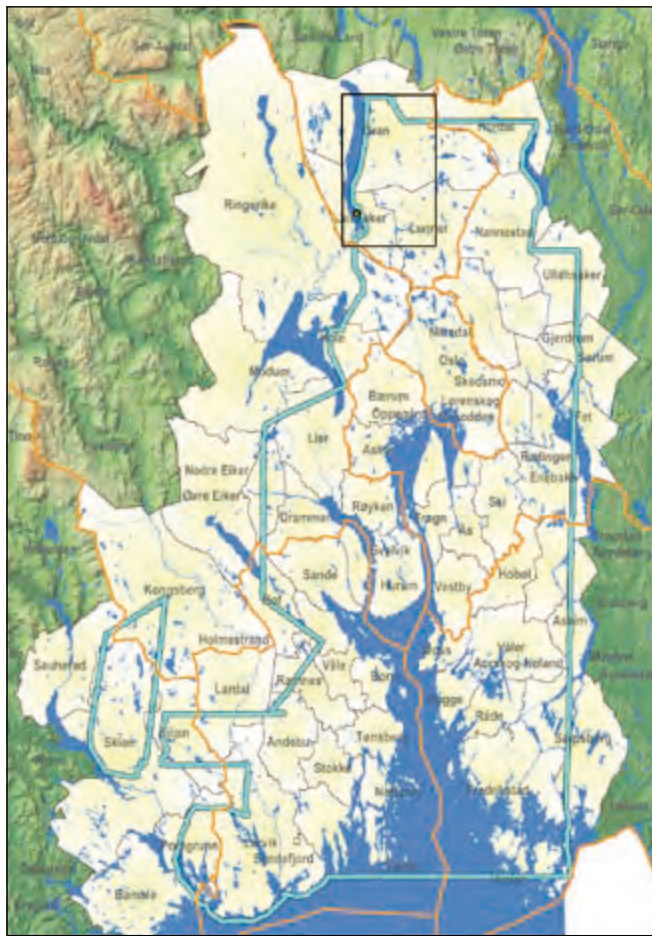


Figure 1. The area around Oslofjord evaluated for radon hazard by Smethurst et al. (2006) is outlined in blue (also see Smethurst et al. submitted). The size and shape of this area is governed by the availability of airborne geophysical surveys in the region—one of the data sets used in the evaluation of radon hazard. We look in detail at the performance of the hazard evaluation within the rectangular area marked in black around Gran in the northern part of the region. The field of view in the figure is approximately 140 × 200 km.

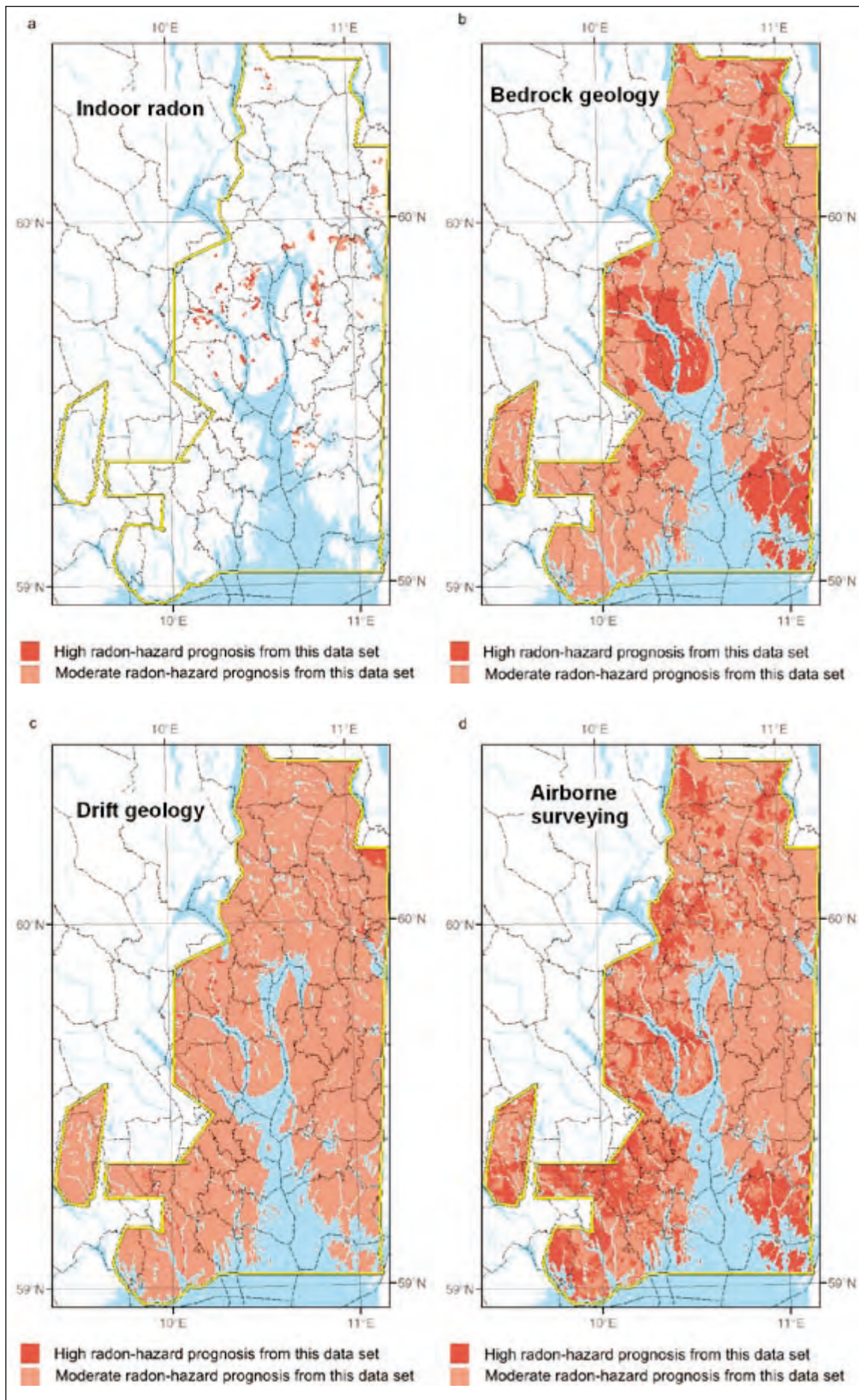


Figure 2. The radon-hazard prognosis of Smethurst et al. (2006) is based upon four data sets. (a) Areas where 20% or more of the indoor radon-concentration measurements exceed 200 Bq m^{-3} (search radius 300 m, $n \geq 9$) are assigned high radon hazard. (b) Alum shale, granite and rhyolite are commonly rich in uranium and areas occupied by these rock types are designated high radon hazard. (c) Highly permeable superficial deposits, in this case largely glaciofluvial deposits, are assigned high radon hazard. (d) Uranium concentrations in the ground from airborne gamma-ray spectrometer surveying. Areas where uranium concentrations exceed 4 ppm are designated high radon hazard. The hazard prognoses from these four data sets are combined into the overall hazard map of Figure 3.

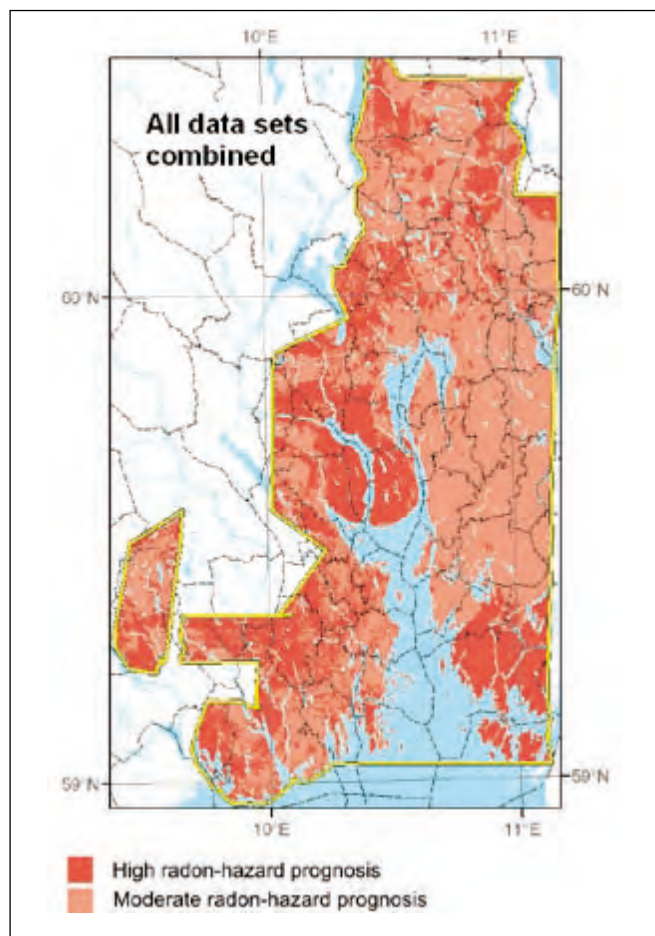


Figure 3. Large-scale radon-hazard evaluation from the study of Smethurst et al. (2006) (sum of the four maps in Figure 2). This map is now available on the Internet in the form of an interactive map service at <http://www.ngu.no/kart/arealis/>. (In Norwegian—select the map theme ‘Radon aktsomhet’.)

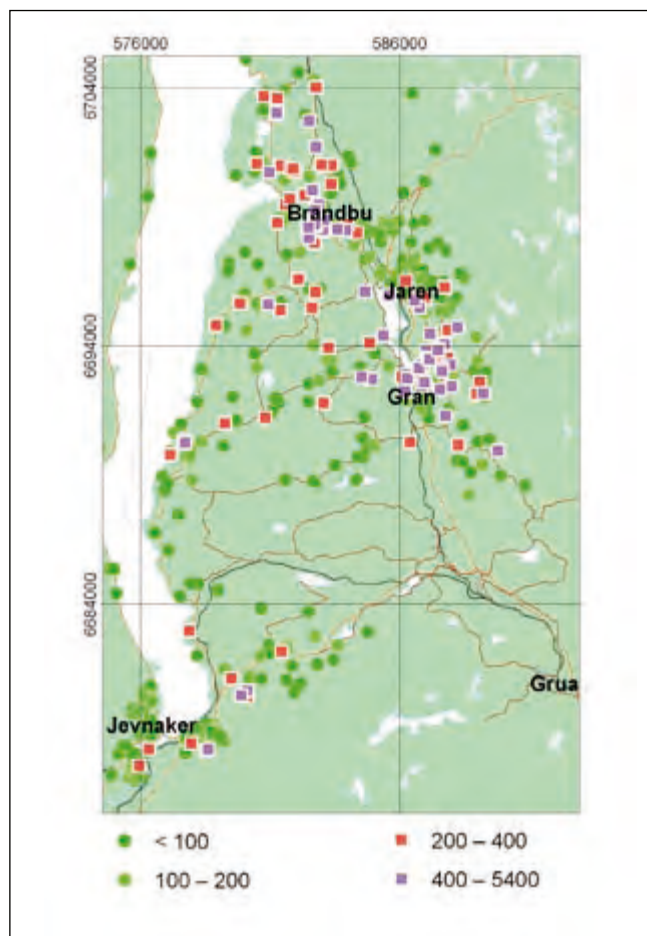


Figure 4. Radon concentrations in indoor air (Bq m^{-3}) for 549 dwellings in the Gran area. Squares denote radon concentrations equal to or above the action level of 200 Bq m^{-3} . Data provided by the Norwegian Radiation Protection Authority, Østerås (Strand et al. 2001, 2003). The measured grid is according to datum WGS1984, projection UTM (zone 32N). The Gran study area (field of view) measures $18 \times 29 \text{ km}$.

Bedrock geology

The bedrock geology around Gran, compiled by Lutro and Nordgulen (2004) and simplified by us, is shown in Figure 5. It is well known that the radon problem area around Brandbu–Jaren–Gran is due to the presence of alum shale in the near surface of the ground. Given that knowledge of the presence of alum shale is sufficient in itself to classify an area as potentially hazardous, the outcrop of the alum shale is classified as a ‘high’ radon-hazard area (Figure 2b). Figure 5 shows that the radon hot-spots, evident through the mapping of radon in indoor air, are enclosed by the outline of the alum shale. It also demonstrates that there are well-defined areas of alum shale that are not delineated by indoor measurements of radon, either because measurements have not been made in dwellings there, or because there are, as yet, no dwellings in those areas.

The rock types listed on the left-hand side of the legend are known to regularly contain sufficient quantities of uranium to result in a significant radon hazard. Smethurst et al. (submitted) show that 46% of the 1169 indoor radon measurements made

in dwellings on granite and rhyolite in the Oslo–Oslofjord area exceed the action level. The areas underlain by these rock types are also classified as high radon hazard (Figure 2b). The bedrock geology map in Figure 5 provides important information on likely sources of radon hazards that are not evident in the indoor radon data set. A notable example is the granite body at Grua, outside the coverage of indoor measurements. Clearly, then, the indoor measurements and bedrock geology complement each other and, together, contribute to a sound hazard evaluation and foundation for follow-up work.

Superficial deposits

At first glance, a surprisingly large proportion of the radon measurements made in dwellings underlain by sedimentary rocks west of Brandbu–Jaren–Gran are high (Figure 6). This illustrates the importance of considering superficial deposits in radon-hazard evaluation. The superficial deposits symbolised as ‘moderate permeability’ in Figure 6 are locally derived and con-

tain material from the alum shale. High radon measurements west of Brandbu–Jaren–Gran may be due to smaller outcrops of alum shale (not in Figure 5) and superficial deposits containing alum shale. In their evaluation of radon hazard, Smethurst et al. (submitted) rated high permeability glaciofluvial sands and gravels as high radon hazard (Figure 2c). Intensive measurement of indoor radon concentrations in dwellings built on such deposits at Jevnaker, show that in this case the only high indoor radon measurements were made where the deposits overlie the alum shale (compare Figures 5 and 6).

Uranium concentration in the near-surface ground from airborne geophysical surveying

Airborne gamma-ray spectrometry detects the decay of radon daughters in the upper 30 to 40 cm of the ground (Otton et al. 1995, Sundevall 2003). Converted to equivalent uranium concentrations, these data are shown in Figure 7 using a simple 3-division colour scale. There is an obvious correlation between uranium concentrations and the incidence of elevated radon concentrations in indoor air. Smethurst et al. (2006) noticed this when examining data for the whole of the Oslo–Oslofjord area and suggested that uranium concentrations of around 4

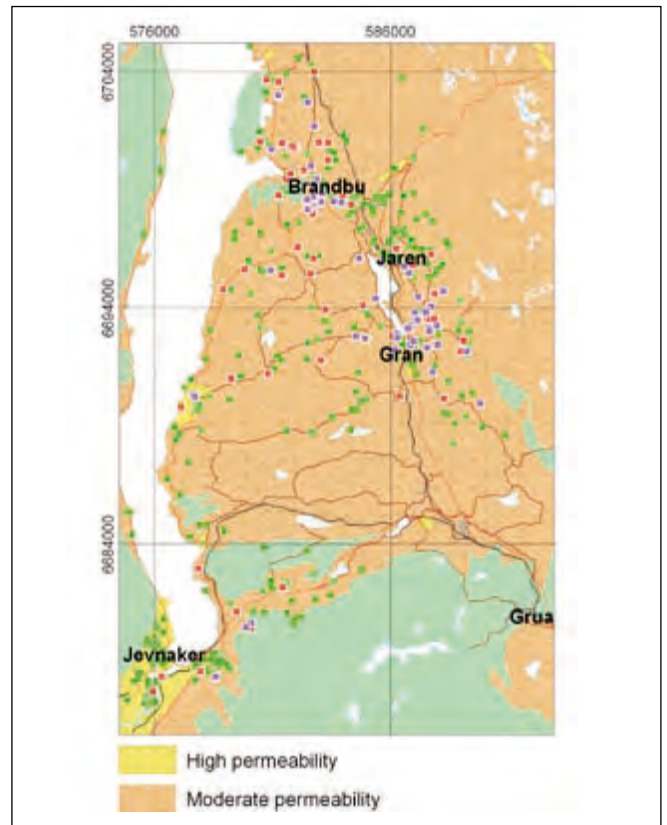


Figure 6. Extract from the 1:50,000-scale drift geology map of Kjernes (1982), simplified to differentiate between deposits with different permeabilities by Bjørn Bergström of the Geological Survey of Norway.

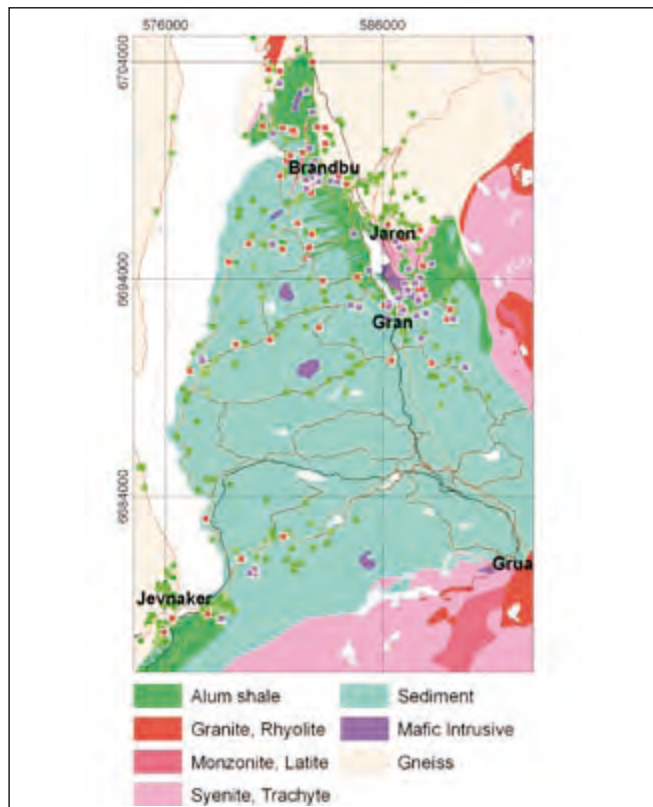


Figure 5. Extract from the 1:250,000-scale bedrock geology map compiled by Lutro and Nordgulen (2004) for the Oslo Rift and surrounding areas. Original rock-type assignments are merged by us into the broader groups shown. ‘Sediment’ includes all sedimentary rock types except for alum shale and unconsolidated deposits.

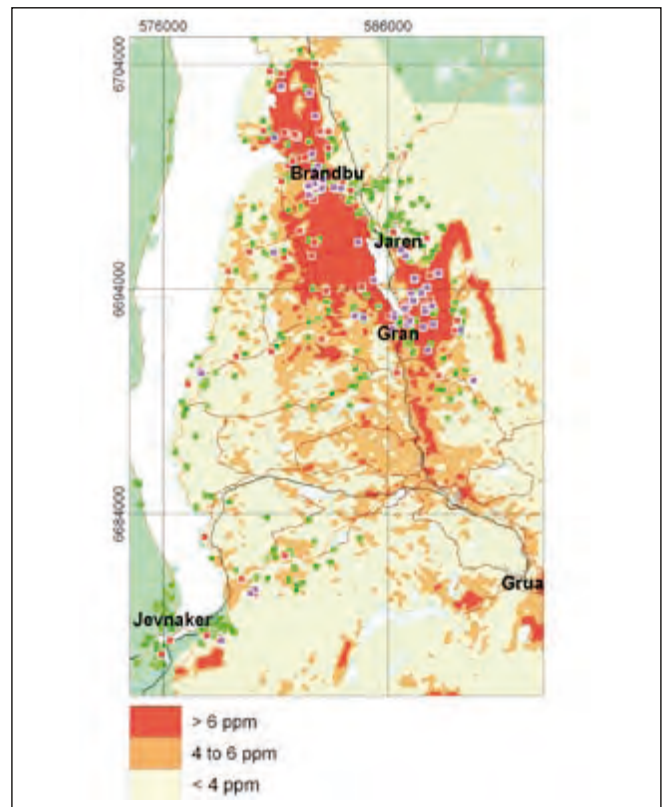


Figure 7. Uranium concentrations in the near surface of the ground (ppm) based on airborne gamma-ray spectrometer surveys carried out by the Geological Survey of Norway (Beard 1998, Beard and Mogaard 2001). Indoor radon measurements are from Figure 4.

ppm and above correspond to rates of occurrence of high radon concentrations in indoor air of 20% or more (high = 200 Bq m⁻³ or more). This led them to classify areas with uranium concentrations of 4 ppm or more as high radon hazard (Figure 2d). This corresponds to the brown and red part of Figure 7.

Addition of the uranium data set in the hazard evaluation of the Gran area very significantly complements the three hazard criteria presented above. The data set confirms and refines our knowledge of the position of the alum shale, including the smaller outcrop near Jevnaker. It indicates significant levels of radon in the superficial deposits above sediments west of Brandbu–Jaren–Gran, and clearly shows that the granite bodies around Grua have high uranium contents.

Before moving on to sum up the combined performance of all four hazard criteria in the Gran area, we test the performance of the uranium map alone as a proxy for radon-hazard level. Using the apparent correlation between uranium concentrations and the incidence of elevated radon concentrations in indoor air of Smethurst et al. (2006), we generate the hazard-prediction map in Figure 8. Figure 8 shows the spatial variation in frequency of occurrence of high radon concentrations predicted by the model of Smethurst et al. (2006). Table 1 shows how well this prediction compares with the actual distribution of elevated radon concentrations in indoor air in the 402 measured dwellings on the uranium map. The prediction is sound and we conclude that the setting of a high radon-hazard threshold at 4 ppm uranium (Figure 7) works well in the Gran region. This threshold is equivalent to 20% in Figure 8.

Summary hazard evaluation in the Gran area

Assembling all of the hazard criteria discussed in the last four sections we arrive at the hazard model in Figure 9a. Straightforward visual inspection of Figure 9a suggests to us that the prediction of elevated hazard conforms well to the actual observations of radon in dwellings in the Gran area. Some conformity is inevitable since clusters of high indoor radon

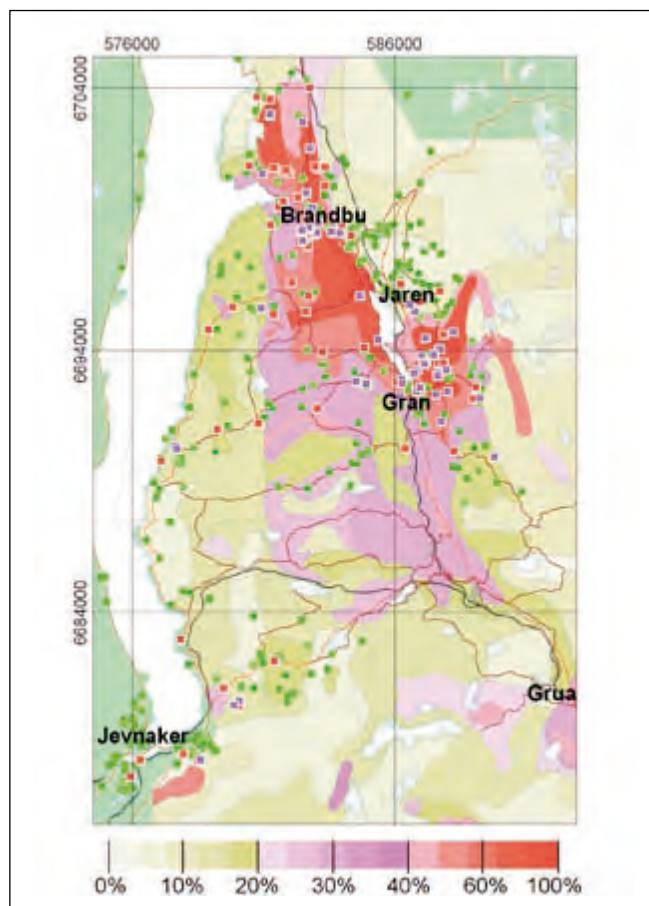


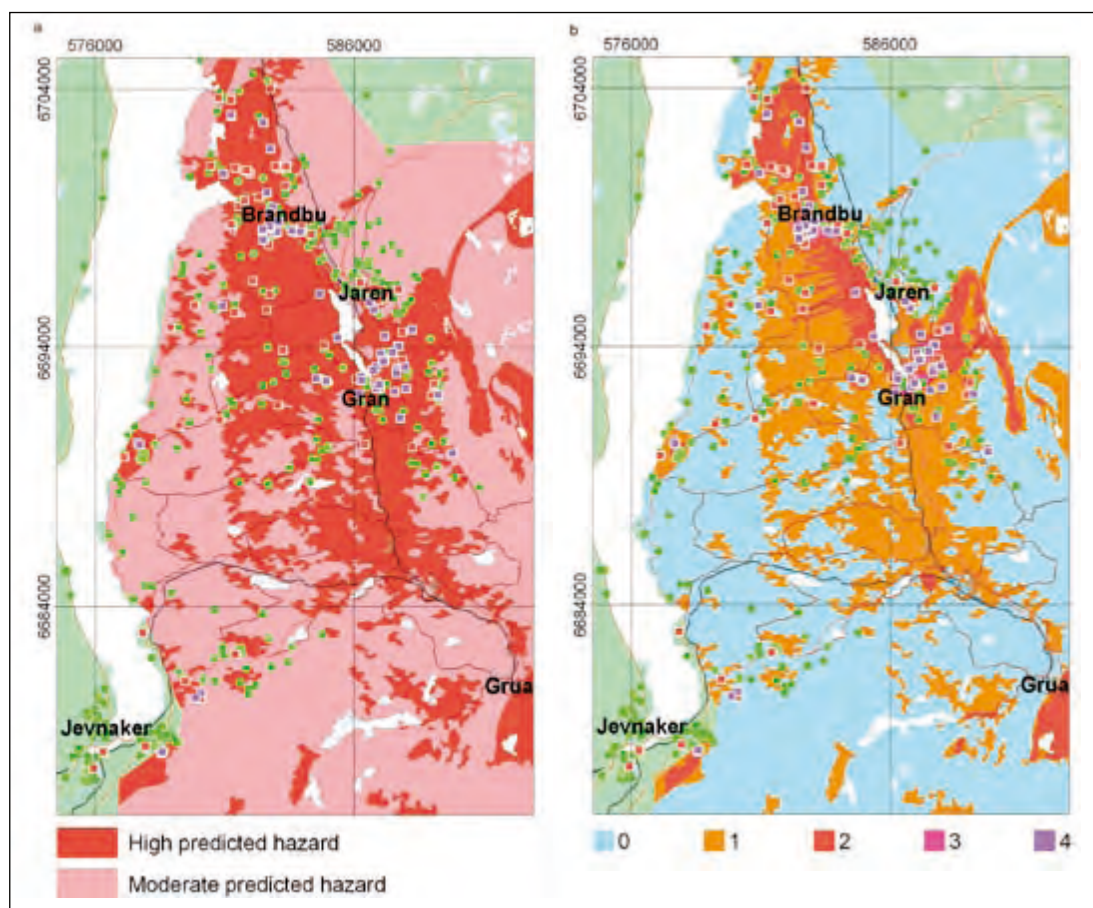
Figure 8. Radon-hazard interpretation based on the relationship reported by Smethurst et al. (2006) between uranium concentrations in the ground and the percentages of indoor radon measurements above 200 Bq m⁻³. The relationship, based on data throughout the Oslofjord area (Figure 1), is here applied to uranium concentrations in the Gran area. The actual uranium map in Figure 7 is here simplified for clarity and average uranium concentrations within the resulting polygonal areas are converted to estimates of the percentages of dwellings with radon levels above 200 Bq m⁻³. The locations of actual indoor measurements are indicated by small, black dots.

measurements are an integral part of the hazard evaluation (Figure 2a). In the Gran region, though, one can remove this element in the hazard evaluation very easily because high-hazard

Table 1. The percentages of dwellings with radon concentrations above the action level predicted from airborne gamma-ray spectrometer measurements (Figure 8) compared with the actual percentages of dwellings with indoor radon concentrations above the action level.

Predicted percentage of dwellings with radon concentrations over 200 Bq m ⁻³	Actual percentage of dwellings with radon concentrations over 200 Bq m ⁻³	Prediction correct	Number of dwellings with indoor measurements	Number of measurements over 200 Bq m ⁻³	Maximum radon concentration Bq m ⁻³
0%–10%	3.6%	YES	56	2	231
10%–20%	18.0%	YES	161	29	832
20%–30%	15.8%	NO	19	3	3134
30%–40%	24.5%	NO	53	13	1143
40%–60%	41.4%	YES	58	24	2001
60%–80%	80.0%	YES	35	28	2330
80%–100%	80.0%	YES	20	16	5400
Total			402	115	

Figure 9. (a) Overall prediction of radon-hazard levels based on the four factors in Figures 4–7. (b) Number of factors suggesting elevated radon hazard.



conditions dictated by the indoor measurements are local to Brandbu and Gran that are both already tagged as high hazard by two other independent data sets. Removing the contribution of indoor measurements from the hazard evaluation (Figure 9a) to facilitate an objective test of the hazard map using measurements of radon indoors does not make any difference to the outcome in the Gran area.

A useful byproduct of this approach to radon-hazard evaluation is shown in Figure 9b. The number of different criteria that indicate high radon-hazard level at any given place can be a measure of how sure we are in the assignment of a hazard level. Of course, real life is not that simple and there will always be room for a more considered evaluation of the reliability of hazard-level assignments. The approach to locating areas of elevated radon-hazard level is a generously inclusive one, leading to the definition of large areas with high, predicted radon hazard. This could be described as a ‘better to be safe than sorry’ approach.

It is interesting at this point to test how efficient the hazard map in Figure 9 is at enveloping high indoor radon measurements within its high radon-hazard zone. Table 2 shows that 41.5% of the indoor measurements in the high-hazard zone are high ($\geq 200 \text{ Bq m}^{-3}$) while 9.9% in the moderate-hazard zone are high.

We want to go further and establish what proportion of *all* high indoor measurements fall within the high-hazard zone.

Table 2. The incidence of ‘high’ ($\geq 200 \text{ Bq m}^{-3}$) and ‘low’ ($< 200 \text{ Bq m}^{-3}$) indoor radon-concentration measurements in what we have designated high- and moderate-hazard regions around Gran (Figure 9a).

Hazard assignment	Percentage of dwellings with radon concentrations over 200 Bq m^{-3}	Number of dwellings with indoor measurements	Number of measurements over 200 Bq m^{-3}
High	41.5%	241	100
Moderate	9.9%	152	15
Total		393	115

For the result to have any significance we need to adjust for any bias there may be in the spatial densities of indoor radon measurements between the two hazard zones, and for the different sizes of the hazard zones (Table 3).

We do this in a simplistic way in Table 4 by adjusting down the number of observations in the high-hazard zone to equalise sampling densities in the two zones and adjusting down the number of observations of high radon in the moderate-hazard zone to equalise the geographic areas occupied by the hazard zones.

After adjustment, 80.7% of high indoor radon values lie in the area designated as high hazard. The probability of this distribution occurring by chance is 0.000543, or 0.054%.

Table 3. Sampling bias in the indoor radon-concentration data set. The spatial density of radon measurements in the area designated as high hazard is almost three times that in the area designated moderate hazard. Furthermore, the moderate-hazard area is almost twice as large as the high-hazard area.

Hazard assignment	Radon observations per km ²	Area (km ²)
High	1.73	139.6
Moderate	0.60	253.0
Total		392.6

So, after adjustment for bias and assuming that high- and moderate-hazard zones have the same size, one might expect to find around 80% of the dwellings with high indoor radon concentrations if one were to target dwellings located within the high-hazard zone.

This is effective, but we do not suggest that dwellings in the moderate-hazard zone be ignored. The hazard assessment is based on potentially flawed data of variable quality from place to place and on data that have a limited spatial resolution. Looking beyond the Gran area, it is quite certain that a large number of smaller areas with strong radon contamination and probably

some larger areas too, will fall within broad tracts categorised as moderate hazard.

Consideration of local conditions is important

The hazard assessment works well around Gran. To balance our evaluation of the technique, we show how the usefulness of one of the data sets used in the evaluation can be compromised. Airborne geophysical surveying over Oslo produced a uranium map that was converted into a prediction of radon hazard in a manner similar to that used to generate Figure 8. The result is shown in Figure 10. The airborne surveying correctly highlights alum shale cropping out in the park at Tøyen (right) that, as would be expected, has caused elevated radon concentrations inside some of the buildings in the museum area. The anthropogenic layer covering much of the inner city prevents radiation from the alum shale reaching the airborne measuring system, explaining the abrupt drop in the signal from the alum shale away from the park. The likely complex distribution of the alum shale beneath

Table 4. The incidence of 'high' ($\geq 200 \text{ Bq m}^{-3}$) and 'low' ($< 200 \text{ Bq m}^{-3}$) indoor radon-concentration measurements in high- and moderate-hazard regions adjusted for sampling bias (Table 3 left). Values are also adjusted as if the high- and moderate-hazard regions have the same size (Table 3 right).

Hazard assignment	Original number of radon measurements	Original number of measurements over 200 Bq m^{-3}	Adjusted number of radon measurements	Adjusted number of radon measurements over 200 Bq m^{-3}
High	241	100	83.9	34.8
Moderate	152	15	83.9	8.3
Total	393	115	167.8	43.1

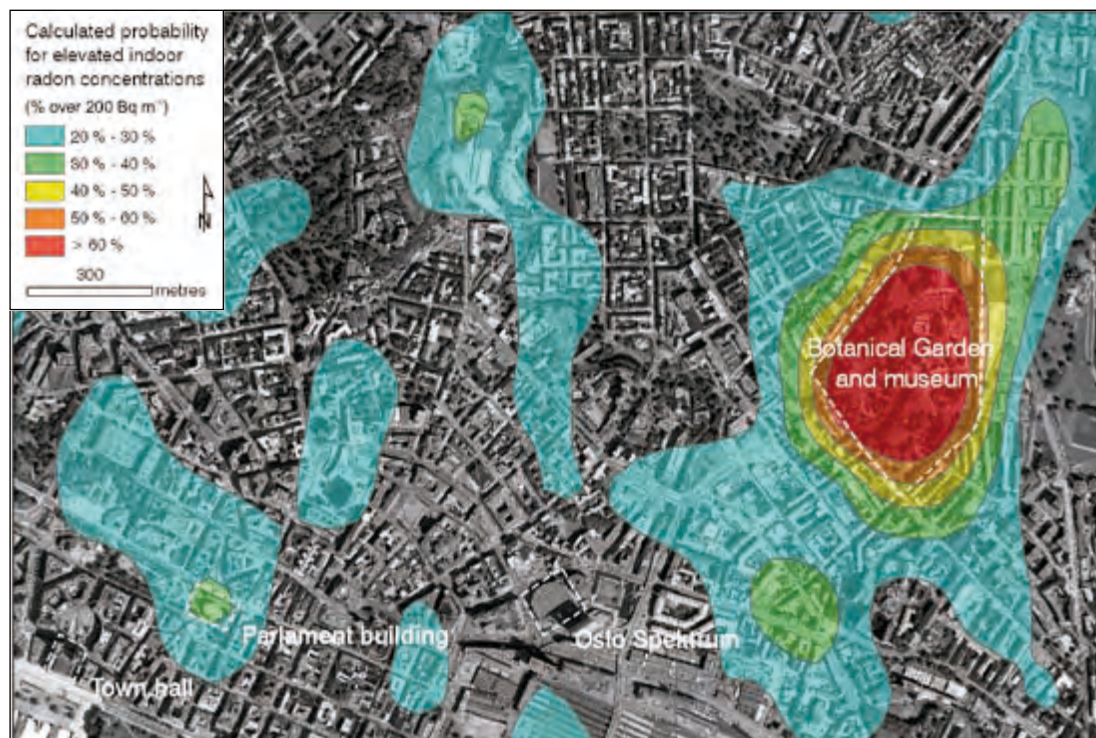


Figure 10. Radon-hazard model for central Oslo based on airborne measurements alone. The methodology used here is akin to that used in Figure 8 for the Gran area. The approach works rather well at Gran, but in Oslo the uranium-rich alum shale is hidden from the airborne detector by a low permeability, anthropogenic covering. Gamma rays from radon daughter bismuth shine out from openings in the cover, most notably over the parkland around the natural history museum (this Figure). Field of view is $2.6 \times 1.6 \text{ km}$.

Oslo is only partially revealed by the airborne data—in areas of open ground. Nevertheless, the adoption of a multi-data set approach to the hazard evaluation in Oslo means that knowledge of the distribution of rock types and superficial deposits beneath the city is not as compromised as the airborne data set, and radon measurements in Oslo dwellings are just as valuable a source of information as measurements anywhere else.

Conclusion

The Geological Survey of Norway and Norwegian Radiation Protection Authority recently reported a multi-disciplinary radon-hazard evaluation for the Oslo–Oslofjord region of eastern Norway (Smethurst et al. 2006; static hazard maps are available for download from <http://www.ngu.no/> and an interactive map is published on the Norwegian AREALIS environmental map-theme resource at <http://www.ngu.no/kart/arealis/>). The evaluation is founded upon (1) measurements of radon concentration in indoor air (2) knowledge of bedrock geology, (3) knowledge of drift geology, and (4) measurements of uranium concentration in the ground from airborne geophysical surveying. The hazard evaluation is intended for use at the large scale and cannot be used to evaluate radon hazards on the scale of individual dwellings or even local housing communities.

We test this hazard evaluation in a 520 km² rectangular area centred on the community of Gran, 40 km north-northwest of Oslo. The uranium-rich alum shale and uranium-rich granite bodies crop out within the test area and indoor radon concentrations reach as much as 25 times the action level. We find that the hazard evaluation describes the distribution of known radon hot-spots well. 41.5% of the indoor radon measurements in the high-hazard areas are above the action level (200 Bq m⁻³) while 9.9% of the measurements in the moderate-hazard areas lie above the action level.

Examining the distribution of high indoor radon concentrations between the high- and moderate-hazard areas, we take account of the different spatial densities of indoor measurements falling in the two hazard categories and apportion high radon measurements between the categories as if the areas occupied by the high and moderate categories were equal. This done, we find that if the high- and moderate-hazard areas were the same size in the Gran area and were sampled equally densely with indoor radon measurements, we would expect 80.7% of all high radon measurements to lie in the high radon-hazard area. In other words, we would expect efficiency in encompassing high-radon dwellings of 80.7%. The probability of this distribution occurring by chance is 0.000543, or 0.054%.

The outcome of this examination, then, is that the radon-hazard mapping of Smethurst et al (2006), later further documented by Smethurst et al. (submitted), works very well in the Gran area by describing known patterns of radon contamination and identifying additional potential radon hazards not yet confirmed by indoor radon measurements.

Acknowledgements

Tor Erik Finne and John F. Dehls are thanked for their valuable participation in the Geological Survey of Norway's RiO project (radon in the Oslo region). We also thank Sverre Iversen, also of the Survey, for his contribution in publishing the radon-hazard evaluation on the Internet in the form of an interactive map (<http://www.ngu.no/kart/arealis/>). Gudmund Løvø of the Survey's information department has served the RiO project extremely well by bringing many of the findings of the project to the attention of the Norwegian public in a very lucid manner. Jon Miles and an anonymous reviewer are thanked for critical comments that helped improve the paper.

References

- Arvela, H., Voutilainen, A., Honkamaa, T. and Rosenberg, A. (1994) High indoor radon variations and the thermal behaviour of eskers. *Health Physics*, **67**, 254–260.
- Beard, L.P. (1998) Data acquisition and processing—helicopter geophysical survey, Oppkuven and Gran, 1997. *NGU Report 1998.079*, 20 pp.
- Beard, L.P. (1999) Data acquisition and processing—helicopter geophysical survey, Larvik, 1998. *NGU Report 1999.026*, 13 pp.
- Beard, L.P. and Mogaard, J.O. (2001) Data acquisition and processing—helicopter geophysical survey, Hurdal, 2000. *NGU Report 2001.018*, 16 pp.
- Beard, L.P. and Rønning, S. (1997) Data acquisition and processing—helicopter geophysical survey, Krokskogen. *NGU Report 1997.134*, 9 pp.
- Fugro Airborne Surveys Central Region (2003) Logistics report, fixed wing borne magnetic, radiometric and VLF–EM survey in the Oslo region, southern Norway. *Fugro Airborne Surveys Report FCR 2241*.
- Håbrekke, H. (1982) Magnetic, electromagnetic, VLF and radiometric measurements from helicopter over an area west of Tønsberg in Vestfold and Telemark counties. *NGU Report 1835*, 13 pp. (in Norwegian).
- Kjærnes, P.A. (1982) Gran, Quaternary geology map 1815 I, scale 1:50,000, *Norges geologiske undersøkelse*.
- Lutro, O. and Nordgulen, Ø. (2004) Oslo Rift, bedrock geology map, scale 1:250,000, *Norges geologiske undersøkelse*.
- Mogaard, J.O. (1998) Helicopter-borne geophysical measurements around Larvik, Vestfold county. *NGU Report 1998.021*, 11 pp. (in Norwegian).
- Mogaard, J.O. (2001) Helicopter-borne geophysical measurements around Sandefjord, Vestfold county. *NGU Report 2001.003*, 12 pp. (in Norwegian).
- Mogaard, J.O. and Beard, L.P. (2000) Helicopter-borne geophysical measurements around Skien, Telemark county. *NGU Report 2000.031*, 12 pp. (in Norwegian).
- NRPA (2000) Radon in indoor air. Health risk, measurements and remedial measures. *StrålevernHefte*, **9** (revised edition), 24 pp., Østerås: Statens strålevern (in Norwegian).

- Otton, J.K., Gundersen, L.C.S., Schumann, R.R., Reimer, G.M. and Duval, J.S. (1995) Uranium resource assessment and exploration data for geologic radon potential assessments in the United States. In *Application of Uranium Exploration Data and Techniques in Environmental Studies, IAEA Technical Document 827*, pp. 135–137.
- Smethurst, M.A., Strand, T., Finne, T.E. and Sundal, A.V. (2006) Airborne gamma ray spectrometry and radon: Application of fixed-wing and helicopter surveying to the identification of radon affected areas—an analysis based on measurements over eastern Norway. *StrålevernRapport 2006:12*, 20 pp., Østerås: Statens strålevern (in Norwegian).
- Smethurst, M.A., Strand, T., Sundal, A.V. and Rudjord, A.L. (submitted) A novel approach to radon-hazard mapping: Utilizing relationships between airborne gamma-ray spectrometer measurements and indoor radon concentrations. *Science of the Total Environment*.
- Strand, T., Ånestad, K., Ruden, L., Ramberg, G.B., Jensen, C.L., Wiig, A.H. and Thommesen, G. (2001) Indoor radon survey in 114 municipalities. Short presentation of results, *StrålevernRapport 2001:6*, 14 pp., Østerås: Statens strålevern (in Norwegian).
- Strand, T., Jensen, C.L., Ramberg, G.B., Ruden, L. and Ånestad, K. (2003) Mapping of radon concentration in 44 Norwegian municipalities. *StrålevernRapport 2003:9*, 10 pp., Østerås: Statens strålevern, (in Norwegian).
- Stranden, E. (1986) Radon -222 in Norwegian dwellings. In *Proceedings of the symposium on radon and its decay products: occurrence, properties and health effects*. New York, US, 13–18 April 1986, *American Chemical Society Symposium Series*, **331**, 70–83.
- Sundal, A.V., Henriksen, H., Soldal, T. and Strand, T. (2004) The influence of geological factors on indoor radon concentrations in Norway. *Science of the Total Environment*, **328**, 41–53.
- Sundevall, S.E. (2003) Regional radon investigations, Kungälv municipality. *Sveriges Geologiska Undersökning Report 2003:22* (in Swedish).



ISBN 82-7385-130-3



9 788273 851307

